THE UNIVERSITY *of* EDINBURGH

Tissue-Engineered Canine Mitral Valve Constructs as In Vitro Research Models for Myxomatous Mitral Valve Disease

Mengmeng Liu

THE UNIVERSITY *of* EDINBURGH

A thesis submitted for the degree of Doctor of Philosophy (PhD)

– The University of Edinburgh – 2014

Declaration

In accordance with the regulation of the University, I hereby declare that all the work included in this thesis has been completed entirely by myself, except where the acknowledgements have been made. This work has not been, and will not be submitted for any other degree or academic qualification.

Mengmeng Liu

August 2014

Acknowledgements

Initially, I would like to give my special thanks to my principle supervisor Professor Brendan Corcoran, for introducing me to this exciting project, for his patience, enthusiasm, excellent academic guidance and supports throughout. I also would like to thank my second supervisor Professor David Argyle, for his brilliant academic advice and the great interest shown in this project. I am grateful to my co-supervisor Dr. Anne French, for the endless encouragement and inspiration in both veterinary research and clinical aspects throughout my PhD as well as for her kind help in proofreading my PhD thesis.

This project is a work of collaboration between four research groups from different international academic institutions. I would like to thank all the collaborators involved. I would like to express my sincere gratitude to my co-supervisor Dr. Thomas Flanagan from the University College Dublin, who is a sound and dedicated scientist specialising in cardiovascular tissue engineering. I would like to thank Dr. Flanagan for his technical assistance in mitral valve construct fabrication, his advices on the design of the study, and for his valuable comments on experimental data analyses as well as on ideas for the future direction of the project. I would like to thank Dr. Alexander Black from the National University of Ireland, Galway for his contribution to the electron microscopy work which is presented in this PhD thesis, including technical assistance with sample preparation, ultrathin sample analyses and expert interpretation of the data. I would also like to thank Professor Stefan Jockenhovel and his PhD students, Luis Hurtado and Stefanos Diamantouros from the Helmholtz Institute of RWTH, Aachen University & Hospital, Germany, for their generous help with the design and manufacture of the bioreactor, and a short-term but helpful training in demonstration of bioreactor operation.

I would like to thank all the members in Professor Argyle's research group for the great supportive company to me, past and present. My special thanks go to Rhona Muirhead, who is the best laboratory technician I have ever known, for her efficient organization, for sorting out my various requests, and also for her training in basic laboratory skills. In addition, my special appreciation goes to Dr. Lisa Pang, for her

technical assistance, helpful advice on experimental trouble-shooting, for kindly proof-reading drafts of my PhD thesis, as well as for her constant encouragement.

My thanks go to Geoff Culshaw and the other clinicians in the cardiopulmonary service of the Hospital for Small Animals in the Easter Bush Veterinary Centre for their help with clinical samples and archive collections, as well as for their opinions regarding my experimental design.

Thanks also to Bob Fleming in the Bio-imaging service at the Roslin Institute for helping me and training me in flow cytometry, FACs and fluorescent microscopy operation.

Thanks also to Gordon Goodall, Neil MacIntyre and the other staff in the Veterinary Pathology Unit for the immunohistochemistry tissue section preparation as well as hematoxylin and eosin staining.

My thanks go to Dr. Daren Shaw for his training and guidance with statistics analyses.

Thanks also to Dr. Shakil Ahmad and Dr. Keqing Wang for their advices on endothelial cell culture.

Thanks also to Steven Mitchell for his kind assistance in sample preparation for transmission electron microscopy, as well as for the toluidine blue staining of samples.

I would like to thank all the scientist friends I met in the Roslin Institute: Virginia Venturina, Shoko Nishiyama, Aayesha Riaz, Chih-Chien Lu, Alexander Cerventas, Anna-Eleonora Karagianni, Stella Mazeri, Uemoto Yoshinobu, Dong Xin Zhu and others, for the ‘research triggered’ warm friendships as well as their academic help and communication.

I would like to thank Professor Jeremy Bradshaw for all his suggestions and assistance since I start to apply for this PhD. My heartfelt thanks to Dr Alastair Macdonald, for ‘spotting’ me when I was a veterinary student in China five years ago

and encouraging me to apply for this PhD, and for all his kind help and friendship throughout. I am also grateful to my previous tutors in the China Agricultural University-Professor Lin Degui and Professor Shi Zhensheng, for always supporting and respecting my decisions.

I would like to give a huge thanks to the Chinese friends I met in Edinburgh. To Qiang and Chen, a lovely couple owning a nice restaurant and the free authentic Chinese food they prepared for me to comfort me a lot particularly during my thesis writing period. To Jun and Meng, a brilliant scientist couple who provided lots of academic help especially in molecular biology and endothelial cell culture, and also to their new-born baby Tinting, who is a cute star who lit up several of my writing afternoons. To Shuo, Xiaolu, Rui, Xin Wang, Xin Ma, Lie and my flatmates Danlei, Tian, Wei, Song and Shaojie and other friends, for their companionship and for looking after me; their wonderful friendship is one of the biggest treasures I've found in Edinburgh. I also would like to thank my vet friends in China, especially Xiao and Lumin, for their kind help and vet news updates, most importantly their constant encouragement and understanding.

Lastly, I would like to give the greatest thanks of all to my loving family, to Dad, Mom and my brother. For their eternal love, endless support, and always believing in me.

I would like to dedicate this thesis to my father, who had a dream of getting high level of education but didn't have an opportunity to accomplish it in his time. And also to my dear grandma who passed away when I was 10 years old. She was a very wise lady and successfully predicted I would become a scientist someday.

Abstract

Myxomatous mitral valve disease (MMVD) is one of the most common degenerative cardiac diseases affecting humans and dogs; however, its pathogenesis is not completely understood. This study focussed on developing tissue-engineered fibrin based canine mitral valve constructs, which can be used as an *in vitro* platform to study the pathogenesis of MMVD.

Prior to three dimensional (3D) construct fabrication, primary canine mitral valve endothelial cells (VECs) and valve interstitial cells (VICs) were isolated, cultured and characterized utilising a variety of techniques. Moreover, preliminary experiments were carried out to optimise the purity of VEC cultures.

It is uncertain if canine MMVD is initiated by long term shear stress damage to the valve endothelium or from abnormalities of VICs. To investigate both hypotheses, three types of models were produced using fibrin/based 3D culture techniques: healthy VEC-VIC co-culture (Type 1); healthy VEC-diseased VIC co-culture (Type 2); healthy VEC-VIC co-culture with endothelial damage during culture (Type 3). Histological examination demonstrated partial native tissue-like morphology of the 3D constructs. Results suggest that current static cultured constructs express MMVD markers irrespective of using healthy or diseased VICs. Simple mechanical stimulation was found to regulate VIC activity in the 3D models. Endothelial damage resulting in VIC phenotypic activation (a change typically observed in MMVD), and decreased mechanical tension appeared to be a negative regulator of this effect. Moreover, there appears to be heterogeneity in the activated VIC population.

Additionally, distinct advanced glycation end product (AGE) carboxymethyllysine (CML) expression was found in canine MMVD valves, which suggesting this biochemical compound (known to affect long living protein) might be a putative regulator of MMVD pathogenesis. The role of CML in MMVD can be further investigated utilizing current 3D static mitral valve construct model in future studies.

Lastly a prototype dynamic tubular construct and a customised bioreactor system were developed. Preliminary data suggest the feasibility of tubular construct

fabrication and endothelialisation, which provides foundation for future dynamic conditioning experiments and will allow examination of the role of endothelial shear stress in triggering MMVD.

In summary, this project successfully developed fibrin based canine mitral valve constructs. It is believed they are promising models for MMVD research, allowing new insights in understanding MMVD pathogenesis.

Table of Contents

List of Tables

List of Figures

Abbreviations

2D	**Two Dimensional**
3D	**Three dimensional**
5HT 2B	**5-Hydroxytryptamine receptor 2B**
5HT	**5-hydroxytryptamine**
AF12	**Advanced DMEM/F-12 medium**
AGE	**Advanced glycation end product**
ANOVA	**Analysis of variance**
AP	**Ammonium persulfate**
AV	**Atrioventricular**
aVIC	**Activated VIC**
α-SMA	**Alpha smooth muscle actin**
BMP-2	**Bone morphogenetic protein-2**
bp	**base pair**
BSA	**Bovine serum albumin**
$CaCl_2$	**Calcium chloride**
CAD	**Computer assisted design**
CAM	**Computer assisted manufacturing**
CD	**Cluster of differentiation**

cDNA	**Complementary DNA**
CKCS	**Cavalier King Charles Spaniel**
CML	**Carboxymethyllysine**
CO_2	**Carbon dioxide**
CT	**Computed tomography**
DAPI	**4', 6-diamidino-2-phenylindole**
DC	**Dendritic cell**
ddH2O	**double distilled water**
DiI-Ac-LDL	**1, 1'-dioctadecyl -3, 3, 3', 3'-tetramethyl-indocarbocyanine perchlorate acetylated low density protein**
DNA	**Deoxyribonucleic acid**
DMEM	**Dulbecco's modified Eagle's medium**
DMEM/F-12	**Dulbecco's modified Eagle medium/Ham's F-12**
DMSO	**Dimethylsulphoxide**
dNTP	**Deoxyribonucleotide triphosphate**
DPS	**Diastolic pulsed stimulation**
DTT	**Dithiothreitol**
DVIC	**Diseased VIC**
EBM	**Endothelial basal medium**

ECM	**Extracellular matrix**
EDTA	**Ethylenediaminetetraacetic acid**
EGF	**Epidermal growth factor**
ELISA	**Enzyme-Linked Immunosorbent Assay**
EndoMT	**Endothelial-mesenchymal-transition**
EPC	**Endothelial progenitor cell**
ERK	**Extracellular-signal regulated kinase**
ETP max	**Maximum early diastolic transmitral pressure gradient**
FACS	**Fluorescence activated cell sorting**
FBS	**Foetal bovine serum**
FGF	**Fibroblast factor**
FGF-2	**Fibroblast growth factor-2**
FITC	**Fluorescein isothiocyanate**
FSF	**Flexure-stretch-flow**
GAG	**Glycosaminoglycan**
GAPDH	**Glyceraldehyde 3-phosphate dehydrogenase**
H&E	**Hematoxylin and eosin**
H_2O_2	**Hydrogen peroxide**
HCL	**Hydrochloric acid**

HEPES	**4-(2-hydroxyethyl)-1-piperazineethanesulfonic acid**
HRP	**Horseradish peroxidase**
HVIC	**Healthy VIC**
IgG	**Immunoglobulin G**
IF	**Immunofluorescence**
kDa	**kilodalton**
KOH	**Potassium hydroxide**
MACS	**Magnetic activated cell sorting**
MCAM/CD146	**Melanoma cell adhesion molecule**
MMP	**Matrix metalloproteinase**
MMVD	**Myxomatous mitral valve disease**
Na_2EDTA	**Disodium ethylenediaminetetraacetate**
NaCl	**Sodium chloride**
NCBI	**National center for biotechnology**
NO	**Nitric oxide**
NOS	**Nitric oxide synthases**
obVIC	**Osteoblastic VIC**
OD	**Optical density**
PBS	**Phosphate buffered saline**

PCR	**Polymerase chain reaction**
PDVIC	**Pooled diseased VIC culture**
PECAM-1 /CD31	**Platelet endothelial cell adhesion molecule**
PG	**Proteoglycan**
PGA	**Polyglycolic acid**
pH	**power of Hydrogen**
PHVIC	**Pooled healthy VIC culture**
PLA	**Polylactic acid**
PVEC	**Pooled VEC culture**
pVIC	**Progenitor VIC**
qVIC	**Quiescent VIC**
RAGE	**Receptor of AGEs**
rER	**rough Endoplasmic Reticulum**
RNA	**Ribonucleic acid**
RT	**Reverse transcription**
RWTH	**Rheinisch-Westfälische Technische Hochschule**
S-100	**Soluble in 100%**
SDCLJ	**Stroma-Dense Cell Layer Junction**
SDS	**Sodium dodecyl sulfate**
SDS-PAGE	**Sodium dodecyl sulphate polyacrylamide gel**

	electrophoresis
SEM	**Scanning electron microscopy**
SM22	**Transgelin**
SMemb	**Embryonic form non-smooth muscle myosin heavy chain**
TAE	**Tris acetate EDTA**
TBS	**Tris buffered saline**
TE	**Tissue engineering**
TEM	**Transmission electron microscopy**
TEMED	**Tetramethylethylenediamine**
TEMV	**Tissue engineered mitral valve**
TGF-β	**Transforming growth factor beta**
TIMP	**Tissue inhibitor of matrix metalloproteinase**
TNF-α	**Tumor necrosis factor alpha**
TPH-1	**Tryptophan hydroxylase 1**
Tris	**Tris(hydroxymethyl)aminomethane**
TβR II	**Type 2 TGF-β receptor**
v/v	**volume for volume**
VEC	**Valve endothelial cell**
VEGF	**Vascular endothelial growth factor**

VEGF-A	**Vascular endothelial growth factor A**
VIC	**Valve interstitial cell**
vWF	**von Willebrand factor**
w/v	**weight for volume**
WB	**Western blot**

Chapter 1: Introduction

1.1 Mitral Valve Biology

1.1.1 Gross Anatomy

The mitral valve, also called bicuspid valve, is a connective tissue structure between the left atrium and left ventricle which functions to separate the two heart chambers and to prevent the blood flow from left ventricle back to left atrium. This delicate structure closes and opens more than 2 billion times during the average human life. The mitral valve was named by Andreas Vesalius, an anatomist in the 16th century (Walmsley, 1929), because the shape of the valve is similar to a bishop's mitre. The term mitral valve complex usually refers to the annulus, the leaflets, chordae tendineae and papillary muscles (Fenoglio et al., 1972; Frater and Ellis, 1961; Silverman and Hurst, 1968). Some literature has suggested that the left atrial and left ventricular myocardium should be considered part of the mitral apparatus as well since myocardial performance is associated with mitral valve regurgitation (Perloff and Roberts, 1972). All these components interact with each other and determine the overall mitral valve function. Among them are the annulus, leaflets and chordae tendineae and these are discussed in detail below.

1.1.1.1 **Annulus**

The annulus is the fibrous junction where the two mitral valve leaflets anchor, at the confluence of the left atrial and left ventricular walls (Fox, 2012; Silverman and Hurst, 1968). It is a discontinuous fibrous ring containing collagen, elastin and scant cartilage in dogs (Evans, 1993; Fenoglio et al., 1972; Silverman and Hurst, 1968). The mitral annulus comprises the anterior and posterior portions in accordance with anterior and posterior leaflets. The anterior part of the annulus consists of a left fibrous trigone and a right fibrous trigone (Evans, 1993). The left fibrous trigone lies in the triangular confluence of anterior mitral valve-aortic valve juncture. The right trigone is situated between the left and right atrioventricular (AV) orifice. The left and right fibrous trigones are united at the central fibrous body (Evans, 1993; Silverman and Hurst, 1968). It is a dynamic structure with capacity to alter shape and diameter during cardiac cycles (Glasson et al., 1996). Apart from serving as hinge

points for valve leaflets and atrial and ventricular muscle, the annulus is essential to modulate dilation of the valve orifice. Annulus dilation, if it occurs, is associated with increased valve regurgitation (Grewal et al., 2010) and altered shear stress distribution on the mitral valve leaflet surface (Misfeld and Sievers, 2007; Salgo et al., 2002).

1.1.1.2 **Mitral Valve Leaflets**

The major components of the mitral valves are two leaflets: anterior and posterior leaflets. Normally they are thin and translucent membrane-like structures without nodules or evidence of thickening (Whitney, 1967). The leaflets attach to the annulus and the chordae tendineae and form a coordinated unit. There are two zones present on the leaflet surface: rough zone, which is near the valve free edge where the chordae tendineae insert while the smooth zone is localized near the annular junction (Connell et al., 2012). Comparing the atrial surface to the ventricular aspect, the former is smooth and relatively transparent while the latter is more rough and irregular and serves as attachment point for the chordae tendineae (Fox, 2012). It has been shown that the leaflet surface area is greater than the mitral orifice area, which indicates that the two leaflets must have contact with each other close to the end of systole (Borgarelli et al., 2011; Kunzelman et al., 1994; Pohost et al., 1975).

The two mitral leaflets are not completely identical. The anterior leaflet is adjacent to the aortic valve, and is also called the aortic leaflet of the mitral valve or septal leaflet. It is anchored by the fibrous region of the continuity of the aortic annulus. The anterior leaflet is longer than posterior leaflet, and has more chordae tendineae attachment (Borgarelli et al., 2011; Frater and Ellis, 1961; Hadian et al., 2007; Han et al., 2010). The posterior leaflet, also called the mural leaflet is smaller and more compliant compared to the anterior leaflet (Fox, 2012; Richards et al., 2012).

Healthy mitral valves are usually considered as avascular. In canine mitral valves, vascular components have been found restricted to the proximal portion of the cusps (Fenoglio et al., 1972; Sonnenblick et al., 1967). Similar to the vascularization, innervation of canine mitral valves occurs predominately in the proximal part of the leaflets (Culshaw et al., 2010; Fenoglio et al., 1972). Most nerves are sympathetic

and there is a dramatic reduction of innervation with advancing aging (Culshaw et al., 2010). Some evidence suggests innervation may be associated with valve function (Bassett et al., 1976; Woollard, 1926). In degenerative mitral valve disease in dogs, however, there is no alteration of innervation pattern or density (Culshaw et al., 2010).

1.1.1.3 **Chordae Tendineae**

Chordae tendineae are columnar structures unique to AV valves which link the valve leaflets and papillary muscle or occasionally are directed to the ventricular walls (Fox, 2012; Frater and Ellis, 1961; Richards et al., 2012). They can transmit the contractility of the left ventricle to the valve leaflet and are arranged in an 'arcade' like fashion (Misfeld and Sievers, 2007). Based on different sites of insertion on valve leaflets, several subtypes of mitral valve chordae tendineae are classified, each of which exhibit differential mechanical properties and functions (Liao and Vesely, 2003; Nielsen et al., 2003; Obadia et al., 1997). In dogs, first order (marginal) chordae tendineae and second order (basal) chordae tendineae are typically seen (Frater and Ellis, 1961). The first order chordae tendineae attach to the free edge of the valve leaflet and are normally thin. They are stiff and bearing high stress, which is essential to maintain mitral valve function: prevent mitral valve leaflet prolapse and insufficiency (Frater and Ellis, 1961; Kunzelman and Cochran, 1990; Obadia et al., 1997). The second order chordae tendineae insert at the junction of the smooth and rough zone of the leaflet ventricular aspect, and are usually thicker in size (Frater and Ellis, 1961). Compared to first order chords, they are more elastic and bearing less stress (Kunzelman and Cochran, 1990). They are not responsible for leaflet function but for promoting valve-ventricle interaction which is crucial for left ventricular geometry and systolic function (Lomholt et al., 2002; Nielsen et al., 2003). Intact chordae tendineae are essential to optimize valve function as well as reduce the stress on the valve (Yacoub and Cohn, 2004).

1.1.2 Mitral Valve Embryonic Development

During mammalian embryonic development, the heart begins with a primary heart tube originating from mesodermal tissue of the late gastrulation. After bending to the right, the primary heart tube divides into an atrial loop and ventricular loop which are

separated by the AV canal. The superior and inferior endocardial cushions are formed from the ventricular wall and grow towards each other on the same plane as the AV canal. The anterior leaflet of the mitral valve is thereafter formed by the fused superior and inferior endocardial cushions. Whereas the mural leaflets of the mitral valve development is based on the AV myocardium protrusion. The mural valve leaflet mesenchyme is formed on the surface of the myocardium and the underneath myocardium undergoes apoptosis in later development. Different from valve leaflets, the papillary muscle is transformed from trabeculae of the muscular ridge, which was separated from the left ventricular wall. Simultaneously to papillary muscle formation, the myocardium is detached from the valve leaflets and the tendinous cords are formed by the cushion tissue of the ventricular layer. By then, the two valve leaflets are completely formed and attached to chordae tendineae and further anchored to the papillary muscle. The whole mitral apparatus complex achieves mature morphology and only increases in size in later development (Anderson et al., 2003; de Lange et al., 2004; Harvey, 2002; Kanani and Deanfield, 2003; Oosthoek et al., 1998).

1.1.3 Mitral Valve Histology

Histologically, the typical mitral leaflet has been described as having three distinct layers: atrialis, spongiosa and fibrosa from the atrial side to the ventricular side (Black et al., 2009; Fenoglio et al., 1972). The aortic valve has an additional ventricularis layer, and more recently a thin distinct layer at the ventricular aspect of the MV has been suggested and is also termed ventricularis (Aupperle et al., 2009a). The atrialis contains a monolayer of endothelial cells with elastic fibres and a few collagen fibres lying underneath. Valve interstitial cell (VIC) population is also present in the atrialis (Aupperle et al., 2009a). In the sub-endothelium layer of the anterior leaflet, there is a smooth muscle cell layer originating from left atrium occupying one fifth the cross sectional thickness of the proximal valve portion (Gross and Kugel, 1931). These myocardial fibres extended from atrial to mitral valve leaflets are thought to contribute to valve closure and competency as they are found to affect mitral valve three dimensional shape and dynamic geometry (Fenoglio et al., 1972; Timek et al., 2003). The second layer is spongiosa. It mainly

consists of proteoglycan (PG) and glycosaminoglycan (GAG) with some loose collagen and elastic fibres interpersed with VICs (Aupperle et al., 2009a; Fenoglio et al., 1972). It extends from the annulus to the free edge of the leaflets. Towards the distal end, the spongiosa layer merges with the fibrosa layer. Spongiosa is more prominent in the posterior leaflet and in the free edge of the anterior leaflet. It has been found water binding PG versican and GAG hyaluronan are rich in the compression load-bearing region (posterior leaflets and distal edge of the anterior leaflets) (Grande-Allen et al., 2004). This suggests they play an important role in buffering shear strain during valve opening and closure. Small PGs such as decorin and biglycan are also detected in the mitral valve and they have been found to co-localize with collagen and elastin fibres in a tension bearing region (central area of anterior leaflets) (Grande-Allen et al., 2004; Yang et al., 2012). They may play a part in regulating collagen fibrillogenesis and elastic fibre formation (Reed and Iozzo, 2002; Reinboth et al., 2002). The fibrosa layer has been considered as a dense collagenous skeleton of the valve which contains predominantly bundles of collagen fibres with scattered VICs (Aupperle et al., 2009a; Fenoglio et al., 1972). This well-organized collagen-based structure is crucial to maintain tension as well as decrease overall bending stress on valve leaflets (Kunzelman et al., 1993). The final layer is the ventricularis. In the canine mitral valves, it has been described as thin collagen layer between ventricular endothelium and fibrosa layer (Aupperle et al., 2009a). It is a similar layer to the atrialis but generally has shorter and thinner elastin fibres and is without smooth muscle cells (Fox, 2012). Chordae tendineae have similar histology to the mitral valve leaflets: a monolayer of squamous endothelial cells, a basal lamina containing loosely organized collagen and elastin (so called elastic sheath) and, a central core formed by densely packed and aligned collagen bundles (Fenoglio et al., 1972; Kunzelman et al., 1993). The alignment of the collagen fibres is parallel to the long axis of the chordae tendineae and in the direction of flow and the major stem of this collagen cord has been considered to contribute to the fibrosa of the leaflet (Fenoglio et al., 1972). Similar to the central region of the anterior leaflets, biglycan and decrorin are present in chordae tendineae (Grande-Allen et al., 2004). It has been suggested they might contribute to tissue strength in the collagenous tissue.

1.1.4 Mitral Valve Cells and Extra Cellular Matrix

1.1.4.1 Mitral Valve Endothelial Cells

Valve endothelial cells (VECs) have the basic endothelial features such as detecting the environmental change of the blood tissue surface, responding to hemodynamic stress and cytokine stimulation and building up a protective barrier to defend the structures underneath (Balachandran et al., 2011; Butcher et al., 2004; Chalajour et al., 2004; Leask et al., 2003; Paranya et al., 2001). The endothelial characteristics of VECs have been demonstrated as being close cell-cell contact, expressing a variety of cell surface marker such as platelet endothelial cell adhesion molecule (PECAM-1) also called CD31, and metabolically having ability to take up acetylated low density lipoproteins (Cuy et al., 2003; Gould and Butcher, 2010; Paruchuri et al., 2006; Wylie-Sears et al., 2011). However, there are some unique characteristics found in VECs when compared with endothelial cells from other anatomic sites. Previous studies have shown that the aortic VECs respond to shear stress differently from vascular endothelial cells, the former aligned perpendicular to the flow while the latter aligned parallel to the flow (Butcher et al., 2004). Moreover, phenotypic differences of VECs have been observed between the inflow surface and outflow surface of the aortic valves. Compared to the ventricular side, VECs of the aortic side are more predisposed to becoming calcified, showing less inhibition of calcification and inflammation protection (Davies et al., 2004; Simmons et al., 2005). These findings suggest that the heterogeneity of the VECs may be a regulatory result of adapting to differential local environment.

Recently, the communications between the VECs and other cell types has become a popular research topic in heart valve research. By using a VECs-VICs three dimensional (3D) co-culture model, Butcher et al. identified that the aortic VECs tend to stabilize the VIC behaviours including inhibition of the VIC activation and modulation of the VIC osteogenic differentiation (Butcher and Nerem, 2006; Richards et al., 2013). In other studies, the VECs have shown the potential to transform into VICs postnatally, known as endothelial mesenchymal transition (EndoMT) which happens in embryonic development. Adult VECs from aortic valves, pulmonary valves and mitral valves can undergo EndoMT in *vitro* in

response to transform growth factor beta (TGF-β) treatment (Paranya et al., 2001). Osteogenic and chondrogenic propensity have also been detected in mitral VECs when cultured in specific differentiation medium, which suggest the differentiation plasticity of the adult VECs (Wylie-Sears et al., 2011).

1.1.4.2 **Mitral Valve Interstitial Cells**

The most dominant cell population in all heart valves are the interstitial cells, which are previously termed as 'valve fibroblasts' or 'myofibroblasts' (Mulholland and Gotlieb, 1996; Taylor et al., 2003). During embryonic development, a group of endothelial progenitor cells in endocardial cushion undergo EndoMT and migrate to cardiac jelly giving rise to the VICs (Markwald et al., 1977; Oosthoek et al., 1998; Patten et al., 1948). This distinct mesenchymal population is different from cells in any other organ and have more complexity and dynamic diversities than fibroblasts or smooth muscle cells. VICs are well known as maintaining normal valve structure and function. They are responsive to tensile mechanical tension (Kural and Billiar, 2013; Stephens et al., 2011; Weston and Yoganathan, 2001), and are responsible for valve contractile activity (Filip et al., 1986; Lester et al., 1988), extracellular matrix synthesis (Dreger et al., 2006; Flanagan et al., 2006a), as well as valve repair and remodelling in disease condition (Disatian et al., 2008; Lester et al., 1993; Lester and Gotlieb, 1988; Rabkin et al., 2002).

It has been widely accepted that the VICs are a heterogeneous population (Durbin and Gotlieb, 2002; Taylor et al., 2003). Liu et al. proposed a more detailed classification of VICs subtypes in 2007 (Liu et al., 2007). They summarized five subtypes of the versatile VICs: embryonic progenitor endothelial cells, quiescent VICs (qVICs), progenitor VICs (pVICs), activated VICs (aVICs) and osteoblastic VICs (obVICs). In normal adult valves, qVICs are the primary VIC phenotype which is characterized by expressing vimentin but lack of alpha smooth muscle actin (α-SMA) expression (Han et al., 2008; Rabkin-Aikawa et al., 2004b; Rabkin et al., 2001). It has been suggested the qVICs can maintain the normal heart valve structure and function and might have some role in extracellular matrix synthesis and degradation (Liu et al., 2007). Once in injury or disease conditions, there is a phenotypic alteration from qVICs to aVICs, which is considered as a key element to

understanding valve disease pathogenesis (Black et al., 2005; Disatian et al., 2008; Han et al., 2008; Rabkin et al., 2001). Activated VICs have been described as myofibroblast-like but actually not smooth muscle cells (Flanagan et al., 2006a; Lester et al., 1988; Taylor et al., 2003). The α-SMA is a common marker for aVICs, but the α-SMA expression level may vary between different aVIC cultures depending on cell density, culture environment and composition of aVIC sub-phenotypes (Blevins et al., 2006; Engler et al., 2006; Stephens et al., 2011; Xu et al., 2012). Other phenotypic markers of aVICs include embryonic form non-smooth muscle myosin heavy chain (SMemb) (Disatian et al., 2008; Rabkin et al., 2001) and transgelin (SM22) (Della Rocca et al., 2000; Wiester and Giachelli, 2003). The VIC activation is believed to be associated with extracellular matrix (ECM) remodelling (Aupperle et al., 2009a; Aupperle et al., 2009b; Disatian et al., 2008; Han et al., 2013; Han et al., 2010; Rabkin et al., 2001). TGF-β signalling is possibly the most important regulatory pathways involved in the VIC activation of myxomatous valves (Aupperle et al., 2008; Disatian and Orton, 2009; Obayashi et al., 2011). This pathway regulates aVIC proliferation, and also has an effect on increasing expression of α-SMA and can regulate ECM synthesis (Jian et al., 2002; Merryman et al., 2007; Walker et al., 2004). It has been hypothesized that TGF-β induced VIC activation and contractility may be the initiating step in the heart valve disease process as this contributes to alteration of valve mechanics (Walker et al., 2004). The pVICs are a group of cells which show stem cell features and can develop into activated VICs. This group is not well characterized to date but two types of cells were thought to belong to this phenotype: endothelial progenitor cells (EPC) and dendritic cells (DC) (Bischoff and Aikawa, 2011; Paruchuri et al., 2006; Skowasch et al., 2005). EPCs are characterized by expressing stem cell markers CD133 and CD34, whereas DCs are characterized by expressing S-100 protein (Skowasch et al., 2005). The valve resident pVICs could possibly originate from valve endothelial cells though the EndoMT process (Dal-Bianco et al., 2009; Paruchuri et al., 2006; Wylie-Sears et al., 2011). The obVICs require osteogenic culture medium for differentiation *in vitro*. They are thought to play a crucial role in aortic valve calcification (Richards et al., 2013; Wylie-Sears et al., 2011). It has been hypothesized that the degenerative valve disease may have similarities to valvulogenesis in embryonic developmental stage:

the aortic calcification may share similar regulatory pathways with osteogenic development, while the myxomatous mitral valve disease may share signalling pathways with chondrogenesis (Caira et al., 2006; Combs and Yutzey, 2009; Orton et al., 2012). *In vitro* adult mitral valve clones also have shown chondrogenesis differentiation in chondrogenic medium culture (Wylie-Sears et al., 2011). Desmin positive chondrocyte-like cells have been detected in myxomatous mitral valves (Han et al., 2008).

It should be noticed that the constitution of the VIC sub-populations is dynamic. Evidence of this is the VIC phenotypic modulation happening in the physiological valve wound healing process as well as in valve disease (Black et al., 2005; Han et al., 2013; Han et al., 2008; Rabkin-Aikawa et al., 2004b; Tamura et al., 2000). Apparently the VICs have the ability to establishing functional adaption once they are exposed to unusual environment/conditions.

1.1.4.3 **Physiological Role of Valve Extracellular Matrix**

Mitral valve ECM is synthesized mainly by VICs (Flanagan et al., 2006a; Latif et al., 2005). As a predominant component of the valve, the ECM plays a key role in shaping the valves. Histologically, a typical canine mitral valve ECM contains collagen, elastin, PGs and GAGs, fibronectin, laminin and heparin sulphate (Aupperle et al., 2009a). Among them, elastin, collagen and PGs and GAGs are major matrix protein types which are predominant in layer of atrialis, fibrosa and spongiosa respectively (Bashey et al., 1992; Cole et al., 1984; Latif et al., 2005; Tamura et al., 1995). The disposition of these matrix proteins reflects differential mechanical behaviour of each tissue layer in the valve (Kunzelman et al., 1993). The elastin provides tissue elasticity, the collagen is responsible for tissue strength and internal force generation and, the PGs and GAGs give flexibility of valve spongiosa (Aupperle and Disatian, 2012; Kunzelman et al., 1993). The normal ECM composition is constantly dynamic to keep the balance between anabolism and catabolism (Dreger et al., 2002; Rabkin et al., 2001). The latter metabolic mechanism is accomplished by matrix metalloproteinase (MMP) family and their tissue inhibitors (TIMP) which are predominantly secreted by the VICs (Aupperle et al., 2009b; Aupperle et al., 2009c; Rabkin et al., 2001; Visse and Nagase, 2003). Apart

from the physiological maintenance of normal valve structure and functions, the ECM is remodelled in the valve disease process which is an underlying cause of valve pathological lesions (Aupperle et al., 2009a; Cole et al., 1984; Gupta et al., 2009a; Hadian et al., 2007; Han et al., 2010; Tamura et al., 1995). The detailed relationship between ECM and myxomatous valve disease will be discussed later in this chapter.

1.2 Canine Myxomatous Mitral Valve Disease

1.2.1 Epidemiology of Canine Myxomatous Mitral Valve Disease

Myxomatous mitral valve disease (MMVD), also called mitral valve endocardiosis or chronic valvular disease is characterized by the progressive degenerative myxomatous change presenting in the mitral valve. So far, similar changes have been found in human, dogs, horses and pigs (Olsen et al.,, 2010). Dogs and humans seem to be more predisposed to it and present similar pathological changes (Kogure, 1980; Pedersen and Haggstrom, 2000; Pomerance and Whitney, 1970). It is the most common acquired cardiac diseases in dogs and approximately accounts for 75-80% of canine cardiac diseases. Risk factors for the disease progression from mild to severe include age, gender, breed, severity of valve lesion, left atrial enlargement, heart rate and arrhythmia (Olsen et al., 2010). Similar to human mitral valve prolapse, the severity of the diseases is strongly associated with age (Han et al., 2010; Han et al., 2008; Pedersen and Haggstrom, 2000; Whitney, 1974). In contrast to low prevalence in young dogs, MMVD is common in old adult dogs. In fact it is more likely that all geriatric dogs have some evidence of the disease. This could due to the degenerative nature of the disease which usually requires several years to progress to be clinically significant. MMVD can occur in any breed but mainly affects small to medium sized breeds, particularly the Cavalier King Charles Spaniel (CKCS), in which the pathological change has been found even at an early age (Beardow and Buchanan, 1993). However, it would appear that the pathological changes (gross and cellular) in CKCS where the disease has an earlier onset are no different than that seen in other dogs, suggesting the inherited component of the disease is mainly affecting the age of onset (Lu. et al., Veterinary Journal in press).

Previous studies suggest polygenic inheritance may play a role in highly susceptible breed like CKCS and Dachshund (Olsen et al., 2003a; Swenson et al., 1996). A genome-wide association study on CKCS identified two potential loci associated with MMVD development (Madsen et al., 2011), but this was not confirmed on a further study (French et al., 2012). Some evidence suggests males have greater tendency of developing MMVD earlier and with more rapid progression than females (Fox et al., 1999; Olsen et al., 2003a; Smith et al., 2005). In humans, degenerative mitral valve disease has also been linked to some inherited connective tissue disorders, such as Marfan syndrome (Ng et al., 2004; Schoen, 2005). The degenerative changes of the valve are possibly an adaptive result of connective tissue weakness.

For clinical features, many affected dogs remain asymptomatic during their lifetime. However, in the severely affected cases, as the disease progresses, it can eventually develop into congestive heart failure, which has a poor prognosis (Kittleson et al., 1984; Olsen et al., 2010).

1.2.2 Gross Morphological Changes

On gross morphology, the MMVD is characterized by thickened, distorted and less transparent valve leaflets, nodule lesions on the valve surface especially the edge and it may affect the whole mitral valve apparatus, e.g. chordae tendineae thickening and rupture, in severe cases. In 1967, Whitney et al proposed a system to classify canine chronic heart valve disease based on gross morphological changes to the valve (Whitney, 1967). Grade 0 represents normal valves. From grade 1 to grade 4, the disease gradually progressed in pathological severity. Generally, the disease starts with a few small discrete nodules appearing on the edge of the leaflet, which might associate with irregular opacities of the more proximal region on the valve (Grade 1). As the disease become more advanced, the nodules are larger, numerous and coalescent. Irregular opacities might be observed in the proximal region of the valve (Grade 2). Chordae tendineae are not affected at this stage. Clinically, there is no valve incompetence in Grade 1 and Grade 2. In Grade 3, the entire valve is thickened and less translucent. The nodules are further enlarged and coalescent forming

irregular plaque-like deformities. The chordae tendineae are thickened as well. In the most severe cases (Grade 4), the edge of the valve has been described as ballooning or billowing (Behar et al., 1967; Bittar and Sosa, 1968). Because of the nodule or plaque formation, the leaflets are grossly distorted and usually rolled upward. The chordae tendineae are proximally thickened, elongated and can rupture eventually (Whitney, 1967). Alternative grading systems of canine MMVD have been proposed by Kogure et.al in 1980 and Disatian et.al in 2008. The former system is based on the progression of pathological changes on the affected leaflets particularly the ECM alteration (Kogure et.al., 1980). The other system is similar to the Whitney grading criteria but is more simplified. It is depending on the nodular thickening area of the valve leaflets and whether the attached chordae tendineae are affected (Disatian et al., 2008). For the purpose of this thesis the Whitney classification was used.

1.2.3 Cellular Changes

The cardinal microstructure alteration in MMVD comprises valve cellular changes and ECM remodelling (Aupperle et al., 2009a; Han et al., 2013; Han et al., 2010; Han et al., 2008). The most dramatic cellular changes are endothelium denudation and interstitial cells activation (Barth et al., 2005; Black et al., 2005; Corcoran et al., 2004; Disatian et al., 2008; Disatian et al., 2010; Han et al., 2008; Mow and Pedersen, 1999; Prunotto et al., 2010; Rabkin-Aikawa et al., 2004b; Stein et al., 1989). Endothelial cell loss has been found in both human and canine diseased valves by topographic studies (Black et al., 2005; Corcoran et al., 2004; Han et al., 2013; Stein et al., 1989). The remaining endothelial cells are less organized than normal and the number of surface micro-appendages are increased which might indicate the cells are activated (Corcoran et al., 2004). Moreover, the endothelial cell denuding is associated with local sub-endothelial matrix degeneration (Han et al., 2013). This suggests there is an interaction between valve endothelium and subjacent matrix which is possibly through nitric oxide (NO) or endothelin signalling pathway (Mow and Pedersen, 1999; Olsen et al., 2003b). It has been well accepted that the endothelium loss is likely to be a consequence of flow induced shear stress impact. Indeed the activity of shear mechanosensor nitric oxide synthases (NOS) has been detected in diseased porcine and canine mitral valves (Moesgaard et al., 2007; Olsen

et al., 2003b). Whether the increased NO release is a mere response to turbulent flow caused by mitral regurgitation or, further serves as a regulator in disease pathological process remains unclear.

As mentioned previously, the VICs undergo phenotype alteration during the MMVD, transform from quiescent fibroblast-like qVICs to activated myofibroblast-like aVICs (Black et al., 2005; Disatian et al., 2008; Disatian et al., 2010; Han et al., 2013; Han et al., 2008). In affected human and dog valve leaflets, the aVICs were found to play a key role in matrix remodelling by secreting excessive MMPs and TIMPs which indicates there is abnormal ECM catabolism (Aupperle et al., 2009b; Aupperle et al., 2009c; Disatian et al., 2008; Obayashi et al., 2011; Rabkin et al., 2001). It has also been noticed the VICs are present in the endothelium denuded area (Black et al., 2005; Lester and Gotlieb, 1988). The wound repair ability of the VICs has been investigated in previous studies. The findings suggest VICs can respond to injury by cell migration, proliferation and de novo matrix protein synthesis (Durbin et al., 2005; Durbin and Gotlieb, 2002; Gotlieb et al., 2002; Lester et al., 1993; Lester et al., 1992; Tamura et al., 2000).

The role of developmental signalling pathway in heart valve disease has caused great attention in recent studies, particularly the EndoMT related pathways (Bischoff and Aikawa, 2011; Dal-Bianco et al., 2009; Orton et al., 2012; Paranya et al., 2001; Paruchuri et al., 2006; Wylie-Sears et al., 2011). Taken the fact that in the embryonic stage the VICs are differentiated from a group of endothelial cells, it cannot be rule out that the adult VECs may possess VIC replenish capability. Previous studies have shown that the adult mitral VECs can undergo EndoMT in response to external mechanical stretch or TGF-β stimulation (Dal-Bianco et al., 2009; Wylie-Sears et al., 2011). Whether the EndoMT process occurring in the MMVD or not requires further investigation.

Inflammation in myxomatous valve disease is generally considered to be rare both in humans and dogs (Han et al., 2008; Rabkin et al., 2001; Stein et al., 1989). Sparsely distributed macrophages and T cells have been detected in both normal and diseased canine valves (Disatian et al., 2008). Gene up-regulation of inflammatory signalling

has been identified in canine MMVD (Oyama and Chittur, 2006). An increase in number of mast cells has been found in canine myxomatous mitral valves, however the role of these inflammatory evidence in the disease pathogenesis is unclear (Han et al., 2008).

1.2.4 Histopathological Changes

The histopathological classification of the disease is mainly based on the alteration of extracellular matrix components. Typical changes in the lesions include excessive expansion of the lamina spongiosa and distortion of fibrosa layer. In the early stage of the disease, accumulation of PGs leads to the expansion of the atrialis and spongiosa particularly in distal edge of the leaflets however the collagen fibers in the fibrosa are not affected. In moderate MMVD, moderately increased PGs are found in the spongiosa which causes the spongiosa to expand, the collagen bundles in the fibrosa degenerate mildly, while the proximal part of the valve remains normal. In marked MMVD, dramatically increased PGs are found in a further expanded spongiosa as well as fibrosa (Aupperle et al., 2009a; Kogure, 1980). Among all the ECM components, it seems that the altered quantity and distribution of PGs, GAGs and collagen in the disease process are the major events. Increased PG and GAG expression has been found in human and canine degenerated mitral valves (Gupta et al., 2009a; Han et al., 2010; Tamura et al., 1995). Specifically, expression of decorin, biglycan and versican increases in human myxomatous valves and hyaluronan metabolism is likely to be altered in the disease (Gupta et al., 2009a). Pronounced collagen bundle reduction and derangement are found in the fibrosa layer of affected canine mitral valve (Hadian et al., 2007). Moreover, increased immature collagen production is found in the lesion area (Hadian et al., 2010; Tamura et al., 1995). This may indicate that the newly produced immature collagen is not capable of normal collagen function which could be a reason for fibrosa distortion.

It should be highlighted that the proteolytic enzymes contribute to the typical ECM degeneration seen in MMVD. Rabkin and colleagues have demonstrated that increased MMP-1, MMP-13, MMP-2, MMP-9 produced by VICs, as well as cysteine endoproteases are associated with collagen and elastin degradation, which suggests

that these enzymes may be responsible for valve weakness and deformation (Rabkin et al., 2001). Similar excessive matrix catabolic activity has been identified in affected canine valves, in which increased MMP-1, MMP-3, MMP-13, MMP-14 and TIMP-2, TIMP-3 and TIMP-4 expression have been detected (Aupperle et al., 2009c; Disatian et al., 2008; Obayashi et al., 2011).

1.2.5 Current Hypothesis of Disease Pathogenesis

In the early days of canine mitral valve studies, Whitney proposed three possible causes of the disease: shear stress on the contacting area of the leaflets, disturbed blood pressure or pulmonary disease related hypoxia (Whitney, 1967). Forty years later, Gupta summarized work of other researchers to identify four possible pathogenesis hypotheses: failure in coping with mechanical shear stress, genetic abnormality, collagen and matrix dissolution and increased expression of proteoglycans (Gupta et al., 2009a). To date, the exact pathogenesis of canine MMVD remains unknown.

The current favoured hypothesis is that the long term flow shear stress causes endothelial denuding, which then leads to changes in metabolic and enzymatic activity of VECs and VICs, resulting in ECM remodelling and further myxomatous pathological changes (Corcoran et al., 2004; Durbin and Gotlieb, 2002; Pedersen and Haggstrom, 2000; Prunotto et al., 2010; Stein et al., 1989). Usually, shear stress induced endothelium denudation is presumed to be an initiator of the MMVD, though the detail signalling mechanism of damaged endothelium to subjacent VICs is still unclear. In canine myxomatous mitral valves, increased endothelin receptors and NOS activity have been found to correlate with the disease severities (Mow and Pedersen, 1999; Olsen et al., 2003b). Induced NOS are found to be essential for mitral VIC migration in a wound repair cell culture model (Durbin and Gotlieb, 2002). Therefore such molecules synthesized by the endothelial cells are possible mediators for sub-endothelial VIC activation in the MMVD disease process. In canine myxomatous valves, subjacent to endothelium loss areas, there is accumulation of activated myofibroblasts under transmission microscopy observation (Han et al., 2013). It is widely accepted that the VIC phenotypic transformation in

MMVD is associated with serotonin or 5-hydroxytryptamine (5-HT) and TGF-β signalling pathways (Orton et al., 2012; Oyama and Levy, 2010). The serotonin hypothesis is supported by the identification of up-regulated serotonin synthesis enzyme tryptophan hydroxylase 1 (TPH-1), increased TGF-β expression as well as the evidence of increased transcripts of serotonin Type 2 receptors in canine myxomatous mitral valves (Aupperle et al., 2008; Disatian et al., 2010; Oyama and Chittur, 2006). It is hypothesized that after the valves injured, the damaged endothelium attracted platelets in which the serotonin is largely stored; release of serotonin from the platelets also induces autocrine serotonin secretion; the extracellular serotonin binds to serotonin receptors on the VICs and further induces TGF-β signalling (Oyama and Levy, 2010). The members of TGF-β family are known to contribute to the VIC myofibroblast activation (Merryman et al., 2007; Walker et al., 2004) and can potentially lead to myxomatous pathological changes such as increased GAGs accumulation (Jian et al., 2002).

Tensile strain induced local serotonin synthesis is alternative hypothesis for the VIC activation in the MMVD (Lacerda et al., 2012a; Lacerda et al., 2012b; Orton et al., 2012; Richards et al., 2012). Hypertension or myxomatous changes of the mitral leaflets and chordae tendineae can alter the valve intrinsic mechanics (Dillon et al., 2012; Han et al., 2010; Richards et al., 2012; Sacks et al., 2006; Singh et al., 1999). In response to the increased tissue stretch, the resident VICs synthesize serotonin and initiate TGF-β signalling pathway through extracellular-signal regulated kinase (ERK) phosphorylation to remodel the local matrix (Grewal et al., 1999; Orton et al., 2012). This hypothesis was tested in *ex vivo* studies, in which 30% cyclic strain has been found to increase the expression of myxomatous disease related proteins in canine and ovine native mitral valves, through induction of autocrine serotonin (Lacerda et al., 2012a; Lacerda et al., 2012b).

Though part of the pathogenesis loop of canine MMVD is understood, there is no definitive evidence that prove whether the disease initiated from shear stress damaged endothelium or from activation of sub-endothelial VICs (Han et al., 2013). This identifies a need to generate mitral valve models with endothelium injured or VIC activation for further investigation of MMVD pathogenesis.

1.3 Tissue Engineering of Heart Valves

1.3.1 Tissue Engineering Overview

Tissue engineering has been defined as an application combining the principles and methods in engineering and life sciences, to develop biological substitutes for native organs (Langer and Vacanti, 1993). The early history of tissue engineering goes back to the 1960s when a type of artificial skin was developed for burn victims (Hall et al., 1966). In the past two decades, tissue engineering has attracted great attention and has gradually become one of the most prevailing technologies in the area of regenerative medicine. By using either native or synthetic materials structural tissues and complex organs have been produced and optimized. Attempts have been made in generating many organs such as liver (Fiegel et al., 2008), pancreas (Opara et al., 2010), skin (Metcalfe and Ferguson, 2007), brain (Cheng et al., 2013), bone (Marolt et al., 2012), heart (Ott et al., 2008), lung (Petersen et al., 2010), blood vessel (Chun et al., 2010), heart valves (Rabkin-Aikawa et al., 2005), bladder (Atala et al., 2006), muscle (Langelaan et al., 2010) and nerve tissue (Penna et al., 2011). Though the major purpose of tissue engineering is for producing therapeutic implants, other applications of tissue engineering include drug testing and establishment of *in vitro* physiological models. The latter approach can assist fundamental studies of tissue biology and physiology as well as improving understanding of pathogenesis of certain diseases (Butcher and Nerem, 2006; Gibbons et al., 2012; Rabkin-Aikawa et al., 2005).

Typically, there are three fundamental elements involved in tissue engineering: cells, scaffolds and bioreactors. All these components work together aiming to best mimic the native tissue structure and function. These three elements, particularly in regard to their role in heart valve tissue engineering will be discussed below.

1.3.2 Heart Valve Tissue Engineering

1.3.2.1 Cell Source

Theoretically cell sources for tissue engineering can be allogenic, xenogenic or autologous cells (Rabkin-Aikawa et al., 2005). Because of the possibility of immune response or pathogen transmission risk, the allogenic and xenogenic cells are not ideal for constructs designed for transplantation purposes (Mendelson and Schoen, 2006; Platt and Nagayasu, 1999; Rabkin-Aikawa et al., 2005). Such concerns do not exist in autologous cells, therefore they are superior for clinical applications (Cebotari et al., 2006; Jockenhoevel et al., 2001a; Metzner et al., 2010; Mol et al., 2006). There are five types of autologous cells used in tissue engineering: (1) differentiated primary tissue cells; (2) tissue specific adult stem cells; (3) bone marrow stem cells; (4) bone marrow-derived, circulating stem cells including endothelial and smooth muscle cell precursors, and (5) pluripotent embryonic stem cells (Ballas et al., 2002; Bertipaglia et al., 2003; Rabkin-Aikawa et al., 2005; Walter et al., 2010). For engineering of cardiac valves, the tissue sources for cell isolation have included vessels, circulating blood, skin, adipose tissue, bone marrow, placenta, amniotic fluid, umbilical cord and primary heart valves (Black et al., 2005; Flanagan et al., 2007; Schmidt and Hoerstrup, 2006; Shinoka et al., 1996; Sodian et al., 2010; Sutherland et al., 2005; Weber et al., 2012). In theory, native valve cells especially valve stem cells probably would be the most ideal cell source. However, their availability is limited, the proliferative ability of adult valve cells may be poor and also the valve stem cells have not been fully characterized yet (Black et al., 2009; Liu et al., 2007). These factors limit the feasibility of using autologous valve cells to create a tissue engineered valve for clinical usage. In contrast, mesenchymal stem cells are thought to be the most attractive cell candidate for heart valve tissue engineering. They are easier to obtain than valve cells and are more likely to satisfy the requirements of differentiating into heterogeneous heart valve cell lineages and developing into functional native valve like structures (Rabkin-Aikawa et al., 2005; Sutherland et al., 2005; Weber et al., 2012). Additionally, adipose tissue derived stem cells have been proven to be a promising cell source. One study has shown that they possess more VIC like properties when compared to mesenchymal stem cells (Colazzo et al., 2011).

1.3.2.2 **Scaffold**

The role of a scaffold in engineered tissues is to act as a skeleton, which provides a platform for cells to attach and proliferate. It is crucial for bio-artificial tissue configuration (Black et al., 2009; Brody and Pandit, 2007; Sacks et al., 2009). The design criteria for a three dimensional (3D) scaffold is to 'mimic natural ECM features sufficiently that cells function in the simulated environment as they would *in vivo*' (Lee et al., 2008). An ideal scaffold should be bio-compatible, restorable and structure-wise it should favour cell attachment, proliferation, differentiation and migration, as well as ECM formation and remodelling (Brody and Pandit, 2007; Mendelson and Schoen, 2006; Rabkin-Aikawa et al., 2005; Sacks et al., 2009). Depending on material origins and properties, the scaffolds can be divided in two categories: synthetic scaffolds and natural scaffolds. Popular synthetic scaffolds for heart valve tissue engineering include polyglycolic acid (PGA), polylactic acid (PLA) and their polymers (Mendelson and Schoen, 2006; Rabkin-Aikawa et al., 2005). The advantage of synthetic scaffolds is that their structures and mechanical properties can be well controlled. However, traditional synthetic scaffolds are not ideal for cell attachment and growth (Mendelson and Schoen, 2006). Other potential drawbacks of synthetic substrates are focal tissue inflammation or fibrosis, slow or incomplete scaffold degradation, and toxicity in the degradation process (Black et al., 2009; Mendelson and Schoen, 2006).

Natural scaffolds comprise ECM components such as de-cellularised connective tissues (Hopkins, 2005), collagen (Chen et al., 2012), GAGs (Flanagan et al., 2006b) and fibrin (Flanagan et al., 2007; Jockenhoevel et al., 2001b). Superior to synthetic scaffolds, the natural scaffolds are better substrates for cell attachment and growth therefore favour cellular and ECM remodelling in engineered tissue. Moreover, they have the advantage of maintaining natural signalling biomaterials and architecture of the native tissue.

In the early tissue engineered heart valves, de-celluarised scaffolds were widely used (Kasimir et al., 2003; Mol et al., 2009; Simon et al., 2003; Vesely, 2005). Using various treatments, cellular components have been removed from donor valve leaflets or small intestinal submucosa, and the ECM structure remained. These

scaffolds have a valve tissue matrix or a collagen based structure, which meets the requirement of mimicking the mechanical properties of native connective tissue (Hopkins, 2005; Kasimir et al., 2003; Metzner et al., 2010). However, this method has caused severe consequences in clinical application, such as immune-incompatibility and tissue degeneration (Simon et al., 2003). Moreover, though many studies claimed that there was potential for cellular growth and remodelling on the re-populated acellular scaffold, clear evidence to support this has not been reported so far (Bouten et al., 2011). This has caused a major concern, as the cellular and ECM regeneration on the scaffolds is essential to maintain tissue structure for long-term durability (Brody and Pandit, 2007; Sacks et al., 2009; Vesely, 2005).

The second category of natural scaffolds is hydrogel systems based on native matrix components. They have become popular in heart valve tissue engineering recently, and are mostly based on collagen and fibrin. The general principle of this scaffold type involves mixing soluble ECM components with appropriate cells initially, and then a gel-like structure is produced through various polymerizations. The cells become entrapped within the hydrogel structure and interact with the surrounding matrix (Jockenhoevel et al., 2001b; Vesely, 2005; Ye et al., 2000). The merits of the hydrogel scaffolds include good bio-compatibility, no toxic degradation or inflammatory reactions and most attractively, they provide a supporting system for ECM synthesis and accumulation within the engineered structure (Pikaart, 2008; Ye et al., 2000). Fibrin is a good example. It is a natural structural protein which participates in the haemostatic process and is formed by fibrinogen reacting with thrombin in the presence of calcium ions. It has been described as ‘a potentially ideal cell delivery vehicle’ for tissue engineering (Black et al., 2009). By using a fibrin gel system, high cell seeding efficiency and uniform cell distribution can be achieved. Cell communication can be conducted in all directions of a 3D configuration (Lee et al., 2008). A tissue engineered fibrin based heart valve using autologous cells has been shown to exhibit excellent tissue remodelling and structure durability *in vivo* (Flanagan et al., 2009). The common drawback of hydrogel scaffolds is cell mediated contraction/shrinkage which is not preventable in static cultures *in vitro*. Dynamic conditioning using a bioreactor system can improve this and optimise the fibrin

based valve constructs (Flanagan et al., 2007). Apart from gel contraction, other concerns of hydrogel scaffolds are inadequate initial mechanical integrity and load bearing properties (Bouten et al., 2011; Brody and Pandit, 2007). A combination of synthetic and natural scaffold materials can improve on this limitation. A fibrin/textile co-scaffold tubular tissue engineered heart valve has been shown to be superior for cell distribution compared to mere fibrin scaffold, which can potentially provide adequate mechanical strength for valve conduit implantation in the aortic position (Weber et al., 2014).

Recently, computational technology has been employed for scaffold design and remodelling. The details of this application will be discussed later. Another recent advance is development of instructive and responsive biomaterial scaffolds which allow specific interaction within the culture system and guide engineered tissue development (Boontheekul and Mooney, 2003; Bouten et al., 2011; Rabkin-Aikawa et al., 2005; Ulijn, 2006).

1.3.2.3 **Bioreactor**

The third important element in tissue engineering is the bioreactor. Usually a bioreactor refers to a dynamic conditioning device which serves as a means to generate a supporting culture environment to maintain tissue viability and to physically stimulate tissue growth *in vitro* (Barron et al., 2003; Gandaglia et al., 2011; Lyons and Prandit, 2005; Wendt et al., 2009). The key functions for tissue engineering bioreactors used in research applications include (1) dynamic cell seeding within 3D culture matrices; (2) maintenance of the culture environment; and (3) physical stimuli to trigger tissue development (Barron et al., 2003; Freed and Vunjak-Novakovic, 2000; Wendt et al., 2009). Cell seeding with bioreactor system assistance allows well controlled and uniform cell distribution on the 3D constructs (Aleksieva et al., 2012; Lee et al., 2009; Lichtenberg et al., 2006; Sierad et al., 2010; Wendt et al., 2009). Dynamic cell seeding and conditioning have been applied to endothelialisation on a de-cellularised valve scaffold. Complete endothelium was achieved and the valve constructs possessed comparable mechanical tension to native ovine pulmonary valves (Lichtenberg et al., 2006). Another similar study utilising gradually increased pulsatile flow to pre-condition manually seeded de-cellularised

valve scaffolds also demonstrated successful endothelialisation on the valve constructs (Lee et al., 2009).

Optimal biochemical culture condition is essential for artificial constructs healthy development *in vitro*. With the assistance of a bioreactor system, nutrient and gas supply as well as waste removal can be efficiently controlled. Moreover, the physiochemical parameters in the culture system (e.g. pH, concentration of O_2 and CO_2, temperature, humidity) can be monitored and optimised with bioreactors (Lyons and Prandit, 2004; Rabkin-Aikawa et al., 2005; Wendt et al., 2009; Ziegelmueller et al., 2010).

Providing mechanical stimuli is another key application of bioreactors in tissue engineering. It has been well recognized that the mechanical stimuli can overcome the common mass transport limitation existing in static culture condition, enhance cell viability and proliferation and improve ECM synthesis and organization (Black et al., 2009; Flanagan et al., 2007; Sodian et al., 2000; Wendt et al., 2009; Weston and Yoganathan, 2001).

Fundamentally the dynamic bioreactor applications aim to mimic physiological parameters *in vivo* (Hoerstrup et al., 2000b; Lyons and Prandit, 2004; Wendt et al., 2009). The majority of the mechanical conditioning studies on heart valves involves providing pulsatile flow stimuli (Aleksieva et al., 2012; Dumont et al., 2002; Flanagan et al., 2007; Hildebrand et al., 2004; Hoerstrup et al., 2000b; Ruel and Lachance, 2009; Sierad et al., 2010; Sun et al., 2011; Weston and Yoganathan, 2001). A typical pulsatile flow bioreactor design contains a left heart replicator and this allows the native heart valves or valve constructs open and close in the system which mimic the valve motion that occurs *in situ* (Gheewala and Grande-Allen, 2010; Goldstein and Black, 1999; Hildebrand et al., 2004; Hoerstrup et al., 2000a; Hoerstrup et al., 2000b). Enhanced cell adhesion and native valve tissue-like properties have been observed after pulsatile conditioning (Schenke-Layland et al., 2003). Moreover increased pulsatile flow with low pressure conditions has been shown to enhance cell attachment and alignment, and affect ECM synthesis and remodelling (Flanagan et al., 2007).

Though dynamic flow conditioning has been proven to be beneficial to heart valve development *in vitro*, the detailed contribution of each individual mechanical stimulus has not been completely elucidated. Major modes of mechanical stimulation on native heart valve leaflets include flow shear stress, cyclic flexure and cyclic stretch/strain (Berry et al., 2010; Engelmayr Jr et al., 2005; Mol et al., 2005). Their effects on heart valve development have been evaluated respectively by different research groups.

Flow shear stress plays a key role for engineered valve construct development *ex vivo*. A low shear stress environment has been recognized to facilitate initial valve construct development (Barron et al., 2003; Weston and Yoganathan, 2001). Shear stress effects on aortic valve leaflets have been estimated previously and it has been suggested the shear stress is essential for cell adhesion and synthesis (Weston et al., 1999). In human aortic myofibroblast based tissue engineered construct, a laminar flow bioreactor providing shear stress for 14 days has been found to direct collagen fibril formation in the shear stress field and tissue mechanical stiffness has increased (Jockenhoevel et al., 2002). Endothelial cell activities are believed to associate with flow shear stress (Davies et al., 2005; Weston et al., 1999). Conditioned with steady laminar flow for up to 48 hours, porcine aortic VECs demonstrated differential responses to aortic endothelial cells regarding cell arrangement pattern and transcriptional profiles. Moreover, the VECs were found to have regulatory effects on VIC proliferation and synthetic activities under shear stress conditioning (Butcher and Nerem, 2006; Butcher et al., 2004; Butcher et al., 2006). Some researchers have suggested bioreactor systems can be applied to study shear stress related cardiovascular disease (Barron et al., 2003; Sun et al., 2011).

The native heart valve is known to be subjected to cyclic circumferential stretch (Berry et al., 2010). The effect of cyclic strain/stretch on the heart valve leaflet has been extensively studied *in vitro*. Cyclic strain effect on aortic valve development has been assessed as an independent factor (Mol et al., 2003). Later on a diastolic pulsed stimulation (DPS) bioreactor was designed to replicate the diastolic phase of the cardiac cycle (Mol et al., 2005). In both studies, better tissue formation and mechanical properties were observed in the strained valves comparing to static

samples. Another application of the DPS bioreactors is allowing estimation of valve compliance by analysing data from a computer based feedback loop (Vismara et al., 2010). Other cyclic tension related studies showed increased VIC synthetic activities and moderate tissue tensile stiffness were observed under stretch conditions (Balachandran et al., 2009; Ku et al., 2006; Merryman et al., 2007; Syedain and Tranquillo, 2009).

Similar to cyclic stretch studies, effect of cyclic flexure stimulus on tissue engineering heart valves has been evaluated independently (Engelmayr et al., 2003; Engelmayr Jr et al., 2005). Increased ECM production and tissue stiffness, as well as homogenous cell distribution were observed in the flex group (Engelmayr Jr et al., 2005). The same researchers further developed a flexure-stretch-flow (FSF) system which combined all three key mechanical stimuli but allowed separate control of each factor (Engelmayr Jr et al., 2006; Engelmayr Jr et al., 2008). Higher collagen production rate and effective tissue stiffness were achieved in the combined conditioned constructs comparing to the static and single stimulus conditioned samples (Engelmayr Jr et al., 2006; Engelmayr Jr et al., 2008; Ramaswamy et al., 2010). This mechanical combination is believed to be tremendously informative and closer to realistic mimicking of the native environment (Berry et al., 2010). It should be noted that optimal conditioning is not only dependent on dynamic stimuli, but a wide range of other factors such as cell source, scaffold materials and their interactions also need to be considered (Gandaglia et al., 2011; Ramaswamy et al., 2010; Sacks et al., 2009).

Innovative technologies such as computerization contribute to more advanced bio-reactor design. Computerization can allow the bioreactor to be customised and controlled by automation, thus allowing more optimal and standardised systems to be achieved (Engelmayr Jr et al., 2008; Lee et al., 2009; Vismara et al., 2010; Wendt et al., 2009). This will be useful in analysing and mimicking complex mechanical stimuli patterns on native tissues, and also help to improve understanding of the unsolved challenges in the area of dynamic conditioning.

1.3.3 Current Progress of Heart Valve Tissue Engineering

The early attempts of cardiac valve engineering go back to late 1980s when the de-cellularised matrix approaches were patented (Brendel and Duhamel, 1989; Klement et al., 1988). However, it is likely that only after the first PGA fibre based pulmonary valve was created and implanted in a lamb model by Shinoka and others in 1995 that heart valve tissue engineering truly started (Shinoka et al., 1995). Compared to the conventional prosthetic heart valves, tissue engineered heart valves have certain advantages including possessing capability for tissue growth and remodelling, facilitating tissue development through dynamic conditioning, and overcoming some limitations existing in traditional valve prostheses (Black et al., 2009; Mendelson and Schoen, 2006; Rabkin-Aikawa et al., 2005).

By using various cell sources, synthetic or native scaffolds, with or without dynamic conditions, tissue engineered heart valves have been produced and evaluated by research groups worldwide (Baraki et al., 2009; Flanagan et al., 2009; Jockenhoevel et al., 2001a; Shinoka et al., 1995; Steinhoff et al., 2000). From a clinical aspect, tissue strength as well as valve ECM content, metabolism and immune compatibility seem to be the major concerns in the bio-engineered valve development area (Mol et al., 2009; Rabkin-Aikawa et al., 2005; Sacks et al., 2009). The aim of heart valve tissue engineering has been described as follows ‘to create or regenerate a living valve that functions well hemodynamically, repairs on-going tissue damage and has long term durability and growth potential similar to those of the natural heart valves’ (Rabkin-Aikawa et al., 2005).

Currently, three approaches have been used in heart valve tissue engineering based on different scaffold types: (1) de-cellularised tissue scaffold with cell pre-seeding *in vitro* or direct implantation; (2) bio-resorbable scaffolds with cell pre-seeding *in vitro* or direct implantation; (3) hydrogel based matrix scaffold with cell entrapment (Vesely, 2005).

As has been discussed before, the acellular matrix based valves have been studied extensively, as the matrix network is considered a key feature for heart valve structure and function and the de-cellularised scaffolds retain native tissue

mechanical conformation (Sacks et al., 2009; Vesely, 2005). The results of acellular xenograft valves for human application, however, are controversial. Complete clinical failure has been reported by Simon (Simon et al., 2003). While in another study, a high success rate was shown using de-cellularised xenograft heart valves (Konertz et al., 2005). Currently, there are continuing attempts to optimize this approach, particularly focusing on complete cellular removal and reduction of immunogenic responses (Kasimir et al., 2003; Tudorache et al., 2007; Wong et al., 2011).

Compared with the acellular matrix approach, bio-resorbable scaffold based valves have better defined chemical and material properties and potentially cause less immunogenic responses (Mol et al., 2009). *In situ* studies on this type of valves are mainly carried out in animal models and the results seem to be promising (Kim et al., 2001; Shinoka et al., 1996). To find an appropriate scaffold is the key challenge for this type of approach. The balance of scaffold resorption rate and ECM synthesis, as well as the scaffold catabolite biocompatibilities, are crucial factors for clinical applications (Mol et al., 2009; Sacks et al., 2009).

The hydrogel approach is relatively novel compared to the above two approaches. It requires the greatest amount of design and engineering work and constructed valve leaflets are usually formed in customised moulds *in vitro* (Mol et al., 2009; Vesely, 2005). Since autologous derivatives seem to be the most ideal cell and scaffold source for tissue engineering, this approach appears to be a promising direction for heart valve engineering. By using naturally derived collagen or fibrin scaffolds, tissue engineered heart valves have been successfully developed by a few groups both *in vivo* and *in vitro* (Chen et al., 2013; Chen et al., 2012; Flanagan et al., 2007; Flanagan et al., 2009; Robinson et al., 2008; Weber et al., 2014; Williams et al., 2006). As was discussed earlier, the major drawback of hydrogel scaffold is the cell mediated contraction that, if used as prosthetics, could conceivably lead to valve regurgitation. It has been suggested a more robust bio-degradable supporting material would be necessary to overcome this issue and it could serve as a valve skeleton for cellular derived ECM to develop over a prolonged time (Flanagan et al., 2009; Weber et al., 2014). Theoretically, this could also improve the intrinsic mechanical

strength of the hydrogel system, which is another concern with these constructs (Bouten et al., 2011).

Novel techniques such as computer assisted design (CAD) and/or computer assisted manufacturing (CAM) have been adapted to the tissue engineering field for more accurate structure analysis and model creation. By using computed tomography (CT) scanning systems, a native heart valve model can be obtained precisely and can be reproduced as a mould or scaffold for artificial valve fabrication (Duan et al., 2013; Schaefermeier et al., 2009; Sodian et al., 2010). Bio-printing or 3D printing technology has also been applied to heart valve tissue engineering very recently. It is suitable for creating layered organ structure with geometric and/or mechanical complexity (Duan et al., 2013). As natural heart valves exhibit unique layered ECM structure, a combination of CAD modelling and 3D printing can simulate this structure precisely and provide the opportunities of replicating customised heart valves on large industrial scale (Mironov et al., 2011). To date, bio-printing of heart valves is still at a preliminary stage. However, fabrication of a heterogeneous aortic valve conduit with CAD and 3D printing techniques has been proven to be feasible (Duan et al., 2013). It is believed that this might become the most dominant approach in the future of heart valve tissue engineering.

To date, numerous exciting achievements have been made in the area of heart valve tissue engineering. To maximally optimise engineering materials and conditions, more advanced understanding of native valve biology is required. Heart valve engineering techniques could aid in this understanding of the native valve and valve response in disease.

1.3.4 Tissue-Engineered Heart Valve as Research Models

Though the main aim of heart valve tissue engineering has been the goal of developing valves for clinical implantation, generating a valve model as an *in vitro* research platform is also of great value. This is extremely useful for preclinical therapeutic tests or examination of tissue function. The classic example is the 3D tumor spheroid model in cancer research, in use since the 1970s (Sutherland 1971). Not only chemotherapeutic drugs and radiation resistances were widely tested using

this model but substantial biological information of tumor cells was also obtained (Mueller-Klieser, 1997; Nehls and Drenckhahn, 1995; Olive and Durand, 1994). There are several advantages of utilising 3D culture or tissue engineered models as *in vitro* research tools: (1) superior to traditional two dimensional (2D) culture, the cells in 3D cultures more resembles to *in vivo* situation in terms of cellular distribution, communication and ECM configuration (Mueller-Klieser, 1997); (2) compared with native tissues, engineered constructs can be produced as needed giving better availability; (3) the artificial constructs could replace animal models for preclinical therapeutic tests and could at least partially answer pathophysiological questions of certain disease conditions.

In the tissue engineering heart valve field, though great efforts have been made in engineering technology, substantial fundamental questions regarding valve cell biology or valve construct *ex-vivo* development remain. As has been stated by Butcher and Nerem: 'advanced understanding in valve cellular biology has not kept up with valve mechanical and scaffold studies' (Butcher and Nerem, 2006). The need to obtain more information on heart valve biology is a clear driving force for using 3D valve constructs as a research model rather than just clinical prosthetics. Valve cells especially VICs play a crucial role in almost all heart valve disease. Therefore, most of the *in vitro* model studies have been focused on VIC biological behaviour and functions. By utilising collagen gel scaffolds, it has been shown that human aortic VICs have the capacity of secreting metalloproteinase and are involved in ECM remodelling *ex vivo* (Dreger et al., 2006). Other studies confirmed the fact that VICs are distinct from other mesenchymal cell types. There are studies comparing VICs with vascular smooth muscle cells and pericardial fibroblasts. The VICs exhibit better ECM synthetic ability than smooth muscle cells (Butcher and Nerem, 2004). Moreover, VICs from different type of heart valves seem to have different force generation ability (Smith et al., 2007). All of these should be considered when selecting appropriate cell sources for specific heart valve tissue engineering.

Heart valve endothelium has been suggested as having a role in valve disease pathogenesis, and the interaction between valve endothelium and sub-endothelial VICs is an interesting area of research. This has been achieved by using a 3D VECs-

VICs *in vitro* co-culture model (Butcher and Nerem, 2006). It has been shown that without endothelium coverage, the VICs-collagen co-culture 3D construct expressed higher α-SMA compared to a VECs-VICs-collagen co-culture. When exposed to dynamic conditioning, VECs-VICs co-culture constructs have greater ECM synthesis comparing to VICs alone constructs. This indicates the valve endothelium is important for maintaining and regulating underlying VIC phenotypes, as well as functions.

Other investigations in heart valve research utilising the 3D culture techniques aim to answer questions of heart valve developmental biology (Li et al., 2013) and to explore optimal engineering materials and mechanical conditions for heart valve regeneration (Colazzo et al., 2011; Grande-Allen and Liao, 2011).

1.3.5 Toward Mitral Valve Tissue Engineering

Compared to aortic and pulmonic valves conduits, fewer attempts have been made in mitral valve tissue engineering due to the complexity of the mitral valve apparatus (Black et al., 2009; Grande-Allen and Liao, 2011). Some studies have been done including a chordae tendinae structure generated by using collagen gel matrix with smooth muscle cells (Shi and Vesely, 2004). To date, making a tissue engineered mitral valve is far away from clinical applications. Current mitral valve tissue engineering is mainly to analyse and to collect fundamental information of the mitral valve tissue and cells, which will establish a solid base for future implantation orientated engineering. At the moment, the major research areas are: mitral valve cellular biology and mechanobiology (Flanagan et al., 2006a; Grande-Allen and Liao, 2011); heart valve embryonic developmental biology and signalling pathways (Butcher and Markwald, 2007; Chiu et al., 2010; Stock and Vacanti, 2001); and developing bioreactor culture systems for *in vitro* valve tissue culture (Gheewala and Grande-Allen, 2010; Lieber et al., 2010).

Though cellular composition of mitral valves share common features with other heart valves, unique properties of mitral valve cells have been found in previous studies (Gotlieb et al., 2002; Grande-Allen and Liao, 2011; Liu and Gotlieb, 2008; Merryman et al., 2006). For example, mitral VICs and aortic VICs demonstrated

differential responses to TGF-β (Liu and Gotlieb, 2008; Walker et al., 2004) and fibroblast growth factor-2 (FGF-2) (Gotlieb et al., 2002). Therefore, the research findings from semilunar valves should be taken with caution when applying them to the mitral valve tissue engineering field. One of the earliest studies assessing mitral valve cell function was carried out on a variety of valve tissue sources (Rabkin-Aikawa et al., 2004b). This classic study compared VIC phenotype from normal adult, myxomatous and foetal mitral valves by using immunohistochemistry technique. The results showed that the majority of VICs in normal adult mitral valves are a quiescent phenotype, whereas in the developmental stage and myxomatous disease, the VICs are a more activated phenotype-expressing α-SMA and SMemb and proteomic enzyme MMP-13. This suggests that ECM remodelling in adult diseased mitral valves share similarities to the foetal valve development process. Moreover, in the same study, tissue engineered valves with *in vitro* dynamic conditioning are comparable to foetal valves regarding ECM distribution pattern. This indicates a developmental-like remodelling had occurred in engineered valves *ex situ*. The cell sources and scaffold materials in the tissue engineered valve constructs in this study were not derived from mitral valves (Rabkin-Aikawa et al., 2004b; Rabkin et al., 2002), which might have had an impact on this result. In another study, the ability of mitral VECs and VICs to synthesise products has been assessed. Cardiovascular regulatory enzyme NOS has been found in 2D cultures of VECs and VICs respectively, and both cell types secreted basement membrane components and collagen Type III. However, Type I collagen was only detected in VIC culture (Flanagan et al., 2006a). This study confirmed VICs are the dominant synthetic cell type in mitral valves. In a later study done by the same group, a 3D collagen-GAG hydrogel mitral valve model has been generated. The collagen-GAG construct has demonstrated native valve-like morphology as well as enhanced ECM distribution and endothelialisation compared to mere collagen construct. This can be a potential model reference for future mitral valve tissue engineering (Flanagan et al., 2006b).

It has been known that VICs with diverse characteristics exist within the mitral valves (Blevins et al., 2008). Differential adhesion, metabolic and synthetic

properties were observed among VICs isolated from the anterior leaflet central region, posterior leaflet free edge and chordae tendineae. It has been suggested this phenomenon corresponds to localisation of physiological stress or altered haemodynamics in pathological conditions (Blevins et al., 2008).

Current understanding of mitral valve leaflet and chordae mechanics has been reviewed by Grande-Allen and Liao (Grande-Allen and Liao, 2011). The mitral valve apparatus's mechanical behaviour is best described as 'heterogeneous'. For example, depending on differential underlying collagen fibre distribution, the stress-strain curves on the leaflets vary and also the tensile stiffness is distinct between valve leaflet clear zone and rough zone (Kunzelman and Cochran, 1992; Stephens et al., 2009), and the chordae tendineae insertion region exhibits uneven tension distribution (Padala et al., 2010). The mechanical interaction between chordae tendineae and mitral valve leaflet certainly is one of the greatest challenges for mitral valve tissue engineering.

Understanding of the developmental biology of the native valves is essential before functional tissue engineered mitral valves can be realized (Butcher and Markwald, 2007). General information for mitral valve embryonic development has been reviewed in Section 1.1.2. However, valvulogenesis *in vitro* requires more advanced understanding of mechanical force effects and signalling pathways involved in valve development. One potential solution to allow examination of this topic is by comparing native embryo implant models with artificial embryo valve constructs to analyse common pathways (Butcher and Markwald, 2007). By using a collagen gel system and embryonic cardiac cushion tissue, avian mitral valve constructs have been developed and remodelled *in vitro*. The results indicate these explants/constructs assemble native embryonic AV valves and the development can be regulated by cardiac myocytes, TGF-β, bone morphogenetic protein-2 (BMP-2) and vascular endothelial growth factor A (VEGF-A) (Chiu et al., 2010; Goodwin et al., 2005). This valvulogenesis study utilising 3D culture techniques is particularly valuable for studying valve development *ex situ*.

Mechanical and biochemical stimulation are important factors in heart valve physiological and pathophysiological conditions. Based on foetal cardiac valve development parameters, the following flow conditions have been suggested to result in reasonable initial development for the heart and vascular system: less than 5% radial strain, low oxygen level and a crescendo heart rate (Stock and Vacanti, 2001). Nevertheless, it has been questioned whether identical conditions should be used for all heart valves as they experience differential mechanical forces and surface shear stress patterns in cardiac cycles *in vivo* (Black et al., 2009). Therefore, bioreactor systems for specific mitral valve tissue engineering are needed. One preliminary study established a bioreactor suitable for entire mitral valve organ culture (Gheewala and Grande-Allen, 2010). This system reproduced physiological pressure and pulsatile flow and a similar mechanical environment to the native status was achieved (Gheewala and Grande-Allen, 2010). Another mitral valve *ex vivo* culture system was based on a splashing rotating bioreactor (Barzilla et al., 2010). This customised design provides perfusion and gentle mechanical stimuli which are essential to maintain mitral tissue ECM integrity. To investigate the role of tensile strain in myxomatous mitral valve disease, a cyclic strain bioreactor was designed and it has shown 30% of cyclic strain can induce myofibroblast activation, MMPs up-regulation and increased GAGs in both canine and ovine mitral valves (Lacerda et al., 2012a; Lacerda et al., 2012b). Moreover, local serotonin synthesis has been found to mediate these changes (Lacerda et al., 2012a). Apart from entire organ culture, bioreactor induced shear stress effects on mitral VIC synthesis and phenotypic alteration have also been investigated. Cyclic strain effect on GAG/PG synthesis from porcine mitral VICs has been assessed in a 3D collagen gel system. Mechanical stretch was found to up regulate total GAG production, and a stretch and relaxation process can reversibly regulate the GAG/PG metabolism in the valve constructs (Gupta et al., 2008a). Another collagen system based study demonstrated that 15% cyclic strain tended to regulate VICs from mild diseased myxomatous mitral valves toward a more quiescent phenotype (Waxman et al., 2012).

As has been mentioned before, the unique heterogeneity of the mitral valve brings up more challenges for tissue engineering compared to the semilunar heart valves.

However, the great need for mitral valve tissues in both clinical and research areas emphasises the need for mitral valve tissue engineering (Black et al., 2009). In the past decade, substantial preparation studies have been carried out which gave rise to more clearer understanding of mitral valve physiological and biological properties both *in vivo* and *ex vivo*. Nevertheless, more unsolved questions remain and additional investigations on the key issues will be required to engineer a functional mitral valve (Grande-Allen and Liao, 2011).

1.4 Aim, Scope and Hypothesis

The aim of the current study is to use tissue engineering techniques to generate *in vitro* research models for an investigation of mitral valve biology and myxomatous disease pathogenesis.

Primary canine mitral valve endothelial and interstitial cells were to be isolated and characterized in 2D culture, and archived as a cell source for tissue engineered mitral valve constructs.

Three types of VECs-VICs 3D co-culture constructs were to be generated using a fibrin based hydrogel system in static culture as follows; Type 1-healthy VECs-healthy VICs co-culture; Type 2-healthy VECs-diseased VICs co-culture; Type 3-endothlium damage model based on healthy VECs-VICs co-culture. The following hypotheses were proposed: (1) 3D models will possess native valve-like features and can be used as a substitute for native valve tissue for research purposes; (2) Myxomatous disease related protein markers indicating VIC phenotypic activation (α-SMA and SMemb) and ECM catabolism (MMP-1 and MMP-3) will be increased in the Type 2 model compared to the Type 1 model; (3) In response to endothelium damage (Type 3 model), VICs will become activated in an attempt to repair the wound.

To examine the hypothesis of shear stress causing endothelium damage and contributing to MMVD pathogenesis, a tissue engineered tubular mitral valve construct and a customised bioreactor system providing pulsatile flow would be developed. For future work, both a physiological and a pathophysiological model

(endothelial injury) would be generated using the dynamic conditioning system. It is hypothesized that (1) pulsatile flow dynamic conditioning will enhance tissue ECM synthesis and the shear flow conditioned construct morphology will be histologically more similar to a native mitral valve than static constructs; (2) endothelial injury of the pulsatile flow conditioned construct will result in a construct resembling a MMVD valve, showing up-regulation of a panel of disease related markers.

Additionally, the expression of advanced glycation end products in MMVD were examined, with the intention of investigating the role of these products in MMVD pathogenesis utilising the 3D mitral valve constructs in future studies

Chapter 2: General Materials and Methods

2.1 Tissue Materials

Tissue samples were collected from The Hospital for Small Animals, the University of Edinburgh with full owner consent and sampling procedure conformed to institutional and national ethical guidelines. All dogs were euthanized for non-cardiac reasons. Canine mitral valve tissue was mainly used in all studies in this project. During collection, mitral valve sample gross morphology was graded by at least two observers independently according to the Whitney grading system. In cell culture based studies, after euthanasia, all mitral valve samples were immediately isolated, rinsed and stored in sterile phosphate buffered saline (PBS) and kept on ice until transferred to a tissue culture laminar hood. For the immunoblotting or immunohistochemistry/immunofluorescence studies, at time of collection, mitral valve samples were either snap frozen on dry ice and stored at -80°C or fixed in 4% paraformaldehyde (VWR International, UK).

Additionally, blood samples were collected for enzyme-linked immunosorbent assay (ELISA) analysis. Plasma was prepared by centrifuging the blood at 3,000 rpm, for 15 min, and then the supernatant was divided into 50 μl aliquots and stored at -80°C. Serum samples were selected from the existing blood sample archive in Cardiopulmonary Department of The Hospital For Small Animal, the University of Edinburgh, which were prepared by the technician of the clinical lab and were stored at -20°C.

2.2 Protein Immunoblot (Western Blot)

2.2.1 Protein Extraction

2.2.1.1 Tissue Protein Extraction

Fresh tissue samples were collected and snap frozen on dry ice, then stored at -80°C before protein extraction. Urea lysis buffer (7 M urea (Fisher Scientific, UK)/0.1 M dithiothreitol (DTT) (Melford Laboratories)/0.05% Triton X-100 (Sigma-Aldrich, USA)/25 mM NaCl (Fisher Scientific, UK)/20 mM HEPES-KOH (Fisher Scientific, UK) pH 7.6) was used for extracting soluble proteins and additional Sodium dodecyl

sulfate (SDS) (BDH Laboratory Supplies) extraction buffer (0.15 M NaCl/50 mM Tris (Fisher Scientific, UK) pH 8.0/0.1 mM Na_2EDTA (Sigma-Aldrich, USA)/10% SDS) was used for extracting less soluble proteins. For protein extraction, Lysing Matrix Tubes (6913, MP-Biomedicals, Germany) with 250 µl urea lysis extraction buffer added were placed for 5 min on ice. Buffer was removed from the tube and replaced with 250 µl fresh buffer. Fifty micrograms tissue samples were thawed and finely cut the tissue into approximate $1mm^3$ in size with a sterile scalpel (Swann Morton, UK). The tissue was added to the lysate tube containing buffer and homogenized for 40 s using Thermo Savant FastPrep FP120 Homogenizer (Thermo Electron Inc, USA) at a speed of 4.0 m/s and then centrifuged at 13,000 g for 2 min at 4°C. Supernatant was collected into 1 ml eppendorf tubes and centrifuged again at 13,000 g for 15 min at 4°C. Supernatant was collected from the second centrifugation and kept on ice. A volume of 250 µl SDS extraction buffer (contained 1% β-mercaptothanol (Sigma-Aldrich, USA)) was added to the tube containing second centrifugation sediments, mixed well and the mixture transferred to the original lysate tubes. The homogenization step was repeated as above and then centrifuged at 13,000 g for 2 min at 4°C. The supernatant was collected into 1 ml eppendorf tubes and centrifuged again at 13,000 g for 15 min at 4°C. The protein supernatant was collected and combined with the protein supernatant extracted by urea lysis buffer, divided into small aliquots and stored at -80 °C.

2.2.1.2 **Cell Protein Extraction**

Primary cultured cells were harvested at 80-90% confluence (the cell harvest protocol is described in details in Section 2.4.3) and re-suspended in 1 ml chilled PBS. They were then centrifuged at 300 g, at 4°C for 3 min. The supernatant was removed and cell pellets snap frozen on dry ice. Cell pellets were stored at -80°C. For cell lysis 2-3 volumes of urea lysis buffer was added to the frozen cell pellets and mixed well until the solution became homogenous. They were then incubated on ice for 30 min, before centrifugation at 13,000 g for 10 min at 4°C. The lysate supernatant was collected and transferred to a new eppendorf tube, before snap freezing on dry ice and storing at -70°C.

2.2.2 Protein Sample Quantification and Preparation

For total protein quantification, a Bradford assay was carried out on each sample. Standard protein solutions were prepared with 10 mg/ml Bovine Serum Albumin (BSA) stock solution (A-7638, Sigma) to 0.125 mg/ml, 0.25 mg/ml, 0.5 mg/ml, 1 mg/ml, 2 mg/ml and 4 mg/ml BSA. Protein samples were thawed out on ice and diluted 1 in 10 with ddH_2O (for sample with low protein concentration, neat sample was used). Either 1 µl of standard solution or sample solution were added to a well in a clear 96-well plate and then 200 µl 1 x Bradford reagent (Bio-Rad, UK) was added and mixed well avoiding bubbles. Both standard assays and protein samples were triplicated. The absorbance reading at optical density (OD) 595 nm was measured by Victor3 V1420 Multilabel Plate Counter (Perkin Elmer, USA). A BSA standard curve was made by plotting each standard assay concentration and OD 595 nm absorbance reading respectively. The equation for the curve was calculated in Microsoft Office Excel software (Microsoft Corporation, USA). The formula was applied to protein samples and undiluted sample protein concentration calculated. Samples were prepared to a concentration of usually 1 µg/µl with 4 x SDS sample buffer (4% SDS/200 mM Tris (pH 7)/20% Glycerol (Fisher Scientific, UK)/10 mM EDTA/50 µl/ml 1% bromophenol blue (Sigma, UK)/0.2 M DTT), stored at -20°C.

2.2.3 Gel Electrophoresis

Proteins were resolved on the basis of their molecular weight by sodium dodecyl sulphate polyacrylamide gel electrophoresis (SDS-PAGE). Different percentage acrylamide gels were prepared according to the size of the protein of interest. For proteins less than 150 KDa, 10% resolving gel was used; for protein size between 150-225 KDa, 6% resolving gel was used. The polyacrylamide gels were prepared and assembled using Bio-Rad Protean II mini-gel system (Bio-Rad, UK). Spacer plates and cover glass plates was cleaned by wiping with 70% ethanol (Fisher Scientific, UK) and assembled in a casting frame. It was ensured that the plates were level before clipping back the side hinges. The plates and casting frame were then secured into a clear casting stand. The space between the plates was tested with water to ensure there was no leakage. The resolving gel for protein band separation contained ddH_2O, 30% acrylamide (National Diagnostics, UK), 1.5 M Tris (pH 8.8),

10% SDS, 10% ammonium persulfate (AP) (Sigma, UK) and tetramethylethylenediamine (TEMED) (Sigma, UK). Just before gel pouring 0.1% AP and 0.08% TEMED were added as they initiated polymerization. The resolving gel was prepared as described in Table 2.1.

Table 2.1 Solutions for SDS-PAGE resolving gel preparation

Solution component	Component volumes (ml) per gel mold volume of					
	5 ml	10 ml	15 ml	20 ml	25 ml	30 ml
6%						
ddH_2O	2.6	5.3	7.9	10.6	13.2	15.9
30% acrylamide	1.0	2.0	3.0	4.0	5.0	6.0
1.5 M Tris (pH 8.8)	1.3	2.5	3.8	5.0	6.3	7.5
10% SDS	0.05	0.1	0.15	0.2	0.25	0.3
10% AP	0.05	0.1	0.15	0.2	0.25	0.3
TEMED	0.004	0.008	0.012	0.016	0.02	0.024
10%						
ddH_2O	1.9	4.0	5.9	7.9	9.9	11.9
30% acrylamide	1.7	3.3	5.0	6.7	8.3	10.0
1.5 M Tris (pH 8.8)	1.3	2.5	3.8	5.0	6.3	7.5
10% SDS	0.05	0.1	0.15	0.2	0.25	0.3
10% AP	0.05	0.1	0.15	0.2	0.25	0.3
TEMED	0.002	0.004	0.006	0.008	0.01	0.012
15%						
ddH_2O	1.1	2.3	3.4	4.6	5.7	6.9
30% acrylamide	2.5	5.0	7.5	10.0	12.5	15.0
1.5 M Tris (pH 8.8)	1.3	2.5	3.8	5.0	6.3	7.5
10% SDS	0.05	0.1	0.15	0.2	0.25	0.3
10% AP	0.05	0.1	0.15	0.2	0.25	0.3
TEMED	0.002	0.004	0.006	0.008	0.01	0.012

Approximately 3 ml of resolving gel solution was added to the space (0.75 mm spacer) between the plates to make the gel level sit just below the green band of the casting frame. Isopropanol (Fisher Scientific, UK) was added on top of the resolving gel to remove air bubbles, and the gel was left to set at room temperature for 20-30 min. Then the isopropanol was removed and 5% stacking gel prepared as described in Table 2.2:

Table 2.2 Solutions for SDS-PAGE stacking gel preparation

Solution component	Component volumes (ml) per gel mold volume of					
	1 ml	2 ml	3 ml	4 ml	5 ml	6 ml
ddH_2O	0.68	1.4	2.1	2.7	3.4	4.1
30% acrylamide	0.17	0.33	0.5	0.67	0.83	1.0
1.0 M Tris (pH 6.8)	0.13	0.25	0.38	0.5	0.63	0.75
10% SDS	0.01	0.02	0.03	0.04	0.05	0.06
10% AP	0.01	0.0.	0.03	0.04	0.05	0.06
TEMED	0.001	0.002	0.003	0.004	0.005	0.006

The stacking gel solution was added on top of the resolving gel to the top of the plates. A 10- or 15-well loading comb was inserted and the gel left to set at room temperature for 20-30 min. Once set the gel was removed from the casting stand and frame, the combs removed and wells washed gently with water to rinse off remaining gel in the wells. The gels were placed in the running module and immersed in SDS-PAGE Running Buffer (192 mM glycine, 25 mM Tris, 0.1% (w/v) SDS) prior to protein sample loading. The samples were thawed and heated at 95^{o}C for 3 min to denature the proteins prior to loading. From 5-30 μg of protein samples were loaded into wells in the stacking gel dependent on experiment. Commercial pre-stained protein markers (Bio-Rad and GE Healthcare, UK) were used to gauge size of the protein bands. The tank lid was secured and subjected to electrophoresis at 180 volts for 45-60 min. Proteins of interest separated in the resolving gel.

2.2.4 Transfer

The resolved protein sample in the gel was transferred to Protran®Nitrocellulose Transfer Membrane (Whatman GmbH, Germany) by electroblotting. In detail, one litre 1 x transfer buffer (192 mM glycine (Sigma), 25 mM Tris, 20% (v/v) methanol (Fisher Scientific, UK)) was prepared. The transfer system was prepared, components included one cassette, two blotting paper, two sponges, one nitrocellulose membrane and the gel. A shallow dish was half filled with the transfer buffer to soak the blotting paper and sponges. The cassette was placed in the dish with black side down. The transfer components were assembled as follows: One sponge → one piece of blotting paper → the gel → the nitrocellulose membrane → one piece of blotting paper → the sponge. Bubbles were removed after placing each layer. The gel was separated from the glass plates by inserting a green wedge in the glass space. The stacking gel part was gently chopped off and the resolving gel lifted from the plate and placed on the blotting paper. After assembling, the cassette was closed. The cassette was inserted into a black and red transfer holder ensuring that the black side of the cassette was facing the black side of the holder. An ice block was placed in the transferring tank. The tank was filled with 1 x transfer buffer. Electroblotting was carried out at 300 mA for 1 h or alternatively run overnight at 30 mA without an ice block. The protein marker was checked to see if it had been transferred to the blot as an indicator for successful electroblotting.

2.2.5 Immunoblotting

The nitrocellulose membrane was removed from the transfer cassette and washed with 1 x PBS-0.1% Tween 20 (Scientific Laboratory Supplies, UK). Ponceau S (kindly provided by Dr Karen Tan) stain was applied to the membrane to check equal protein loading. The membrane was washed with PBS-0.1%Tween 20 and blocked in 5% milk/PBS-0.1%Tween 20 for 1 h at room temperature. The primary antibody was diluted with 5% semi-skimmed milk (Sigma-Aldrich, USA)/PBS-0.1%Tween 20 and membranes probed with the primary antibody for 1 h at room temperature or overnight at 4^{o}C. The membrane was washed with PBS-0.1%Tween 20 for 3 x 5 min and then incubated for 1 h at room temperature with a secondary horseradish peroxidase (HRP) conjugated antibody diluted in 5% milk/PBS-0.1% Tween20. The

membrane was washed 3 x 15 min with PBS-0.1%Tween 20. Amersham™ ECL™ Western Blot Detection Reagent (RPN2290, GE Healthcare, UK) was applied to drained blot on a clear glass plate, left for 1-2 min, excessed reagent was removed and blot covered with cling film and placed in a film cassette. Radiographic film (GE Healthcare) was loaded into the cassette in a dark room and developed for 30 s-20 min depending on signal strength of different proteins of interest based on trial and errors. Protein bands were visualised by developing films in a SRX-101A radiographic processor (Konica Minolta, UK). After development, the molecular weight size of target protein was checked by comparing with the standard protein markers on the blot.

2.3 Enzyme-Linked Immunosorbent Assay (ELISA)

For ELISA study, the protocols provided in the commercial kit were followed. Details of the protocols are described in Section 6. Once all reactions had been completed, OD value of each well was measured at 450 nm using a Victor3 V1420 Multilabel Plate Counter. Standard curves were obtained using MasterPlex® EX 2010-Multiplex Expression Data Analysis Software (Hitachi Solutions America, USA).

2.4 Cell Culture

2.4.1 Canine Mitral Valve Endothelial Cell and Interstitial Cell Isolation

Canine mitral valves were dissected immediately post mortem by using sterile surgical instruments. Blood was rinsed from the valve surface with cold sterile pH 7.4 PBS, the valves was kept in 50 ml conical tubes (Greiner Bio-One, UK) with 20 ml sterile PBS on ice. In a tissue culture hood, excess annular, visible myocardium on the leaflets and chordae tendineae were carefully dissected from the valve leaflets to avoid cell contamination. Usually both anterior and posterior leaflets were collected; in some experiments only anterior leaflets were used due to other experiment needs. The valve leaflets were rinsed with sterile PBS or culture medium (details described in Section 2.4.2), then placed in a 35 mm sterile petri dish with 3-5 ml (depending on the size of the leaflets) pre-warmed 600 Units/ml collagenase II

(17101-015, Invitrogen, UK) solution. Tissue was incubated at 37°C and 5% CO_2 for 10 min. Mitral valve endothelial cell (VEC) population was obtained by gently rotating a dry sterile swab over the surface of the leaflet (approximate 5 times for each side) and then dabbing the swab in the collagenase solution to release cells from the swab. The collagenase solution was aspirated and the cells pelleted in a Heraeus®Labofuge 400 centrifuge (Thermo Scientific, UK) at 1,000 rpm for 5 min at room temperature. The supernatant was removed and cells washed in 5 ml culture medium. The cell solution was centrifuged again at 1,000 rpm for 5 min and the cells re-suspended in 10 ml of culture medium. The cells were seeded on 2% gelatin (Sigma, USA) pre-coated cell culture flasks/plates (Thermo Scientific, UK) and the cells cultured at 37°C and 5% CO_2 for at least 2 days before the first medium change.

Mitral valve interstitial cell (VIC) population was isolated either by using an explant or collagenase digestion technique. The explant technique was used in earlier experiments and was replaced by the collagenase digestion in later experiments. For the explant technique, after VEC isolation, the rest of the valve tissue was finely minced into small pieces (around 2 x 2 mm) with sterile scalpels and the pieces were immediately transferred to T80 culture flasks. A couple of minutes allowed for the pieces to adhere to the flasks, and then 10 ml culture medium was gently added to each flask. The explants were incubated under standard tissue culture conditions. Once the VICs substantially migrated from the tissue (6-8 days), the valve explants were removed and discarded.

The explants technique was only used in the earlier VICs isolation experiments, due to the concerns that the VICs that migrate from the explants might not represent the entire VIC population; a collagenase digestion technique was used instead for further experiments. All VICs used in Section 4-5 were isolated by collagenase digestion.

For collagenase digestion, after VEC isolation the valve tissue was placed in a 15 ml conical tube with 10 ml collagenase II solution (600 Units/ml), the tissue was digested for 18 h at 37°C and 5% CO_2. Then the degraded tissue was mixed with a serological pipette until cells and collagenase solution became homogenized. The cell suspension was centrifuged and cells washed using the same protocol which was

described above for harvesting VECs. The VICs were re-suspended in 10 ml culture medium, seeded on 1 x T80 culture flasks and incubated at 37°C and 5% CO_2. VIC primary cultures were normally left for 2 days before changing medium, and usually reached confluence within 2-4 days under light microscopy observation.

2.4.2 Culture Medium

Advanced DMEM/F-12 medium (26134, Life Technologies) with supplement (10% foetal bovine serum (FBS) (Life Technologies, UK), 1% penicillin G and streptomycin (100 U/ml-100 µg/ml) (Invitrogen, UK) and 1% L-glutamine (2 mmol/L) (Gibco, UK) was used for both VECs and VICs culture.

In endothelial culture condition optimization experiments, canine endothelial basal medium kit (Cn211K-500, Cell Application Inc., USA) was also used for VECs culture. Commercial medium supplement in the kit contains antibiotics, FBS, hydrocortisone, fibroblast growth factor-2 (FGF-2) and epidermal growth factor (EGF).

2.4.3 Cell Harvest and Sub-culture

Once the cells reached confluence the medium was removed and sterile PBS was added into the flasks to wash the cells. PBS was removed and the cells were incubated at 37°C and 5% CO_2 with 0.05% 1 x Trypsin/EDTA (253000, Life Technologies, UK) or 1 x TrypLE Express (12604, Life Technologies, UK) (volume: one well of six well plate or T25 flask-1 ml, T80 flask-3 ml, T175 flask-5 ml) for 5-30 min to dissociate the cells. After trypsinization/TrypLE Express dissociation, the cell suspension was diluted with 3-10 ml (depending on the culture vessel) culture medium and centrifuged at 1,500 rpm for 5 min. If cell counting was being performed, the medium was removed, cells were re-suspended in 1-5 ml (depending on the cell number, which was estimated by observing cell pellets) medium then counted; if cell counting was not required, the cells were re-suspended in medium (one well of 6 well plate-3 ml; T25-5 ml; T80-10 ml; T175-30 ml) and seeded on the culture flasks/plates.

2.4.4 Cell Counting

A haemocytometer was used for cell counting. 10 µl cell suspension was mixed with 10 µl Trypan Blue (Sigma-Aldrich, UK) and was added into each side of the counting chamber. Live cells were counted (no Trypan Blue staining) in the two central big squares of the haemocytometer. One cell in one single big square represents 10^4 cells. Therefore Cell Number/ml suspension = Cell Counting Number (sum of the two central big squares) x 10^4.

2.4.5 Cryopreservation

Freezing medium (70% culture medium, 20% FBS, 10% dimethylsulphoxide (DMSO) (Invitrogen, UK)) was prepared into 5 ml aliquots, stored at -20 °C until used. The cells were counted as described previously and re-suspended in freezing medium at approximately 1.5 x 10^6 cells per ml for VICs; 2 x 10^6 cells per ml for VECs and cell suspensions transferred to pre-labelled cryogenic tubes (Wheaton, USA). The tubes were placed in a cryopreservation canister (Thermo Scientific, UK) which contained isopropyl alcohol in the base, the coolant allowing a cooling rate of 1°C/min when transferred to a -80°C freezer. For long term storage, tubes were transferred to a -150°C freezer or stored in liquid nitrogen.

2.4.6 Reviving Cells from Cryopreservation

The cell culture vial was retrieved from the freezer and immediately transferred to a water bath at 37°C and cells thawed without allowing the water to penetrate the cell tube. When the vial contents thawed (generally 1-2 min), the contents were transferred to a 15 ml centrifuge tube in the laminar hood and 5 ml pre-warmed medium slowly added to the cell suspension. The cells were centrifuged at 3,000 rpm for 5 min to remove the freezing medium components, especially DMSO. The supernatant was aspirated, and cells re-suspended in a volume of culture media appropriate for the flask or culture plate, and cultured at 37°C with 5% CO_2.

2.4.7 Cell Morphology Observation

Cell morphology was observed by using a light microscope during culture period. Representative cell images were captured by using a camera connected Zeiss

Axiover 40 microscope (Carl Zeiss, Germany) at different magnifications: x 50, x 100 and x 200.

2.5 Polymerase Chain Reaction (PCR)

2.5.1 Primer Design and Preparation

Canine nucleotide sequences of the selected markers were found either in National Centre for Biotechnology Information (NCBI) Gene Bank (USA) or Ensembl Genome Browser Website (UK). Based on the published genome sequences, the primers pairs were designed by utilizing Primer 3 Input software (Version 4.0) and intron spanning pairs were selected. The specificity of the chosen primers was checked by using NCBI BLAST online program. All primers were ordered through MWG Eurofins Operon online service (Eurofins MWG Operon, Germany) and diluted to 50 pmol/µl, then aliquoted and stored at -20°C.

2.5.2 Cell Ribonucleic Acid (RNA) Extraction

Canine mitral valve cells were trypsinized, counted, re-suspended in cold PBS and centrifuged for 10 min at 300 g, 4°C. Removed the supernatant and snap froze the cell pellets. Frozen cell pellets were stored at -80°C until ribonucleic acid (RNA) extraction. Less than 5 x 10^6 cells were pelleted and washed in 1 ml cold PBS. The cell suspension was centrifuged at 300 g for 10 min at 4°C. Supernatant was removed and cells snap frozen on dry ice. Samples were stored at -80°C until RNA extraction was performed. Cell total RNA was isolated by utilising RNeasy Mini Kit (74106, Qiagen, UK), following the manufacture's instruction. Cells were disrupted by mixing with 350 µl Buffer RLT (provided in the kit), the lysate transferred directly into a QIAshredder spin column (79656, Qiagen, UK), and centrifuged for 2 min at full speed. Then 350 µl 70% ethanol was added to the homogenized lysate, mixed well and the solution transferred to an RNeasy spin column (provided in the kit) and centrifuged for 15 s at ≥ 10,000 rpm. The flow-through was discarded. Buffer RW1 (provided in the kit) 700 µl was added to the RNeasy spin column and centrifuged for 15 s at ≥ 10,000 rpm to wash the spin column membrane. Flow through was discarded. 500 µl Buffer RPE (provided in the kit) was added to the RNeasy spin column, and centrifuged for 2 min at ≥ 10,000 rpm. The RNeasy spin

column was placed in a new 2 ml collection tube and centrifuged at full speed for 1 min. RNeasy spin column was placed in a new 1.5 ml collection tube. 50 µl RNase-free water (129112, Qiagen, UK) was added directly to the spin column membrane and centrifuged for 1 min at ≥ 10,000 rpm) to elute the RNA.

The RNA was subsequently cleaned up using RNase-Free DNase Set (79254, Qiagen, UK) using the following protocol: mixed ≤ 87.5 µl RNA solution, 10 µl Buffer RDD and 2.5 µl DNase I stock solution (provided in the kit) in a micro centrifuge tube, and made up the final volume to 100 µl with RNase-free water, the allowed to react for 10 min at room temperature. Afterwards, 350 µl Buffer RLT and 250 µl 100% ethanol was added to the diluted RNA, mixed well and the sample transferred to an RNeasy Mini spin column. The column was centrifuged for 15 s at ≥ 10,000 rpm and flow-through discarded. 500 µl Buffer RPE was added to the RNeasy spin column and centrifuged for 15 s at ≥ 10,000 rpm and flow-through was discarded. Another 500 µl Buffer RPE was added to the RNeasy spin column and centrifuged for 2 min at ≥ 10,000 rpm and flow-through was discarded. To ensure that no excessive RPE buffer was remained, the RNeasy spin column was placed in a new 2 ml collection tube and centrifuged at full speed for 1 min. Then the RNeasy spin column was placed in a new 1.5 ml collection tube, 40 µl RNase-free water added directly to the spin column membrane, centrifuged for 1 min at ≥ 10,000 rpm to elute the RNA. The total RNA extracted was quantified and quality evaluated by reading absorbance ratio 260 nm: 280 nm and 260 nm: 230 nm on Nanodrop™ machine (Thermo Scientific, USA).

2.5.3 Complementary Deoxyribonucleic Acid (cDNA) Synthesis

Before reverse transcription (RT), the RNA was diluted to the desired concentration using Nuclease Free water (129114, Qiagen, UK) and was denatured at 65℃ for 5 min, and stored on ice. Complementary Deoxyribonucleic acid (cDNA) was synthesized using Omniscript Reverse Transcription Kit (205111, Qiagen, UK). The solutions and their volumes used in the reaction system are described in Table 2.3. The solutions were added to a 200 µl PCR tube in the following order: Nuclease Free water, 10 x Reverse Transcription Buffer, 5 mM dNTP, 0.1 M DTT, random primers,

RNA template, RNase Inhibitor and Ominiscript Reverse Transcriptase. The mixture was incubated for 60 min at 40℃, cooled down on ice, and then stored at -20℃.

Table 2.3 Reverse transcription PCR system

Components	µl
10 x Reverse Transcription Buffer	2
Deoxyribonucleotide triphosphate (dNTP) Mix (5 mM)	2
DTT (0.1 M)	2
Random primers	2
RNase Inhibitor (10 units/µl)	0.25
Ominiscript Reverse Transcriptase	1
Nuclease Free water	8.75
RNA Template	2 (500 ng)
Total Volume	20

2.5.4 Polymerase Chain Reaction (PCR) Amplification

Undiluted or 1 in 20 diluted cDNA template was used in the experiment. Polymerase chain reaction (PCR) was performed using Go taq PCR Core System I (M7650, Promega, USA). The solutions and their volumes used in the reaction system are described in Table 2.4. The solutions were added to a 100 µl PCR tube in the following order: Nuclease Free water, 5 x colourless Go taq Buffer, 10 mM dNTP, $MgCl_2$, primers, cDNA template and Go taq DNA polymerase. After experimental trials, optimal reaction conditions were developed. The PCR results presenting in this thesis were all amplified under the optimized conditions which are described as follows: the reaction started from initial denaturation at 95℃ for 5 min, followed by 30 cycles of 95℃ for 1 min, 58℃ for 1 min, 72℃ for 1 min and final extension at

72℃ for 10 min. For short term storage, PCR products were kept at 4℃; long term, samples were stored at -20℃.

Table 2.4 PCR system

Component	µl
Nuclease Free Water	31.75
dNTP (10 mM)	1
$MgCl_2$	4
5 x colorless Go taq Buffer	10
Primer(forward)	0.5 (25 pmol)
Primer(reverse)	0.5 (25 pmol)
Go taq DNA polymerase	0.25
cDNA template	2
Total volume	50

2.5.5 Agarose Gel Electrophoresis Analysis

Two percentage agarose (Sigma-Aldrich, USA) gel was used for PCR products analysis. Agarose gel powder was dissolved in 1 x Tris acetate EDTA (TAE) buffer (Invitrogen, UK). Gel Red (Biotium, USA) was added at a ratio of 1 in 10,000 (volume). The gel was dissolved by microwaving, poured into a gel casting frame, comb inserted and left for 40-60 min to set. The comb was removed, gel with casting frame placed in a gel tank, and 1 x TAE buffer added to cover the gel. Before loading, PCR products were mixed with 6 x Blue/Orange Loading Dye (Promega, UK). A100 base pair (bp) DNA ladder (Promega, UK) was loaded as a size control. Samples were run in the gel at 60 volts for 1-1.5 h to allow DNA band separation. Molecular Imager Gel Doc system (Bio-Rad, UK) was used to visualize the results after electrophoresis.

2.6 Immunocytochemistry

After dissociation, cells were counted and adjusted to 0.5 x 10^5/ml for both VECs and VICs. Cell pellets were re-suspended in culture medium. 200 µl (i.e. 1 x 10^4

cells) cell suspension was added into each well of culture glass slides (BD, USA) (slides for VECs were pre coated with 2% gelatin). Cells were incubated on the slides at 37°C, 5% CO_2 for 24-48 h until the cells attached to the bottom of the slide. Culture medium was removed from chamber slide wells and cells washed with 1 x PBS several times. Cells were then fixed in acetone for 10 min at -20°C. Fixation was followed by two washes with 1 x PBS, 5 min each time. Subsequently slides were incubated with blocking buffer (10% goat serum (Invitrogen, UK)/0.1% Tween 20/PBS) for 1 h at room temperature to eliminate unspecific protein binding to antibodies. Primary antibodies were diluted with buffer (0.1% goat serum/0.1% Tween 20/PBS) to desired concentrations and prepared in a volume of 100 µl for each sample. The primary antibody was added to each sample well and slides placed in a humid chamber and incubated overnight at 4°C. The slides were washed twice with 1 x PBS, 5 min each time. A volume of 100 µl fluorescent secondary antibodies were applied to the slides and slides incubated for 1 h at room temperature in a dark humid chamber. The wells were removed and slides placed in a staining jar and washed with 1 x PBS for three times, 5 min each. Slides were mounted using the VECTASHIELD Mounting Medium with 4', 6-diamidino-2-phenylindole (DAPI) (H-1200, vector, UK). Nail polish was used to seal the edge of the slide. The slides were left to dry in a dark humid chamber before observation by a LEITZ DMRB fluorescent microscope (Leica, UK).

Images were captured by using Leica Firecam imaging software (Leica, UK). Antibody staining and DAPI staining images of the same sampled field were merged by Adobe Photoshop CS6 software (Adobe System Incorporated, USA). After observing, the slides were stored at 4°C for short term and at -20°C for long term.

2.7 Acetylated Low Density Lipoprotein Labelling

Acetylated low density lipoprotein conjugated with fluorescence dye1, 1'-dioctadecyl -3, 3, 3', 3'-tetramethyl-indocarbocyanine perchlorate (DiI-Ac-LDL) was used as an endothelial cell marker. Cells were seeded on a chamber slide at the concentration of 1 x 10^4 cells per well for at least 36 h. Chamber slides for VEC cultures were pre-coated with 2% gelatin. DiI-Ac-LDL (BT902, Biomedical Technologies, UK)

reagent was diluted to 5 μg/ml with cell culture medium and was added to a cell chamber in a 200 μl volume. The following steps were carried out avoiding light exposure. After 4 h incubation at 37°C, 5% CO_2, cells were washed several times with sterile 1 x PBS and slides observed immediately under a LEITZ DMRB fluorescent microscope. Images were captured by using Leica Firecam imaging software (Leica, UK). For long term storage of the slides, cells were fixed in 3% paraformaldehyde/1 x PBS solution for 20 min, rinsed with distilled water for 5 s, the liquid drained and inverted coverslip on a drop of 90% Glycerol and 10% PBS on the slide. The edge of the slides were sealed with paper tape and stored them at 20°C in dark environment.

For live construct endothelium labelling, the protocol is similar to above. Constructs were rinsed several times with sterile 1 x PBS and remained in culture well (static construct) or transferred to a culture plate (tubular construct). Diluted DiI-Ac-LDL reagent was added to each construct well in a volume of 0.5-1 ml (enough to cover the tissue). The treated constructs were kept away from alight in the following steps. After 4 h incubation at 37°C and 5% CO_2, constructs were rinsed 3 x 5 times with 1 x sterile PBS. The constructs were transferred to an inverted glass chamber slide and maintained in warm PBS immediately followed by observation with a LSM710 confocal microscope (Carl zeiss, Germany) and the images were processed by using ZEN software (Carl zeiss, Germany).

2.8 Flow Cytometry

Cells were harvested, washed and adjusted to 1 x 10^6 for each sample in 50 μl cold washing buffer (0.1% NaN_3/1% FBS/PBS). The experimental protocol was based on a BD company flow cytometry protocol. Antibody was diluted with washing buffer. Then 50 μl of antibody and 50 μl cell suspension were added to a 1.5 ml eppendorf tube and gently mixed well before incubation for 1 h at 4°C in a dark environment. Cells were washed twice with 200 μl cold washing buffer and centrifuged at 300 g for 5 min after each wash. The cell samples were re-suspended in 0.5 ml ice cold washing buffer and cells pellets transferred to polystyrene round-bottom tubes with

cell strainer caps (BD, Bioscience, UK), kept on ice and light exposure avoided until analysed by BD FACsAria^{TM} IIIu Cell Sorter (BD Biosciences, UK).

2.9 Fluorescence Activated Cell Sorting (FACS)

Cells were harvested, washed and adjusted to a concentration of 1 x 10^7 cells per 500 µl cold washing buffer (1% FBS/PBS). Antibody was diluted 1:50 with cold washing buffer in a total volume of 500 µl. Diluted antibody was added to the conical tube containing 1 x 10^7 cells, following mixing the solution was incubated for 1 h at 4°C in the dark. For the unstained control, 500 µl cold washing buffer was added instead of the primary antibody.

Following incubation, cells were washed with 2 x 200 µl ice cold washing buffer, centrifuged at 300 g for 5 min at 4°C and re-suspended in 2 ml advanced DMEM/F-12 medium supplemented with 1% L-glutamine and 1% antibiotics. For unstained cells, cells were re suspended in 0.5 ml medium (to above). Samples were kept in the dark and immediately analyzed and sorted by BD FACsAria^{TM} IIIu Cell Sorter. After sorting, both positive and negative cell populations were collected for culture and kept in 1 ml cell culture medium respectively. The collected cells were subsequently centrifuged, re-suspended in 10 ml culture medium, seeded on T80 flasks and cultured at 37°C, 5% CO_2.

2.10 Mitral Valve Construct Tissue Engineering

2.10.1 Fibrinogen Preparation

Fibrinogen powder from bovine plasma (F8630, Sigma) was stored at -20°C. Before use, the fibrinogen powder was allowed to warm up by being kept at room temperature for 20 min. Bovine fibrinogen (50-70 mg) was gently sprinkled onto 3 ml distilled water or pH 7.4 Tris buffered saline (TBS) in one well of a six well tissue culture plate (Thermo Scientific, UK). The culture plate lid was left off for several minutes to avoid the surface fibrinogen powder sticking on the lid due to static electricity. The lid was placed on the plate and the plate left at room temperature for at least 4 h or at 37°C for 3-4 h to dissolve the fibrinogen. An appropriate length (3.3 ml volume/cm) of dialysis membrane Spextra/Pro®1 (1956.1,

Carlroth, Germany) was prepared. The dialysis tube was soaked in 0.05% NaN_3 (S8032, Sigma), then rinsed/soaked with a large amount of distilled water immediately before use. Once the fibrinogen solution was ready, it was transferred into the prepared dialysis tube, and the two ends of the tube secured with dialysis tubing closures (Z371009-10EA, Sigma). The dialysis tube was placed in 4 L pH 7.4 TBS solution on a stir plate and the fibrinogen solution purified at room temperature overnight. On the following day, the dialyzed fibrinogen solution was filtered through a 5.0 µm syringe filter (Sartorius Stedim, UK) and sterilized by passing it through a 0.22 µm syringe filter (Sartorius Stedim, UK) in a laminar hood. The solution was kept under sterile condition from this point on. Measurement of the fibrinogen solution concentration was based on its 280 nm absorbance using a Nanodrop™ analyser. To get a reliable absorbance value (between 0.5-1), normally it required 1 in 20 dilution of the neat fibrinogen solution. The concentration of original fibrinogen was determined using the following formula: Concentration [mg/ml] = (A280/1.55)*dilution factor. For fibrinogen stock, the solution was made into 1 ml aliquots, labelled with the date and concentration and stored at -80°C.

2.10.2 Fibrin Based Mitral Valve Constructs in Static Culture

Four solutions were used for the preparation of fibrinogen gels: TBS, 50 mM $CaCl_2$ (BDH, UK) in TBS (pH 7.4), 40 IU/ml bovine thrombin (T4648, Sigma, UK) and fibrinogen. All the solutions were prepared under sterile conditions. TBS and 50 mM $CaCl_2$ were kept at 4°C. Bovine thrombin (40 IU/ml) solution aliquots were stored at -20°C. Either freshly prepared fibrinogen solution or -80°C fibrinogen stock aliquots were used in experiments. Dissociated canine VICs were counted and re-suspended in warm TBS. The final concentration of the VICs in TBS was approximate 5.7 x 10^6 per ml. A 24 well plate was prepared and the following solutions added to each well in order: 37.5 µl 40 IU/ml bovine thrombin, 37.5 µl 50 mM $CaCl_2$, 175 µl TBS cell pellet (1 x 10^6 cells/gel) and 250 µl fibrinogen (10 mg/ml). The control fibrin gel was made at this stage using the same protocol but using TBS solution instead of VICs-TBS suspension. The gels were placed in the tissue culture incubator for 40-60 min to polymerise. Dissociated VECs were re-suspended in customised bioreactor

medium (advanced DEME/F-12 medium/0.003% ascorbic acid (857653, Sigma)/10% FBS/1% penicillin G and streptomycin (100 U/ml-100 µg/ml)/1% L-glutamine (2 mmol/L)/0.0001% tranexamic acid (857653, Sigma, UK)) at the concentration of 1.8 x 10^4/ml (1 x 10^3 cells/cm^2). The recipe of the bioreactor medium was kindly provided by Dr Thomas Flanagan from the University College Dublin, Ireland. Once the gels were completely polymerized, 1 ml bioreactor medium-VECs suspension was seeded on the top of each fibrin/VICs construct. Constructs were cultured at 37°C, 5% CO_2 for 2 weeks. Culture medium was changed every day.

2.10.3 Fibrin Based Mitral Valve Tubular Constructs

Similar to the static constructs all the fibrinogen gel ingredients i.e. pH 7.4 TBS, 50 Mm $CaCl_2$ in TBS and 40 IU/ml bovine thrombin and fibrinogen were prepared. Additionally, the following components were autoclaved in advance: one customized mould, one medium reservoir and connectors (provided by collaborators in Aachen, Germany), corn oil (Sigma, UK), Tygon® SI 3350 silicone tubes (SC0584A, IDEX, Germany) and PharmMed®-BPPT tubes (MF0013, IDEX, Germany). One MCP process pump (ISM915/ISM734B, IDEX, Germany) was assembled and thoroughly sprayed with 70% ethanol before placing it in the tissue culture hood. Using a six well tissue culture plate, fibrinogen solution (Solution 1) was added in one well and 50 mM $CaCl_2$ in pH 7.4 TBS and 40 IU/ml bovine thrombin (Solution 2) were added in a separate well on the same plate. The inner side of the mould and inner cylinder was painted with sterile corn oil, and the mould assembled. The VICs were harvested, cells counted and re-suspended in warm TBS. The concentration of the VICs in TBS was approximately 5.7 x 10^6 per ml. The VICs-TBS solution was well mixed with $CaCl_2$ and thrombin. Two 5 ml syringes were used to take out 3.5 ml of Solution 1 and Solution 2 respectively, bubbles were carefully removed from the syringes, and the volume adjusted to 3 ml for both solutions. The syringes were attached to a customised syringe applicator and 2.6 ml of each solution injected into the mould at a constant rate.

The construct was left standing in the tissue culture incubator for 45-50 min to polymerise according to visual observation. VECs were harvested and re-suspended in bioreactor medium to get a concentration at 1.8 x 10^4/ml.

The inner cylinder of the construct was carefully removed and the VEC suspension added to the construct lumen. A T80 flask gas filter cap was connected to the open end of the mould. The cap neck was secured with parafilm (Pechiney Plastic Packaging, USA). In the first and second experiment, four and eight vertical directions were marked on the cap and the device placed in tissue culture incubator respectively. The device was rotated by 90^o every 15 min for 2 h and 45^o every 15 min for 4 h respectively. An illustration of the seeding devise is shown in Figure 5.2.

After seeding, the remaining VEC suspension was removed and the construct gently rinsed once with the bioreactor medium. The construct was carefully separated from the mould and a 2 ml syringe (BD, USA) with plug, inserted into the construct lumen to provide support.

Before the construct was placed in the medium reservoir, the supporting syringe plug was removed to allow the construct stand in the reservoir. Medium was added and reservoir connected to the MCP process pump. The pump was turned on and bubbles removed in the connecting tubes. Lastly, flow rate was set at 30 rpm.

The whole device was transferred to the tissue culture incubator. Constructs were cultured for 7 days before harvesting.

2.11 Histological Staining and Immunohistochemistry

2.11.1 Native Mitral Valve Tissue Section Preparation

Canine mitral valve tissue was harvested post mortem and washed with PBS. After scoring with Whitney grading system, the valve leaflet was fixed in 4% paraformaldehyde overnight and transferred to 70% ethanol on the next day for storage. Fixed tissues were dehydrated and embedded in paraffin blocks. Sections were cut into 5 μm thickness and mounted on coated glass slides. Unstained slides were stored at room temperature.

2.11.2 Tissue Engineered Mitral Valve Constructs Section Preparation

Fresh fibrin based mitral valve constructs were collected and rinsed with 1 x PBS several times before fixing in Methacarn fixative (60% methanol/30% chloroform (Fisher Scientific, UK)/10% acetic acid (VWR International, UK)) for 4 h at room temperature or overnight at 4°C. Samples were stored in 30% ethanol at 4°C before further processing. Samples were dehydrated in serial ethanol solutions and embedded in paraffin blocks. Sections were cut into 5 μm thickness and mounted on coated glass slides. Unstained slides were stored at room temperature.

2.11.3 Hematoxylin and Eosin (H&E) Staining

Paraffinized tissue sections were de-waxed through three changes of xylene then three changes of ethanol, 2 min each. Sections were rinsed with running water for 2 min, then Harris Haematoxylin stain applied to the sections for 18 min, then rinsed twice with running water for 1 min each. Sections were placed in acid alcohol for 10 s, then washed with running water for 2 min. Sections were stained with Scott's tap water substitute for 2 min, rinsed with running water for 2 min, stained with Eosin for 30 s and then rinsed with running water for 4 min. Sections on the slides were dehydrated through three changes of absolute ethanol and three changes of xylene, mounted with glass cover slips in DePex mounting medium. Slides were dried out in the fume hood at room temperature. Slides were observed under a LEITZ DMRB microscope and the images were captured by using Leica Firecam imaging software.

2.11.4 Russel-Movat Pentachrome Staining

Russell-Movat Pentachrome Stain kit (KTRMP, American MasterTech) was used for detecting and differentiating connective tissue components. Staining process followed product instruction and all solutions were prepared within the kit except xylene and ethanols. In detail, slides were de-paraffinised using xylene for 10 min and sections hydrated through 100%, 95%, 90%, 70% ethanol and distilled water for 5 min each. Slides were stained with freshly prepared Verhoeff's Elastic Stain (2.5% alcoholic hematoxylin/25% ethanol/2.5% ferric Chloride/25% universal Iodine) for 15 min. Slides were rinsed in warm running tap water for 5 min, followed by distilled water. Sections were differentiated under light microscope in 2% ferric chloride until

elastic fibers were sharply defined. Slides were rinsed in distilled water and stained with 5% sodium thiosulphate for 1 min. Slides were washed in running tap water for 5 min and then immersed in 3% glacial acetic acid for 3 min. Slides were placed directly in 1% alcian blue solution for 15 to 30 min and then rinsed thoroughly in warm running tap water for 1 min, followed by distilled water. Slides were placed in crocein scarlet-acid fuchsin for 2 min, followed by rinsing with 3 changes of distilled water. Slides were dipped 5 times in 1% glacial acetic acid then stained in 2 changes of 5% phosphotungstic acid for 2-5 min each. Sections were checked under the microscope and reaction stopped when connective tissue was clear but without de-staining elastic fibres. Slides were dipped 5 times in 1% glacial acetic acid. After dehydrating tissue sections through 3 changes of fresh absolute alcohol, slides were placed in alcoholic safferon solution for 15 min to stain collagen. Slides were dehydrated through 3 changes of fresh absolute alcohol and 3 changes of fresh xylene, mounted with glass cover slips in DePex mountant and dried in the fume hood at room temperature. Slides were observed under a LEITZ DMRB microscope and the images were captured by using Leica Firecam imaging software.

2.11.5 Native Mitral Valve Tissue Immunohistochemistry

Tissue sections were de-waxed in xylene (Fisher Scientific, UK) for 10 min and re-hydrated through a series of graded ethanols and ddH_2O for 5 min each. If antigen retrieval was required (positive control shows negative signal), sections were incubated with 40 μg/ml Proteinase K (19131, QIAGEN, UK) in 20 mM Tris-HCl (pH 8.0). Slides were then incubated in 0.3% H_2O_2 (Sigma, UK) in methanol to block endogenous peroxide for 30 min at room temperature. Slides were washed with tap water for 2 min. Sections on one slide were separated using an ImmEdge™ pen (H-4000, Vector Laboratories Inc., UK) to isolate sections. Sections were blocked with 10% normal horse serum (provided in the kit)/PBS for 20 min, primary antibody was applied to sections and incubated for 30 min at room temperature or 4°C overnight. For the negative control sections, primary antibody was omitted. Slides were washed with 1 x PBS (pH 7.5) for 3 x 3 min on a rocker. R.T.U. VECTASTAIN Elite ABC Kit (Universal) (PK7200, Vector Laboratories, UK) was used for immunohistochemistry staining. Sections were incubated with a

secondary antibody (provided in the kit) for 30 min at room temperature, followed by 30 min incubation with VECTASTAIN Elite ABC reagent (provided in the kit) and developed with NovaRed^{TM} Substrate kit (SK-4800, Vector Laboratories, UK) for 5-10 min until desired staining intensity appeared. Sections were rinsed in ddH_2O for 2 x 3 min on a rocker. Slides were counter-stained with Mayer's haematoxylin (Sigma) for 3 min and washed under the tap for 30 s and then counter-stained in pH 8.0 Scott's Tap Water (0.35% sodium hydrogen carbonate/2% magnesium sulphate (VWR International, UK)) for 30 s. Slides were placed in distilled water, 70% , 90%, 95% graded ethanol solutions for 2 min each, 100% clear ethanol for 5 min and clear xylene for 10 min before mounting glass cover slips with DePex mounting medium (VWR International, UK).

Slides were left to dry in the fume hood overnight at room temperature and staining was observed under Slides were observed under a LEITZ DMRB microscope and the images were captured by using Leica Firecam imaging software.

2.11.6 Immunofluorescence

Native mitral valve sections or tissue engineered construct sections were prepared as has been described in Sections 2.11.1 and 2.11.2. The sections were de-paraffinised in xylene for 10 min and rehydrated through serial ethanol: 100%, 95%, 90% and 70% and 1 x PBS for 5 min each. For native mitral valve samples, additional antigen retrieval step was required, which was carried out by incubating the sections in pH 9.0 Tris-EDTA buffer (10 mM Tris Base/1 mM EDTA/0.05% Tween 20) in a microwave at high power setting or in a 95°C water bath for 30 min. When sections were cooled down they were rinsed with distilled water. Individual sections were delineated on slides with ImmEdgeTM wax pen. Blocked Non-specific protein sites were blocked with 10% goat serum in 0.5% PBS-Tween for 30 min at room temperature. In some experiments, Image-iT TM FX Signal Enhancer (I36933, Invitrogen) was used to improve nonspecific protein blocking prior to common blocking step, by incubating the slides for 30 min with the reagent and then rinsing off with 1 x PBS. After blocking, the primary antibody was diluted with diluting buffer (same recipe as blocking buffer) to desired concentration and the sections

probed with primary antibody in a humid chamber at room temperature for 1 h or overnight at 4°C. For negative control samples, the primary antibody was omitted. Primary antibody incubation was followed by 3 x 5 min wash with 1 x PBS on rocker. The fluorescent secondary antibody was prepared with diluting buffer and sections incubated in a dark humid chamber at room temperature for 1 h. After probing, excess secondary antibody was rinsed off with 1 x PBS on rocker for 3-5 times x 5 min. Slides were mounted using the VECTASHIELD Mounting Medium with DAPI. Nail polish was used to seal the edges of the slides. The slides were left to dry in a dark humid chamber before observation by a LEITZ DMRB fluorescent microscope. Images were captured by using Leica Firecam imaging software. Antibody staining and DAPI staining images of the same sampled field were merged by Adobe Photoshop CS6 software. After observing, the slides were stored at 4°C for short term and at -20°C for long term.

2.12 Electron Microscopy

2.12.1 Scanning Electron Microscopy (SEM) Sample Preparation

Construct samples were collected from the culture plates and briefly washed in culture medium or sterile PBS, followed by 2 x 5 min wash in 0.1 M sodium cacodylate (C0250, Sigma, UK)/HCl buffer (pH 7.2). Samples were fixed in 2% glutaraldehyde (23114.02, AMS Biotechnology, UK)/2% paraformaldehyde in 0.1 M sodium cacodylate buffer (pH 7.2) at room temperature for 1 h. Samples were then rinsed for 2 x 5 min in 0.1 M sodium cacodylate/HCl buffer (pH 7.2) and stored in airtight containers in 0.1 M sodium cacodylate/HCl buffer (pH 7.2) at 4°C before future processing.

2.12.2 Transmission Electron Microscopy (TEM) Sample Preparation

Construct samples were collected from the culture plates and briefly washed in culture medium or sterile PBS, followed by 2 x 5 min wash in 0.1 M sodium cacodylate/HCl buffer (pH 7.2). Samples were fixed in 2% glutaraldehyde/2% paraformaldehyde in 0.1 M sodium cacodylate buffer (pH 7.2) at room temperature

for 20-24 h. Samples were then rinsed for 2 x 5 min in 0.1 M sodium cacodylate/ HCl buffer (pH 7.2) and stored in airtight containers in 0.1 M sodium cacodylate/HCl buffer (pH 7.2) at 4°C before future processing.

Chapter 3: Canine Mitral Valve Cells Isolation and Characterization

Abstract

Mitral valve cells especially VECs and VICs are believed to play a crucial role in valve physiology and pathophysiology. It is hypothesized that by using previous reported methods for porcine aortic valve cell separation, canine mitral VECs and VICs can be isolated and cultured *in vitro*. Moreover the two populations can be differentiated by specific markers.

Canine mitral valves were harvested immediately post mortem. Mitral VECs and VICs were isolated by collagenase digestion sequentially. Primary mitral VECs and VICs were expanded and characterized utilising a variety of techniques. Moreover, preliminary experiments were carried out to optimise the purity of VEC cultures.

VECs and VICs were successfully isolated from canine mitral valves and cultured *in vitro*. Relatively pure cultures were obtained for both populations. In general, cells in VEC and VIC cultures exhibited differential morphology and growth patterns. Endothelial markers were expressed in VEC cultures alone only. Expressions of mesenchymal, activated mesenchymal and myofibroblast marker were detected in both cultures at transcriptional level. These findings were consistent at protein level except myofibroblast marker alpha-smooth muscle actin expression was absent in majority of examined VEC cultures. In order to obtain a higher purity of VECs, the current results indicated that additional cell sorting followed by endothelial basal medium culture proved the most promising.

In this study, both canine mitral VECs and VICs were isolated, sub-cultured and characterized *in vitro*. It provides new insights to the fundamental understanding of canine mitral valve cell biology which will help in interpreting the pathogenesis of canine MMVD.

3.1 Introduction

Cellular components play a key role in heart valve biology and mechanical functions. They are actively involved in valve tissue development (Armstrong and Bischoff, 2004; Person et al., 2005), maintenance of physiological function (Mulholland and Gotlieb, 1997; Tao et al., 2012; Taylor et al., 2003) and also in the valve remodelling process under pathophysiological conditions (Durbin and Gotlieb, 2002; Lester et al., 1992; Lester and Gotlieb, 1988). Knowledge of cellular biology is essential for understanding of the heart valves in both healthy and diseased conditions, especially for investigating disease pathogeneses such as myxomatous mitral valve disease (Bischoff and Aikawa, 2011; Black et al., 2005; Han et al., 2013; Han et al., 2010; Han et al., 2008; Prunotto et al., 2010; Salhiyyah et al., 2011).

Recent research on heart valve cells has mainly focused on valve endothelial cell (VEC) and valve interstitial cell (VIC). The VECs form a monolayer lining both the atrial and ventricular side of the valve leaflets. They possess common endothelial features such as sensing environmental alteration of the blood tissue interface and response to haemodynamic shear stress and cytokine stimulation (Balachandran et al., 2011; Butcher et al., 2004; Chalajour et al., 2004; Leask et al., 2003; Paranya et al., 2001). VECs have been characterized by having close cell to cell contacts and expressing endothelial markers such as CD31 (Gould and Butcher, 2010; Paruchuri et al., 2006; Wylie-Sears et al., 2011) and DiI-Ac-LDL (Cuy et al., 2003; Gould and Butcher, 2010). Additionally, the VECs also have unique features which differentiate them from endothelial cells of other organs. For example, in response to laminar flow conditioning the aortic VECs show perpendicular arrangement to flow direction rather than the parallel pattern that is observed in aorta endothelial cells, and also have differences in transcriptional profiles (Butcher et al., 2004; Butcher et al., 2006). Compared to semilunar valves, there is little information on mitral VEC biology. However, the mitral valve endothelium has been shown to be an important factor involved in pathological conditions such as myxomatous mitral valve disease (Moesgaard et al., 2012; Mow and Pedersen, 1999), functional mitral regurgitation (Dal-Bianco et al., 2009) and pulmonary hypertension due to mitral stenosis (Snopek et al., 2000). In both human mitral valve prolapse and canine myxomatous mitral

valve disease, there is evidence of the endothelial cell damage (Corcoran et al., 2004; Han et al., 2013; Stein et al., 1989) and abnormal endothelial related synthesis activity (Mow and Pedersen, 1999; Olsen et al., 2003b). Endothelium dysfunction seems to be associated with sub-endothelial VIC activation in myxomatous mitral valve disease and physiological remodelling process which emphasizes the importance of VECs in maintaining normal mitral valve function (Black et al., 2005; Han et al., 2013; Lester et al., 1993; Rabkin et al., 2001). Regional pleomorphism has been found in mitral VECs indicating cells ability to adapt to different environments (Corcoran et al., 2004; Sarphie, 1980; Sarphie and Allen, 1978). The plasticity of mitral VECs has been further confirmed in a recent study by Wylie-Sears et al., 2011 where osteogenic and chondrogenic features were induced in mitral VECs through endothelial mesenchymal transition (EndoMT) process (Wylie-Sears et al., 2011).

The VICs are the major cell type in all four heart valves. In the embryonic stage, they derive from the a subset of foetal VECs that are activated by myocardial signalling, migrate to the cardiac jelly and transform into mesenchymal cells through EndoMT process (Armstrong and Bischoff, 2004; Markwald et al., 1977; Oosthoek et al., 1998; Patten et al., 1948; Person et al., 2005). Mature interstitial cells are localized in the sub-endothelium and disperse through valve ECM layers. It has been proven that the VICs are responsible for valve ECM production and remodelling (Flanagan et al., 2006a; Gupta et al., 2009b; Rabkin-Aikawa et al., 2004b), valve tension (Smith et al., 2007), wound repair (Durbin et al., 2005; Durbin and Gotlieb, 2002; Gotlieb et al., 2002; Lester and Gotlieb, 1988) and are actively involved in pathological conditions such as mitral valve prolapse (Prunotto et al., 2010) and myxomatous mitral valve disease (Rabkin et al., 2001). The VICs have been found to be heterogeneous (Blevins et al., 2006; Lester et al., 1988; Taylor et al., 2000; Zacks et al., 1991) and their composition of sub-phenotypes is dynamic in response to trauma (Durbin and Gotlieb, 2002; Tamura et al., 2000), myxomatous valve disease (Disatian et al., 2008; Han et al., 2013; Han et al., 2008) and environment alteration (Rabkin-Aikawa et al., 2004b; Rabkin et al., 2002). In normal adult heart valves, most VICs are described as a quiescent phenotype, which are characterized by expressing vimentin but not alpha smooth muscle actin (α-SMA) (Han et al., 2008; Rabkin-Aikawa et al.,

2004b). In disease or remodelling processes, there is phenotypic alteration with increased activated myofibroblast-like VIC (aVIC) presumed to be actively involved in the repairing process (Black et al., 2005; Disatian et al., 2008; Han et al., 2008; Lester et al., 1993; Rabkin et al., 2001). The aVICs are positive for activated mesenchymal marker embryonic form non-smooth muscle myosin heavy chain (SMemb) (Disatian et al., 2008; Disatian et al., 2010; Rabkin et al., 2001), myofibroblast marker α-SMA (Blevins et al., 2006; Disatian et al., 2008; Han et al., 2008; Stephens et al., 2011) and smooth muscle cell marker transgelin (SM22) (Della Rocca et al., 2000; Wiester and Giachelli, 2003). Similar to mitral VECs, VICs from mitral valves have also been found to have distinct features from other VICs. As mention in Section 1.3.5, mitral VICs demonstrated a differential response to transforming growth factor beta (TGF-β) compared to aortic VICs: exogenous TGF-β promotes proliferation of mitral VICs but inhibit proliferation and apoptosis in aortic VICs (Liu and Gotlieb, 2008; Walker et al., 2004). Moreover human mitral VICs and aortic VICs were found to have differences in transcriptional profiles and in cell proliferation and the mitral VICs are more susceptible to calcification *in vitro* (Sun et al., 2013). This addresses the needs of developing specific VIC study systems derived from mitral valves for mitral valve related research.

Cell culture techniques provide opportunities to investigate valve cellular biology *in vitro*. Enzymatic digestion techniques have been reported to isolate VECs and VICs (Cheung et al., 2008; Gould and Butcher, 2010; Simon et al., 1993). Although general success has been achieved with these techniques, contamination with other cell types or cell differentiation are particular confounding factors in VEC cultures (Bischoff and Aikawa, 2011; Cheung et al., 2008). Additional cell sorting techniques can improve these issues to obtain higher endothelial cell purity (Cheung et al., 2008; Hoerstrup et al., 1998).

A number of studies have been done cultivating and characterizing mitral VECs and VICs *in vitro* (Blevins et al., 2006; Blevins et al., 2008; Flanagan et al., 2006a; Liu and Gotlieb, 2008; Simon et al., 1993; Stephens et al., 2011; Stephens et al., 2010b; Sun et al., 2013; Xu et al., 2012), but only a few are reported in veterinary field (Heaney et al., 2009; Waxman et al., 2012). The aim of this study was to isolate and

culture canine mitral VECs and VICs using a previously reported protocol and moreover characterize canine mitral VECs and VICs by using a variety of techniques *in vitro*. It was hypothesized that: (1) canine mitral VECs and VICs can be successfully isolated and cultured *in vitro* using current methods; (2) in phenotypic characterization, mitral VECs exhibit common endothelial cell features and express mesenchymal marker vimentin; while VICs are negative for the endothelial markers but express vimentin and a panel of selected activated VIC markers; (3) fluorescent activated cell sorting can separate VECs from other contaminating cell types; and endothelial specific medium is superior in maintaining VEC endothelial properties than standard culture medium.

3.2 Materials and Methods

3.2.1 Isolation and Culture of Canine Mitral Valve Cells

Cells were isolated from 26 canine mitral valves in total. Mitral VECs were isolated by collagenase digestion from healthy valves only (n=14). Mitral VICs were harvested using an explant technique in the first 6 dogs (2 healthy mitral valves and 4 MMVD valves). All remainder of the VICs were isolated by collagen digestion (12 healthy mitral valves and 8 MMVD valves). Due to time limitation, later cell characterization was only carried out in cell cultures isolated by enzymatic digestion but not in explant derived cells. The characterized mitral VEC and VIC cultures were collected from 1.5-5 year old MV healthy dogs, which were potential cell source for later construct engineering. A summary of the 1.5-5 year old MV healthy dog information is shown in Table 3.1. Details of the cell isolation protocol have been described in Section 2.4.1.

Details of cell culture medium, sub-culture and cryopreservation were described in Section 2.4.2-2.4.5. In this project, VECs were expanded up to passage 3 while VICs were cultured up to passage 8.

Table 3.1 Details of dogs from which healthy mitral valve cells were collected using collagenase digestions.

Age (Year)	3.2 ± 1.2
Gender	Male n=7 Female n=5
Breed	Large breed n=4 Small/middle breed n=8

3.2.2 Canine Mitral VEC and VIC Characterization

3.2.2.1 Morphology Observation

Cell morphology was observed by using a light microscope during culture period for cell morphology and confluence assessment. Representative cell images were captured by a Zeiss Axiover 40 microscope at different magnifications: x 50, x 100 and x 200.

3.2.2.2 Cell Characterization at Gene Transcriptional Level

Isolated VECs and VICs were characterized by using RT-PCR. Canine nucleotide sequences of target makers were found in either NCBI Gene Bank or Ensembl website. Primers were designed, ordered and prepared as has been described in Section 2.5.1. The following markers were selected to characterize the VECs and VICs: CD31 and von Willebrand factor (vWF) (endothelial specific); α-SMA, SMemb and SM22 (aVIC markers) and vimentin (a marker for mesenchymal origin cells) (Flanagan et al., 2006a; Heaney et al., 2009). Glyceraldehyde 3-phosphate dehydrogenase (GAPDH) was used as an internal control gene in PCR amplification. The vWF-1, α-SMA and GAPDH primers were kindly provided by Dr. Hannah Hodgkiss-Geere and vWF-3 primers were from a previous publication (Fulton et al., 2000). All other primer pairs were original in design. Primer details are listed in Table 3.2.

Total RNA extraction, cDNA synthesis, PCR reaction system and agarose gel electrophoresis was carried out following the protocols described in Section 2.5.2-

2.5.5. In each RT-PCR reaction, RNA template from cultured cells were amplified with GAPDH primers and served as a negative control. The PCR results were accepted only if the negative controls were completely clean for target transcripts.

When comparing marker expression in differential cell lines, transcript band intensity was quantified by using Image J software and the genes of interest were normalized to GAPDH. Ratio of Target gene band intensity to GAPDH band intensity was illustrated in histograms.

3.2.2.3 **Immunocytochemistry and Acetylated LDL Labelling**

The immunocytochemistry protocol for VEC and VIC characterization was detailed in Section 2.6. The antibodies used are listed in Table 3.3. DiI-Ac-LDL labelling for detecting endothelial cells was carried out using the protocol in Section 2.7. After staining, the slides were observed with a Leica DMRB fluorescence microscope using the red fluorescence channel (excitation wavelength of 568 nm) or green fluorescence channel (excitation wavelength of 488 nm) for target antibody staining. DiI-Ac-LDL was assessed at 568 nm (excitation wavelength of DiI dye = 554 nm). Cell nuclei stained with DAPI was observed using the blue fluorescence channel. Positive staining was defined as fluorescence signals detected above background threshold (unstained negative control).

Images were captured by using Leica Firecam imaging software. The antibody staining and DAPI staining images were converted into grayscale with Image J software. Colour antibody staining and DAPI staining images of the same sampled field were merged by Adobe Photoshop CS6 software. The immunocytochemistry data in this thesis is presented as a DAPI staining in grayscale, an antibody staining in grayscale and an antibody-DAPI merged image. For DiI-Ac-LDL assay, bright field images were taken from the same sampled area demonstrating cell distribution. The bright field images were converted into grayscale with Image J software when presented.

Table 3.2 Primer sequences used in PCR analysis for cell characterization.

Gene	Primer Sequence (5'-3')	Product size
CD31	(F) AATCCCAAATTCCACGTCAG (R) GAATGGAGCACCACAGGTTT	346bp
vWF-1	(F) CTGGGAGAAGAGAGTCACGG (R) GTGGATGGAGTACACGGCTT	235bp
vWF-2	(F) GGCTGTACCTGGATGAGAGG (R) GACAGGACAGGCTCCTTTTG	228bp
vWF-3	(F) AATATAGGGCCCCGGCTCACTCAA (R) ACATCCCCGGGCCTCTTCTCATTC	512bp
SM22	(F) AAGAACGGCGTGATTCTGAG (R) CGGTAGTGCCCATCATTCTT	269bp
α-SMA	(F) GGGGATGGGACAAAAGGACA (R) GCCACGTAGCAGAGCTTCTCCTTGA	525bp
SMemb	(F) AGAAGCGAGCTGGAAAACTG (R) TCTTGCTCTGTCCGATTCTG	252bp
Vimentin	(F) GGAGCAGCAGAACAAGATCC (R) AGACGTGCCAAAGAAGCATT	282bp
GAPDH	(F) CATCAACGGGAAGTCCATCT (R) GTGGAAGCAGGGATGATGTT	428bp

F, forward primer; R, reverse primer.

Table 3.3 Antibodies for VEC and VIC immunocytochemistry characterization

Primary antibody	Cat No. and company	WC
Anti-CD31 (RP)	Ab28364, Abcam, UK	1:200
Anti-SMemb	Ab24761, Abcam, UK	1:400
Anti-vimentin (MM)	V6389, Sigma, USA	1:1600
Anti-α-SMA	A2547, Sigma, USA	1:400
Secondary antibody	**Cat No. and company**	**WC**
Goat Anti rabbit IgG (H+L) Alexa Fluor568	A11011, Invitrogen, UK	1:500
Goat Anti mouse IgG (H+L) Alexa Fluor488	A10667, Invitrogen, UK	1:500

RP, rabbit polyclonal; MM, mouse monoclonal; WC, working concentration.

3.2.3 Optimization of Canine Mitral VEC Culture

3.2.3.1 Endothelial Purity Evaluation by CD146 Flow cytometry

To check purity of the VECs, two endothelial markers CD31 and CD146 also called melanoma cell adhesion molecule (MCAM) were evaluated in VEC cultures by flow cytometry. As described in Section 2.8, cells were harvested, washed and adjusted to 1 x 10^6 concentration for each sample in 50 µl cold washing buffer (0.1% NaN_3/1% FBS/PBS). Mouse monoclonal [WM-59] to CD31 with fluorescein isothiocyanate (FITC) conjugated (ab13466, Abcam) or mouse monoclonal [P1H12] CD146 (FITC) antibody (ab78451, Abcam) was diluted (1:2.5 for CD31; 1:25 for CD146) with washing buffer in a volume of 50 µl. 50 µl of antibody and 50 µl cell suspension were added to a 1.5 ml eppendorf tube and gently mixed before incubation for 1 h at 4°C in dark. For the unstained control, 50 µl cold washing buffer was added instead

of CD146 antibody. Cells were washed twice with 200 µl cold washing buffer and centrifuged at 300 g for 5 min after each wash. The cell samples were re-suspended in 0.5 ml ice cold washing buffer and cells pellets transferred to polystyrene round-bottom tubes with cell strainer caps, kept on ice and protected from light exposure. Samples were analysed by BD FACsAria^{TM} IIIu Cell Sorter to obtain data and histograms. The cell gating strategy was done by arbitrarily circling obvious live cells and separating them from cellular fragments and dead cells.

3.2.3.2 **CD146 Based FACs for Purifying Canine VECs**

The detailed sorting protocol has been described in Section 2.9. The same CD146 antibody and cell sorter used in flow cytometry was used in FACs. After sorting, CD146 positive and negative cell populations were collected in 1 ml cell culture medium and the purity was checked with the same cytometer. Histograms of fluorescence intensities were obtained. The collected cells were subsequently centrifuged, re-suspended in 10 ml culture medium, plated on T80 flasks and cultured at 37°C, 5% CO_2. Cell morphologies were observed during culture with Zeiss Axiover 40 microscope for cell shape and confluence assessment, representative images were captured. A series of characterization were done, and the details will be discussed in Section 3.3.3.

3.2.3.3 **Comparison of Two Culture Media in Culturing Canine VECs**

Two experiments were undertaken to compare canine endothelial basal medium (EBM) with standard culture medium i.e. advanced DMEM/F-12 medium with supplements (AF12). In the first experiment, primary VECs (passage 0) were cultured with standard culture medium. After one passage, the standard culture medium was replaced with canine EBM. In the second experiment, canine EBM was used to culture primary VECs (passage 0) right after cell isolation. Standard medium cultured VECs from the same dogs were compared as controls in both studies.

Cell morphologies and biomarker expressions for the two experimental protocols were compared.

3.3 Results

3.3.1 Canine Mitral VEC Characteristics

On morphological observation with light microscopy, endothelial progenitor cells usually started to appear randomly in canine mitral VEC culture flasks in 1-2 days post primary isolation. They presented typical cobblestone morphology and formed clusters (Figure 3.1A). In later stage of the primary culture, cells started to proliferate extensively and usually reached confluence within 6-8 days in one T80 flask (Figure 3.1B). In confluent cultures, most cells exhibited growth contact inhibition and formed a monolayer. However, heterogeneous cell morphologies were observed in the culture; cobblestone morphology cells were dominant but elongated and spindle shape cells were also present (Figure 3.2). As passage times increased, cuboid cells decreased and the spindle shapes cells gradually became dominant in the culture (data not shown).

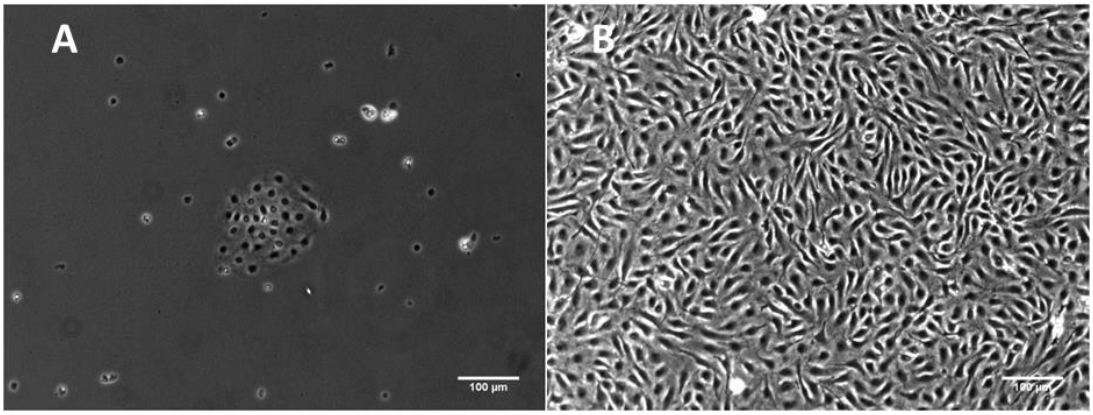

Figure 3.1. Primary isolated canine mitral VECs morphology. A. At the early stage (1-2 day culture), single colony clusters randomly appeared in the culture. B. Once the cells reached confluence, the majority exhibited cobblestone morphology and were growth-contact inhibited. Scale bar = 100 μm.

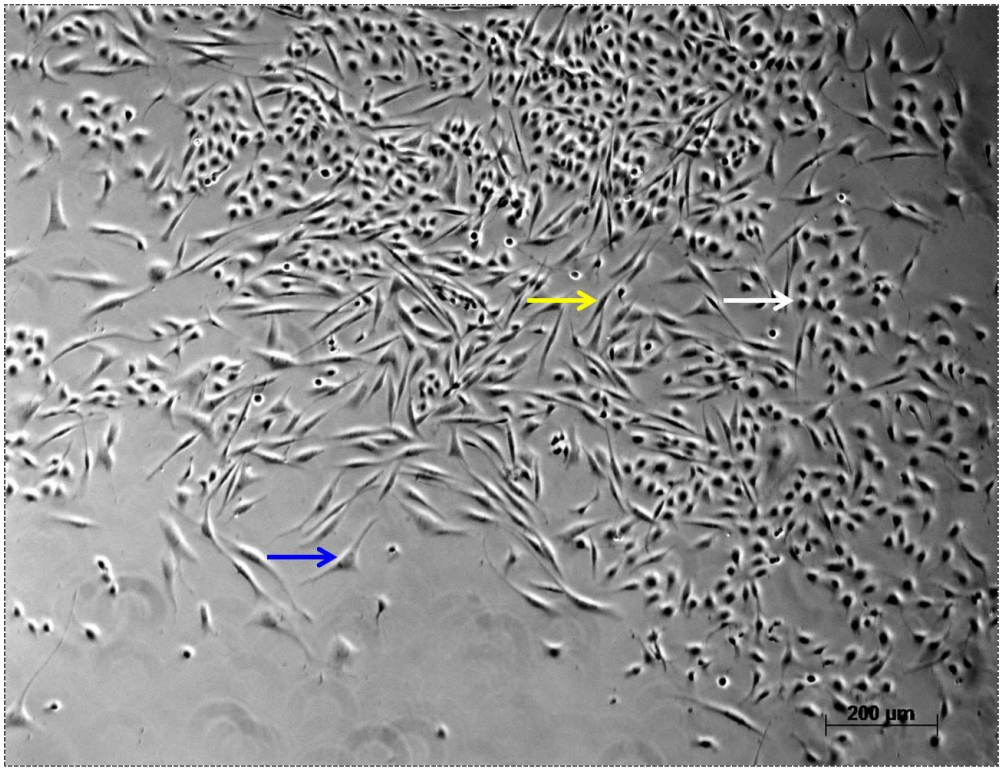

Figure 3.2. Cells in primary VEC culture exhibited varying morphologies. Though the majority of cells were cuboidal (white arrow), elongated spindle shape cells (yellow arrow) and polymorphic cells (blue arrow) with multiple cytoplasmic extensions were also observed. Scale bar = 200 µm.

Results of canine mitral VEC phenotypic characterization are summarized in Table 3.4. Endothelial marker CD31, mesenchymal marker vimentin and activated mesenchymal marker SMemb were detected in VECs at gene level. Moreover, myofibroblast marker α-SMA and smooth muscle cell marker SM22 were also found in VECs by RT-PCR (Figure 3.3). Endothelial marker vWF primers were designed to characterize the VECs at gene level, however, no obvious positive expression was observed in canine VECs whereas the target products were expressed by other cell lines having endothelial nature, such as a human umbilical vascular endothelial cell line and a canine haemangiosarcoma cell line (Thamm et al., 2006; Fosmire et al., 2004) (Figure 3.4).

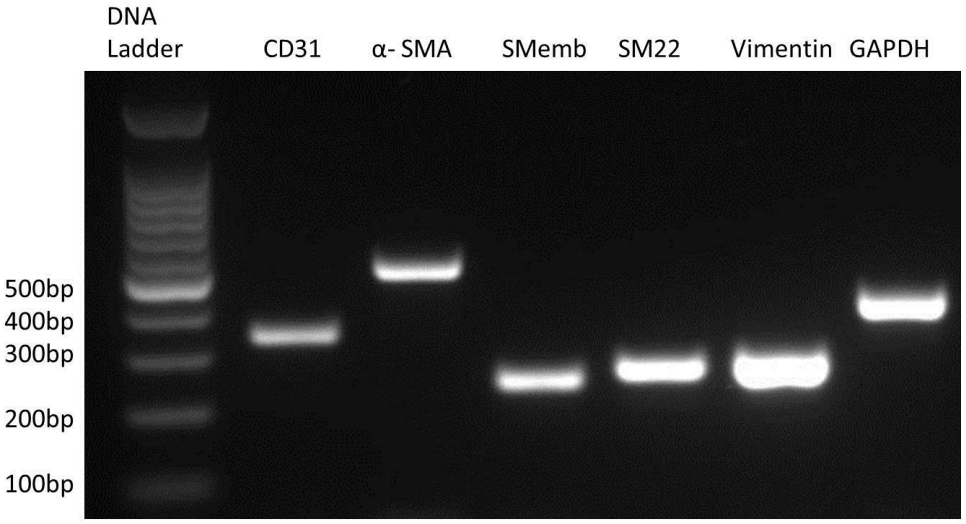

Figure 3.3. RT-PCR characterization on primary canine mitral VECs. Total RNA of cultured cells were used in the amplification. Endothelial marker CD31 and activated VIC markers i.e. α-SMA, SMemb and SM22 were detected in VEC cultures at transcriptional level. Vimentin and GAPDH were used as internal controls.

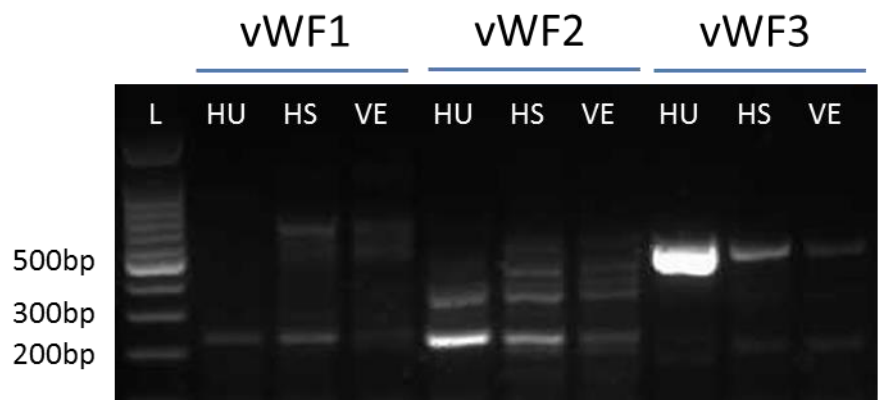

Figure 3.4. The vWF gene expression was not evident in primary canine mitral VECs. Three vWF primer pairs were used to detect the target gene expression. In contrast to the limited expressions in primary canine mitral VECs (VE), the vWF1 gene (235bp), vWF2 gene (228bp) and vWF3 gene (512bp) were clearly expressed by the two positive control cell lines-human umbilical vascular endothelial cell line (HU) and a canine haemangiosarcoma cell line (HS).

On fluorescence/immunofluorescence, cells in VEC cultures exhibited endothelial features by expressing two endothelial markers: DiI-Ac-LDL (Figure 3.5) and CD31 (Figure 3.6). Vimentin and SMemb protein expressions were detected in cytoplasm of all cells in VEC cultures (Figure 3.6). The majorities of cells did not express α-SMA protein in the VEC cultures (Figure 3.6), except in one VEC culture limited α-SMA protein expression was detected in some cells (data not shown).

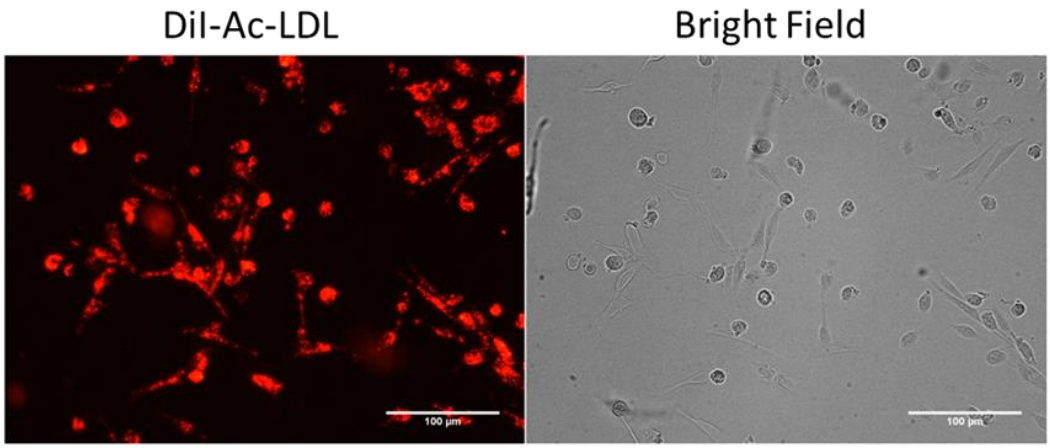

Figure 3.5. DiI-Ac-LDL labelled canine mitral VECs. A. The acetylated low density protein (red in A) was up taken by cells in VEC culture through endocytosis pathway. B. A bright field image provided the cells distribution information. Scale bar = 100 µm.

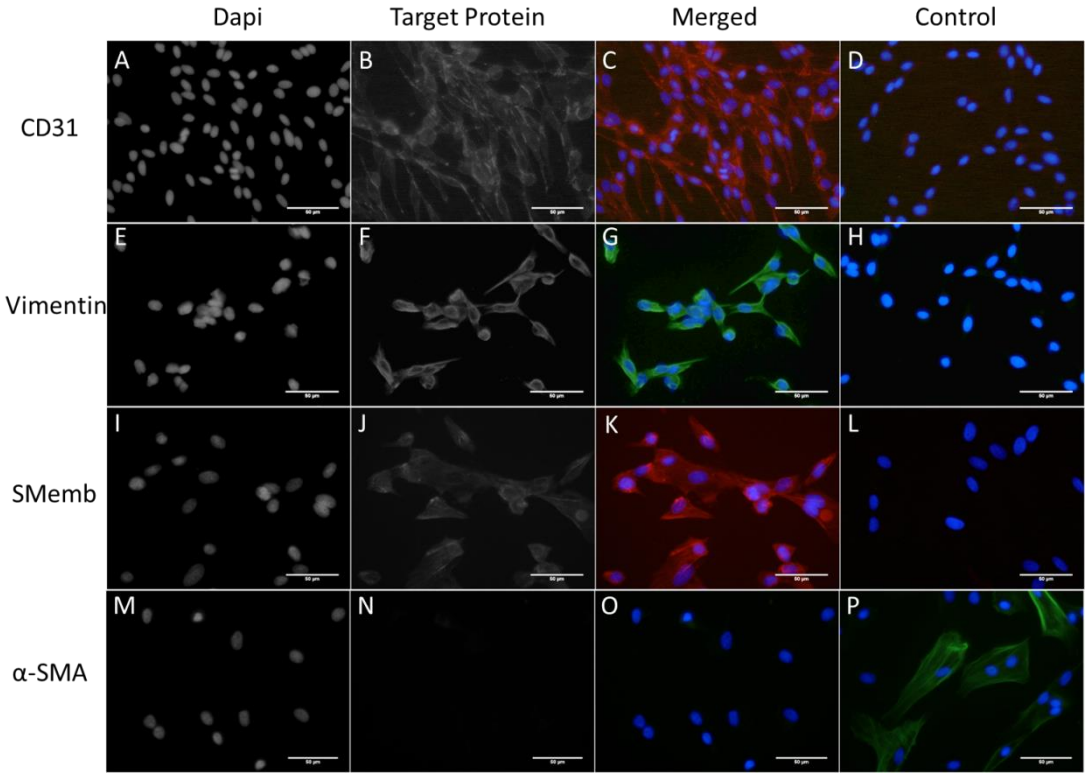

Figure 3.6. Immunofluorescent characterization on canine mitral VEC cultures. Cells expressed CD31 (red in C), vimentin (green in G) and SMemb (red in K), but was generally negative for α-SMA (O). DAPI stained cell nuclei (blue). DAPI channel (A, E, I, M), target protein channel (B, F, J, N) and merged images (C, G, K, O) were showed respectively for each marker. Same cell lines served as negative controls on which primary antibodies were omitted (D, H, L). Cells from a VIC culture expressed α-SMA which served as a positive control (P). Scale bar = 50 μm.

3.3.2 Canine Mitral VIC Characteristics

Canine mitral VICs typically had elongated cell process, though polymorphic and cuboidal cells were also present. By using the explant technique, substantial cell outgrowth from the tissue was usually observed within 7 days, with the explants then being removed and the cells were not harvested until they reached 80% confluence. By using collagenase digestion, in early primary VIC culture, cell growth was in a random distributed pattern. When at confluence, the cells tended to form a vortex pattern with multiple layers and did not show growth contact inhibition (Figure 3.7). Primary VICs usually reached at confluence in a T80 flask within 3 days.

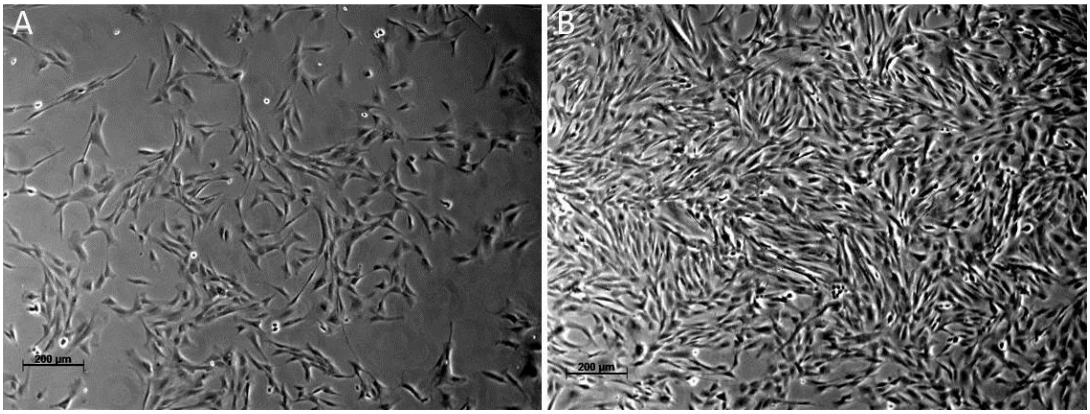

Figure 3.7. Primary isolated canine VIC morphology. A. The mitral VIC appearance under light microscopy before confluence, and B. At confluence. Cells in VIC cultures exhibited fibroblast-like morphology, cells tended to arranged in a 'hill and valley' pattern in confluent cultures. Scale bar = 200 µm.

Results of mitral VIC phenotypic characterizations are summarized in Table 3.4. On RT-PCR, cells in VIC cultures were negative for the endothelial marker CD31, but positive for aVIC marker α-SMA, SM22, SMemb and mesenchymal marker vimentin (Figure 3.8). The absence of endothelial features in VICs has been supported by findings in acetylated low density lipoprotein metabolic analysis and immunofluorescence where the VICs were negative for endothelial markers DiI-Ac-LDL (Figure 3.9) and CD31 (Figure 3.10), but expressed vimentin, SMemb and α-SMA proteins (Figure 3.10).

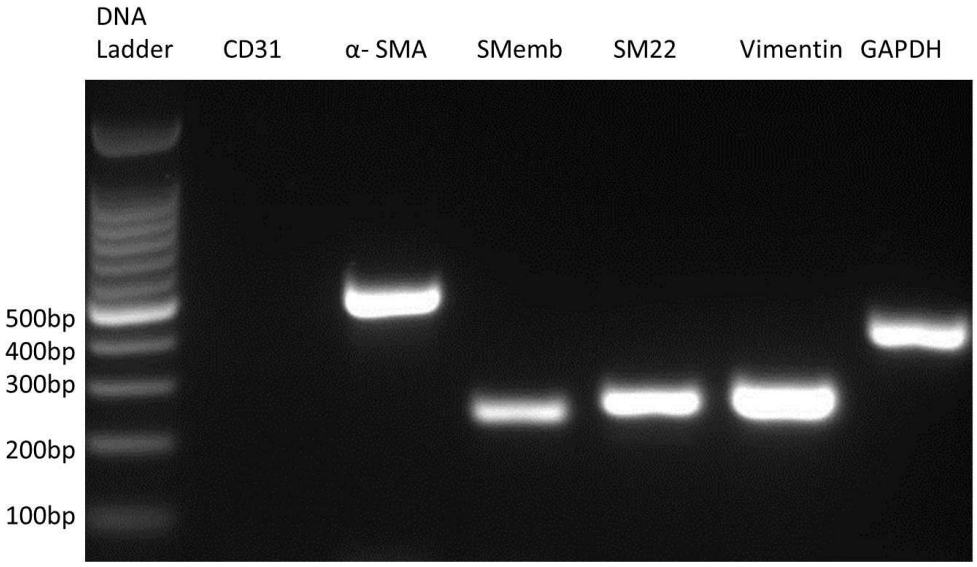

Figure 3.8. RT-PCR characterization on primary canine mitral VICs. They were negative for CD31, but positive for α-SMA, SMemb, SM22 and vimentin. As a positive control, cDNA template derived from cells in a VEC culture was used to amplify CD31 transcripts in the same experiment (data not shown).

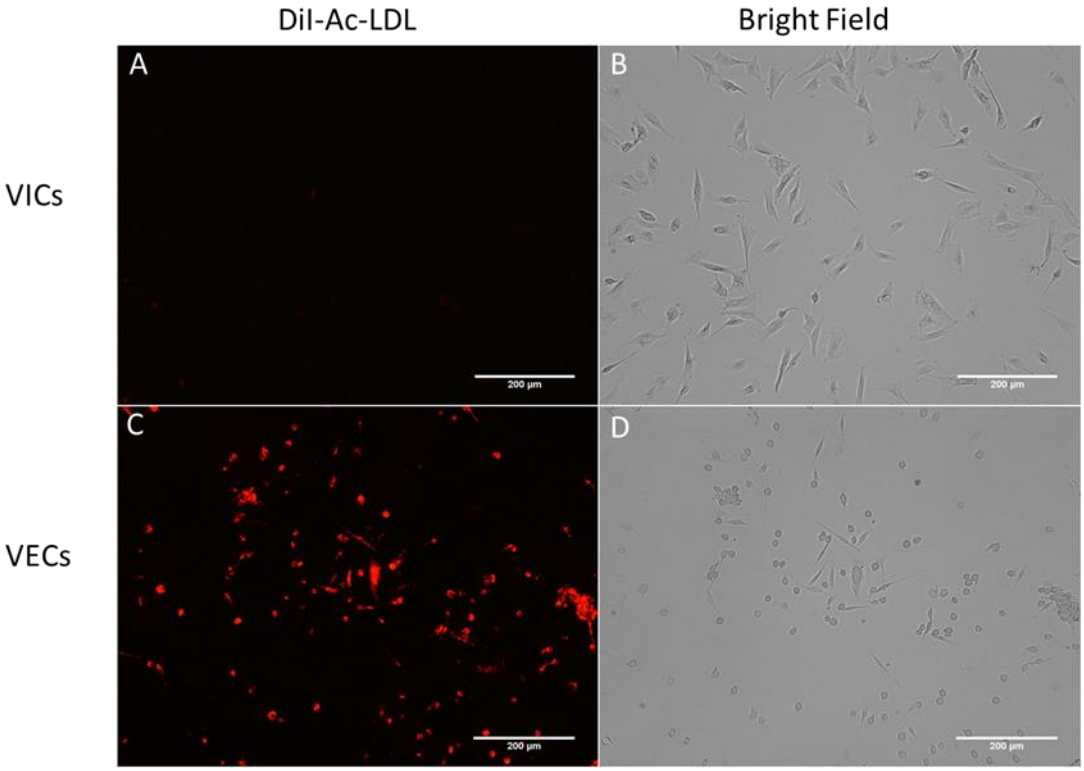

Figure 3.9. DiI-Ac-LDL expression was absent in the primary canine mitral VIC culture. Cells in VIC cultures did not up take DiI-Ac-LDL and had a background level staining (red in A). Cells from VEC cultures were assessed in the same experiment and served as a DiI-Ac-LDL positive control (red in C). Bright field images of corresponding VICs and VECs in the experiments are shown in B and D respectively. Scale bar = 200 µm.

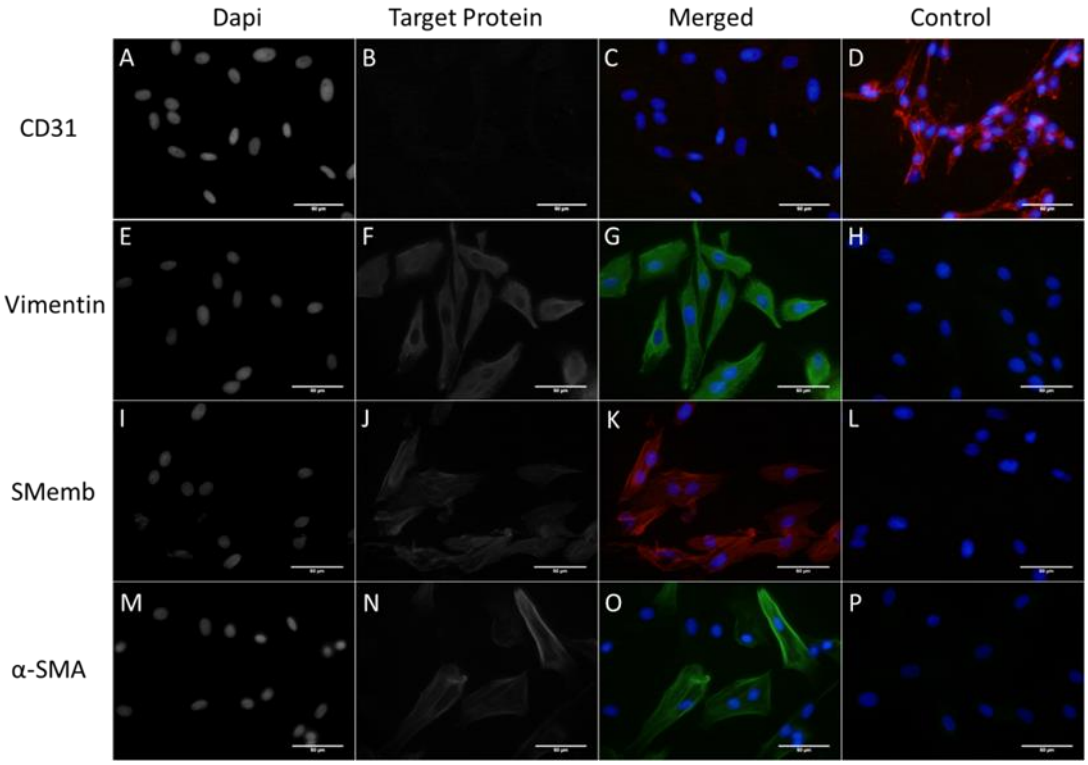

Figure 3.10. Immunofluorescence characterization on canine mitral VIC cultures. Cells were negative for endothelial marker CD31 (C), but positive for vimentin (green in G), SMemb (red in K) and α-SMA (green in O). DAPI (blue) stained nuclei. DAPI channel (A, E, I, M), target protein channel (B, F, J, N) and merged images (C, G, K, O) were showed respectively for each marker. Cells from a VEC culture were used in the same experiment and served as a positive control for CD31 primary antibody (D), while sample from same VIC cell lines without primary antibody incubation served as negative controls respectively (H, L, P). Scale bar= 50 μm.

Table 3.4 Result summary of mitral VEC and VIC culture characterization

	PCR characterization				
	Endothelial	Activated VIC			Mesenchymal
	CD31	SMemb	α-SMA	SM22	vimentin
VEC	+ (n=4)	+ (n=4)	+ (n=4)	+ (n=3)	+ (n=4)
VIC	– (n=4)	+ (n=3)	+ (n=4)	+ (n=3)	+ (n=4)
Immunocytochemistry and acetylated LDL labelling					
	Endothelial		Activated VIC		Mesenchymal
	DiI-Ac-LDL	CD31	SMemb	α-SMA	vimentin
VEC	+ (n=5)	+ (n=4)	+ (n=3)	+ (n=1); – (n=3)	+ (n=4)
VIC	– (n=4)	– (n=4)	+ (n=3)	+ (n=3)	+ (n=4)

The ‘n’ indicates the number of dog mitral valves used to derive the cell lines.

3.3.3 Optimization of Canine Mitral VECs *in vitro* Culture

3.3.3.1 Purity Evaluation of Canine Mitral VECs by Endothelial Marker Based Flow Cytometry

As described, heterogeneous cells were observed in the primary VEC cultures. VIC contamination in primary isolated VECs seem to be an issue thus additional cell sorting was undertaken (Cheung et al., 2008; Hoerstrup et al., 1998). After isolation and sub-culture, the purity of VECs was assessed by using endothelial cell surface marker based flow cytometry. Both CD31 and CD146 antibodies were tried in preliminary experiments. The CD31 antibody labelled 0.6%-2.6% (mean percentage of replicate samples) positive cells in the VEC cultures. This result did not fit the morphological observation according to which a much higher number of VECs were expected, suggesting this antibody didn’t identify canine VECs efficiently. Therefore, the CD31 antibody for flow cytometry was not selected in later experiments. While for antibody CD146, in VEC culture at passage 1, 77.4% cells (mean percentage of replicate samples) were identified as positive (Figure 3.11), which suggested the majority of the cells in VEC culture exhibited the endothelial cell marker. The experiment has also been done in VICs using the same protocol and

in contrast, 3.6% (mean percentage of replicate samples) cells were found to possess CD146 antigen (Figure 3.12).

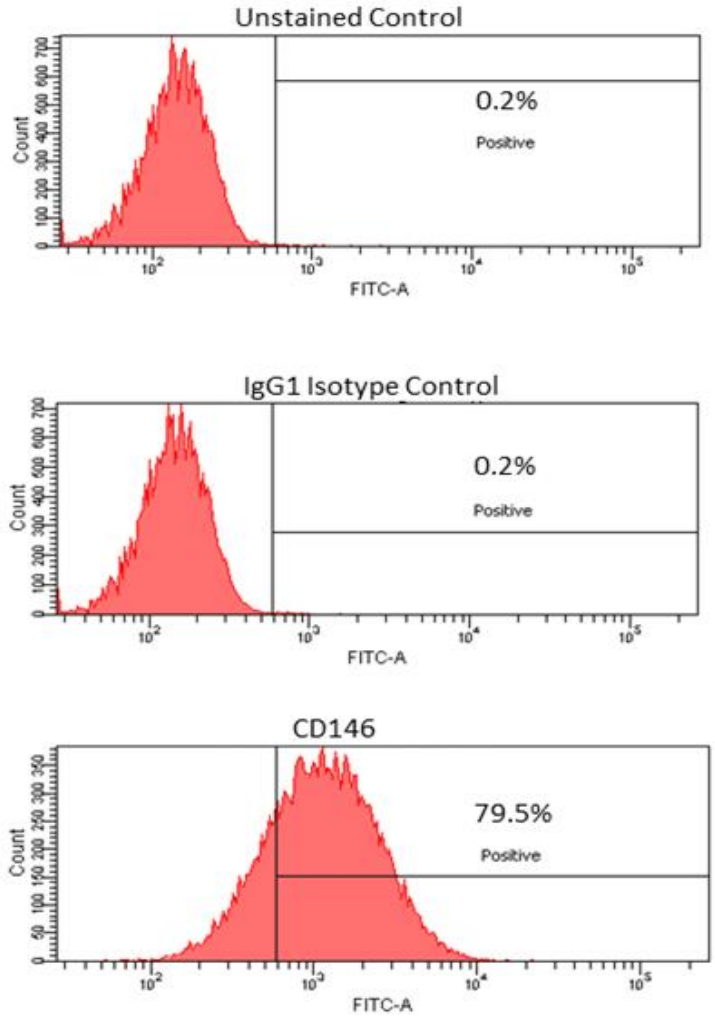

Figure 3.11. Representative results of CD146 flow cytometry on primary canine mitral VECs. The majority of cells in VEC culture (79.5%) showed affinity to endothelial marker CD146. The horizontal axis indicates FITC tagged CD146 fluorescence intensity; the vertical axis indicates cell count in each sample. Cells incubated with antibody diluting buffer instead of CD146 antibody served as an unstained control and cells incubated with IgG1 antibody served as an isotope control.

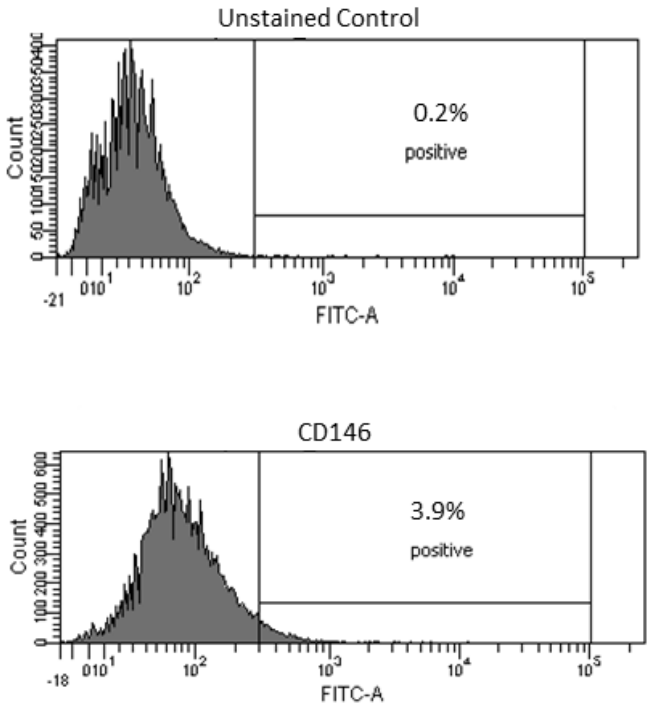

Figure 3.12. Representative results of CD146 flow cytometry on primary canine mitral VICs. Under the same experimental conditions to VEC CD146 flow cytometry, a small number of CD146 positive cells (3.9%) were found in VICs, the majority of cells were unstained. The horizontal axis indicates FITC tagged CD146 fluorescence intensity; the vertical axis indicates cell number in each sample. Cells incubated with antibody diluting buffer instead of CD146 antibody served as an unstained control.

3.3.3.2 **CD146 Positive VEC Separation**

Since the primary isolated VECs would be used for 3D tissue construction in the later stage of this project, it was considered ideal to have pure VECs population. Therefore cell sorting by FACs was carried out to separate VECs from contaminating cell types. It was hypothesized that the purified VEC population would have typical endothelial appearance in morphology and reduced activated VIC marker expression than unsorted cells.

As previous flow cytometry results suggested CD146 to be a promising marker for differentiating VECs and VICs, the sorting experiments were based on the same antibody. Cells positive for CD146 were identified and separated from the remaining cell populations. Isolated cell purities were checked right after sorting (Figure 3.13). Both CD146 positive (CD146+) and CD146 negative (CD146-) populations were collected and subsequently plated in cell culture flasks using the same culture conditions prior to sorting. Cell morphologies were observed during the culture (Figure 3.14). In the early days after the separation, CD146+ and CD146- cell populations exhibit apparently different morphologies. CD146 positive cells showed close growth contact with each other and possessed typical endothelial morphology; while the CD146 negative cells had elongated cell bodies and formed networks with their long extensions, which were similar to cells in VIC culture. The two populations were further characterized by using DiI-Ac-LDL. DiI-Ac-LDL labelled cells were found in both populations, though CD146+ population appeared to have more positive cells than CD146- population (Figure 3.14).

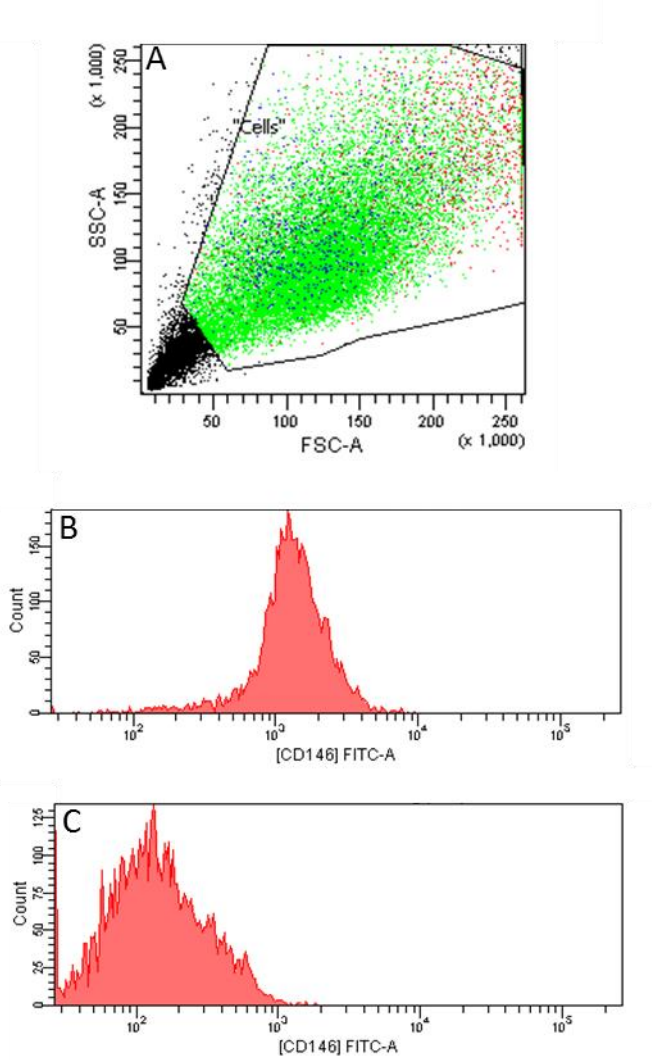

Figure 3.13. Primary canine mitral VEC cultures were separated by CD146 FACs. The cell gating strategy was illustrated in A: Blue dots indicate CD146+ cells and green dots represent CD146- cells. The red dots represent cells having fluorescence intensities in between of these two populations, which were not collected in the sorting procedure. Cell purities were checked immediately after sorting, CD146+ population (B) and CD146- (C) population have apparent differential fluorescent magnitudes, which suggest the sorting technique was effective. The horizontal axis indicates FITC tagged CD146 fluorescence intensity; the vertical axis indicates cell number in each sample. SSC, side scatter intensity value, indicating the complexity of the cell inner structure; FSC, forward scatter intensity value, reflecting the cell size.

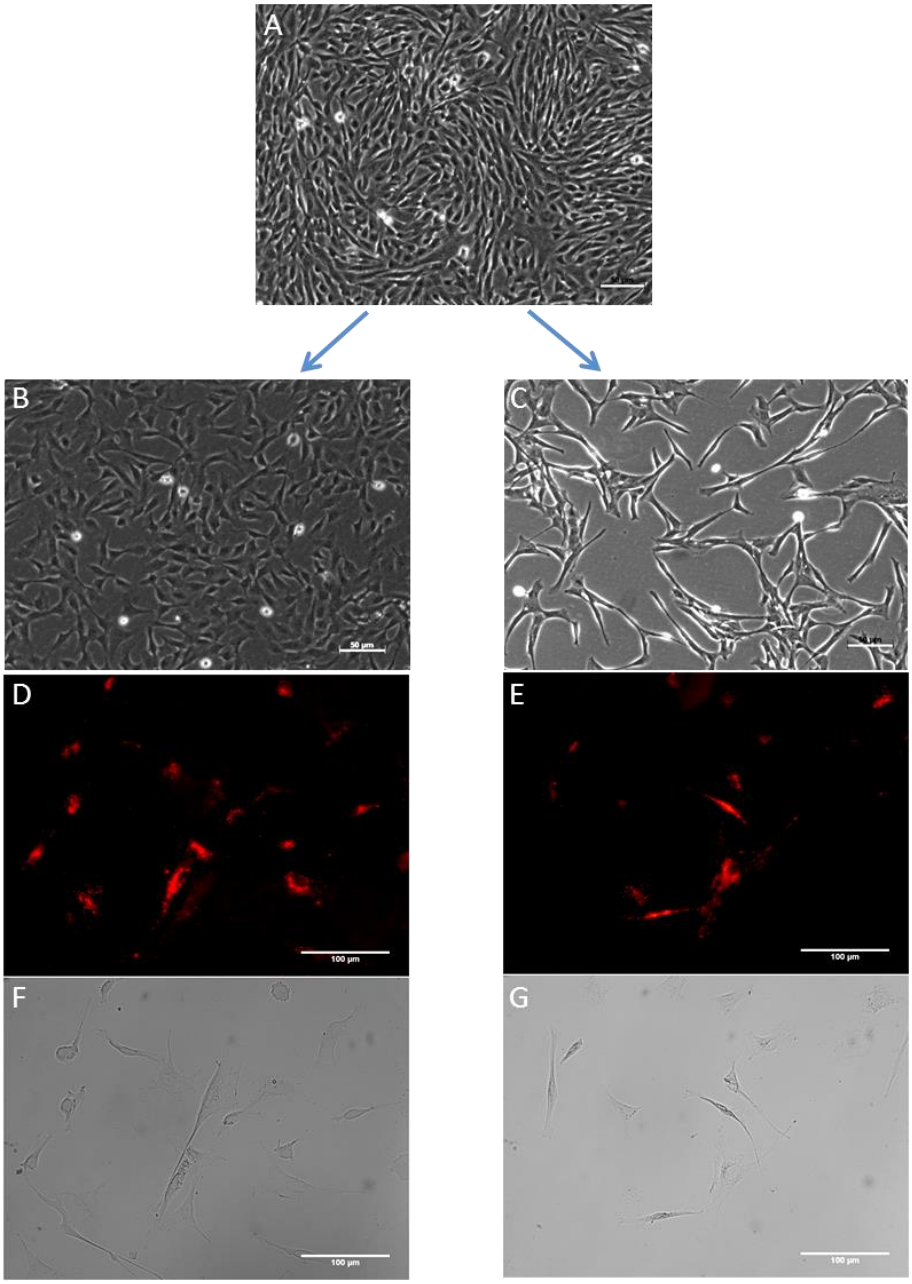

Figure 3.14. Primary canine mitral VEC morphologies at Day 3 post CD146 FACs sorting. Apparent differential morphologies were observed in CD146+ (B, D, F) and CD146- cell cultures (C, E, G). DiI-Ac-LDL staining was evaluated and both populations had cells uptake it. However, more intense red fluorescence was observed in CD146+ VEC culture (D) then CD146- culture (E). Light field images of cells in CD146+ and CD146- culture were shown in (F) and (G) respectively.

Furthermore, CD146+ VECs have been evaluated for activated VIC marker expression by RT-PCR (Figure 3.16). Previous data suggested that, cells in VEC culture and VIC culture expressed similar levels of SM22 (Figure 3.15). In contrast to VECs without FACs, CD146+ VECs have much lower SM22 expression than the VICs (Figure 3.16 B and C). Moreover, the α-SMA expression was minimal in CD146+ VECs (Figure 3.16 B and C). These results indirectly indicate the activated VIC characteristics in CD146+ VECs were reduced compared to unsorted VECs. However, myofibroblast morphology was observed in the CD146+ VECs confluent culture (Figure 3.16A).

To summarise, CD146 FACs sorting was efficient to separate a more pure endothelial population from primary VEC culture. However, the isolated CD146+ population still acquired activated VIC features, though maker expression levels seemed to be much reduced than the unsorted VECs.

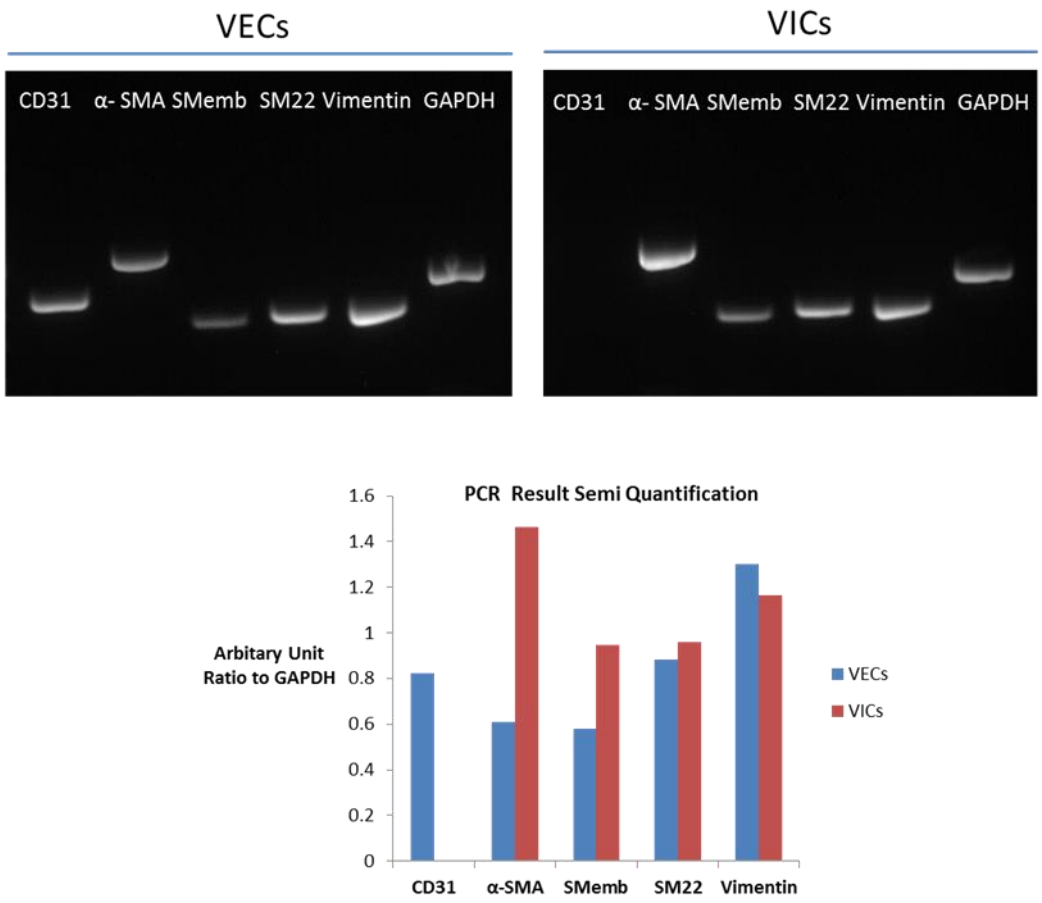

Figure 3.15. RT-PCR marker comparisons between primary canine mitral VECs and VICs. The transcripts were amplified in the same RT-PCR reaction and analysed on the same agarose gel. The VECs and VICs expressed similar levels of SM22 and vimentin; the VICs expressed higher levels of α-SMA and SMemb than VECs and did not express endothelial marker CD31.

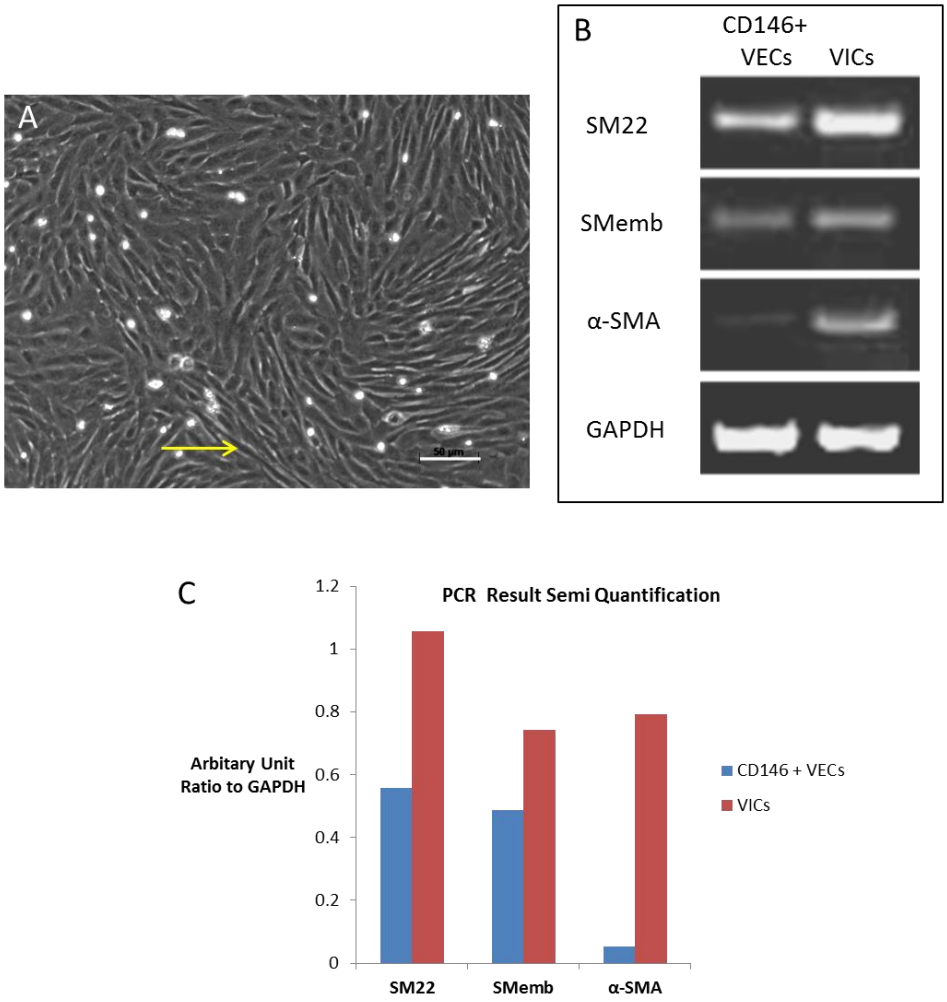

Figure 3.16. Reduced activated VIC marker expressions in CD146+ VEC culture. Myofibroblast-like morphology (yellow arrow in A) was present in CD146+ VEC confluent culture, notice that cells tend to form a vortex pattern. Compared to VICs, SM22 was much less in CD146+ VECs at transcriptional level (B and C) and α-SMA expression was minimal in CD146+ VECs.

3.3.3.3 Comparison of Canine Endothelial Basal Culture Medium and Standard Culture Medium in Canine Primary VEC Culture

The primary VECs are well known as being less stable in long term culture. There are two reasons resulting in this: VIC contamination in VEC culture and/or the VECs undergo differentiation *in vitro* (Bischoff and Aikawa, 2011; Cheung et al., 2008; Hoerstrup et al., 1998). In Section 3.3.3.2, FACs was tried to purify the VECs, however, the purified VECs only maintained typical endothelial cell morphology for a short period (within one Passage) then cells altered to mesenchymal phenotype in confluent culture. This phenotypic transformation has been considered to be similar to the foetal EndoMT process (Bischoff and Aikawa, 2011; Butcher and Markwald, 2007; Butcher and Nerem, 2007; Person et al., 2005). This complex transition process involves multiple signalling pathways and can be modulated by a number of biochemical factors such as endothelial growth factors and TGF-β (Armstrong and Bischoff, 2004). To maintain endothelial properties, VECs *in vitro* culture usually require specific culture medium containing growth factors favouring endothelial proliferation (Ci et al., 2013; Paranya et al., 2001; Wylie-Sears et al., 2011). In this study, a commercial canine endothelial culture medium (EBM) was compared with standard culture medium i.e. Advanced DMEM/F-12 medium with supplements (AF12) to culture canine VECs. It has been hypothesized that canine EBM would maintain the endothelial phenotype better than the standard medium.

Two experiments were done comparing canine EBM with standard culture medium. In the first experiment, primary VECs (passage 0) were cultured with AF12 medium. After one passage, the AF12 medium was replaced with canine EBM. In the second experiment, canine EBM was used to culture primary VECs (passage 0) right after cell isolation. Standard medium cultured VECs from the same dogs served as controls in both studies.

In medium replacement experiment, VECs (passage 1) were cultured in canine EBM or AF12 for 24 h. Cell morphologies were evaluated at passage 1 and passage 2 (Figure 3.17). At passage 1, EBM medium replacement seemed to drive VECs to a differentiation state, as cells with thin long cellular extensions were widely seen in the culture, though overall cell morphologies were similar to VECs cultured in

standard medium. At passage 2, differential VEC morphologies and arrangement patterns were observed in EBM and in AF12. Cells in EBM culture were smaller in size comparing to VECs in AF12, and substantial spindle shape cells were observed in the culture and some of them tended to arrange into a whirling pattern.

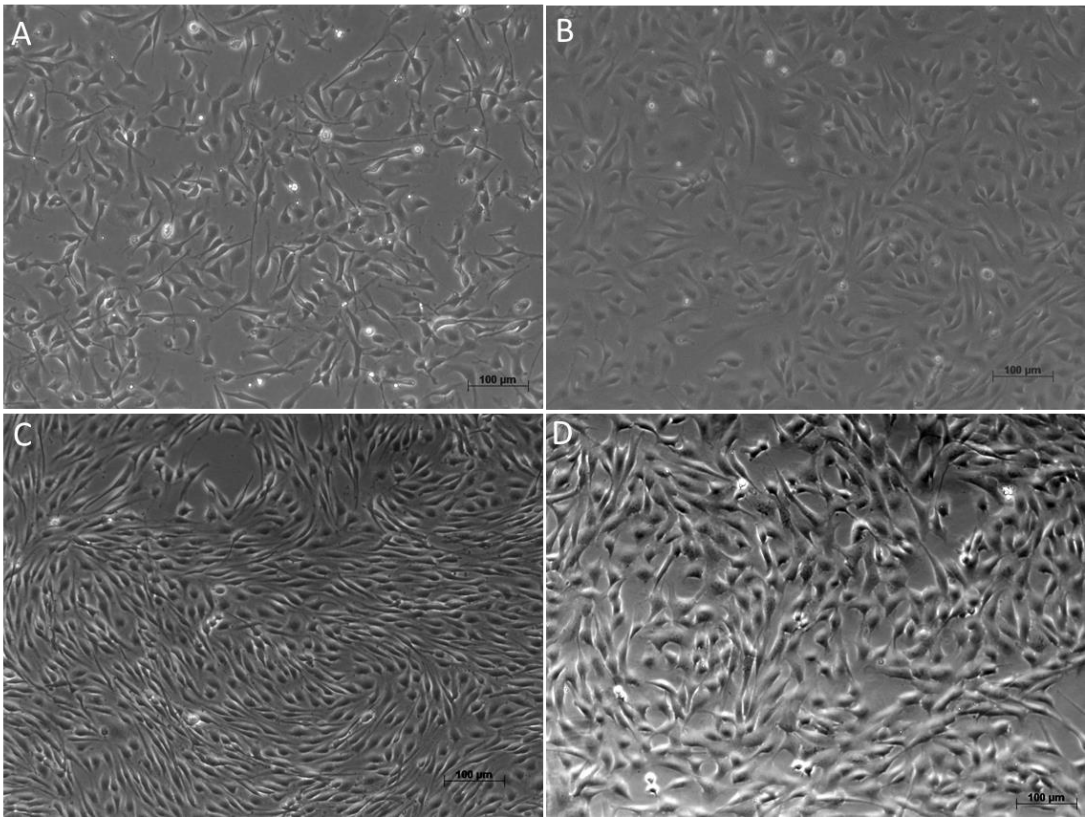

Figure 3.17. Cell morphologies in primary canine mitral VEC sub-cultures in EBM and in AF12 medium. In early culture time of the medium replacement, cells in EBM (A) had similar morphologies to cells cultured in standard AF12 medium (B), though the former cells exhibited long extensions. In later confluent cultures, cell sizes were decreased in the EBM culture (C) comparing with cells in AF12 culture (D) and spindle shape cells forming whirling pattern were noticed in the culture (C). Scale bar =100 µm.

Canine VECs (passage 2) in EBM and in AF12 were characterized by expression of endothelial markers DiI-Ac-LDL (Figure 3.18) and CD31 (Figure 3.19). Both cultures were positive for the endothelial markers, and VECs in EBM have higher fluorescence intensity than cells in AF12. At transcriptional level, α-SMA expression diminished in EBM cultures, which indicated a dramatic decrease of the myofibroblast feature in EBM cultured VECs (Figure 3.20).

To summarise, replacing standard culture medium with specific endothelial medium to culture canine VECs seemed to maintain a more endothelial phenotype for the cells in culture.

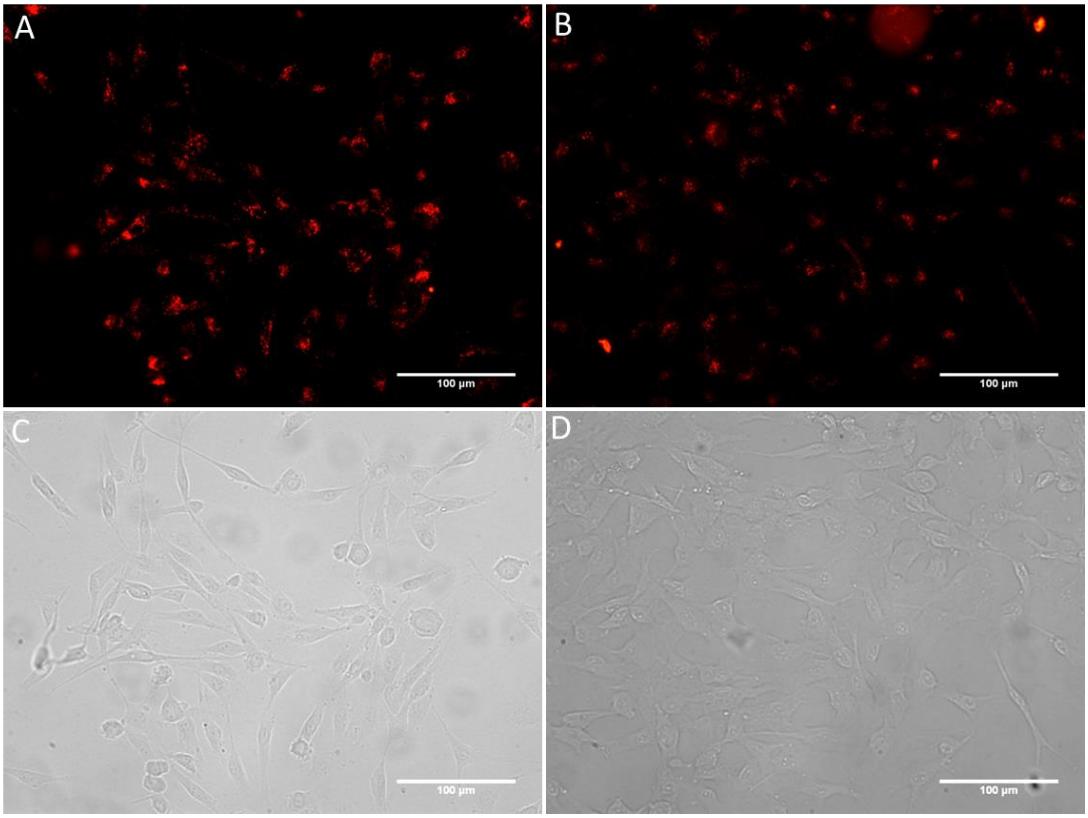

Figure 3.18. DiI-Ac-LDL labelled EBM and AF12 cultured VECs. VECs in EBM (A) appear to have more intense red fluorescence than cells in AF12 (B). Bright field cell images of the DiI-Ac-LDL labelled VECs in EBM and in AF12 are shown in C and D respectively. Scale bar = 100 µm.

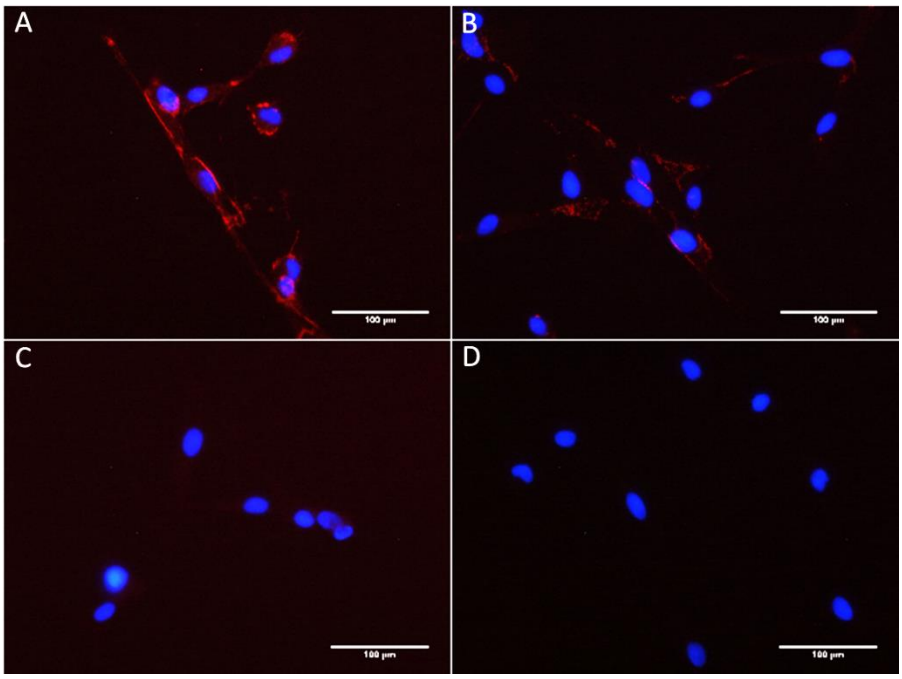

Figure 3.19. Endothelial marker CD31 expression in EBM cultured and in AF12 cultured primary VECs. Higher CD31 expression was observed in EBM VEC cultures (red in A) than in AF12 VEC cultures (red in B). Secondary antibody alone served as negative controls (C for VECs in EBM, D for VECs in AF12). DAPI (blue) stained nuclei. Scale bar = 100 μm

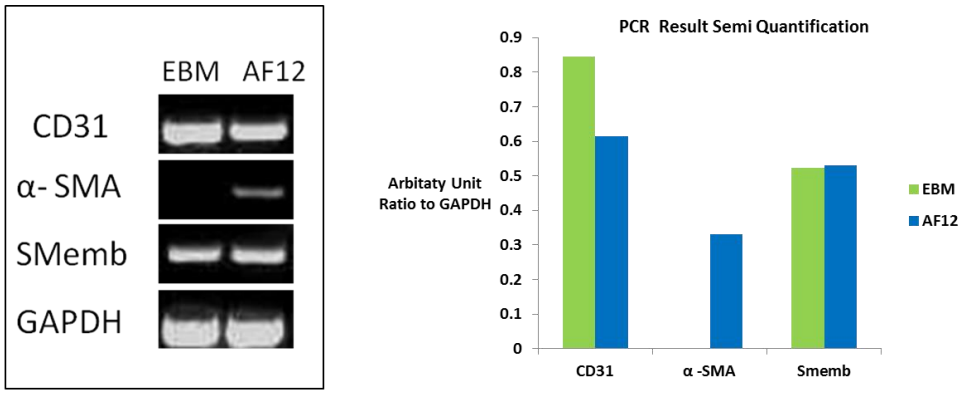

Figure 3.20. RT-PCR characterization on EBM cultured and AF12 cultured primary VECs. Higher CD31 expression but much reduced α-SMA expression was detected in EBM cultured VECs comparing with AF12 cultured VECs on RT-PCR. The expression of SMemb was not apparently different between the two cultures.

Since the results of using commercial canine EBM for VECs sub-culture suggested that EBM is superior in maintaining endothelial properties comparing with AF12 medium, it was hypothesized that using canine EBM to culture primarily isolated VECs (passage 0) could stabilize their endothelial features immediately after the *in vitro* isolation.

Primary isolated VECs from the same individual mitral valve leaflet (n=5) were cultured in both EBM and AF12 medium respectively. Cell morphologies were observed during the cultures. All primary VEC cultures in EBM experienced same fate: from initial endothelial progenitor colonies to altered morphologies in later culture. At Day 3, endothelial progenitor cell colonies were observed in both EBM and AF12 culture, with no apparent differences between the two. At Day 6, VECs in AF12 medium reached approximate 80% confluence with the majority of cells exhibiting a cobblestone morphology, spindle shape cells also existed in the culture which was consistent with previous findings. Whilst in the EBM medium, typical endothelial colonies diminished in the culture by Day 6. Cells remaining in the culture were spindle shape with very elongated cell process and less robust according to visual observation under light microscope. No obvious cell growth was observed in the EBM culture between Day 6 to Day 10. At Day 11, cells in EBM started to proliferate; heterogeneous morphologies of cells were observed in the culture. At Day 13, three types of cell growth patterns were observed in a 70%-80% confluent EBM VEC culture (Figure 3.21). They are a sparse distribution of cells with long extensions; confluent arrangements formed by spindle shape cells and another type of confluent colony containing both spindle shape and cobblestone morphology cells.

The EBM cultured primary VECs were evaluated by RT-PCR techniques (Figure 3.22). Compared to standard medium cultured VECs and VICs, VECs in EBM expressed higher level of CD31 and lower level of α-SMA, which was consistent with the medium replacement results.

In conclusion, using canine EBM to culture primary isolated VECs resulted in an unexpected morphology alteration process, which indicated differential phenotypes

were existing in the cultures. Enhanced endothelial marker expression and reduced activated VIC feature were observed in primary VECs cultured in EBM.

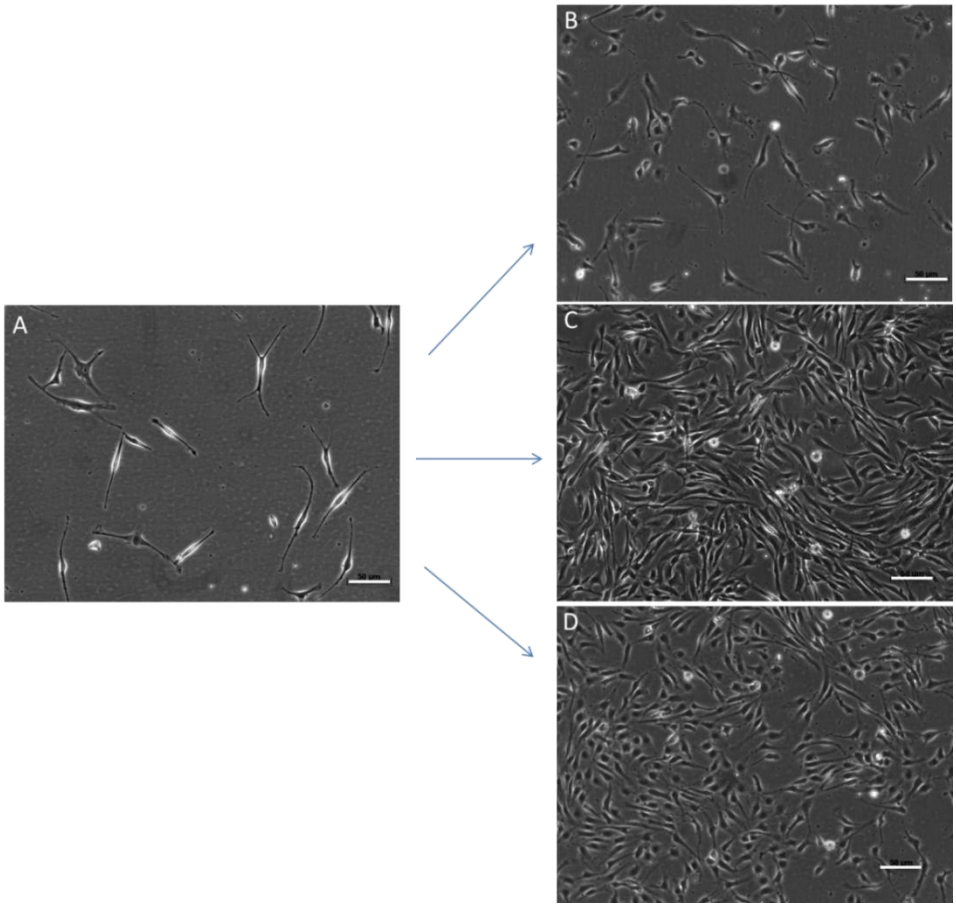

Figure 3.21. Primary isolated VECs cultured in EBM morphologies altered in the early culture days. A. On Day 6, cells with long extensions were observed in primary VEC EBM culture, where typical endothelial cobblestone colonies disappeared. On Day 13, morphological heterogeneities were observed in the same culture. There were three patterns: B. Sparse distribution of cells with long extensions; C. Confluent fibroblast-like colony formed by spindle shape cells and D. another type of confluent colony containing both spindle shape and cobblestone morphology cells. Scale bar = 50 μm.

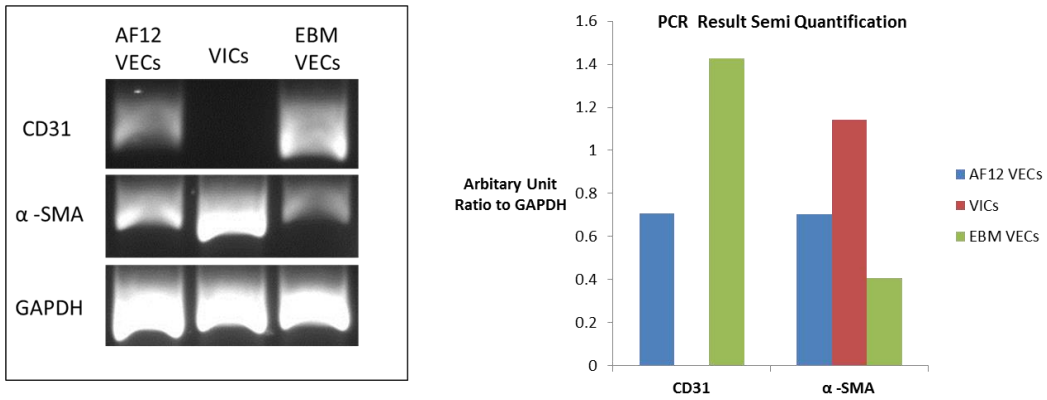

Figure 3.22. Primary isolated VECs consistently cultured in EBM characterized by RT-PCR. Cells (passage 2) demonstrated higher expression of CD31 and decreased expression of α-SMA than VECs cultured in AF12 medium.

3.4 Discussion

3.4.1 Primary Canine Mitral VEC Exhibit Endothelial Properties and Differentiation Potentials *in Vitro*

Primary canine mitral VECs possessed common endothelial properties such as expressing endothelial specific cell surface molecule CD31 and uptake of acetylated low density protein through endocytosis. CD31 is a 130 kilodalton (kDa) cell adhesion molecule which is involved in inflammation and vascular structure development (Ilan and Madri, 2003; Woodfin et al., 2007). It has been well accepted as one of the classic markers to characterize endothelial cells (Ferrer et al., 1995; Gould and Butcher, 2010). DiI-Ac-LDL has been found to be specifically taken up by macrophages and endothelial cells through scavenger pathway which is not present in other cell types and it has been used to identify endothelial cells for more than two decades (Cuy et al., 2003; Voyta et al., 1984). Therefore a combination of these two markers confirms endothelial identity of the cells in VEC culture in aspects of both surface molecule synthesis and unique metabolic function.

In initial studies, vWF was tried as a marker to identify endothelial cells. Unexpectedly, this common endothelial marker was not obviously expressed in our VEC cultures. Three pairs of vWF primers were used for RT-PCR amplification along with annealing temperature optimization. All the primer pairs were successfully amplified in both human umbilical endothelial cell line and canine haemangiosarcoma cell line (tumor in endothelial nature) (Thamm et al., 2006; Fosmire et al., 2004), which indicate that the absence of vWF in VECs was unlikely due to technical issues. This could be a result of tissue specific heterogeneous expression of vWF, as has been previously observed in endothelium from different anatomic sites (Pusztaszeri et al., 2006). Interestingly, in one previous report vWF expression in porcine mitral VECs at transcriptional level was also weak (Flanagan et al., 2006a). To enhance the vWF expression signal in VEC cultures, possibly using stimulating cytokines such as tumor necrosis factor alpha (TNF-α) could boost the vWF synthesis in the culture (Bernardo et al., 2004).

Consistent with marker characterization, the majority of cells in VEC culture exhibit typical cobblestone morphology in early culture (< 3 passages). However cellular

pleomorphism was seen. This non-cobblestone phenotype of cells in the VEC culture might arise from three sources: endothelial cells with differential morphology, other cell type contamination or endothelial cell differentiation.

Previous reports have showed the presence of different endothelial cell morphologies in native mitral valves (Corcoran et al., 2004; Sarphie and Allen, 1978). Endothelial cells on the ventricular side of canine mitral valve leaflet seem to be larger, with more prominent nuclei and in a more orderly arrangement than the atrial side (Corcoran et al., 2004; Sarphie and Allen, 1978). Consistently, the side specific heterogeneity has also been observed in aortic VECs (Simmons et al., 2005).

Apart from the above possibility, it is more likely the use of an enzymatic digestion technique released sub-endothelial cells (i.e. VICs) from the valve leaflet during VECs isolation. This technical issue has been discussed in studies isolating VECs from semilunar valves (Cheung 2008; Butcher 2004). Additional cell sorting or single cell clonal expansion might be a possible solution (Cheung 2008; Hoerstrup 1998; Parayan 2001; Gould 2011).

Lastly, the possible identity of these spindle shaped cells might be transformed VECs which undergone EndoMT *in vitro*, as occurs in embryonic development. The possibility of EndoMT potential in adult valve cells has been examined in recent studies (Bischoff and Aikawa, 2011; Mahler et al., 2013; Paranya et al., 2001; Paruchuri et al., 2006). It has been proposed to be one of the key remodelling mechanisms in heart valve disease, where a subset of adult VECs possess foetal cell characteristics such as differentiation potential, and can replenish the VIC population when needed, for example during disease or remodelling process (Bischoff and Aikawa, 2011; Liu et al., 2007; Paruchuri et al., 2006). Hallmarks of EndoMT include induction of mesenchymal marker expression and decreased endothelial marker properties (Bischoff and Aikawa, 2011). In this study, myofibroblast marker expression was present in VEC cultures at the transcriptional level, but as stated above VIC contamination might contribute. A more convincing finding of EndoMT is SMemb expression in VECs at both gene and protein levels. Extensive expression of SMemb in cells from VEC culture on immunofluorescence would suggest VIC

contamination was not responsible for all SMemb expression. SMemb is a 200 kDa non-muscle type myosin heavy chain which was first reported in embryonic vascular structures (Aikawa et al., 1993; Kuro-o et al., 1991). This protein has been considered as an activated mesenchymal marker and has been found expressed highly in foetal VECs, but minimally in normal adult VECs in semilunar valves (Aikawa et al., 2006). Moreover, it has been shown the SMemb is expressed by the majority of VICs in MMVD, but absent in normal human mitral valves (Rabkin et al., 2001). Similarly, SMemb phenotype VIC transformation has also been observed in canine MMVD (Disatian et al., 2010). These studies suggest SMemb is involved in VIC activation during the disease remodelling process. To our knowledge, this is the first study showing apparent SMemb expression in adult VECs. This suggests VECs from adult canine mitral valves are activated *in vitro* and possibly still possess developmental EndoMT potential, which is consistent with the VEC progenitor cell hypothesis (Bischoff and Aikawa, 2011).

For further confirmation, it will be necessary to counterstain endothelial markers with mesenchymal markers on VEC populations to detect whether there is co-expression of these proteins in individual cells. A more straightforward method of confirming the EndoMT hypothesis will be evaluating a series of markers involved in the EndoMT process.

3.4.2 Primary Canine Mitral VIC Characteristics *in Vitro*

In this study, canine mitral VICs were isolated by using both explant culture and collagen digestion techniques. Cells were successfully cultured on standard tissue culture vessels without additional coating substrates. In a previous report, coating substrate such as collagen has been necessary for primary canine mitral VIC growth from explants (Heaney et al., 2009). The collagenase digestion method was used to isolate primary VICs, after several explant cultures were undertaken, as it was believed a digestion of the entire leaflet tissue would be less selective and so results in obtaining a complete set of VIC sub-phenotypes.

Regarding cell morphology, distinct from VECs, primary mitral VICs typically exhibited fibroblast-like morphology, which is consistent with previous reports

(Gould and Butcher, 2010; Heaney et al., 2009). Heterogeneous populations (based on morphology) were also observed in the VIC cultures. Apart from morphological differences, it was noticed that cells in VIC cultures showed different responses to enzymatic dissociation, with a number of cells in the culture showing stronger adhesion properties to culture substrate compared to others (data not shown). The same phenomenon has been observed previously. It has been shown that trypsinization sensitive mitral VICs expressed low levels of α-SMA (15-35%) whereas the more adhesive VICs expressed α-SMA highly (>98%) (Blevins et al., 2006). A similar study also managed to obtain mitral VIC sub-populations by utilising their differential adhesion properties to fibronectin (Stephens et al., 2010b). Factors such as anatomic region and age are associated with mitral VIC phenotypic and synthetic differences in culture, which might be linked with incidence of myxomatous mitral valve disease *in vivo* (Blevins et al., 2008; Stephens et al., 2011).

The heterogeneity of native VICs has been reviewed by Liu et al. in 2007, where at least 5 sub-phenotypes are reported to exist in native VICs (Liu et al., 2007). Moreover, the relative density of these sub-populations is proposed to respond dynamically to stimulation and environment alterations (Liu et al., 2007). The complex mechanism under-pinning this heterogeneity is not known.

To date, there is no definitive marker panel for differentiating each VIC sup-phenotype. In this study, the identity of VICs was determined by their lack of endothelial properties, but being positive for vimentin (Heaney 2009). Endothelial markers were absent in all VIC cultures examined. The expressions of activated VIC markers SMemb, SM22 and α-SMA were detected in VIC cultures at the transcriptional level. SMemb protein was found to be expressed by all cells in VIC culture, while α-SMA expression varied between different cultures on immunofluorescence. The α-SMA positive cells were generally estimated on visual examination at less than 10% in VIC cultures. This figure is much less than previously reported (Taylor et al., 2003). Culture conditions such as cell density and substrate types have been reported to be associated with α-SMA expression (Engler et al., 2006; Stephens et al., 2011; Xu et al., 2012).

Mitral aVIC function and properties have been studied both *in vivo* and *in vitro*. Most *in situ* studies have focused on the roles of aVICs in myxomatous mitral valve disease (Black et al., 2005; Disatian et al., 2008; Han et al., 2013; Han et al., 2008; Rabkin et al., 2001). The number of aVICs are reported increased in disease remodelling (Disatian et al., 2008; Han et al., 2008) or repair processes (Durbin and Gotlieb, 2002; Tamura et al., 2000), and they are possibly associated with cell migration (Black et al., 2005), increased ECM synthesis (Aupperle et al., 2009a; Gupta et al., 2009a; Han et al., 2010) and degradation activity (Aupperle et al., 2009b; Disatian et al., 2008; Rabkin et al., 2001).

In vitro studies on mitral VICs mainly refer to the activated phenotype (aVIC) (note: caution has to be exercised in equating cultured VIC phenotypic characteristics with native valve VICs, but for the purpose of this discussion the VICs appear to be activated). The ECM synthetic ability of VICs has been evaluated (Flanagan et al., 2006a; Gupta et al., 2008b), as well as wound repairing capacity (Durbin et al., 2005; Fayet et al., 2007; Lester et al., 1993). Similar to aortic VICs, the mitral VICs have been found to be 'mechanosensitive'-with differential α-SMA expression and collagen synthesis activity in response to different culture substrates and conditions (Stephens et al., 2011), which might better explain VICs-valve matrix interaction *in vivo*. Recent studies have also identified other mitral VIC properties, such as osteogenic, chondrogenic and adipogenic potentials, and a higher predisposition to calcification comparing to aortic VICs (Sun et al., 2013; Wylie-Sears et al., 2011). In the current study, due to time constraints, only cell phenotypic markers have been evaluated in cultured mitral VICs, without further function investigation of activated VICs.

In future studies, it would be worth obtaining accurate percentages of activated VICs in the culture by additional techniques such as flow cytometry and separating aVICs from the main VIC culture population, to investigate biological functions targeting this specific VIC sub-population.

3.4.3 Evaluation and Improvement of Primary Canine Mitral VEC Purity

The marker CD146 has been used to identify canine circulating endothelial cells previously (Wills 2009). In this study, CD146 expression was evaluated in passage 1 VEC cultures by flow cytometry and over 75% of cells were positive. This suggests that the majority of cells in proposed VEC cultures were actually endothelial. There was no well-characterized canine VEC cell line available to serve as a positive control; however there was marked differential CD146 expression in primary isolated VECs and VICs (less than 4% CD146 positive cells) under the same experimental conditions. The results of VEC flow cytometry is consistent with the morphological observation (judging by estimating the typical endothelial cobblestone appearance cell numbers in the VEC cultures). Therefore this suggests CD146 would be reasonable efficient in detecting endothelial cells in primary VEC culture, and be a potential marker for VEC purification. As this experiment was only undertaken in samples from one dog further work is required to confirm this finding.

It should be noted that around 4% of cells were positive for CD146 in VIC culture. In the other characterization protocols, VICs were negative for all endothelial markers, suggesting the identity of these CD146 positive VICs was not endothelial. Furthermore, caution should be exercised in using CD146 as a lone endothelial marker, not least as it can be present in other cell types such as vascular smooth muscle cells (Ren et al., 2002).

Mouse monoclonal [WM-59] CD31 antibody (ab13466) was also used for the VEC flow cytometry. However, this antibody seemed to fail to label canine mitral VECs possibly due to species differences of the antigen epitope. Another rabbit polyclonal CD31 antibody (ab28364) successfully labelled canine mitral VECs on immunocytochemistry which proved the presence of CD31 protein on the canine VECs. However, as polyclonal antibodies can bind to multiple antigen epitopes which might intensify the fluorescence quantification, they are not ideal for flow cytometry. Therefore, the rabbit polyclonal CD31 antibody was not applied to current flow cytometry study. A limitation of the sorting experimental design is a common endothelial cell surface marker was used to identify VECs. It is likely that

other endothelial cell types such as circulating endothelial cells might also exist in the VEC cultures. Therefore, to ensure a pure VEC population, it would be necessary to use additional cell markers to differentiate VECs from other types of endothelial cells (Gould and Butcher, 2010).

Cell sorting techniques have been commonly used in optimizing primary isolated endothelial cells (Cheung et al., 2008; Hoerstrup et al., 1998). Magnetic sorting has been tried to separate pulmonary VECs from contaminating cell types (Cheung et al., 2008). Based on evaluation of CD31 expression, VEC purity increased to 96 $\pm$ 3%. However, it has been shown that the interstitial cells re-appeared in the culture once they reach confluence (Cheung et al., 2008). This is similar to the observation in the current study. Although the sorting technique seemed to be efficient to separate endothelial cells from the VEC culture, mesenchymal cell morphology re-occurred in a later confluent CD146+ VEC culture.

An alternative method for getting high purity VECs would be single clonal expansion followed by specific endothelial medium culture (Cheung et al., 2008). However, this method results in selected VEC clones which might not be representative for the entire population. Also cell doubling number of the clones is very limited in each expansion, and extensive expansion may affect cell quality (Gould and Butcher, 2010).

Specific endothelial culture medium or adding additional endothelial growth factors should be helpful in maintaining endothelial properties and preventing the development of mesenchymal properties (Armstrong and Bischoff, 2004). With that in mind, a commercial canine endothelial basal culture medium (EBM) was used in this study and compared with standard culture medium (AF12). Endothelial colony forming cells in VEC culture occurred in both EBM and AF12 medium at the early stages of culture. However, cells appeared undergone an unexpected differentiation, particularly in the EBM VEC cultures. Moreover, when cells in EBM reached confluence, their morphologies were not limited to typical endothelial type, but showed morphological heterogeneity. The exact mechanism of this phenomenon was not investigated. It should be noted that other cell types rather than VECs could also

survived in endothelial basal medium (Cheung et al., 2008; Gould and Butcher, 2010). A further concern is the commercial canine EBM used in this study is for culturing aortic endothelial cells, but not specific for mitral VECs. As has been reported previously the vascular endothelium and valve endothelium possess differential inflammatory and mechanical responsive characteristics (Butcher et al., 2004; Butcher et al., 2006), it is possible that the mitral VECs could respond to the culture medium in a manner distinct from vascular endothelial cells. Customising media in the laboratory would be another solution for mitral VECs culture. Despite the above mentioned transformation process in EBM culture, characterization results suggested EBM is superior to AF12 in maintaining endothelial characteristics, as higher expressions of endothelial markers and dramatically decreased α-SMA expression were observed in the EBM culture compared to AF12 culture.

In summary, cell sorting can separate VECs from a mixed population culture but standard culture media cannot maintain the endothelial properties in long term culture. Specific endothelial basal medium can preserve endothelial properties and down regulate mesenchymal marker expressions, but cannot eliminate contaminated cell types in the culture. To obtain the purest VEC population, a combination of cell sorting followed by specific endothelial medium culture should give better results. In this study, due to sample number and time limitation, this purification approach was not undertaken.

To guarantee a relatively pure VEC population (for endothelial lining of tissue engineered constructs), the VECs used in later experiments were not passaged more than three times and over-confluent cultures were avoided to reduce the chance of EndoMT differentiation (Gould and Butcher, 2010).

3.5 Conclusion

Primary canine mitral VECs and VICs were successfully isolated, cultured and characterized *in vitro*. Relatively pure cell populations were obtained. Endothelial markers differentiated VECs from VICs and mesenchymal features existed in both cultures. Additional cell sorting and specific culture medium can contribute to endothelial cell purity in VEC cultures. This study provides fundamental information

for canine mitral valve cellular biology, which will benefit mitral valve disease research and valve constructs in tissue engineering.

Chapter 4: Fibrin Based Canine Mitral Valve 3D Constructs in Static Culture

Abstract

It is uncertain if canine myxomatous mitral valve disease (MMVD) is initiated by long term shear stress damage to the valve endothelium or from abnormalities of valve interstitial cells (VICs). Examining these questions is problematic *in vivo*. In this study, an alternative approach was taken and tissue-engineered fibrin based canine mitral valve constructs were developed which can be used as an *in vitro* platform to study the pathogenesis of MMVD.

Canine mitral valves were collected post mortem and categorized into two groups: healthy (Whitney grade 0/4) and diseased (Whitney grade 1/4-2/4). Dogs in 1.5-5 years age range were used in current study. Mitral valve endothelial cells (VECs) and VICs were cultured and characterized as described in Section 3 prior to three dimensional (3D) culture (VECs passage 2-3; VICs passage 4-7). Three types of models were generated by using fibrin based 3D culture techniques. Samples were maintained in static culture for 14-20 days and analysed by using light microscopy, immunofluorescence microscopy, Western blot and electron microscopy techniques.

Histological examination demonstrated partial native tissue-like morphology of the 3D constructs. Relatively comparable expression of cellular and ECM associated markers was detected between artificial constructs and native valves. Comparing healthy VIC constructs (Type 1) with diseased VIC based models (Type 2), no apparent difference was detected in expression of the VIC activation markers (α-SMA and SMemb) and matrix catabolic enzymes (MMP-1 and MMP-3). The partial ultrastructure analysis using transmission electron microscopy revealed cells in the construct with variable morphologies. Atypical endothelial cells or cell loss/degradation were observed in the proposed endothelium surface, and the VICs typically were either in active or degraded state.

In endothelium damaged model (Type 3), without changing mechanical tension, up-regulated VIC activation (SMemb up-regulation) was observed after damaging; while in Type 3 with decreased external mechanical tension, generally the VIC phenotype appeared to be more quiescent based on marker expression (decreased SMemb and α-SMA expression) and showing some signs of degradation or decreased proliferation (vimentin down-regulation). However, some cellular activities were observed at the wound sites which may indicate an undergoing repair process. Additionally, distinct association patterns of SMemb and α-SMA to some of the ECM proteins suggested aVIC heterogeneity. These findings were further supported by ultrastructure analysis using TEM, where differences in cell activity were observed within a "smooth muscle" cell phenotype population.

In conclusion, canine fibrin-based 3D mitral valve constructs have been successfully developed using cells from both normal and diseased dogs, and appear to be promising models for valve research. Results suggest that current static cultured constructs express MMVD markers irrespective of using healthy or diseased VICs. Simple mechanical stimulation was found to regulate VIC activity in the 3D models. Endothelial damage resulting in VIC phenotypic activation (a change typically observed in MMVD), and decreased mechanical tension appeared to be a negative regulator of this effect. Moreover, there appears to be heterogeneity in the aVIC population.

4.1 Introduction

Myxomatous mitral valve disease (MMVD) is the most common cardiac disease in dogs and also accounts the leading cause for human mitral valve prolapse (Buchanan, 1977; Connell et al., 2012; Olsen et al., 2010). It has been proven this disease is strongly associated with age (Beardow and Buchanan, 1993; Davies et al., 1978; Whitney, 1974). Affected leaflets have been described as thickened, distorted and less transparent when compared to normal valves, and with myxomatous nodule lesions occur on the valve surface progressing from distal free edge to more proximal region (Buchanan, 1977; Han et al., 2010; Kogure, 1980; Whitney, 1967).

Underlying microstructural alterations on the affected leaflets mainly comprise valve resident cell changes and extracellular matrix (ECM) remodelling. In the case of cells, the most dramatic features are valve endothelium denudation and valve interstitial cell phenotypic transformation (Barth et al., 2005; Black et al., 2005; Corcoran et al., 2004; Disatian et al., 2008; Disatian et al., 2010; Han et al., 2008; Mow and Pedersen, 1999; Prunotto et al., 2010; Rabkin-Aikawa et al., 2004b; Stein et al., 1989). Typical ECM changes in myxomatous valves include collagen abnormalities (Aupperle et al., 2009a; Cole et al., 1984; Hadian et al., 2010; Tamura et al., 1995) and increased proteoglycan (PG) and glycosaminoglycan (GAG) accumulation (Gupta et al., 2009a; Han et al., 2010; Tamura et al., 1995). Resident cellular change and ECM alterations lead to abnormal mechanical properties in diseased valves (Butcher and Nerem, 2007; Richards et al., 2012; Schoen, 2008), and adversely affect valve physiological functions *in vivo*.

To date, the pathogenesis of MMVD is not completely understood. Studies on two highly susceptible dog breeds the Cavalier King Charles Spaniel (CKCS) and Dachshund suggest polygenetic inheritance may play a role in canine MMVD development (Olsen et al., 1999; Olsen et al., 2003a; Swenson et al., 1996). Another study on CKCS identified two potential loci associated with MMVD development (Madsen et al., 2011), but this was not confirmed in a later study (French et al., 2012). Recent study of CKCSs suggests the inheritance component of the disease is mainly affecting the age of onset but not pathological changes (Lu. et al., in press). In

humans, mitral valve prolapse has been found to associate with some general connective tissue disorder such as Marfan syndrome and Ehlers-Danlos syndrome (Grau et al., 2007; Jaffe et al., 1981; Ng et al., 2004; Schoen, 2005). Considering majority of MMVD cases develop through a chronic degenerative process, genetic factors certainly would not be the only contributor. A current hypothesis for myxomatous degeneration is that the lesion is a result of valve leaflet responsive adaption to long-term shear stress damaging on valve endothelium which triggers sub-endothelial VIC activation and ECM remodelling (Corcoran et al., 2004; Durbin and Gotlieb, 2002; Pedersen and Haggstrom, 2000; Prunotto et al., 2010; Stein et al., 1989). However, so far there is no definitive evidence that can clarify whether this disease is initiated from damaged endothelium or from abnormal valve interstitial cells (Corcoran et al., 2004; Han et al., 2013). It has been shown that VIC abnormalities exist in MMVD in respect to cell phenotypic alteration (Black et al., 2005; Disatian et al., 2008; Disatian et al., 2010; Han et al., 2013; Han et al., 2008; Rabkin-Aikawa et al., 2004b) and excessive ECM remodelling (Aupperle et al., 2009c; Disatian et al., 2008; Obayashi et al., 2011; Rabkin et al., 2001). VICs in diseased mitral valve transform from a quiescent fibroblast phenotype into an activated myofibroblast-like phenotype (Black et al., 2005; Disatian et al., 2008; Disatian et al., 2010; Han et al., 2013; Han et al., 2008; Prunotto et al., 2010; Rabkin-Aikawa et al., 2004b). The latter phenotype is usually characterized by expressing the myofibroblast marker alpha smooth muscle actin (α-SMA) and/or an embryonic form of non-muscle myosin heavy chain (SMemb) (Disatian et al., 2008; Disatian et al., 2010; Han et al., 2008; Lester et al., 1992; Rabkin-Aikawa et al., 2004b; Rabkin et al., 2001). Activated VICs have been found to have a number of properties and functions including contractile and force generation (Filip et al., 1986; Mulholland and Gotlieb, 1997; Smith et al., 2007; Stephens et al., 2010a) ECM related synthesis (Disatian 2008; Disatian 2010; Rabkin 2001) as well as migration and proliferation potential in early stage valve injury (Durbin et al., 2005; Durbin and Gotlieb, 2002; Gotlieb et al., 2002; Lester et al., 1993; Lester et al., 1992; Lester and Gotlieb, 1988; Tamura et al., 2000). Matrix metalloproteinases (MMPs) and their tissue inhibitors (TIMPs) secreted by aVICs are major enzymes involved in valve matrix remodelling which play a crucial role in valve ECM dynamics (Aupperle et al., 2009b; Aupperle

et al., 2009c; Disatian et al., 2008; Dreger et al., 2002; Obayashi et al., 2011; Rabkin et al., 2001).

In contrast to increased understanding of the role of VICs in MMVD, the mechanism of how VECs might contribute to the disease is still uncertain. Since endothelium loss is a commonly seen in MMVD, an endothelial damage model has been previously generated and investigated utilising mitral valve organ culture (Lester and Gotlieb, 1988). With endothelium denuding, activated VICs were found to migrate and proliferate in response to the injury (Lester and Gotlieb, 1988). Later studies showed that mitral VICs possess wound repair ability in response to injury by migration, proliferation and secreting ECM components at wound sites (Durbin et al., 2005; Durbin and Gotlieb, 2002; Gotlieb et al., 2002; Lester et al., 1993; Lester et al., 1992; Lester and Gotlieb, 1988; Tamura et al., 2000). Since then there have been no further studies reported using injury mitral valve models.

Tissue engineering is a novel technology in regenerative medicine field, which provides opportunities for developing artificial organs *in vitro*. Apart from clinical orientated development, 3D culture constructs have also been utilised as research models particularly for improving understanding of cell biological behaviour and functions (Butcher and Nerem, 2004, 2006; Dreger et al., 2006; Gibbons et al., 2012; Griffith and Swartz, 2006; Gupta et al., 2008a; Gupta et al., 2008b).

In the present study, primary canine mitral valve cells used to develop a fibrin based 3D valve construct as a research platform to investigate pathogenesis of MMVD. Generally three types of models were generated: healthy VECs-VICs co-culture (Type 1), healthy VECs-diseased VICs co-culture (Type 2) and an endothelium damage model (Type 3). It was hypothesized that (1) Type 1 models possess some features of normal mitral valve, and can be used as a substitute for native tissue in *in vitro* studies; (2) phenotypically, VICs in Type 2 models would be more active, and there would be greater ECM remodelling activity in Type 2 constructs compared to Type 1; and (3) after damaging construct endothelium, VIC activation and migration would occur to repair the wound in Type 3 models.

4.2 Materials and Methods

4.2.1 Cell Source

Canine mitral VECs and VICs were isolated and cultured as described in Section 3.2.1. VEC cultures derived from healthy mitral valves (n=3, 'n' indicates the number of dog mitral valves) were used. While VIC cultures (n=3 respectively) were derived from both healthy and diseased mitral valves (Whitney Grade 1/4-2/4) for construct fabrication. Since age is strongly associated with MMVD disease progression (Davies et al., 1978; Whitney, 1974) and VIC heterogeneity (Stephens et al., 2011), cells were collected from 1.5-5 year old dogs for all cultures to reduce the influence of age. One elderly adult dog was included in the diseased VIC group, this was due to limited sample availability. Because of the same limitation and to control for the variation effect of using individual dogs, pooled cell cultures were used in the later experiment. Identical numbers of cells, at same passage, were derived from each individual culture (n=3-4 for each cell type) and all contributed to each cell pool.

All cells were assessed for the expression of vimentin and CD31, prior to 3D culture, using immunocytochemistry, which was described in Section 3.2.2.3. VEC identity was confirmed by expressing vimentin and CD31, while VICs were defined as positive for vimentin but negative for CD31 (Heaney et al., 2009). VECs at passage 2-3 and VICs at passage 4-7 were used for 3D construct fabrication.

4.2.2 Fibrin Based Canine Mitral Valve Models Fabrication

4.2.2.1 Fibrin/VECs-VICs Co-culture Hydrogel System

Fibrin based canine mitral valve constructs in static culture were produced as described in Section 2.10.1 and 2.10.2. The schematic image below briefly demonstrates the fabrication process (Figure 4.1). Fibrin/VICs constructs were generated by mixing VICs suspension (1 million cells per gel) with fibrinogen, thrombin and $CaCl_2$ solution. Once the solid hydrogel formed, VECs suspension (1, 000 cells/cm^2) was seeded on the upper surface of the Fibrin/VICs gels. The co-culture constructs were maintained in standard tissue culture conditions for 14 days before manipulation or analysis.

Detailed construct types are described in Table 4.1.

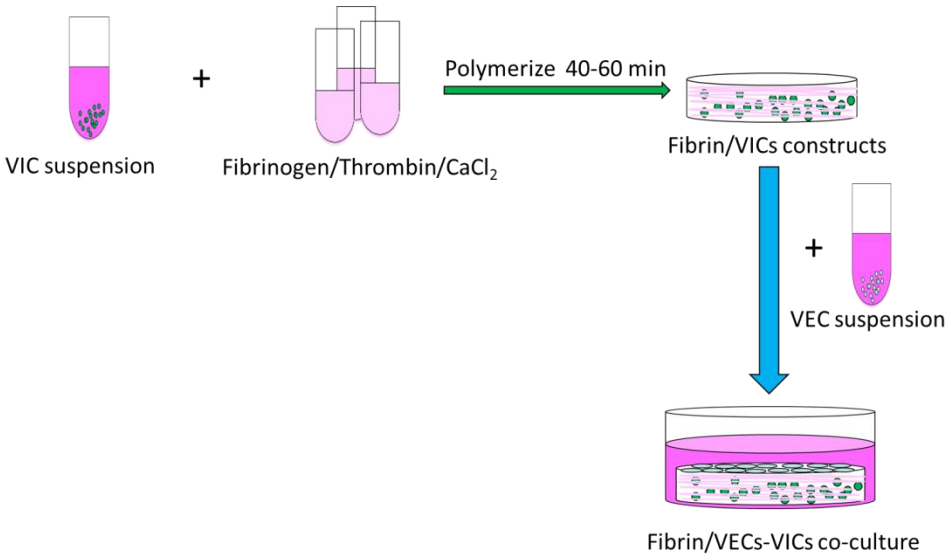

Figure 4.1. Fabrication of fibrin/VECs-VICs 3D co-culture constructs in static culture.

Table 4.1 Types of fibrin based canine mitral valve 3D construct in static culture

Construct Name	Description
Type 1	Healthy VECs-healthy VICs 3D co-culture on fibrin matrix, cultivate for 14 days in standard tissue culture system (static culture).
Type 2	Healthy VECs-diseased VICs 3D co-culture on fibrin matrix, cultivate for 14 days in static culture.
Type 3-A	Healthy VECs-healthy VICs 3D co-culture on fibrin matrix, cultivate for 14 days in static culture. On Day 14, damage the proposed construct endothelium and maintain the construct in static culture for up to 6 days. The constructs attach to culture plate during the entire culture period.
Control-A	Sham control for Type 3-A.
Type 3-F	Healthy VECs-healthy VICs 3D co-culture on fibrin matrix, cultivate for 14 days in static culture. On Day 14, damage the proposed construct endothelium and detach the construct from culture plate to float them, and maintain the construct in static culture for up to 6 days.
Control-F	Sham control for Type 3-F.

4.2.2.2 Experimental Design Comparing Healthy and Diseased Mitral Valve Constructs

Four separate Type 1 and Type 2 experiments were carried out using cells derived from different dogs. Six constructs of each type were fabricated and cultured in one 24 well plate in each experiment. The sample plate arrangement is illustrated in Figure 4.2. Fibrin gels without added cells served as cell free controls. Constructs were harvested after 14 days culture. Two samples of each type were collected and prepared for full panel analysis (illustrated in Figure 4.2). Each construct was divided into four parts each of which was processed as follows: methacarn fixation (histology and immunofluorescence), snap frozen and protein extraction (Western blot), and glutaraldehyde/paraformaldehyde fixation (electron microscopy). Detail of protocols for methacarn fixation, protein extraction and EM sample pre-fixation are described in Section 2.11.2, Section 2.2.1, Section 2.12.1 and Section 2.12.2. Remaining construct samples of each type were pooled and snap frozen as tissue protein stock for Western blot analysis.

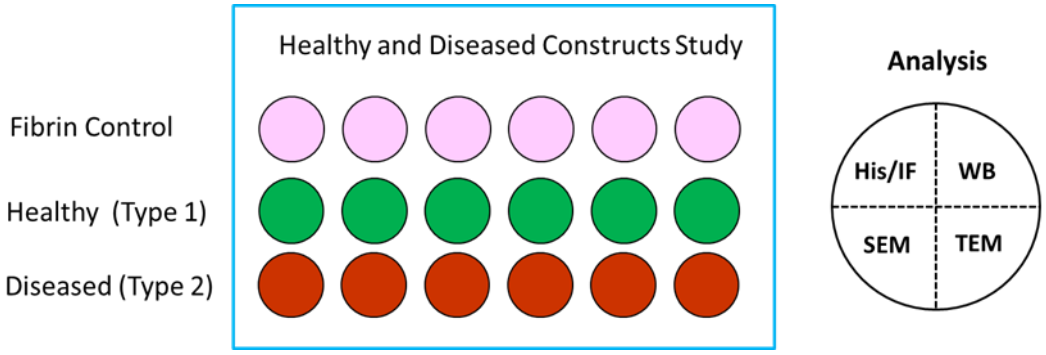

Figure 4.2. Typical culture plate design and analysis plan for Type 1 and Type 2 constructs comparison study. His/IF, histology and immunofluorescence; WB, Western blot; SEM, scanning electron microscopy; TEM, transmission electron microscopy.

4.2.2.3 Experimental Design and Wounding Procedure for Endothelium Damaged Mitral Valve Constructs

4.2.2.3.1 Construct Endothelium Damage

Three separate endothelium wounding experiments were carried out using cells derived from different cultures. Fibrin based healthy VECs-VICs co-culture constructs were made and maintained in static culture for 14 days on one 24 well culture plate. On Day 14, the culture medium was removed and the constructs were rinsed with sterile PBS. The constructs were divided into two groups: intact control and wounded (Type 3). Constructs in the wounded group were manually damaged on their upper surface (presumed endothelium) using the flat end of surgical forceps. Several linear wounds (scratch) were made all through construct endothelium surface. The constructs were rinsed with sterile PBS to remove detached cells before adding fresh culture medium. Both wounded and control constructs were maintained in static culture for 0-6 days. Based on differential manipulation techniques, the Type 3 constructs were further divided into 'adherent' and 'floating' groups.

4.2.2.3.2 Adherent Type 3 Construct and Analysis

Constructs remained attached to the culture plate in the first construct endothelium damage experiment (T3-1). To be differentiated from later Type 3 models, the wounded constructs in T3-1 were designated as adherent Type 3 (Type 3-A). The adherent constructs with intact endothelium served as controls (Control-A). Experimental design of T3-1 is shown in Figure 4.3. One construct pair was collected at Day 0, Day 1, Day 2, Day 4 and Day 6 respectively (Lester and Gotlieb, 1988).

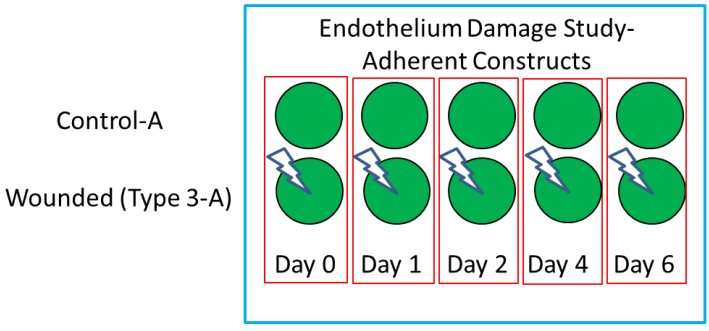

Figure 4.3. Culture plate design of endothelium damage experiment-adherent constructs. Ten healthy constructs were fabricated and divided into two groups. One pair of constructs was collected at each time point (identified in red squares).

Samples were prepared for histology and immunofluorescence study using methods described in Section 2.11.2.

4.2.2.3.3 Floating Type 3 Constructs and Analysis

Generation of floating constructs was not planned as part of the original study design. However, occasionally construct detachment occurred during wounding in the second (T3-2) and third (T3-3) Type 3 experiments. To eliminate potential effects of adherence affecting mechanical tension across the constructs, all constructs including controls were detached from the culture plate using a sterile forceps and lab spatula in T3-2 and T3-3. The endothelium damaged constructs are so called floating Type 3 (Type 3-F). Floated constructs with intact endothelium served as controls (Control-F).

Following on from results from T3-1 experiments, the harvesting time points in later experiments were reduced to three (Day 0, Day 2 and Day 6) as this was most likely to allow identification of the most evident changes as well as to increase repeatability. Sample arrangement and collection plan are shown in Figure 4.4. Two pairs of samples were harvested at each time point. Samples were prepared for histology, immunofluorescence and Western blot using methods described in Section 2.11.2 and Section 2.2.1.

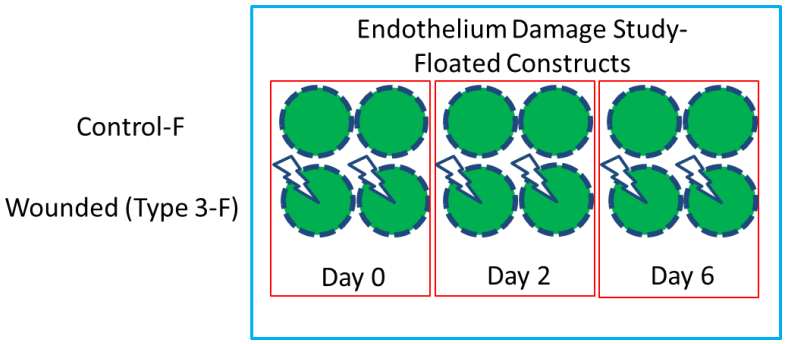

Figure 4.4. Culture plate design for endothelium damage experiment-floating constructs. Twelve healthy constructs were fabricated and divided into two groups. Two sample pairs were collected at each time point (circled in red squares).

4.2.3 Constructs Analysis

4.2.3.1 Histology and Immunofluorescence

Type 1 and Type 2 construct histological features were assessed by hematoxylin and eosin (H&E) staining and Russel-Movat Pentachrome staining. Detailed staining protocols are described in Section 2.11.3 and 2.11.4.

On Day 14 fibrin/VECs-VICs co-culture constructs were assessed for endothelium layer formation using DiI-Ac-LDL labelling and the protocol is described in Section 2.7. Stack images were processed by using Zen imaging software and maximum intensity image was presented.

On immunofluorescence, Type 1, Type 2 and Type 3-F constructs were assessed for activated VIC phenotype and ECM related markers. Healthy canine mitral valve tissue was also assessed for the same marker panel to have a comparison with the Type 1 construct. Type 3-A constructs were only assessed for activated VIC phenotypes. Staining protocol details are described in Section 2.11.6. Antibody information and working concentrations are listed in Table 4.2. Secondary fluorescence-labelled antibodies and working concentrations are the same as used for immunocytochemistry in Table 3.3. Fluorescent image capture and processing was as described in Section 3.2.2.3, and images were captured at x 100 and x 200 magnification.

Table 4.2 Primary antibody source and dilution used for fibrin based constructs analysis using immunofluorescence and Western blot.

Primary antibody	Cat No. and company	WC	
		IF	WB
Anti-vimentin (MM)	V6389, Sigma, USA	1:1600	1: 2000
Anti-SMemb (RP)	Ab24761, Abcam, UK	1:1000	1 in 1000
Anti-α-SMA (MM)	A2547, Sigma, USA	1:200	1 in 1000
Anti-Collagen I and III (RP)	Ab24137, Abcam, UK	1:10	/
Anti-MMP-1 (RP)	Ab38929, Abcam, UK	1:200	1 in 5000
Anti-MMP-3 (RP)	Ab53015, Abcam, UK	1:100	1 in 500
Anti-GAPDH (MM)	CB1001, Calbiochem, Finland	/	1 in 1000

MM, mouse monoclonal; RP, rabbit polyclonal; WC, working concentration; IF, immunofluorescence; WB, Western blot.

4.2.3.2 **Western Blot**

Type 1, Type 2 and Type 3-F constructs were analyzed by using immunoblotting (Western blot) to semi-quantify cell activation and matrix metalloproteinase (MMP) synthesis. Samples derived from four (Type 1 and Type 2) or two (Type 3-F) separate experiments were analyzed. 50mg construct tissue was used for protein extraction. Related experimental protocols for protein extraction and Western blot are described in Section 2.2. Primary and secondary antibody details for Western blot are listed in Table 4.2 and 4.3 respectively.

As sample number of Type 3-F construct was limited, triplicated protein sample loading was carried out in each Western blot experiment to eliminate loading error. The mean value of triplicate sample data is used in the semi-quantification analysis.

Table 4.3 Secondary antibody source and dilution used for construct Western blot

Secondary antibody	Cat No. and company	WC
Polyclonal Rabbit Anti-Mouse Immunoglobulins/HRP	P0260, Dako, Denmark	1 in 1000
Polyclonal Swine Anti-Rabbit Immunoglobulins/HRP	P0217, Dako, Denmark	1 in 3000

WC, working concentration

4.2.3.3 Western Blot Data Semi-Quantification and Statistical Analysis

Protein bands on radiographic film were scanned by using an office photocopier and the protein band intensity was quantified using ImageJ software.

For the comparison of Type 1 and Type 2 models, data was initially semi-quantified by normalizing protein band intensity of interest to internal control GAPDH intensity, then normalised further by calculating the mean value of Type 2/Type 1 ratio for each marker. Statistical analysis was carried out on Type 1 and Type 2 Western blot semi-quantitative data. One way analysis of variance (ANOVA) test was performed to determine the difference between two groups of data. Statistical significance was considered at $p< 0.05$. The results are presented as mean ± standard deviation.

For Type 3-F model, data was initially semi-quantified by normalizing protein band intensity of interest to internal control GAPDH intensity, followed by further normalization to Day 0 control. Sample data directly normalized to Day 0 control without semi-quantified with GAPDH is also shown.

4.2.3.4 Transmission Electron Microscopy (TEM)

Construct samples were prepared for electron microscopy analysis using the protocols stated in Section 2.12. Due to time constrains, only transmission electron microscopy (TEM) analysis has been carried out in examples of the 3D constructs. One sample of the following construct types were used for TEM analysis: Type 1, Type 2, Type 3-F Day 0, Control-F Day 0, Type 3-F Day 6 and Control-F Day 6. The prefixed TEM samples were sent to the Electron Microscopy Service in School of Biological Sciences in the University of Edinburgh, where they were further processed and embedded in resin blocks. A toluidine blue staining was applied and areas of interest were selected in a view of light microscopy images. The sample blocks and selected toluidine blue staining images were sent to Dr. Alexander Black in National University of Ireland, Galway for TEM analysis. Dr. Alexander Black kindly contributed to all TEM image processing and interpretation, and the TEM results in this chapter is based on a summary report provided by Dr. Alexander Black.

4.3 Results

4.3.1 Cell Identity Authentication Prior to 3D Culture

Prior to 3D culture experiment, cell identities were assessed. All individual VEC cultures (n=3) were positive for both vimentin (Figure 4.5) and the endothelial marker CD31 (Figure 4.6), while both healthy and disease VIC cultures (n=3 respectively) were positive for vimentin, but negative for CD31.

Pooled cells were checked with same marker panel and they demonstrated similar marker expression pattern for each individual culture: i.e. on immunofluorescence pooled VECs are CD31+/vimentin+; pooled VICs are CD31-/vimentin+ (Figure 4.7 & Figure 4.8). No apparent differences in cell morphology or abnormal cell death were observed in the pooled cells during culture compared to individual cultures.

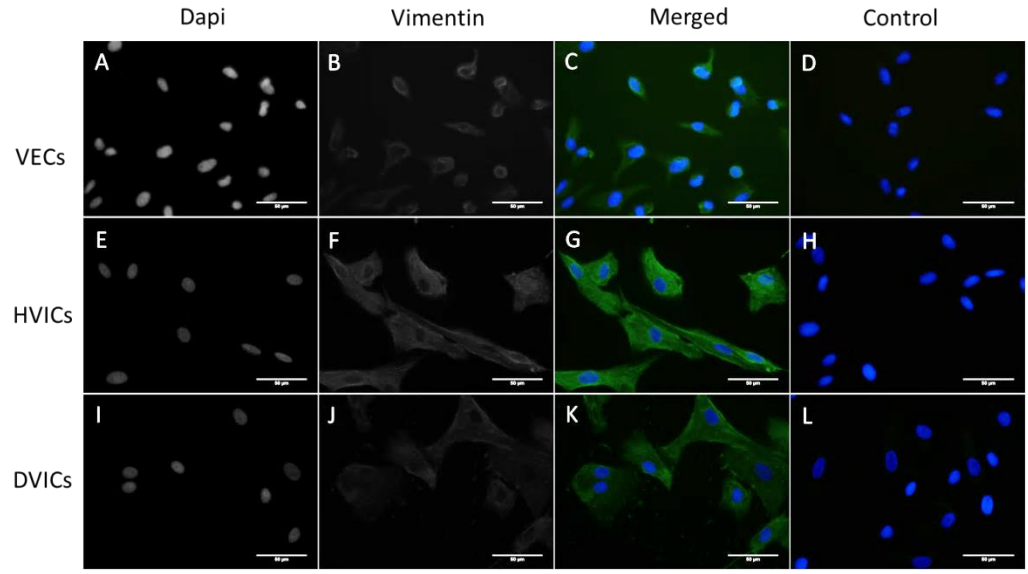

Figure 4.5. Vimentin expression in canine mitral valve cell cultures used for 3D construct fabrication. Vimentin (green) was expressed by VECs (A-C), healthy VICs (HVICs) (E-G) and diseased VICs (DVICs) (I-K). Same cell lines served as negative controls in which vimentin primary antibody was omitted (D, H, L). DAPI (blue) counterstained cell nuclei. Scale bar = 50 µm.

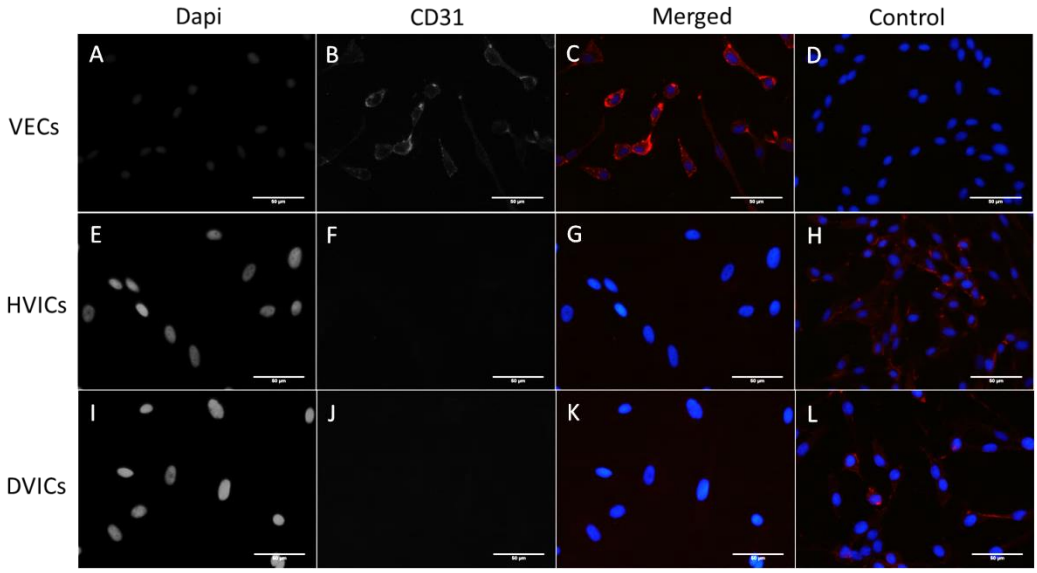

Figure 4.6. CD31 expression in canine mitral valve cell cultures used for 3D construct fabrication. CD31 (red) was expressed by VECs (A-C) but not HVICs (E-G) or DVICs (I-K) in 2D culture. Same VEC cell line served as a negative control on which CD31 primary antibody was omitted (D); cells from a VEC culture expressed CD31 served as a positive control for HVICs and DVICs (H and L respectively). DAPI (blue) counterstained cell nuclei. Scale bar = 50 µm.

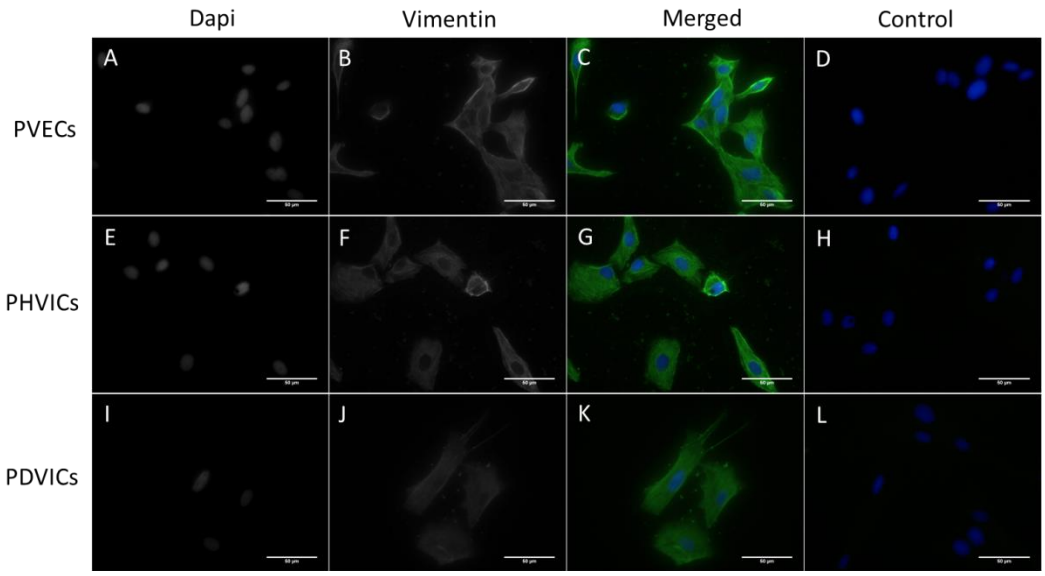

Figure 4.7. Vimentin expression in canine mitral valve cell culture pools used for 3D construct fabrication. Vimentin (green) was expressed by pooled VECs (PVECs) (A-C), pools of healthy VICs (PHVICs) (E-G) and diseased VICs (PDVICs) (I-K). Same cell lines served as negative controls on which vimentin primary antibody was omitted (D, H, L). DAPI (blue) counterstained cell nuclei.

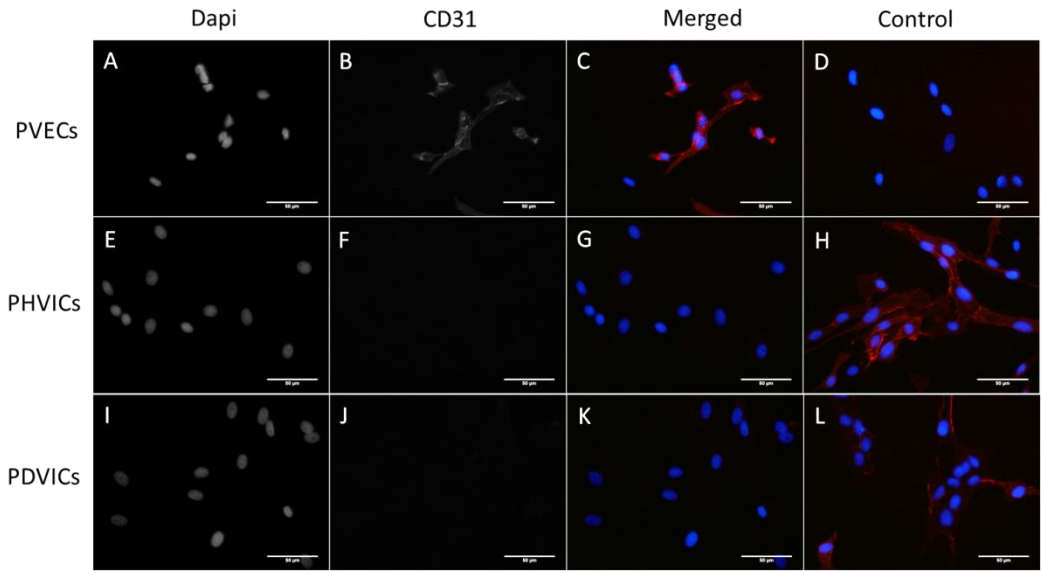

Figure 4.8. CD31 expression in canine mitral valve cell culture pools used for 3D construct fabrication. CD31 (red) was expressed by PVECs (A-C) but not PHVICs (E-G) or PDVICs (I-K). Same PVEC cell line served as a negative control on which CD31 primary antibody was omitted (D); cells from a VEC culture expressed CD31 served as a positive control for PHVICs and PDVICs (H and L respectively). DAPI (blue) counterstained cell nuclei. Scale bar = 50 µm.

4.3.2 General Features of Fibrin Based Canine Mitral Valve Constructs in Static Culture

After 14 days static culture, fibrin based VECs-VICs co-culture mitral valve constructs shrunk in size and exhibited tissue-like morphology, which were less transparent than cell-free fibrin control constructs (Figure 4.9A).

H&E staining showed cells were distributed all through construct thickness, with an even distribution in the construct stroma and a dense cell/matrix layer toward the surface (presumed endothelial layer) (Figure 4.9B). Russel-Movat Pentachrome staining showed there was de novo valve ECM synthesis in the constructs (n=4) (Figure 4.9C). Collagen fibres were detected mainly in the construct stroma, while GAGs production was localized in the loose matrix layer in the immediate sub-endothelial area.

Live constructs without endothelium damage were treated with DiI-Ac-LDL on Day 14 and patchy positive expression was observed on the construct medium contact surface only (n=4) (Figure 4.9D). This is the proposed endothelial layer.

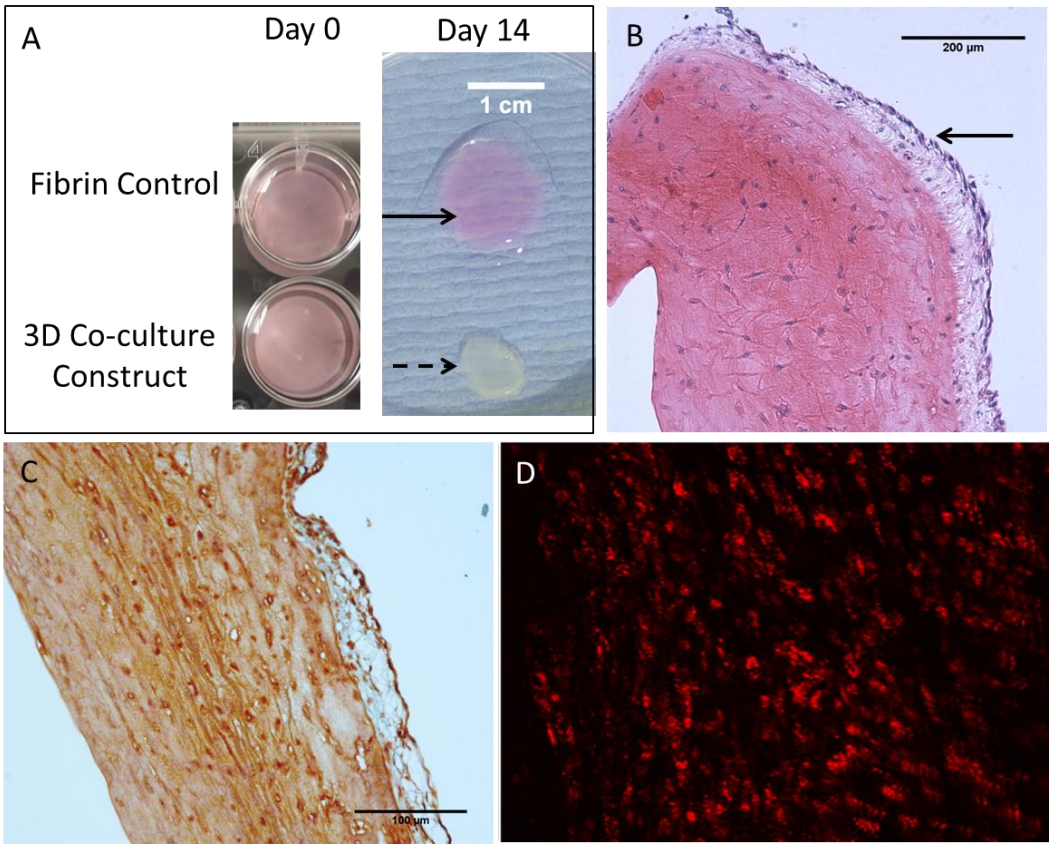

Figure 4.9. Gross morphology of fibrin based canine mitral valve constructs. A. the VECs-VICs co-culture construct (dash arrow) shrunk in size after 14 days culture compared to the cell free control (solid arrow); B. H&E staining shows construct histology, with arrow indicating 'endothelial' surface; C. ECM expression in 3D construct using Movat Pentachrome staining; collagen fibers in stroma (yellow), GAGs in sub-endothelial area (blue to green); D. proposed construct endothelium labelled by DiI-Ac-LDL for identification of endothelial cells, magnification in D: x 200.

Healthy VECs-VICs co-culture constructs (Type 1) were compared with native mitral valves on immunofluorescence. Cell phenotypes and ECM related proteins were evaluated. Positive cells for mesenchymal marker vimentin were evenly distributed all through the thickness of tissue section for both valves and constructs (Figure 4.10A and B). SMemb, an activated mesenchymal marker, was expressed in a similar pattern to vimentin (Figure 4.10C and D). Positive cells were mainly seen in valve/construct stroma whereas endothelium was either negative or exhibited weaker SMemb expression. The expression pattern of α-SMA was different between native valves and constructs. In healthy canine mitral valve, α-SMA expression was limited and mainly localized to the sub-endothelial atrialis layer (Figure 4.10E). While in the Type 1 construct α-SMA was expressed by a number of stroma cells (Figure 4.10F). Usually the most prominent expression was found in the junction area between construct stroma and sub-endothelial dense cell layer, named as 'Stroma-Dense Cell Layer Junction (SDCLJ)' (arrows in Figure 4.10F). The majority of cells in the densely accumulated cell layer and endothelium were negative for α-SMA.

Collagen type I and III are major ECM components in the native heart valve (Aupperle et al., 2009a; Cole et al., 1984; Latif et al., 2005) and mainly resident in the valve fibrosa layer (Figure 4.11A). In the Type 1 construct, weak to moderate collagen I and III expression was found in the stroma on immunofluorescence (Figure 4.11B). The expression was primarily co-localized with cells. A wavy staining pattern was observed on some constructs in the SDCLJ (n=2/6, 'n' indicates the number of the constructs). MMPs are important enzymes involved in valve ECM remodeling. Moderately diffused staining of collagenase MMP-1 was detected in both mitral valve and 3D construct (Figure 4.11C-D). The expression was mainly in valve/construct stroma. Stromelysin MMP-3 was found to be minimally expressed in healthy mitral valve (Figure 4.11E) and in the majority of Type 1 constructs examined on immunofluorescence (n=4/6, 'n' indicates the number of the constructs). Occasional and randomly dispersed MMP-3 positive cells were detected in stroma of the remaining constructs (n=2/6) (Figure 4.11F).

Primary antibody omitted negative controls for each tissue type is shown in Figure 4.12 and only background level of staining was detected.

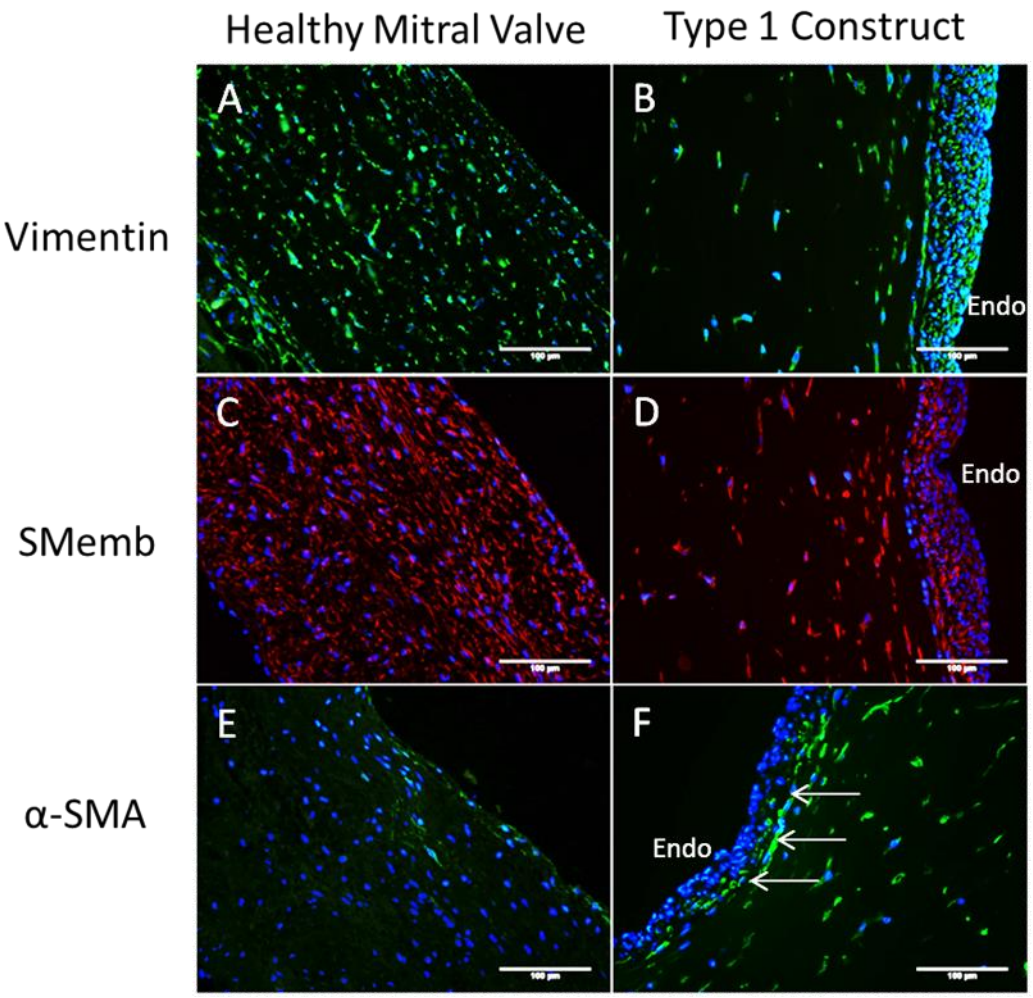

Figure 4.10. Cell phenotypes in canine healthy mitral valve and fibrin based mitral valve construct. Valve cell markers vimentin (green in A and B), SMemb (red in C and D) and α-SMA (green in E and F) expression in canine mitral valves (A, C, E) and 3D constructs (B, D, F). Arrows in F indicate junction area between construct stroma and sub-endothelial dense cell layer, i.e. 'Stroma-Dense Cell Layer Junction (SDCLJ)', where prominent α-SMA is present. Construct endothelium (Endo in B, D and F) was identified as outer surface layer of the densely packed cell layer. DAPI (blue) counterstained cell nuclei. Scale bar = 100 μm.

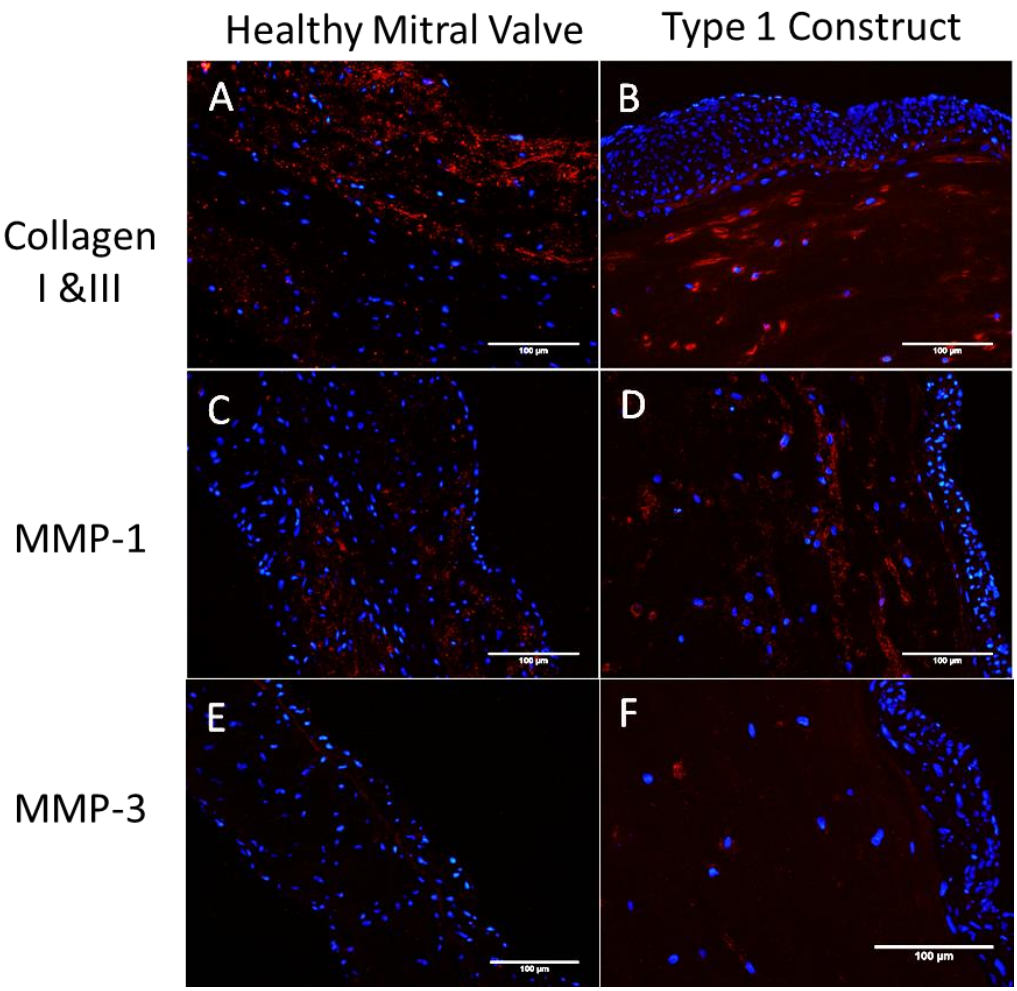

Figure 4.11. ECM related protein expression in canine healthy mitral valve and fibrin based mitral valve construct. Collagen I & III (red in A and B), MMP-1 (red in C and D) and MMP-3 (red in E and F) were expressed in canine mitral valves (A, C, E) and 3D constructs (B, D, F). Construct endothelium was identified as outer cell layer of the densely packed cell layer. DAPI (blue) counterstained cell nuclei. Scale bar = 100 µm.

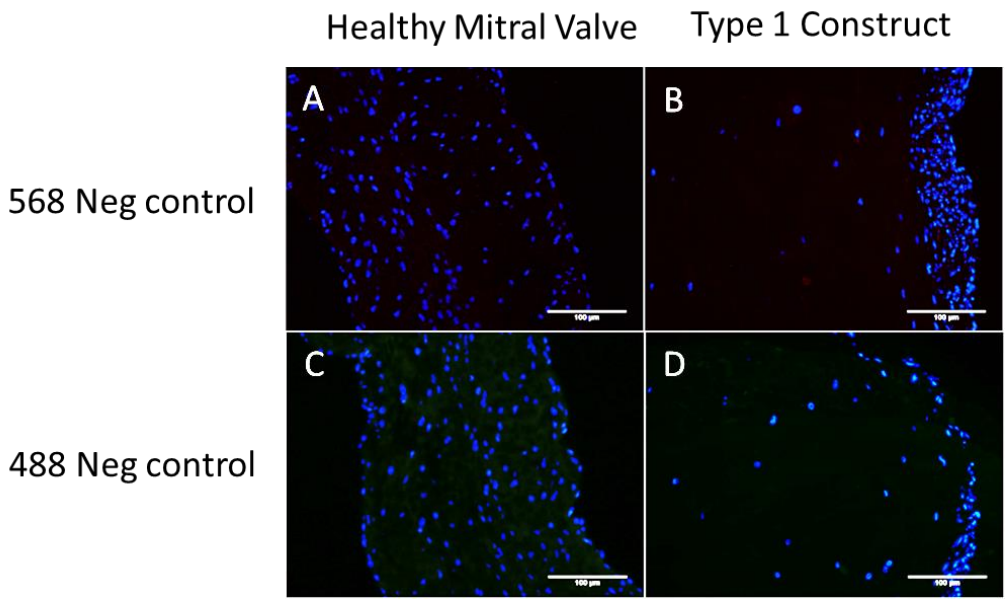

Figure 4.12. Negative controls for healthy mitral valve and fibrin based mitral valve construct tissue using immunofluorescence. With primary antibodies omitted, fluorescence secondary antibody Alexa Fluo568 (A and B) and Alexa Fluo488 (C and D) only stained tissue samples at a background level. Construct endothelium was identified as the outer cell layer of the densely packed cell layer. DAPI (blue) counterstained cell nuclei. Scale bar = 100 µm.

4.3.3 MMVD Related Marker Expression in Healthy and Disease VICs Based Fibrin/VECs-VICs Co-culture Models

Cell phenotype and matrix related synthesis activity (markers in Table 4.2) were compared between proposed healthy (Type 1) and diseased constructs (Type 2) constructs (n=6 respectively). Two samples were derived from one 3D construct fabrication experiment, and three 3D experiments were carried out.

On immunofluorescence, no apparent differential expression pattern was observed between Type 1 and Type 2 constructs. Vimentin was expressed by cells all through construct thickness (Figure 4.13A and B). SMemb exhibited similar expression pattern to vimentin but was predominantly expressed by stroma cells (Figure 4.13C and D). Endothelial cells and the sub-endothelial dense cell layer were also positive for SMemb, but the expression was less pronounced than stroma. In the SDCLJ area, spindle shape cells strongly positive for SMemb were observed in the majority of constructs (n=4/6 respectively) (arrows in Figure 4.13C and D). The expression of α-SMA was mainly found in stromal cells (Figure 4.13E and F). The expression was usually most prominent in SDCLJ area (n=4 respectively) (arrows in Figure 4.13E and F) and was not evident in outer side of the dense cellular layer closest to endothelial surface.

Weak to moderate collagen I and III expression was observed in both construct types and predominantly localized in the construct stroma (Figure 4.14 A and B). The staining was diffuse and some of which was localized close to cells. On some constructs, wavy collagen staining was seen in the SDCLJ area (data not shown). MMPs expression was usually associated with cells. MMP-1 was found to be expressed mainly in construct stroma (Figure 4.14 C and D). Occasionally, positive cells were found in construct endothelium (n=2/6). MMP-3 expression was not apparent in the majority of Type 1 and Type 2 constructs examined by immunofluorescence (n=4/6 respectively) (Figure 4.14 E and F). Occasionally, weak to moderate MMP-3 expression was found in stromal cells (n=2/6 respectively) (Data not shown).

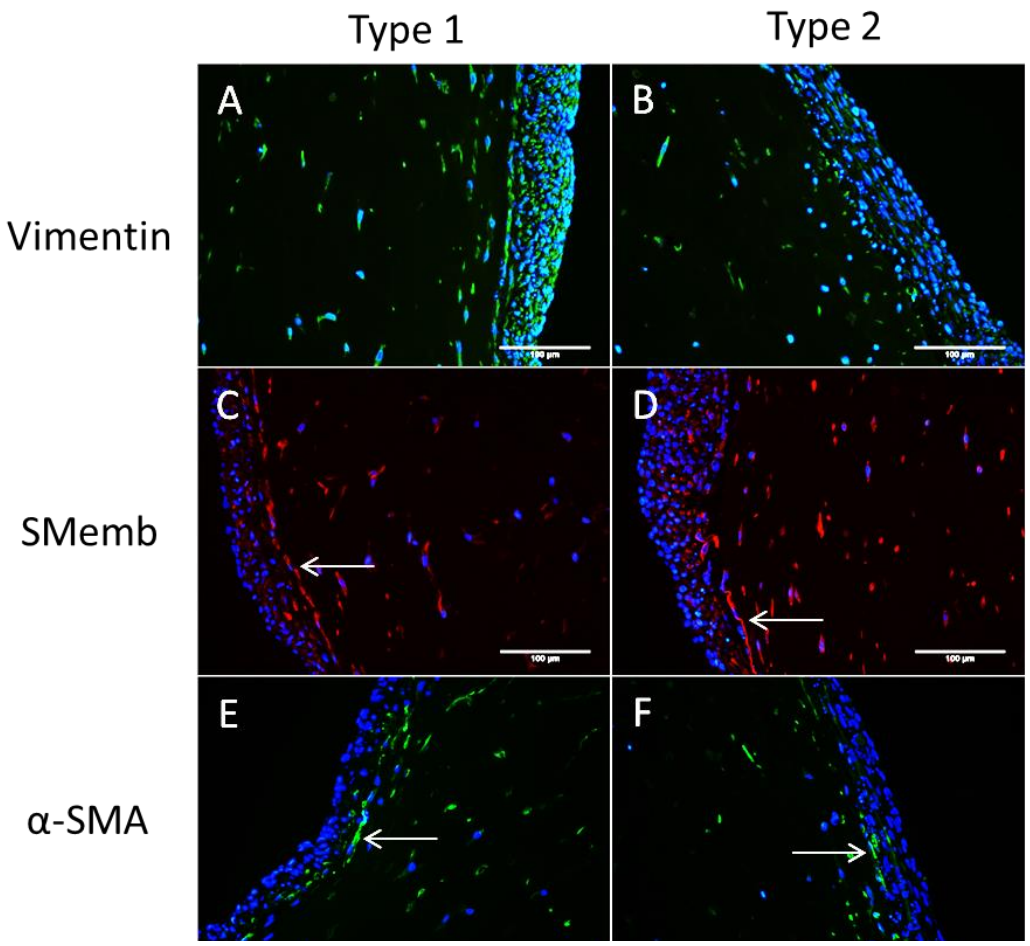

Figure 4.13. Cell phenotype marker expression in Type 1 and Type 2 constructs. In general, similar cell phenotypic distribution was observed in the two construct types. Vimentin positive cells (green in A and B) were found all through construct depth in Type 1 (A) and Type 2 (B) constructs. SMemb (red in C and D) expression pattern was similar to vimentin in Type 1 (C) and Type 2 (D). A linear cluster of spindle-shaped positive cells were identified on some constructs (arrows in C and D). Prominent α-SMA (green in E and F) expression was generally seen in the SDCLJ area (arrows in E and F). Positive cells were also found in the deep stroma, but not commonly on the outer side of the densely packed cell layer. Construct endothelium was identified as the outer surface of the densely packed cell layer. DAPI (blue) counterstained cell nuclei. Scale bar = 100 µm

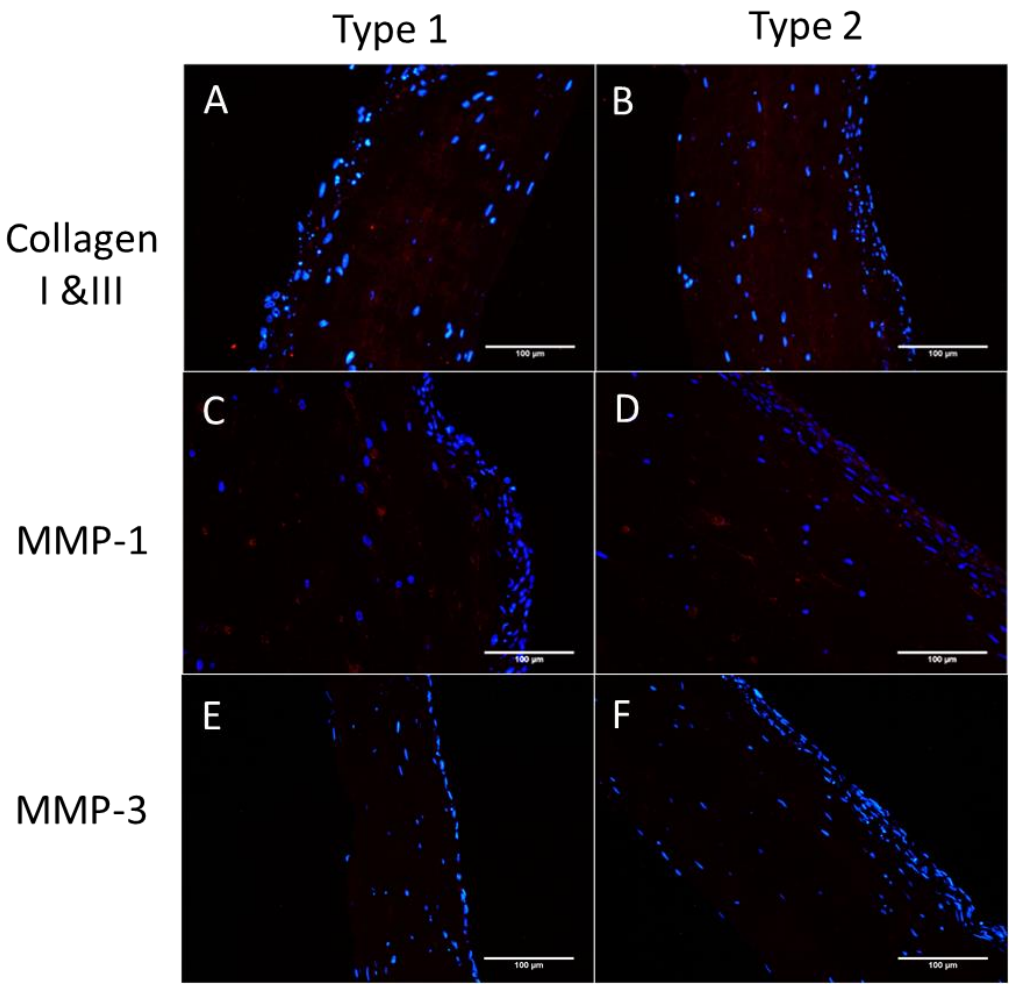

Figure 4.14. ECM related protein expression in Type 1 and Type 2 constructs. Weak Collagen I&III (red in A and B), MMP-1 (red in C and D) and minimal MMP-3 (red in E and F) expression was found in Type 1 (A, C, E) and Type 2 construct (B, D, F). No clear differences in expression were observed between the two types. Construct endothelium was identified as the outer surface of the densely packed cell layer. DAPI (blue) counterstained cell nuclei. Scale bar = 100 µm.

Primary antibody omitted negative control for each tissue type is shown in Figure 4.15. Only background level of staining was detected.

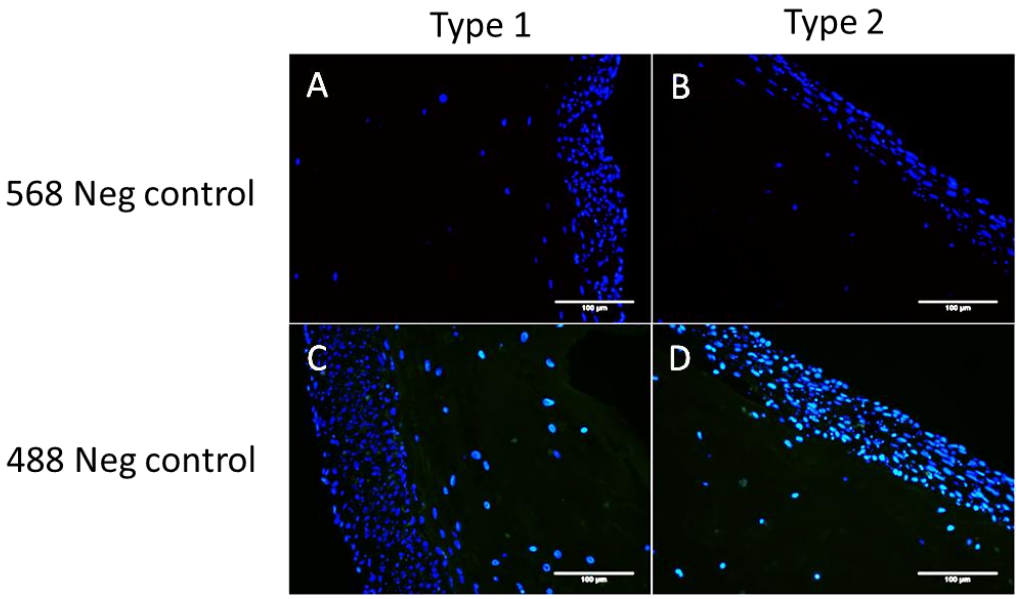

Figure 4.15. Negative controls for Type 1 and Type 2 constructs using immunofluorescence. With primary antibodies omitted, fluorescence secondary antibody Alexa Fluo568 (A and B) and Alexa Fluo488 (C and D) only stained tissue samples at the background level. Construct endothelium was identified as the outer surface of the densely packed cell layer. DAPI (blue) counterstained cell nuclei. Scale bar = 100 µm.

The endothelial marker CD31 was used to label construct endothelium using immunofluorescence. However, no obvious expression was detected in both native valve tissue and constructs using current immunofluorescence protocols. Nevertheless, on Western blot CD31 protein was detected in native mitral valve tissue and in all constructs examined, but the expression varied between different batches of constructs (Figure 4.16).

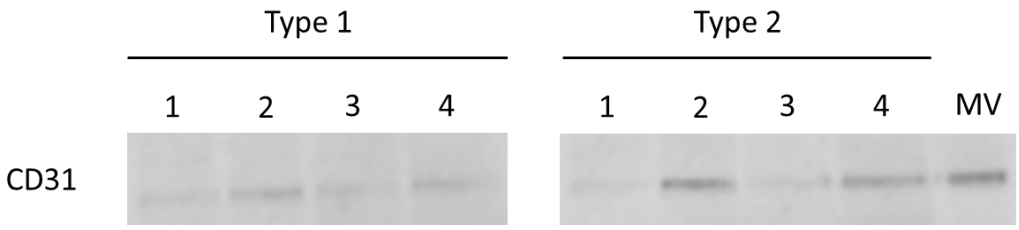

Figure 4.16. Variable CD31 (130 kDa) expression was detected in Type 1 and Type 2 constructs on protein immunoblotting (Western blot). Samples were collected from four separate experiments. Equal amount of total protein was loaded for each sample. Native mitral valve (MV) sample served as a positive control.

Construct cell phenotype and matrix degradation activity was also assessed using Western blot (Figure 4.17). Target protein band intensity did not show substantial difference between Type 1 and Type 2 constructs. Semi-quantitative analysis showed there was no statistically significant difference (P>0.01) in expression of MMP-1, MMP-3, SMemb, α-SMA and vimentin between two construct types.

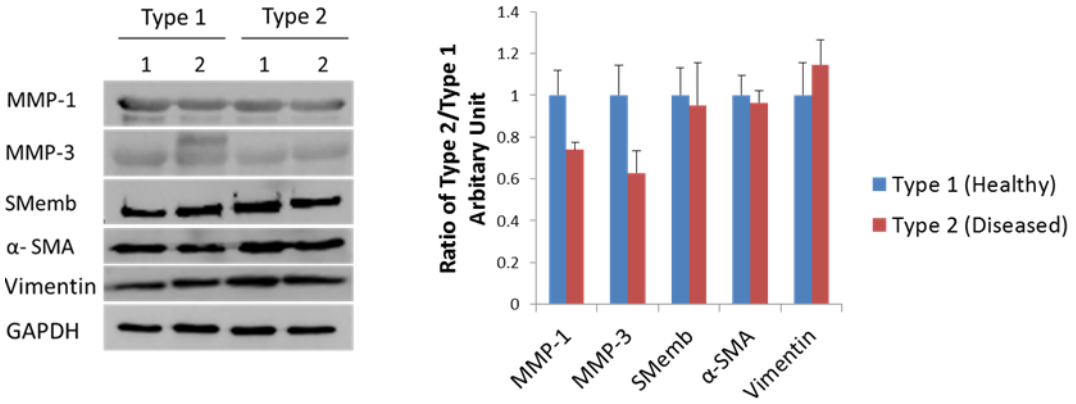

Figure 4.17. Representative images (results of two experiment runs) of MMVD related marker expression in Type 1 and Type 2 constructs on Western blot. Healthy and diseased VIC based constructs expressed MMVD associated markers MMP-1 (54 kDa), MMP-3 (54 kDa), SMemb (200 kDa) and α-SMA (42 kDa) at similar levels (n=4). Vimentin (58 kDa) served as an internal control for cells of mesenchymal origin. GAPDH (36 kDa) served as a loading control. Data was initially semi-quantified by normalizing protein band intensity of interest to GAPDH intensity, then normalised further by calculating the mean value of Type 2/Type 1 ratio for each marker and the data are presented in the column diagram. One way ANOVA analysis (n=4) confirmed that statistically no significant difference was detected between the two groups in all above markers examined (P>0.1).

4.3.4 The Ultrastructure of Healthy and Disease VICs Based Fibrin/VECs-VICs Co-culture Models

The ultrastructure of one Type 1 and Type 2 samples was examined by using TEM in a limited sample. Cells within both construct types were variable in morphology and the proposed construct endothelium appeared to be abnormal, either presenting atypical endothelial cells or showing evidence of cell degradation. Cell activation and de novo ECM production, as well as cell degeneration was detected in both construct types. Incomplete intercellular connections of the VICs were also observed.

In detail, live cells with variable morphologies were identified in the Type 1 construct medium contact surface (proposed endothelium). An elongated cell (Figure 4.18A and B) was found highly activated displaying a complex folded nucleus with a high degree of euchromatin and contained large rough endoplasmic reticulum (rER) in the peri-nulcear region and substantial mitochondria at one edge. Incomplete basement membrane was also seen in the same cell. All the above cellular features typically are not seen in endothelial cells. Some ECM components were seen at the base of the cell possibly produced by the cell itself. Cell degeneration (apoptosis/necrosis) (Figure 4.18C) was also suggested in the proposed endothelium layer by the presence of cellular organelle remnants and peripheral chromatin aggregation in the cell nucleus. Deep to the cell, there was large accumulation of fibril-form ECM interspersed with cellular organelle remnants. The boundary between fibrin matrix and cell derived ECM were clearly seen. While in the Type 2 construct, no cells were observed on the proposed endothelium in the selected area of this single specimen (Figure 4.18D). However, degraded cellular fragments were commonly seen.

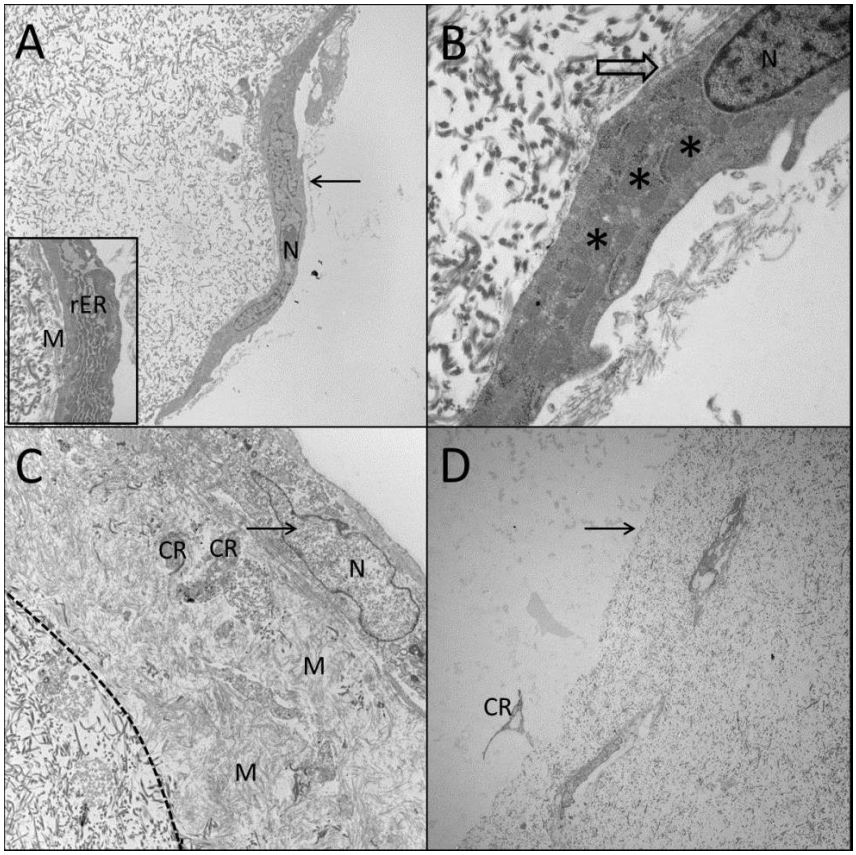

Figure 4.18. The ultrastructure of proposed endothelium in Type 1 and Type 2 constructs. A. An elongated active cell was observed in proposed endothelium (arrow in A) of the Type 1 construct. The inset image at high magnification showed well-developed rER and possibly cell-derived ECM were associated with the cell. Accumulation of mitochondria (*in B) and patchy basement membrane (hollow arrow in B) were observed in the same cell. Possible cell-derived ECM was seen at the base of the cell (M in A); C. Cell degeneration in the proposed endothelium of the Type 1 construct. Peripheral chromatin aggregation in cell nucleus was observed (arrow in C). Substantial fibril ECM accumulated deep to this cell (M in C), with cellular remnants interspersed (CR in C). A clear boundary between fibrin matrix and de novo ECM (dash line in C) was observed. In the Type 2 construct, no viable cells were present in the proposed endothelium surface (arrow in D), however dead cell fragment was seen (CR in D). N, cell nucleus; rER, rough endoplasmic reticulum; M, extracellular matrix; CR, cell remnant. Magnification in A, 4000 x; in inset image of A and in B, 20,000 x; in C, 5,000 x; and in D, 2,000 x.

The VICs in both construct types were variable in morphology, particularly in the Type 1 construct. The VIC intercellular connection was commonly seen in the Type 1 model (Figure 4.19A and B). A ‘lumen’ appearance formed by some connected cells may suggest a degree of angiogenic activity. These cells appeared to be highly active in matrix synthesis; well-developed rER network was observed and the cell was surrounded by ECM elements and patchy basement membrane. The VICs in the Type 2 construct were either active or appeared to undergo degeneration. Similar to the VICs in the Type 1 construct, not well formed intercellular junctions were seen in some cells in close proximity to each other in the Type 2 (Figure 4.19C). Cell degradation was noticed within the connected cells. De novo ECM production was also seen to be associated with the active cells (Figure 4.19D). Some of the VICs were elongated suggesting the presence of a more “smooth muscle” cell phenotype, though most cells in the construct were compact. Some degraded cellular fragments were observed in both construct types.

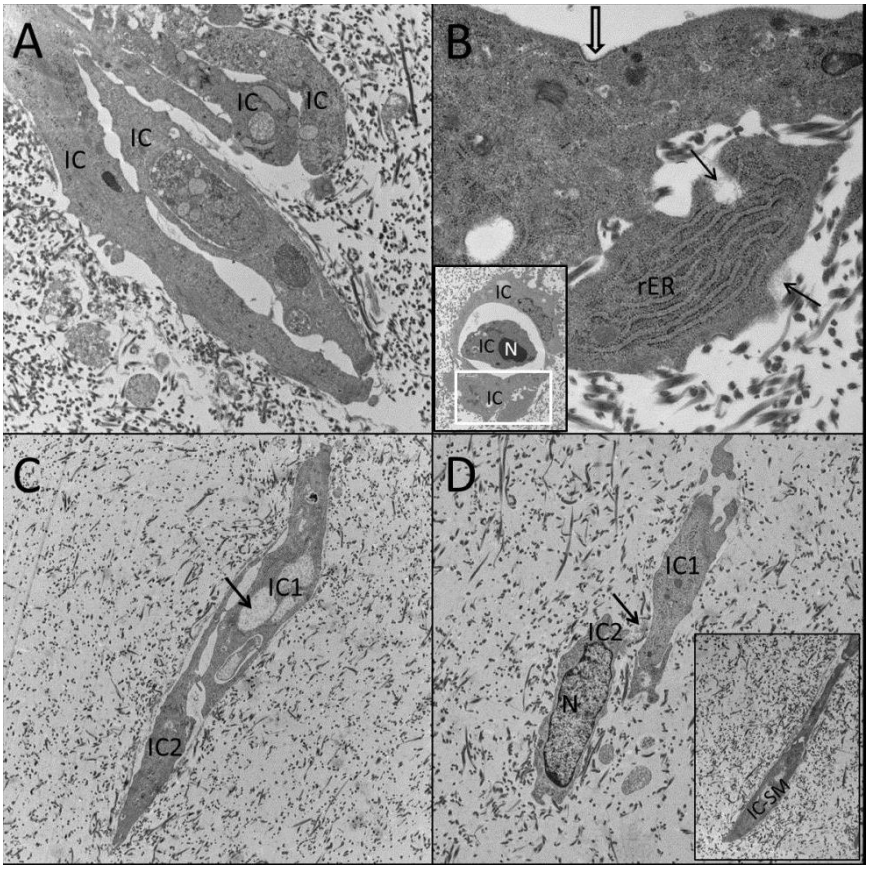

Figure 4.19. The ultrastructure of the VICs in the Type 1 and Type 2 constructs. A. Intercellular connections were noticed in the Type 1 construct. A 'lumen' cell arrangement pattern (inset image in B) was observed. The cell in the lumen was in apoptosis and the interconnected cells appeared to be highly active. High magnification image of the cell in the white box inset is shown in B. Well-developed rER, ECM synthesis (solid arrows in B) and patchy basement membrane (hollow arrow in B) were identified in the cell. C. The incomplete intercellular connections of VICs were also identified in the type 2 construct. The upper cell (IC1 in C) appeared to have abnormal cellular organelles and vacuolae (arrow in C) in cytoplasm indicating degradation. D. Active VICs in the Type 2 construct. A large nucleus with high euchromatin/heterochromatin ratio and de-novo ECM (arrow in D) was seen in one cell (IC2 in D). Highly attenuated cell morphology (IC-SM in the inset of D) suggested a smooth muscle phenotype. IC, interstitial cells; N, cell nucleus; rER, rough endoplasmic reticulum; IC-SM, smooth muscle phenotype interstitial cell. Magnification in A, 8,000 x; in B 20,000 x; in C 5,000 x; in D 7,000 x and in insets, 6,000 x.

4.3.5 Cell Activity Assessment in Endothelium Wounded Model

4.3.5.1 Gross Morphology Alteration

In endothelium wounding experiments, construct morphology altered after manipulation on macroscopic evaluation (Figure 4.20). In the wounded/adherent experiment (T3-1), Type 3-A constructs contracted usually within one to two days after insult, whereas on gross morphology adherent control constructs (Control-A) showed consistent morphology over the 6 day period. In wounded/floating experiments (T3-2 and T3-3), contraction occurred in both the control (Control-F) and wounded constructs (Type 3-F). Similar to the adherent constructs, the most dramatic change was in the first two days after detachment and endothelium damage, although the floating constructs appeared to have a more curled edge appearance. Construct morphology then remained stable on after 48 hours.

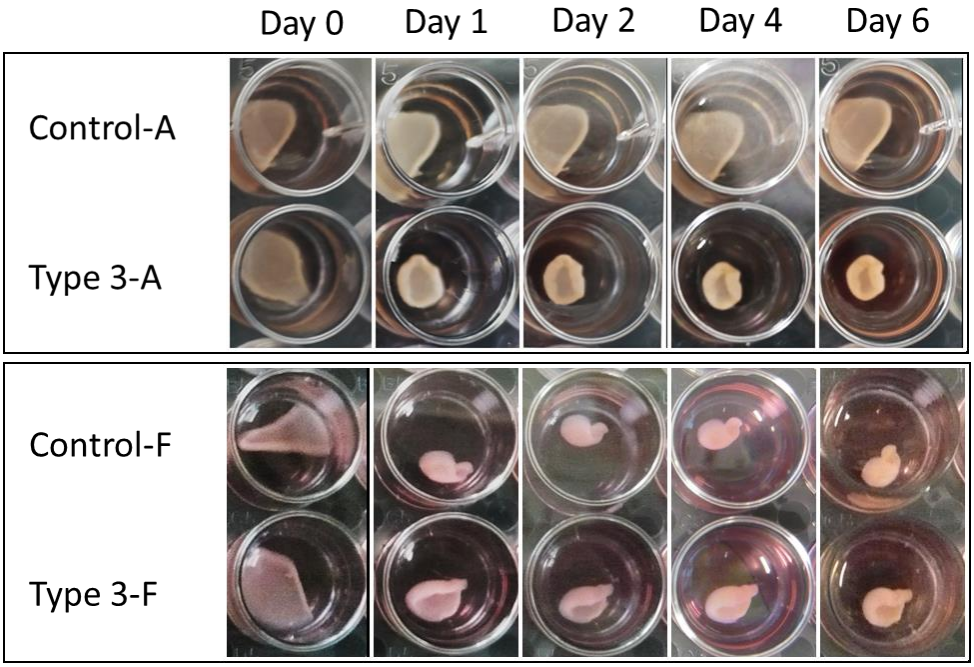

Figure 4.20. Gross morphology of adherent and floating Type 3 constructs and controls in culture after manipulation. Control-A construct showed consistent morphology during the 6 day period (Row 1). Type 3-A (Row 2), Control-F (Row 3) and Type 3-F (Row 4) all showed contraction within the first two days.

4.3.5.2 SMemb Expression in Adherent Wounded Constructs

In adherent wounded constructs (Type 3-A), α-SMA and SMemb were evaluated as indicative markers for VIC activation on immunofluorescence. Construct samples collected at Day 0, Day 1, Day 2, Day 4 and Day 6 were examined. The expression of α-SMA was not detected in all construct samples as well as in the positive control tissue (diseased canine mitral valve) (data not shown). However, increased SMemb expression was observed in Type 3-A constructs collected on Day 1, Day 2 and Day 6 post wounding. Type 3-A constructs from Day 2 and Day 6 demonstrated most prominent SMemb up-regulation (Figure 4.21).

In details, on Day 0, minimal to weak SMemb expression was observed in both Control-A (Figure 4.21A) and Type 3-A constructs (Figure 4.21B), with the latter having slightly higher level of expression. No expression was observed in the endothelium or wounded surface. On Day 1, SMemb expression in Type 3-A (Figure 4.21D) appeared to be more intense than Control-A (Figure 4.21C). On Day 2, Control-A constructs showed weak to moderate SMemb expression in endothelium and construct stroma (Figure 4.21E), while in Type 3-A, higher SMemb expression was observed primarily in an area subjacent to the wounded surface (Figure 4.21F). On Day 4, limited SMemb expression was observed in both Control-A (Figure 4.21G) and Type 3-A (Figure 4.21H). On Day 6, SMemb expression was minimal in Control-A construct (Figure 4.21I) while the expression in Type 3-A construct was much greater particularly in the area closed to the wounded edge (Figure 4.21J).

Primary antibody omitted negative control for each sample was shown in Figure 4.22. Only background level of staining was detected with Alexa 568 fluorescent antibody alone.

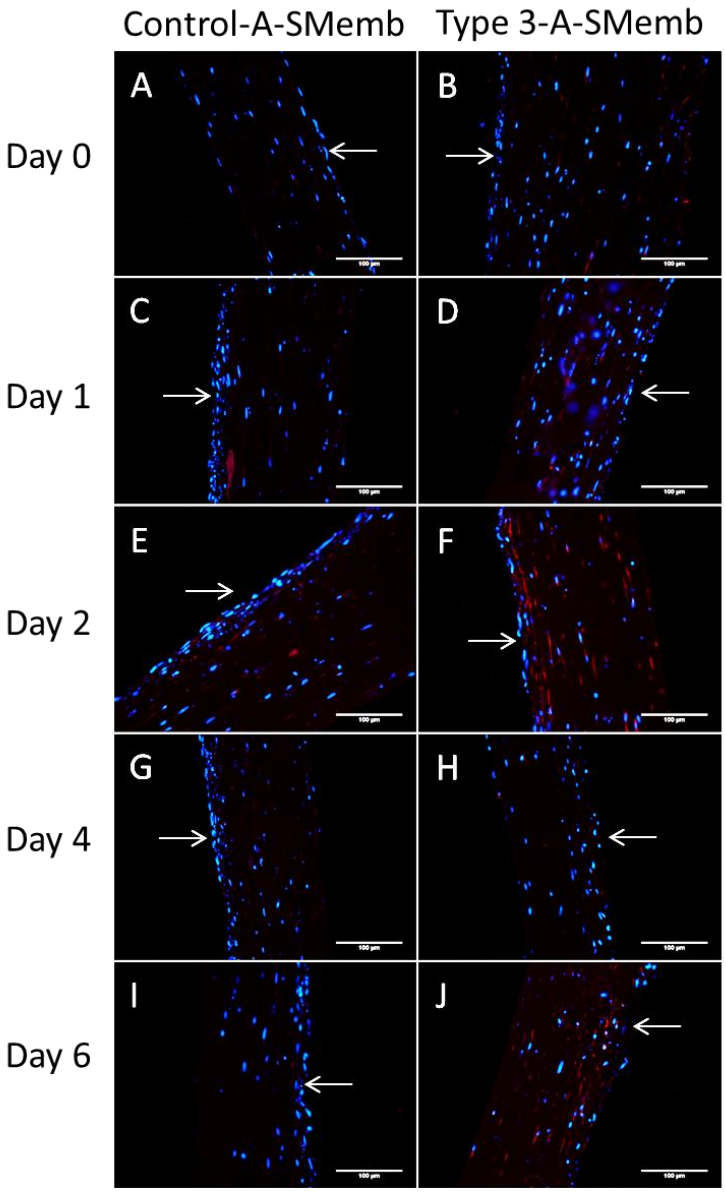

Figure 4.21. SMemb up-regulation in adherent Type 3 constructs. On Day 0, minimal to weak SMemb (red) expression was observed in both control (A) and Type 3-A (B). On Day 1 slightly higher SMemb expression was observed on Type 3-A (D) than Control-A (C). On Day 2, Type 3 constructs showed clear up-regulation of SMemb (F) subjacent to the wounded surface compared to Control-A (E). On Day 4, minimal expression was detected in both construct types (G and H). On Day 6, higher SMemb expression was observed on Type 3-A particularly towards the wounded surface (J) compared to Control-A (I). White arrows indicating construct endothelium or wounded surface. DAPI (blue) counterstained cell nuclei. Scale bar = 100 µm.

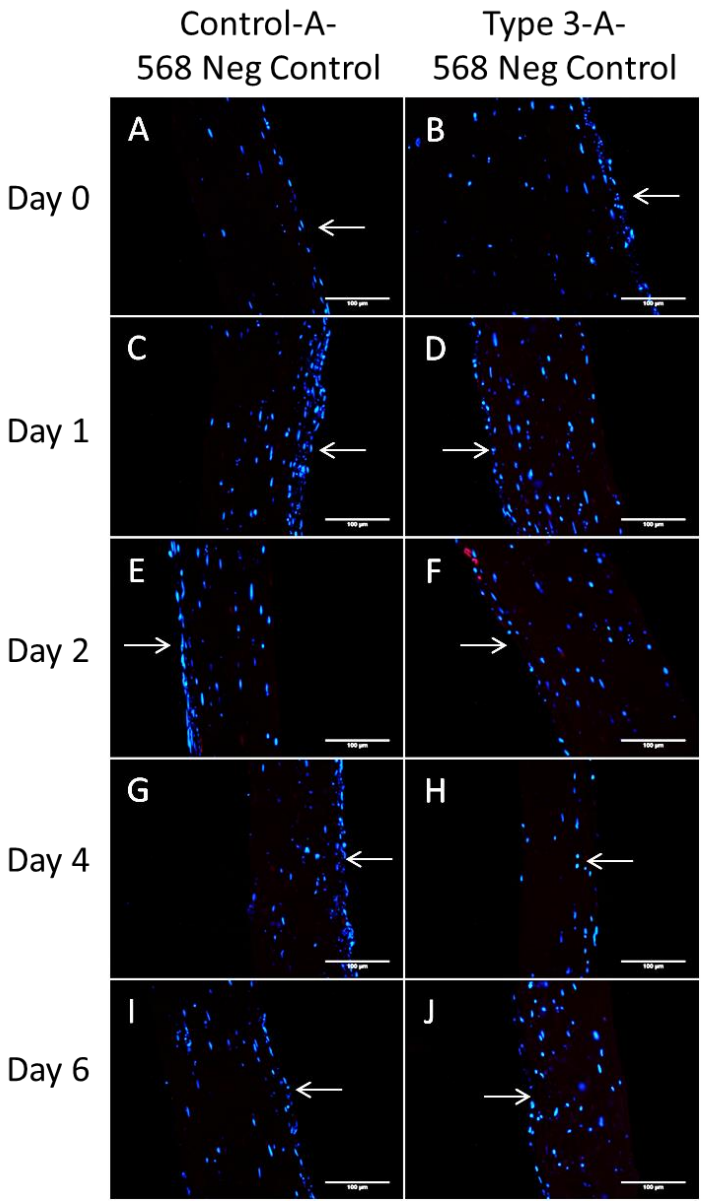

Figure 4.22. Negative controls for SMemb expression in adherent Type 3 and control construct on immunofluorescence. With SMemb primary antibody omitted, fluorescence secondary antibody Alexa Fluo568 only stained Control-A (A, C, E, G, I) and Type 3-A (B, D, F, H, J) constructs at background level. White arrows indicating construct endothelium or wounded surface. DAPI (blue) counterstained cell nuclei. Scale bar = 100 µm.

4.3.5.3 **Alteration of Cell Activity on Floated Wounded Constructs**

To evaluate cell phenotypic activation on Type 3-F constructs, construct protein was probed with α-SMA, SMemb and vimentin antibodies using Western blot. Construct sample collected on Day 0, Day 2 and Day 6 were analyzed. In general, reduced expression of the activated VIC makers SMemb and α-SMA was observed on Day 2 and Day 6 compared to Day 0 (Figure 4.23.1 and 4.23.2). Vimentin expression was in a similar pattern. There were no differences between Control-F and Type 3-F constructs. Although protein expression was not identical between two experiments (T3-2 & T3-3), α-SMA and SMemb expression was similar in the same sample when comparing each sample with Day 0 control (without normalizing to GAPDH) (Figure 4.23.2).

GAPDH was used as a loading control for Type 3-F constructs Western blot, however it was noticed that the expression of GAPDH was not consistent between samples (Figure 4.23.1). When proteins of interest were normalized to GAPDH, expression trends altered dramatically compared to data without normalization (Figure 4.23.2). Triplicate experiments confirmed GAPDH inconsistent expression and the expression pattern was similar in each repeat. This suggested the GAPDH inconsistency was less likely due to a technical error. Other common loading control proteins such as β-actin and α-tubulin were also tried in the current study (data not shown), but GAPDH expression appeared to be the most consistent among the three.

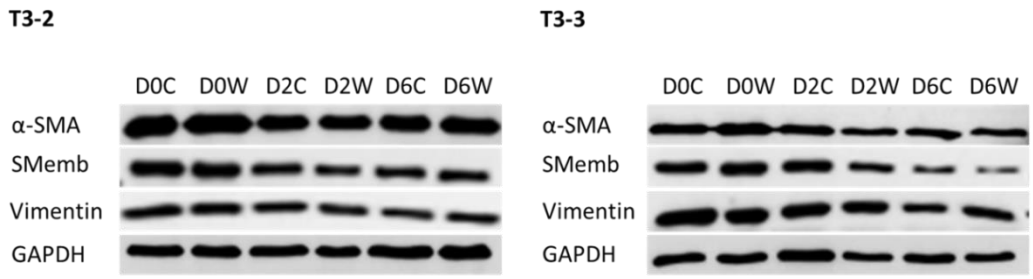

Figure 4.23.1. Cell phenotypic alteration in floating Type 3 constructs on Western blot. Data for construct samples derived from two independent 3D experiments are shown (T3-2 and T3-3). A decreasing trend for α-SMA and SMemb expression was observed as culture time increased. D0, Day 0; D2, Day 2; D6, Day 6; C, Control-F; W, Type 3-F.

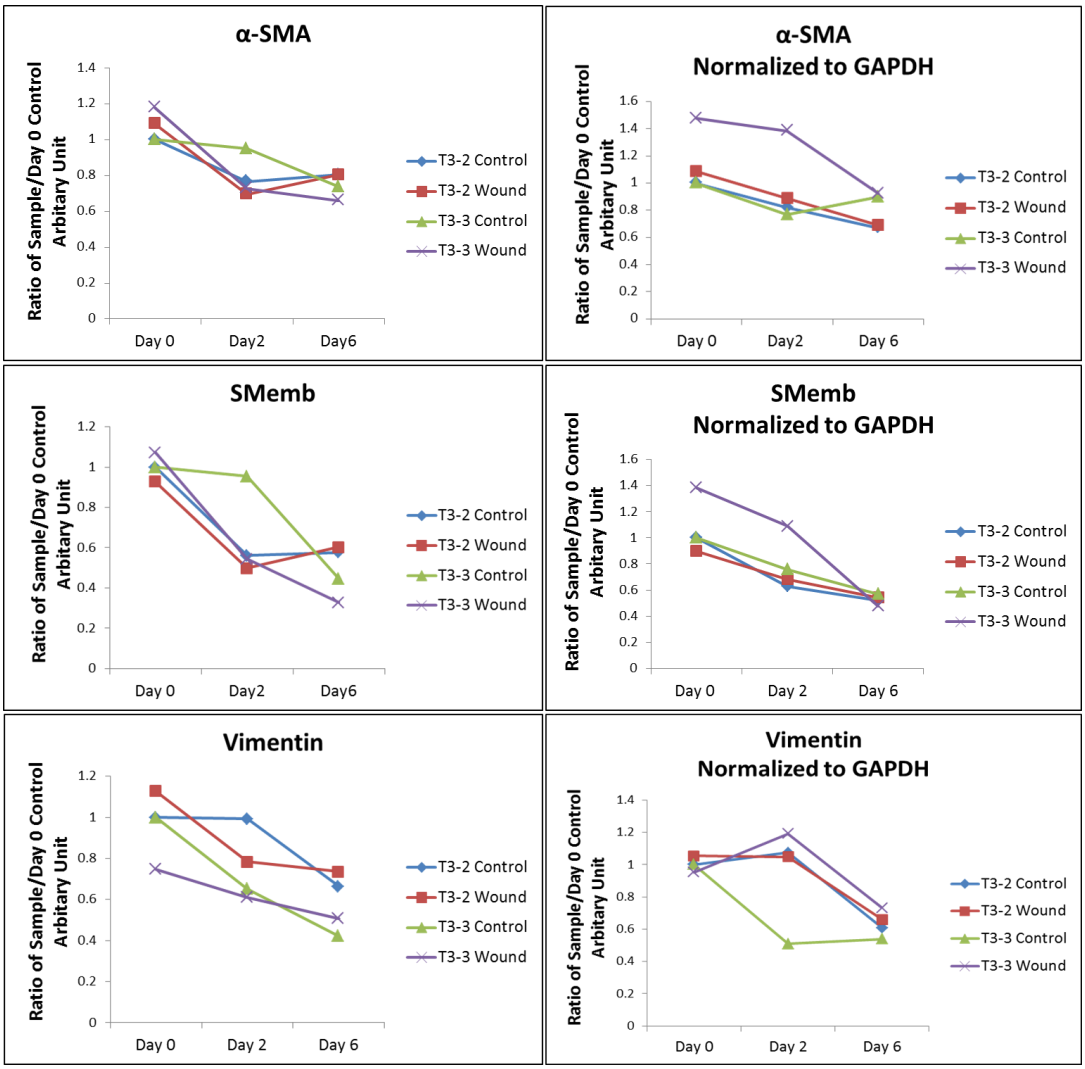

Figure 4.23.2. Tendency for changes in cell phenotypic markers in floating Type 3 constructs (Western blot data). Mean value (n=3, n' indicates the number of the construct protein sample in each Western blot experiment) of each sample/Day 0 control ratio is shown. Consistent with the visual examination of immunoblots, there was a decreasing trend observed in α-SMA and SMemb expression in both Type 3-F and Control-F constructs at the different time-points. Vimentin expression was also decreased. Left panels show neat protein levels, while Right panels shows protein levels after normalization to GAPDH.

Cell phenotypic markers for Type 3-F and Control-F constructs were identified on immunofluorescence. Though expression varied between each individual sample, and for 4/12 constructs there was absence of endothelium/dense cellular layer making it difficult to identify the construct wound surface, a general description of any alteration can be summarized as follows. The overall expression of α-SMA and SMemb in floating construct was consistent with Western blot data, however the expression patterns were distinct for the two markers.

On Day 0 Control-F constructs expressed α-SMA in the construct stroma, sub-endothelial dense cell layer and typically prominent expression was found at the SDCLJ (Figure 4.24A). Day 0 Type 3-F constructs exhibited similar α-SMA expression pattern to the control and occasional positive cells were also observed on the wounded surface (Figure 4.24B). By Day 2 and Day 6, α-SMA positive cell numbers were markedly decreased in both Type 3-F and Control-F constructs (Figure 4.24C-F). At this stage positive cells were mainly distributed in the construct stroma. A few positive cells were identified in SDCLJ area in some samples (arrow in Figure 4.24C). No apparent differential expression was observed between Control-F and Type 3-F constructs, except for one wounded sample derived from T3-2 which showed prominent expression on the wounded surface and the subjacent area (data not shown).

Primary antibody omitted negative control for each tissue sample is shown in Figure 4.25. Only background level of staining was detected.

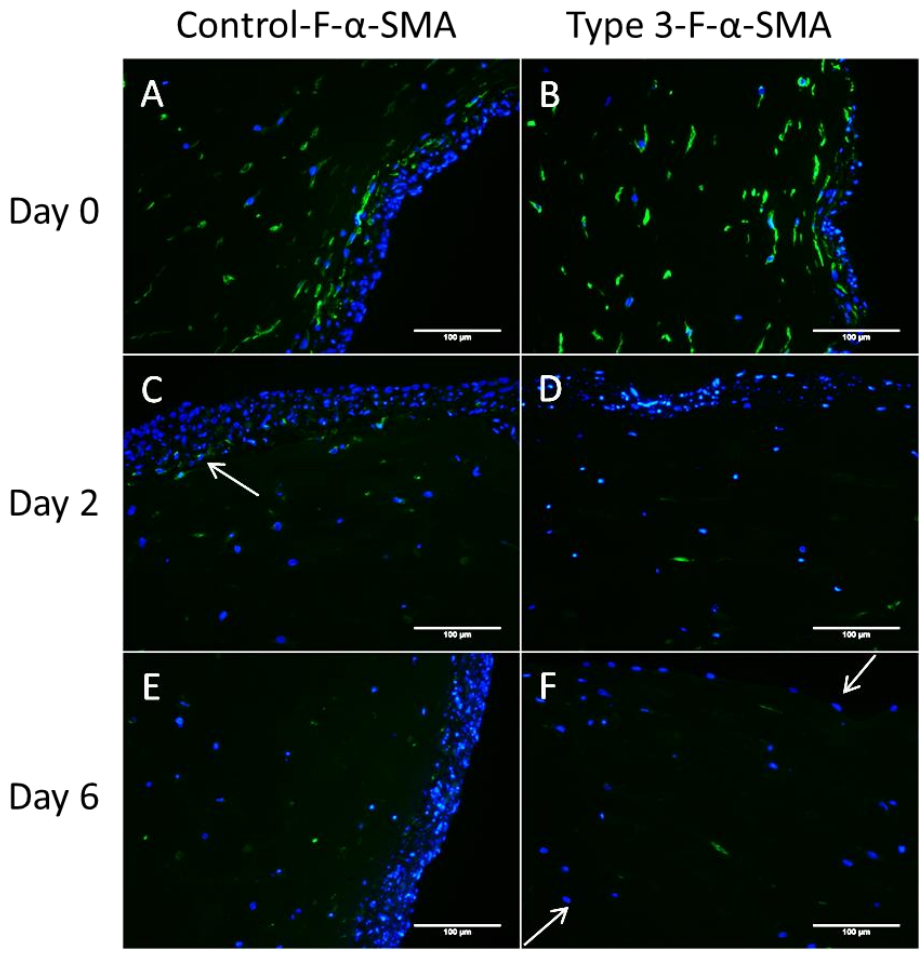

Figure 4.24. Expression of the myofibroblast marker α-SMA in floating Type 3 constructs. Day 0, α-SMA (green) positive cells were evident in both Control-F (A) and Type 3-F (B); the expression was most prominent in construct stroma and the SDCLJ area. On Day 2 and Day 6, a minority of cells were expressing α-SMA in both Control-F (C and E) and Type 3-F (D and F). The staining was randomly distributed in the construct stroma. A few positive cells were observed in the SDCLJ area in some constructs (arrow in C). Construct endothelium or wounded surface was usually identified as the outer surface of the densely packed cell layer. For samples where there was complete endothelium or dense cell layer loss, two images along the construct long axis were captured (arrows in F indicating construct two surfaces parallel to the construct long axis). DAPI (blue) counter-stained cell nuclei. Scale bar = 100 µm.

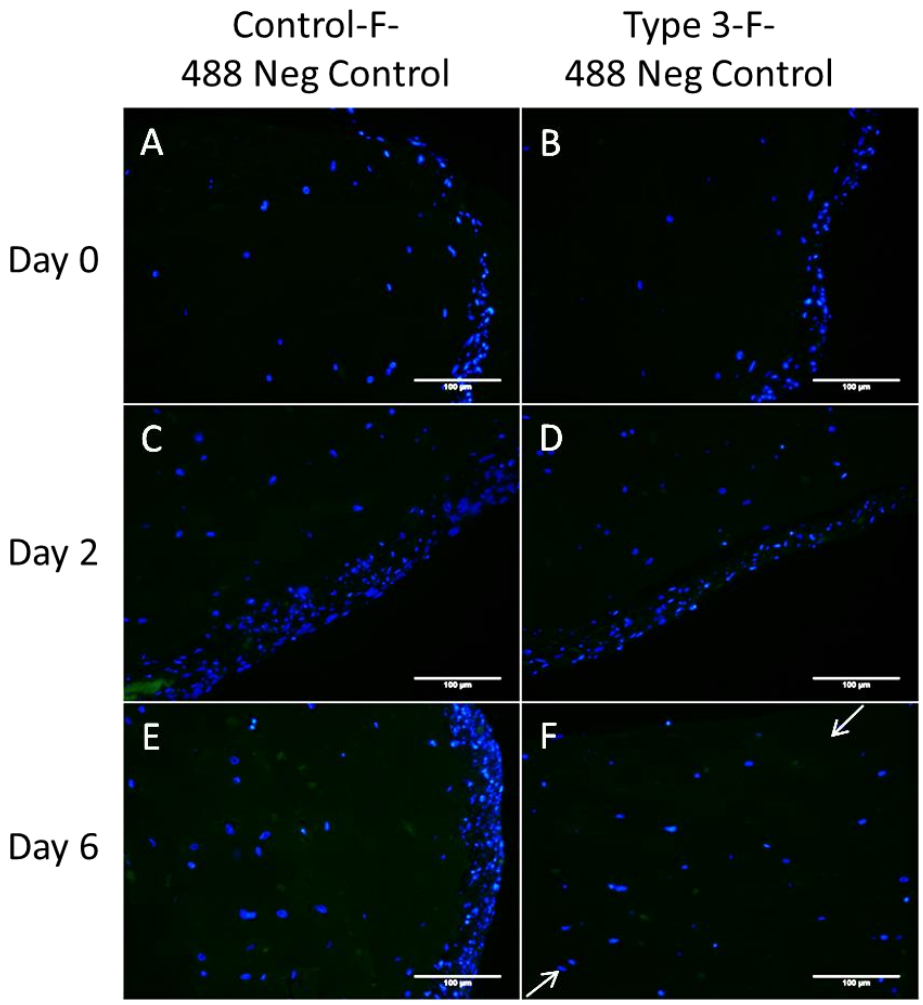

Figure 4.25. Negative controls for α-SMA and vimentin immunofluorescence in floating Type 3 constructs. With primary antibodies omitted, fluorescence secondary antibody Alexa Fluo488 only provided background level staining on all samples examined. Construct endothelium or wounded surface was usually identified as the outer surface of the densely packed cell layer. For samples where there was complete endothelium or dense cell layer loss, two images along the construct long axis were captured (arrows in F indicating construct two surfaces parallel to the construct long axis). DAPI (blue) counterstained cell nuclei. Scale bar = 100 µm.

SMemb expression in floating constructs demonstrated a different pattern compared to α-SMA on immunofluorescence. On Day 0, SMemb positive cells were found all through the construct thickness in both Control-F and Type 3-F (Figure 4.26A and B). On Day 2 and Day 6, in the Control-F, SMemb expression was predominantly in the stroma and expression in dense cellular layer became less evident compared to Day 0 (Figure 4.26C and E). Whilst in majority of Day 2 and Day 6 Type 3-F constructs (n=6/8, 'n' indicates the number of the constructs), apart from stroma expression, weak to moderate SMemb staining was observed in cells on or close to the wounded surface (Figure 4.26D and F).

SMemb primary antibody omitted negative control for each tissue sample is shown in Figure 4.27. Only background level of staining was detected.

Vimentin positive cells were distributed through the entire construct thickness from Day 0 to Day 6 in both Control-F and Type 3-F constructs (Figure 4.28), and the staining intensity did not differ appreciably between each time point. However, the staining was not uniform in later cultured constructs particularly evident in the Control-F constructs, with a number of cells being negative for vimentin staining in the dense cell layer which may suggest cell apoptosis (arrow in Figure 4.28E).

Vimentin primary antibody omitted negative control for each tissue sample is shown in Figure 4.25. Only background level of staining was detected in control samples.

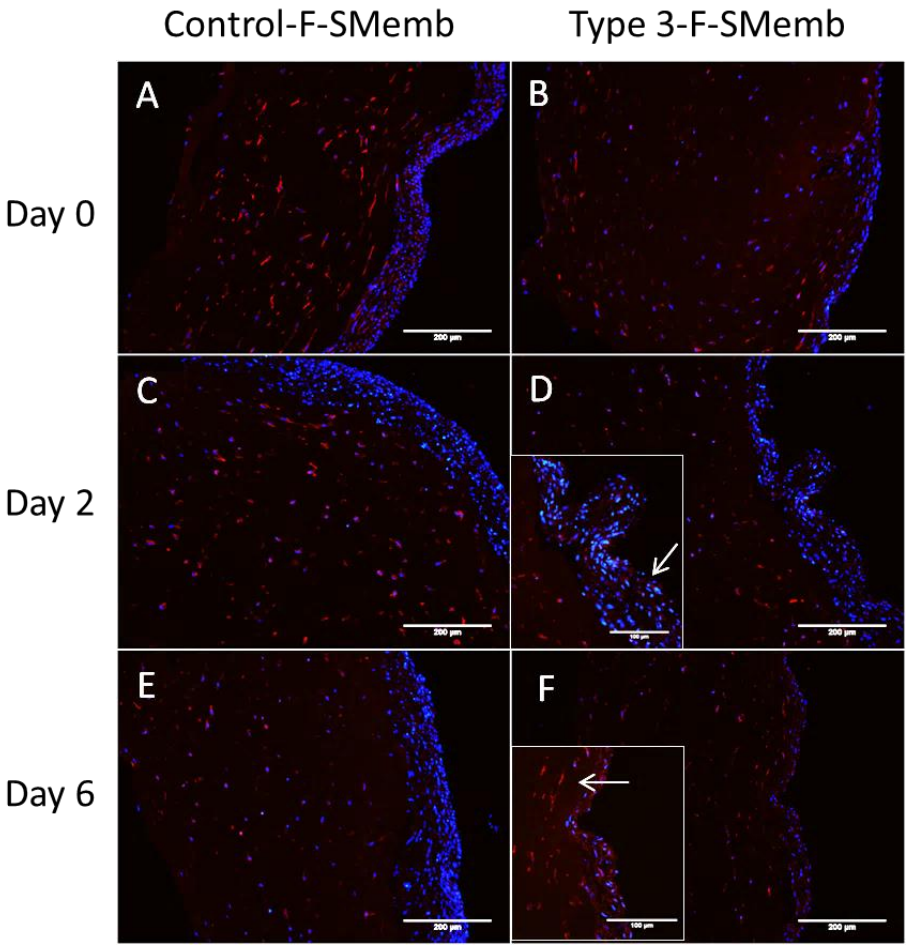

Figure 4.26. Expression of the activated mesenchymal marker SMemb in floating Type 3 constructs. On Day 0, SMemb (red) expression was evident in the construct stroma and dense cell layer subjacent to the endothelium/wounded surface (A, B). On Day 2 and Day 6, SMemb expression was primarily observed in the construct stroma. Less evident expression (compared to Day 0) was detected in the dense cell layer in Control-F at later time points (C, E); while SMemb positive cells were found on (arrow point in D) or close to the wounded surface (arrow point in F) in several Type 3-F constructs (D, F). Construct endothelium or wounded surface was identified as the outer surface of the densely packed cell layer. DAPI (blue) counterstained cell nuclei. Inset images, scale bar = 100 µm. Other images, scale bar = 200 µm.

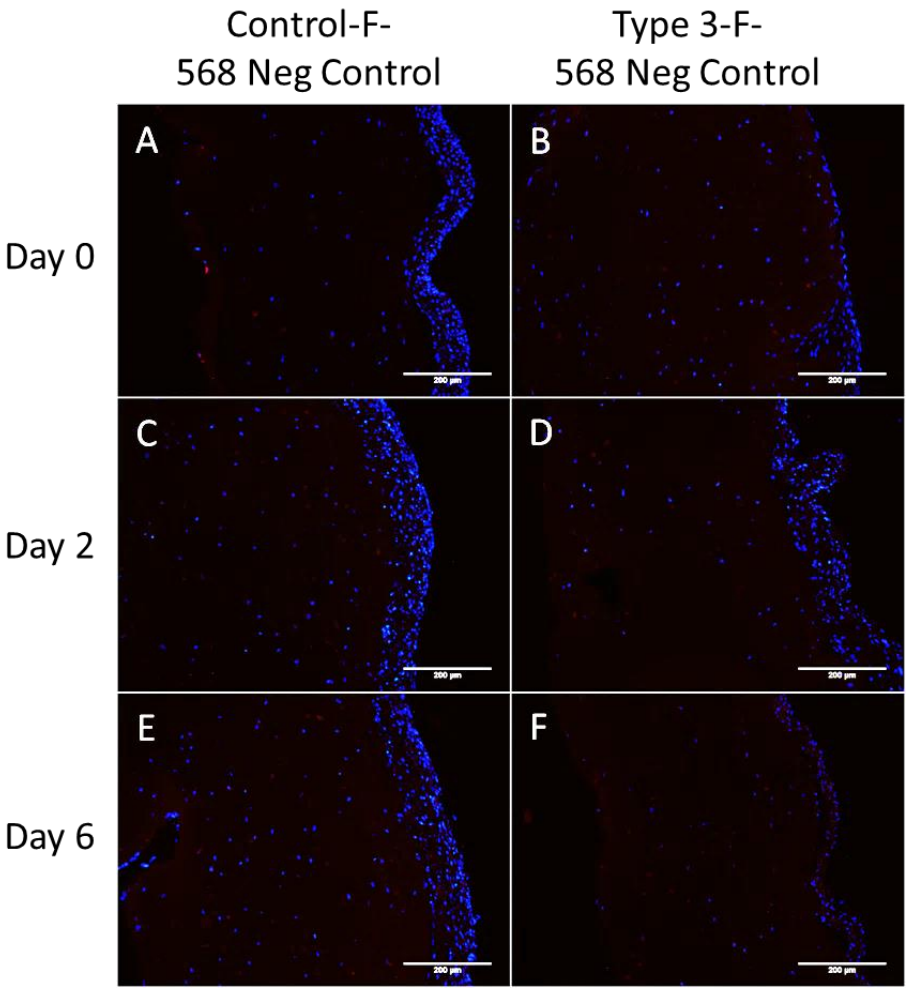

Figure 4.27. Negative controls for SMemb immunofluorescence in floating Type 3 constructs. With primary antibodies omitted, fluorescence secondary antibody Alexa Fluo568 only caused background level staining on all samples examined. Construct endothelium or wounded surface was identified as the outer surface of the densely packed cell layer. DAPI (blue) counterstained cell nuclei. Scale bar = 200 µm.

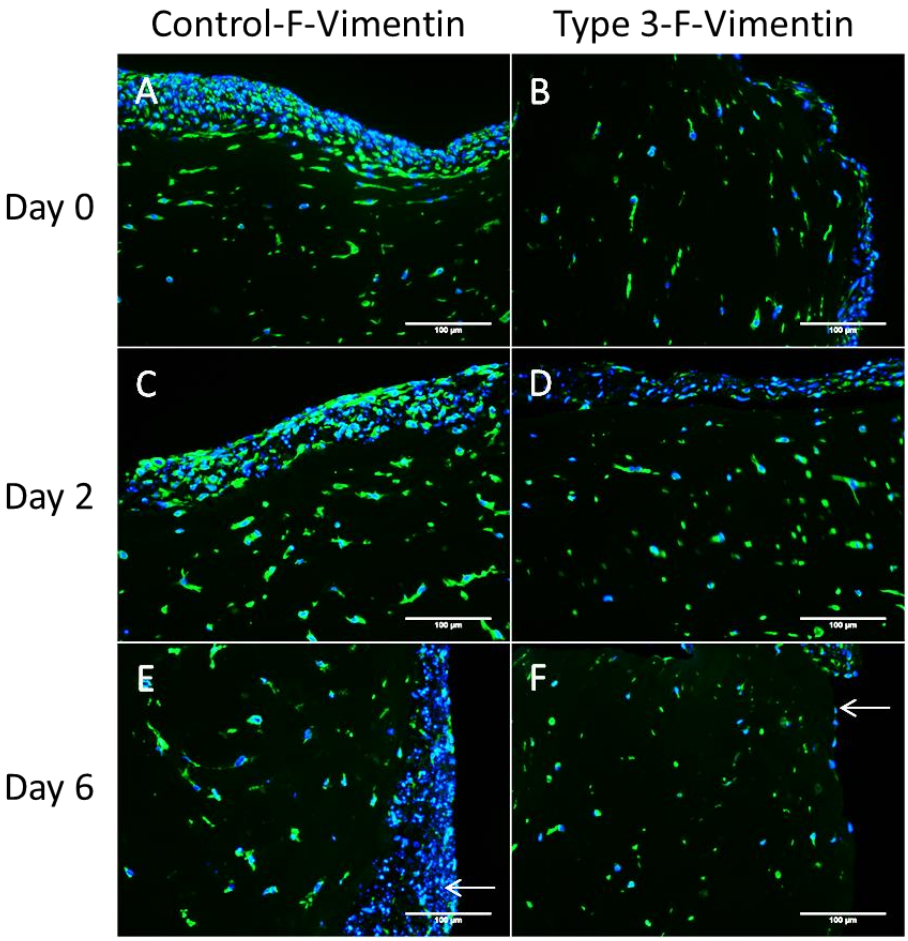

Figure 4.28. Expression of the mesenchymal marker vimentin in floating Type 3 constructs. From Day 0 to Day 6, vimentin (green) staining intensity was consistent in both Control-F (A, C, E) and Type 3-F (B, D, F). It was noticed that a non-uniform distribution existed in the sub-endothelial dense cell layer (arrow in E, a cluster of cells were negative for vimentin), and particularly in Control-F constructs at later time points. Construct endothelium or wounded surface was identified as the outer surface of the densely packed cell layer. Arrow in F indicating wound surface of Day 6 Type 3-F. DAPI (blue) counter-stained cell nuclei. Scale bar = 100 µm.

4.3.5.4 Correlation of ECM Synthesis and Cell Phenotype in Floating Constructs

Collagen I&III and MMP-1 expression were assessed in Control-F and Type 3-F constructs using immunofluorescence. When evaluating ECM and cell phenotype markers on the same floating construct, it was noticed collagen I&III and MMP-1 expression was not associated with α-SMA positive cells, but in a manner that was more similar to SMemb distribution (Figure 4.29). This finding was not evident in Day 0 Control-F (standard Type 1 construct) (Figure 4.29D, G, J, M). While in Day 2 Control-F constructs, where markedly decreased α-SMA staining was observed (Figure 4.29H), collagen I&III (Figure 4.29K) and MMP-1 (Figure 4.29N) expression appeared to be not affected by this cell phenotypic alteration. Their distribution appeared to be more associated with SMemb positive cells (Figure 4.29E). Examination of cultured Type 3-F (Day 2) constructs showed similar findings to Control-F, though SMemb expression was weaker (Figure 4.29F, I, L, O).

Primary antibody omitted negative control for each specific construct is shown in Figure 4.30. Only background level of staining was detected in control samples.

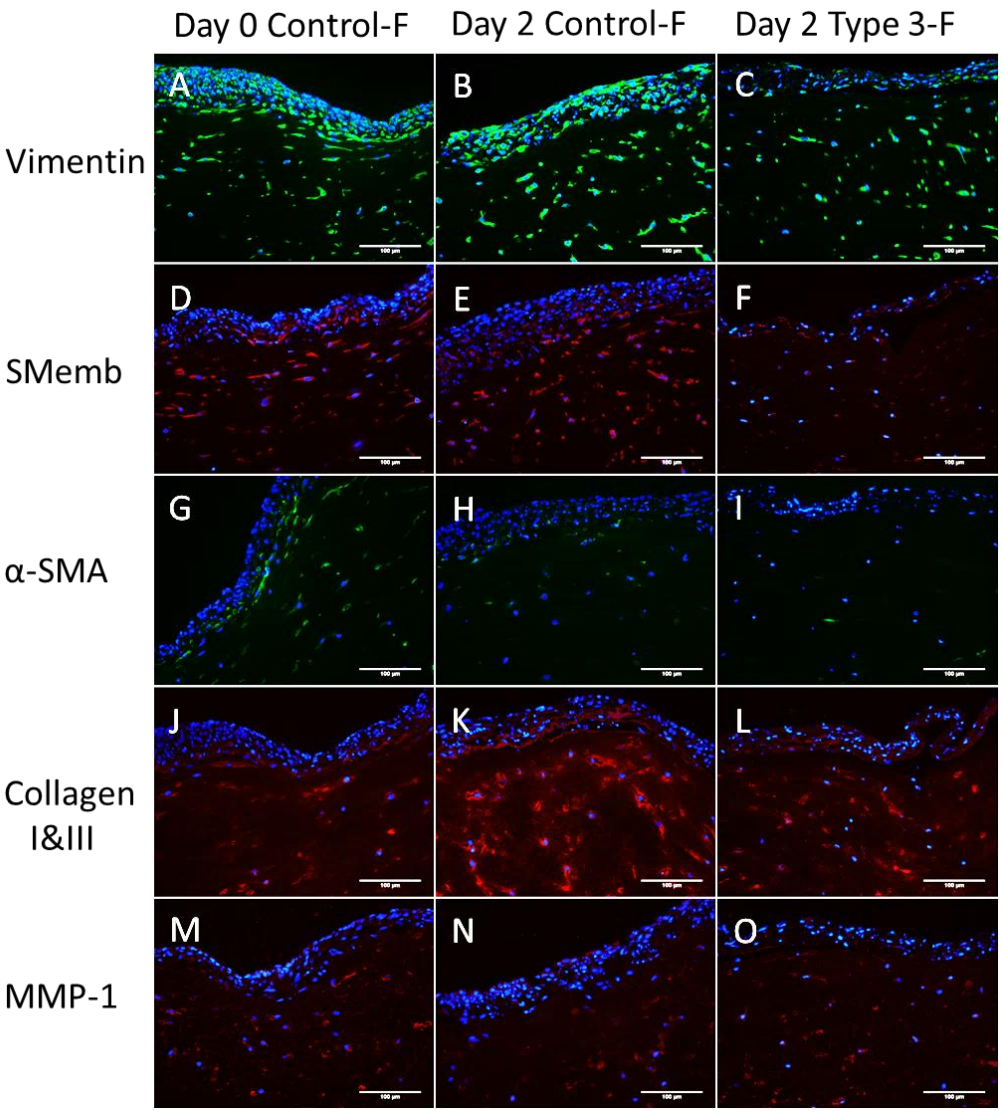

Figure 4.29. ECM related proteins and cell phenotypic markers in the same floating constructs. One representative construct of Day 0 Control-F, Day 2 Control-F and Day 2 Type 3-F are shown. ECM association with cell phenotype was not evident in Day 0 Control-F (D, G, J, M), but was in longer cultured floating constructs where collagen I&III (red in K, L) and MMP-1 (red in N, O) were more associated with SMemb positive cells (red in E, F) than α-SMA (green in H, I). Vimentin demonstrated mesenchymal cell distribution in each construct sample (green in A-C). Construct endothelium or wounded surface was identified as the outer surface of the densely packed cell layer. DAPI (blue) counterstained cell nuclei. Scale bar = 100 μm.

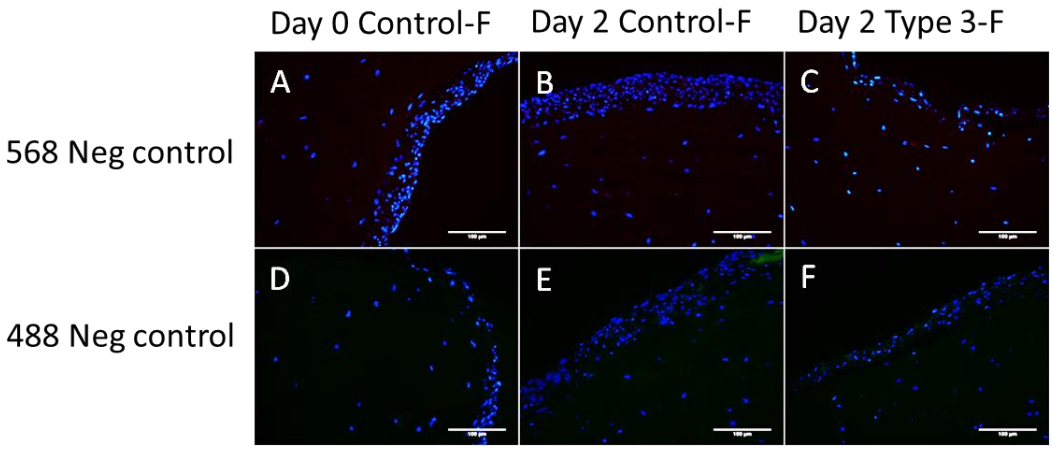

Figure 4.30. Negative controls for the three representative constructs shown in Figure 4.29 with immunofluorescence. With primary antibodies omitted, fluorescence secondary antibody Alexa Fluo568 (A-C) and Alexa Fluo488 (D-F) only stained tissue sample at background level. Construct endothelium was identified as the outer surface of the densely packed cell layer. DAPI (blue) counterstained cell nuclei. Scale bar = 100 µm.

4.3.6 The Ultrastructure of Endothelium Damaged Model (Floating Constructs)

The ultrastructure of one wounded floating construct (Type 3-F) and one intact floating control construct (Control-F) was examined on Day 0 and Day 6 after injury. On Day 0, apart from the wounded area, there was no apparent difference between the Type 3-F and Control-F constructs. The proposed endothelial cells and the VICs were variable in morphologies and some degree of degradation was seen. On Day 6, although both samples possessed multiple layered cell mass at the wound site (in Type 3-F) or proposed endothelium (in Control-F), cells at the wounded site showed a relatively healthy appearance and were surrounded by ECM. A linear arrangement of cells was observed on the surface of the fibrin matrix in the examined Type 3-F construct. While in its counterpart, cells were generally in a degradation state in the proposed endothelium of the Control-F construct. The VICs in Day 6 Type 3-F showed relatively healthy cell profile, however the cell number was small in this specimen; in Day 6 Control-F construct, smooth muscle-like cells were observed and some of them were in degeneration state, while the others were viable and producing ECM.

In detail, immediately after wounding (Day 0), the proposed endothelium surface of the Type 3-F construct was severely damaged with a few cells present. However, in some areas of the wound site, a large number of cells with varying morphology were observed and most of them contained large vacuoles (Figure 4.31A). Some cells showed distended and disrupted mitochondria and a large nucleus with fragmented chromatin which was evidence of degradation (Figure 4.31B). While in the intact Control-F construct multiple layers of cells were present in the proposed endothelium surface with variable morphologies. In some areas this cellular multi-layer was mainly consisted of highly degraded cells (Figure 4.31C). Cells in the uppermost layer appear to be synthetically active possessing large nuclei, obvious rER and ECM production (Figure 4.31D). Moreover, some cells contained filaments not typically seen in endothelial cells (data not shown).

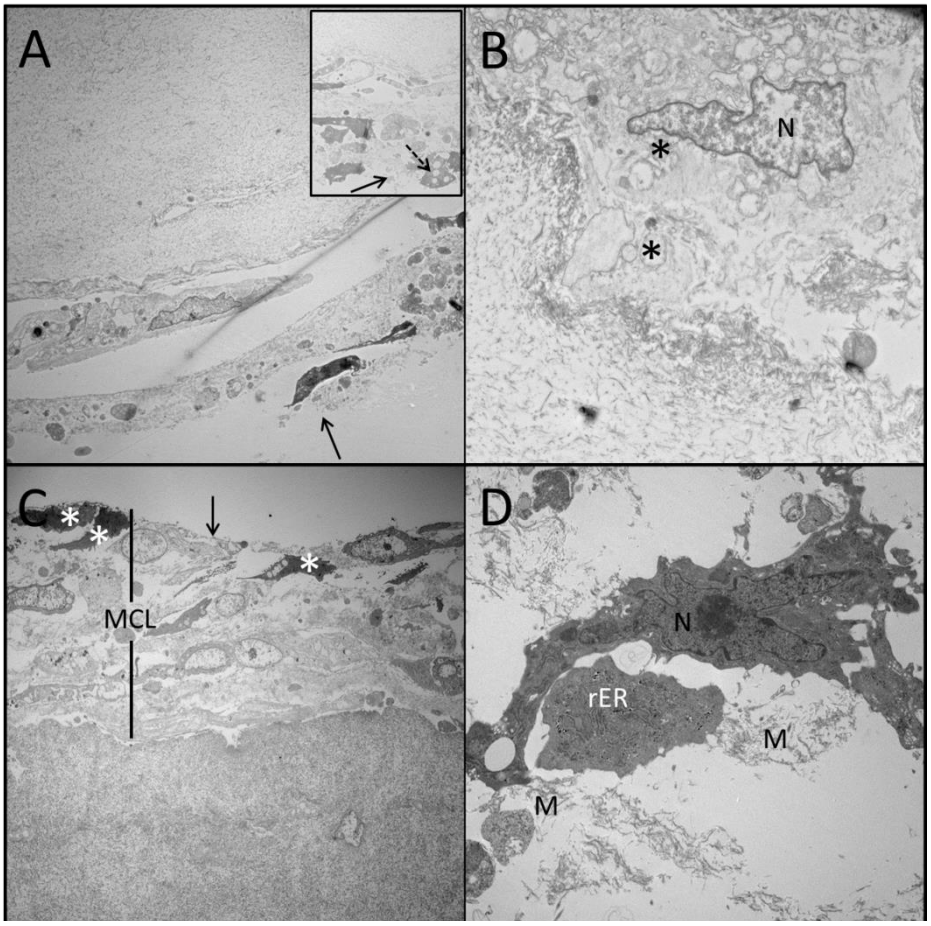

Figure 4.31. The ultrastructure of wound or proposed endothelium of the floating Type 3 constructs on Day 0 after manipulation. A. The proposed construct endothelium (arrows in A) was destroyed after wounding showing few intact cells. In some other areas of the wound (inset in A), multiple layered cells with variable morphology were observed most of which contain large vacuoles (dash arrow in the inset); B. A cell at wound site showed large nucleus (N in B) with fragmented chromatin, distended and disrupted mitochondria (* in B) were also seen. C. Multiple-layered cells (MCL in C) were observed on the proposed endothelium surface (arrow in C) of Day 0 Control-F construct. Viable cells (* in C) were typically lying on the uppermost surface. Most of the cell layers contained highly degraded cells. D. Viable cell in proposed endothelium possess large nuclei (N in D), obvious rER with evidence of de novo ECM production (M in D). N, nucleus; rER, rough endoplasmic reticulum; M, extracellular matrix. Magnification in A, 2,500 x; in B, 6,000 x; in C, 1,500 x; in D, 8,000x; in inset of A, 2,000 x.

The interstitial cells in the construct stroma of both Day 0 constructs varied in morphology and some of them showed evidence of degradation (Figure 4.32). The signs of degradation include electron dense inclusions.

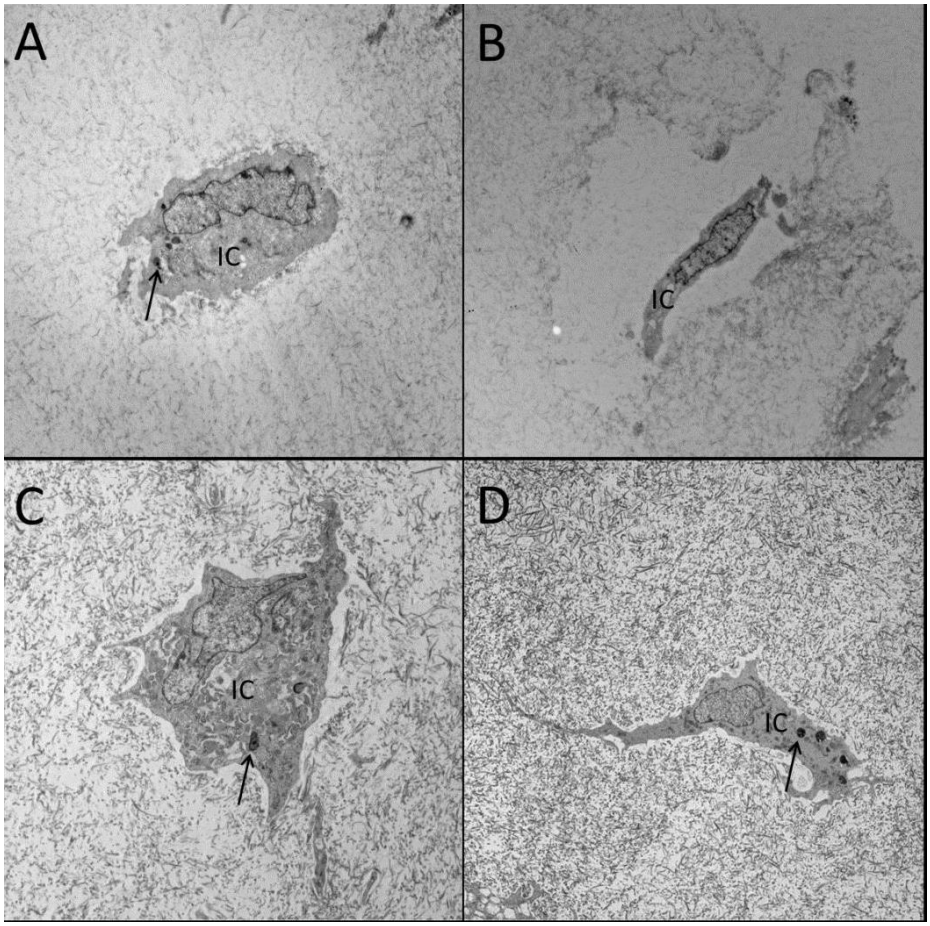

Figure 4.32. The ultrastructure of the VICs in Day 0 floating Type 3 constructs. Various VIC morphologies were seen in both construct types. For example, compact VIC (IC in A) and elongated VIC (IC in B) were present in the Type 3-F construct; and pleomorphic VIC (IC in C) and smooth muscle-like VIC (IC in D) were observed in the Control-F construct. The presence of electron dense inclusions in some cells (arrow in A, C and D) suggested a degraded state. IC, interstitial cell. Magnification in A and B, 3,500 x; in C, 6,000 x; in D, 4,000 x.

Apparent differences were detected at the construct medium contact surface in the Day 6 Type 3-F construct compared to the Control-F. In the Type 3-F construct, multiple layers of cells of variable morphologies with no apparent order were observed at the wound site (Figure 4.33 A). These cells seemed to be surrounded by fibrillar ECM. Interestingly, a group of cells arranged into a monolayer lying at the junction between the fibrin matrix and the multiple layered cell mass (Figure 4.33 B and C). The monolayer cells possessed large oval nuclei and elongated profiles with scant organelles which were broadly fitting with endothelial-like characteristics. The fibrin matrix subjacent to these cells displayed an uneven surface indicating destruction by the prior wounding procedure. While in the Day 6 Control-F construct, multiple layers of cells generally in a degraded state were seen in the proposed endothelium (Figure 4.33 D). Most of the cells contain large vacuoles and lipid-like inclusion.

In construct deep stroma of the Day 6 Type 3-F construct, only a few VICs were seen in the selected area of the this specimen. The cells generally displayed a relatively healthy profile with large nuclei, rich rER plexus and scattered mitochondria (Figure 4.34 A). Some electron-dense inclusions are seen however, which indicates cellular destruction. While in Control-F construct, a number of smooth muscle phenotype cells were observed to be in a degraded state (Figure 4.34 B). Despite that, other cells remained viable and showed evidence of de novo ECM production (Figure 4.34 C and D). The active cells also appeared to be a smooth muscle phenotype, with elongated cell shape and some cytoplasmic processes.

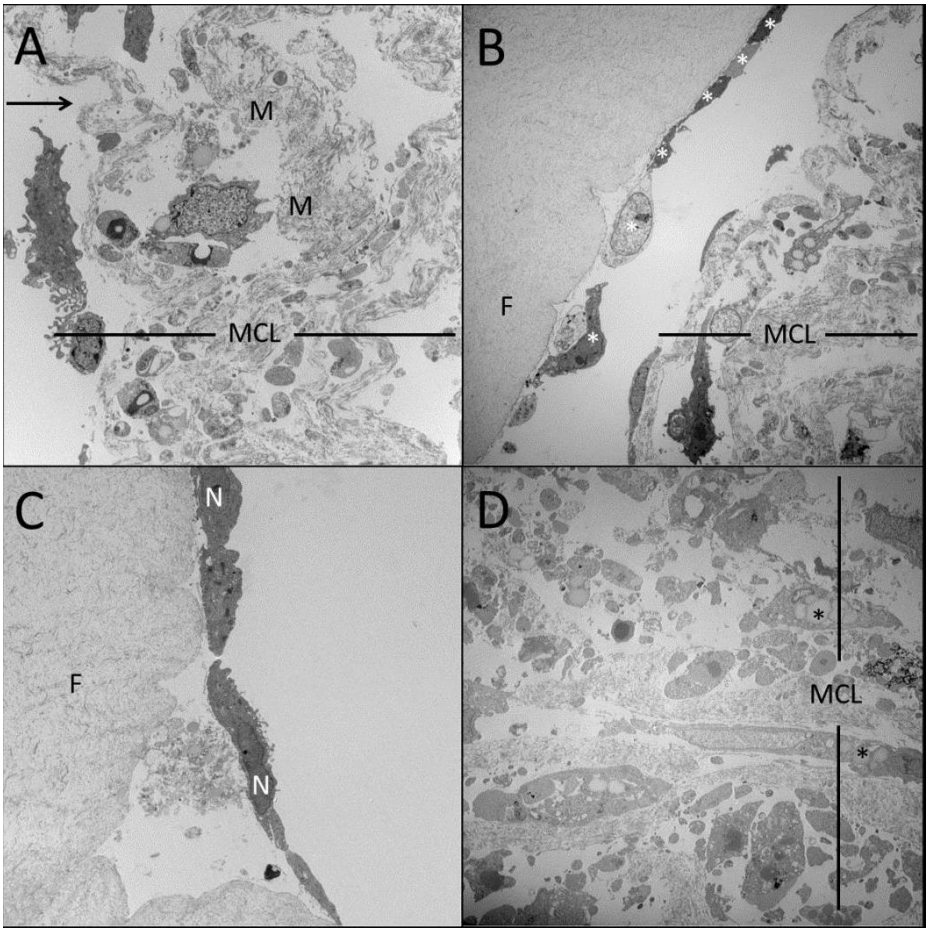

Figure 4.33. The ultrastructure of wound site or proposed endothelium in Day 6 floating Type 3 constructs. Multiple layers of cells (MCL) were observed on the upper surface of both Type 3-F (A-C) and Control-F construct on Day 6. A. In the Type 3-F construct, cells within the wound site (arrow in A) were variable in morphology with no apparent order and, were surrounded by fibril ECM (M in A). B. Subjacent to the multiple-layered cells at the wound site (MCL in B), cells (* in B) in a mono layer were observed lying on the fibrin matrix (F in B). C. These cells possessed large oval nuclei (N in C) and elongated profiles, displaying an endothelial-like morphology. The fibrin matrix (F) showed an uneven surface which appeared had been destroyed. D. While in the proposed intact endothelium of the Control-F construct, majority of cells in the multiple cell layers (MCL in D) exhibited a degradation state showing large vacuoles and possible lipid inclusions (* in D). N, nucleus; M, extracellular matrix. Magnification in A, 3,500 x; in B, 2,000 x; in C, 4,000 x; in D, 2,500 x.

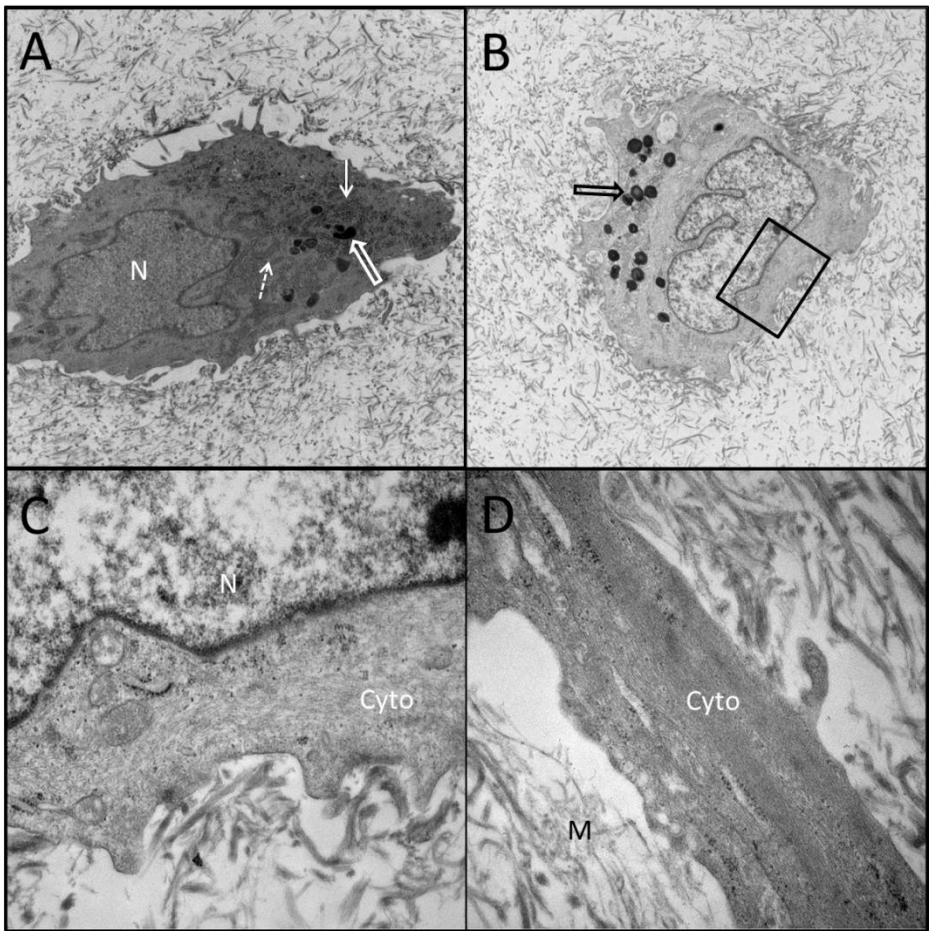

Figure 4.34. The ultrastructure of the VICs in Day 6 floating Type 3 constructs. A. A VIC in the Type 3-F construct with large nucleus (N), scattered mitochondria (dash arrow), rich rough endoplasmic reticulum (solid arrow) and some electron dense inclusion (hollow arrow). B. A VIC in the Day 6 Control-F construct was in degeneration state and showing a number of electron dense inclusions (hollow arrow). The selected area (in black box) is present in C. The filamentous cytoplasm (Cyto in C) of this cell suggested a smooth muscle phenotype. D. A viable cell in the Day 6 Control-F construct displayed a smooth muscle phenotype and possibly involved in ECM synthesis. Notice the elongated cellular process with longitudinal filaments in the cytoplasm (Cyto in D). There was extracellular matrix components (M) in proximity to the cell. N, nucleus; Cyto, cytoplasm; M, extracellular matrix. Magnification in A, 5,000 x; in B, 6,000 x; in C, 30,000 x; and in D, 40,000 x.

4.4 Discussion

4.4.1 The Potential for Using Fibrin Based Canine 3D Mitral Valve Construct as An *In vitro* Research Model

As described in Section 1, though the mainstream of heart valve tissue engineering is for clinical transplantation, it can also be used as an *in vitro* model for heart valve research. In the present study, a 3D mitral VECs-VICs co-culture construct was developed using fibrin based culture system.

Theoretically, the most ideal cell source for heart valve regeneration is primary valve cells. In native heart valves, the principle cell types are VECs and VICs. Therefore, a VECs-VICs 3D co-culture system is expected to at least partially resemble native mitral valve. In the present study, healthy VECs-VICs based (Type 1) 3D constructs were compared with native canine mitral valves. The 3D constructs possess some native valve like features, including tissue-like gross and histological morphology; expression of native cell phenotypic markers (vimentin, SMemb and α-SMA) in a relatively comparable manner to native valve, and cells in the co-culture constructs synthesized some key valve matrix components (collagen and GAGs) and also demonstrated ECM degradation capability (collagenase MMP-1 and stromelysin MMP-3 expression). These data suggested mitral valve cells in the current fibrin 3D model still possessed potential for organizing a native valve structure. The results are consistent with a previous study which also showed porcine mitral VECs and VICs were capable of synthesizing a native-like ECM profile *in vitro* (Flanagan et al., 2006a). Similarly, aortic VICs were also found to synthesize collagenases, stromelysins and membrane-type MMPs on a collagen hydrogel system; ECM related mRNA was detected in these cells suggesting potential for matrix production (Dreger et al., 2006). All above findings indicate that native valve cells are capable of conducting ECM synthesis and remodelling *in vitro*. This is crucial for heart valve regeneration, as one of the major concerns in current heart valve tissue engineering is whether the seeded cell source could generate sufficient native ECM components to replace degraded scaffolds.

Moreover, the expansive ability of the native mitral valve cells is another positive feature which make them attractive cell source for establishing 3D culture models.

For example, without excessive sub-culturing (i.e. cells in culture appear to be robust and morphologically stable), cells derived from a single middle-sized breed of dog mitral valve can contribute to hundreds of static constructs using the current system. This can provide substantial numbers of substitutes for native valve tissue which could improve a tissue shortage problem for research work. However, particularly in the current study design, an issue arose regarding cell availability: there was difficulty in getting sufficient number of affected young adults, since most MMVD cases develop the disease later in life. To overcome this issue as well as to limit potential inherent variability between different dogs (Stephens et al., 2010b; Warnock et al., 2006), pooled cells were used in one experiment. When cells were pooled, an equal number of cells from each individual cell culture at the same passage was used, and excessive passages were avoided (< 7 passages). There was no apparently difference in morphology between individual cultures of each group and no abnormal cell morphology or behaviour in the pooled cultures.

Fibrin scaffolds have been widely used in cardiovascular tissue engineering in recent years (Flanagan et al., 2007; Jockenhoevel et al., 2001b; Vesely, 2005; Ye et al., 2000). It serves as an excellent cell supporter as it is favourable for cell distribution, cell communication, ECM synthesis and accumulation within the 3D culture system (Lee et al., 2008; Pikaart, 2008; Ye et al., 2000). The most common drawback of hydrogel systems is cell-mediated contraction and shrinkage. The current constructs dramatically decreased in size within a 14 day static culture. VICs are known to have contractility and force generation properties, and this might be a contributing factor (Filip et al., 1986; Mulholland and Gotlieb, 1997; Smith et al., 2007; Stephens et al., 2010a). Though altered macromorphology of the construct was not a major concern in this study (as current constructs are not used for *in vivo* implantation), it should be noted that VIC induced gel contraction must have effects on matrix configuration and feedback to regulate cell behaviour. Another concern for fibrin scaffolds is that fibrin is not a native valve ECM component. Valve cells might respond to this foreign protein differently than they do to native ECM. This will be discussed in Section 4.4.2.

For this study the 3D valve constructs were cultured in a static system. A 3D static culture system is superior to 2D culture system in regards to resembling native tissue configuration. In native heart valve, VECs and VICs are in a sandwich like structure: the VECs line two surfaces of the valve leaflet and cover valve stroma which contains dispersed VICs and ECM. The current co-culture model created a fibrin-VICs based stroma structure with one endothelial surface, which allows VECs and VICs interaction within the 3D system. On histological evaluation, cell distribution in the intact construct stroma appeared to be uniform. Whereas, towards the medium contact surface, densely accumulated cell layers were observed between the fibrin-VICs stroma and construct endothelial surface. This phenomenon is possibly due to imbalanced culture nutrient and gas distribution in the culture system with VICs in stroma possibly tending to migrate to the medium contact surface for optimal culture environment. One piece of supporting evidence is in Day 0 Control-F construct (actually same as Type 1), TEM showed the viable cells tended to situate in the upper most surface of the multiple cell layers. This has been described as a common limit of static culture systems (Carrier et al., 1999; Kofidis et al., 2003). However, it cannot be ruled out that the accumulated cell mass was not from proliferation of an endothelial source, since multiple layer endothelium has been observed in previous vascular organ *in vitro* cultures (Gotlieb and Boden, 1984; Lester and Gotlieb, 1988; Merrilees and Scott, 1982). Attempts were made using endothelial markers CD31 and vWF to detect construct endothelial cells by immunofluorescence, but both antibodies failed to label either constructs or endothelium of the native valve tissue. The endothelium formation on the construct was finally confirmed by DiI-Ac-LDL positively labelled live construct surface and CD31 protein expression on Western blot. DiI-Ac-LDL positive cells were arranged in a patchy pattern on the constructs which suggested uneven endothelium coverage. Additionally, variable CD31 expression was detected between different batches of constructs. This suggests differences may exist between each individual VEC culture for 3D construct fabrication. Alternatively it might be a limitation of manual cell seeding techniques that resulted in uneven endothelial cell distribution between constructs. Limited ultrastructure examination suggested cell degradation was frequent in the static cultured 3D construct. It is not certain whether this is a pathological response to the

culture substrate (fibrin matrix/tension), or is due to (more likely) poor nutrient/gas perfusion. A thinner fibrin based construct is under consideration for future static construct experiments, which is predicted to give better gas/nutrient perfusion to embedded cells. It would be necessary to carry out cell viability assays in the future constructs.

Investigation of valve cell behaviour in 3D culture system is not a novel concept. The early history of 3D culture from the 1980s used valve organ culture systems to study valve ECM degradation (Decker et al., 1986; Decker and Dingle, 1982) and mitral VIC response to wounding (Lester et al., 1993; Lester et al., 1992; Lester and Gotlieb, 1988). With the increased use of tissue engineering technology in regenerative medicine, novel TE scaffolds, such as the hydrogel system, were adapted to establish 3D research models for heart valve biology and disease study (Butcher and Nerem, 2004, 2006; Colazzo et al., 2011; Dreger et al., 2006; Flanagan et al., 2006b; Li et al., 2013; Smith et al., 2007). The *ex-vivo* 3D culture models provides opportunities for advanced understanding of valve cell biology and pathology, answering questions in heart valve tissue engineering field which will eventually benefit heart valve regeneration projects.

In this study, haemodynamic factors affecting construct behaviour were not examined. Future designing of a more optimal tissue engineering mitral valve model possibly would use a combination of computed tomography based valve modelling, bio-printing valve fabrication and customised dynamic conditioning culture systems (Duan et al., 2013; Flanagan et al., 2007; Schaefermeier et al., 2008; Sodian et al., 2010).

4.4.2 Healthy and Diseased VICs Showed Similar Activity on Fibrin Based 3D VECs-VICs Co-Culture Constructs

It is still uncertain whether canine MMVD initiates from abnormalities of VICs or from damage to the overlying endothelium. It has been proposed that the activated VICs in diseased mitral valve may be a primary initiator for pathological change of valve ECM structure (Prunotto et al., 2010; Walker et al., 2004). In the current study, the expression of a series of MMVD related markers has been compared between

diseased VICs and healthy VICs, to see if they contribute differently to expression of the selected MMVD markers in an *in vitro* 3D system.

α-SMA and SMemb have been considered as hallmarks of transformed VICs and both of them are reported to be up-regulated in canine and human MMVD (Disatian et al., 2008; Disatian et al., 2010; Han et al., 2008; Rabkin-Aikawa et al., 2004b; Rabkin et al., 2001). Using immunofluorescence techniques, a number of α-SMA and SMemb positive cells were detected in both healthy and diseased VIC based constructs, but no apparent differential expression pattern was observed between these two types of models. This suggests the presence of the activated VIC phenotype in both models. It was also been noticed that the expression manner of α-SMA and SMemb appeared to be different from each other: α-SMA was mainly expressed by stroma cells with a prominent accumulation in the SDCLJ area, while SMemb positive cells were distributed throughout the construct thickness, covering stroma, the dense cellular layer as well as surface endothelial cells. The distinct expression patterns between α-SMA and SMemb indicates heterogeneity existing within the aVICs population. Interestingly, the accumulated α-SMA positive cells clustered between the construct endothelium and deep stroma, and is similar to that observed in native samples. Even if healthy or diseased, α-SMA positive cells are commonly seen in the atrialis or ventricularis layers of heart valves, though with disease progression this can extend to the valve stroma (Bertipaglia et al., 2003; Chester and Taylor, 2007; Disatian et al., 2010; Han et al., 2008; Mulholland and Gotlieb, 1997; Taylor et al., 2003). Native valve α-SMA expression might be in response to mechanical stimuli (shear flow) in which cells align in response to flow and considering their contractile properties might also generate force to contribute to valve mechanical integrity. The origin of α-SMA positive cells on constructs, however, was not investigated. There are at least two possible explanations: VICs migrating from deep in the construct stroma towards the more optimal culture conditions or transformed VECs replenishing VIC population in a manner similar to EndoMT seen with embryonic heart valve development (Markwald et al., 1977; Oosthoek et al., 1998; Patten et al., 1948; Person et al., 2005). A recent review proposed that progenitor cells exist in the adult VEC populations, and that they can

replenish sub-endothelial VIC population through an EndoMT process triggered by injury or disease (Bischoff and Aikawa, 2011).

MMPs and their inhibitors play a crucial role in valve ECM remodelling. In the previous studies MMP-1 and MMP-3 had been found to be up-regulated in MMVD (Aupperle et al., 2009c; Disatian et al., 2008; Obayashi et al., 2011; Rabkin et al., 2001). MMP-1 is an interstitial collagenase present in heart valves in both normal and pathological conditions and mainly functions to cleave collagen Type I, II and III (Disatian et al., 2008; Dreger et al., 2002; Visse and Nagase, 2003). The up-regulation of MMP-1 indicates increased ECM catabolic activity, presumably excessive degradation of collagen Type I and III. Considering Type I and III are the major collage types in native valve fibrosa, MMP-1 must be one principle proteinase that is responsible for destruction of the fibrosa and further tissue weakening in MMVD (Prunotto et al., 2010). Extracellular MMP-1 expression was found to mainly co-localize with VICs, but occasionally expressed by VECs in both healthy and diseased VICs based constructs. Combined with the finding that collagen Type I and III are present, it is clear that one of the key native valve ECM remodelling function was ongoing in the culture system. Stromyslin-1 MMP-3 activates a number of proMMPs including MMP-1 and is also involved in degradation of a range of ECM components (Visse and Nagase, 2003). It has been reported to be absent in normal canine mitral valve but present in disease valve leaflets (Obayashi et al., 2011). Moreover, this catabolic enzyme is capable of digesting numerous ECM components as well as cleaving fibrin cross-link *in vitro* (Bini et al., 1996). Investigation of this MMP might be particularly important for fibrin gel-based tissue engineering constructs when considering achieving a balance between fibrin degradation and accumulation of newly synthesized ECM. In the current study MMP-3 was not evident in a majority of constructs on fluorescence staining. However, Western blot data did suggest the presence of MMP-3 on all constructs examined. This indicates potentially fibrin scaffolds can be degraded by native mitral valve cells without introducing any external proteolytic enzymes, though the efficacy of degradation was unknown.

In vivo studies have shown that diseased VICs exhibit excessive synthetic activity and transformed phenotypes compared to VICs in healthy mitral valves (Black et al., 2005; Disatian et al., 2008; Disatian et al., 2010; Han et al., 2008; Rabkin-Aikawa et al., 2004b). The selected disease markers were expected to exhibit higher expression levels in constructs containing diseased VICs. However, Western blot semi-quantification data suggested diseased VICs and healthy VICs did not contribute differently to all investigated markers the 3D models. Since most of the markers were minimally expressed in native mitral valve, clearer presence of them in both types of constructs suggests they are more close mimicking a MMVD valve rather than a health mitral valve. There are several explanations for this; construct matrix and cell source. Healthy VICs might be activated by the fibrin environment. Fibrin is not a native ECM component and in response an activated VIC phenotype is needed to enable production of MMPs (such as MMP-1 and MMP-3) and TIMPs in order to initiate ECM remodelling. Moreover, the fibrin hydrogel system is mechanically similar to a GAGs rich environment, which itself is a hallmark of the myxomatous valve (Gupta et al., 2009a; Han et al., 2010; Tamura et al., 1995). This "matrix" might signal to cells that they are in a pathological condition, triggering ECM remodelling. Substrate stiffness is also known to contribute to VIC activation (Kural and Billiar, 2013; Pho et al., 2008). For the cell source, the diseased VICs were derived from valves with mild to moderate MMVD lesions only, with cells from severe diseased valves not being investigated. It is possible that many VICs from mildly diseased valves would behave similarly in culture as those derived from healthy valves. One previous study compared TGF-β1 effects on canine healthy VICs compared to VICs from mild disease in a collagen gel compaction study and there was no evident differential response was observed (Waxman et al., 2012).

Apart from the markers evaluated, other markers were also found to associate with MMVD (all summarized in Table 4.4). Due to time limitations, it is not possible to assess all the markers in the models. One important consideration that needs to be investigated in future studies is the potential effect of diseased VICs on healthy VECs. The pilot ultrastructure EM analysis suggested abnormalities existed in the proposed endothelium of these constructs, with atypical endothelial features and cell

loss somewhat similar to that observed in native MMVD (Corcoran et al., 2004; Han et al., 2013). Future work will evaluate endothelial function and it particular the question of whether the endothelium damage in MMVD is a cause or a consequence to sub-endothelial VIC activation.

In summary, a MMVD-like 3D construct was obtained using either healthy or diseased canine mitral valve cells, and this could be a potential model for disease studies. For future work, studies on the combination of the current models with customized bioreactor maintained dynamic conditioning on construct morphology will be needed, and the specific effects of drugs and/or chemical components associated with MMVD (such as advanced glycation end product) will be investigated.

Table 4.4 MMVD associated marker review

Category	Marker		Roles in MMVD			
			Gene		Protein	
			Regulation	References	Alteration	References
Endothelial function	Endothelin-1 receptor				↑	(Mow and Pedersen, 1999)
	Endothelin-1		↑	(Oyama and Chittur, 2006)		
	Nitric oxide synthase:		↑	(Oyama and Chittur, 2006)	↑	(Olsen et al., 2003b)
Activated VIC phenotype	α-SMA				↑	(Rabkin et al., 2001)
	SMemb				↑	(Rabkin et al., 2001)
ECM components	Collagen Type I				↑	(Aupperle et al., 2009a) (Cole et al., 1984)
	Collagen Type III				↑	(Aupperle et al., 2009a) (Cole et al., 1984)
	Collagen Type V				+	(Aupperle et al., 2009a)
					↑	(Cole et al., 1984)
	Collagen Type VI				↑	(Aupperle et al., 2009a)
	Fibronectin				↑	(Aupperle et al., 2009a)
	laminin				↑	(Aupperle et al., 2009a)
	proteoglycans	Total			↑	(Aupperle et al., 2009a) (Kogure, 1980) (Han et al., 2010)
		Biglycans			↑	(Gupta et al., 2009a)
		Decorin			↑	(Gupta et al., 2009a)
		Versician			↑	(Gupta et al., 2009a)

Table 4.4 MMVD associated marker review-continued with previous page

Category	Marker	Roles in MMVD			
		Gene		Protein	
		Regulation	References	Alteration	References
MMPs and TIMPs	MMP-1	↑	(Aupperle et al., 2009c)	↑	(Rabkin et al., 2001) (Disatian et al., 2008)
	MMP-2	No change	(Aupperle et al., 2009c) (Oyama and Chittur, 2006)	↑	(Rabkin et al., 2001)
				↓	(Aupperle et al., 2009b)
	MMP-3			+	(Obayashi et al., 2011)
	MMP-9	No change	(Aupperle et al., 2009c) (Oyama and Chittur, 2006)	↑	(Rabkin et al., 2001)
				-	(Aupperle et al., 2009b)
	MMP-13	No change	(Oyama and Chittur, 2006)	↑	(Disatian et al., 2008) (Rabkin et al., 2001)
	MMP-14	↑	(Aupperle et al., 2009c)	↑	(Aupperle et al., 2009b)
	TIMP-1	↑	(Oyama and Chittur, 2006)		
	TIMP-2	↑	(Aupperle et al., 2009c)	↑	(Aupperle et al., 2009b)
	TIMP-3	↑	(Aupperle et al., 2009c)	↑	(Aupperle et al., 2009b)
	TIMP-4	↑	(Aupperle et al., 2009c)		
Serotonin pathways	5-Hydroxytryptamine receptor 2B (5-HT_{2B})	↑	(Oyama and Chittur, 2006)		
	Tryptophan hydroxylase 1 (TPH1)			↑	(Disatian et al., 2010)
	TGF-β3			+	(Obayashi et al., 2011)
	TβR II			+	(Obayashi et al., 2011)

+, presence; -, absent

4.4.3 Mechanical Stresses Regulate VICs Activity on Fibrin Based 3D VECs-VICs Co-Culture Constructs

A potential cause of MMVD is a response to valve endothelium injury. An *in vitro* valve endothelium damage model was generated based on the fibrin 3D co-culture constructs, to investigate effect of endothelium injury as well as altered culture substrate stiffness on 3D cultured valve cells.

With endothelium damage, there was an overall up-regulation of SMemb expression towards the wounded endothelial surface on adherent Type 3 (Type 3-A). On floating Type 3 (Type 3-F), however, overall SMemb protein expression in the constructs was decreased, but SMemb positive cells were still observed on the wounded surface of most samples. While in their counterparts (floating entire controls i.e. Control-F), SMemb expression was decreased on the endothelial aspect. The partial TEM results suggest this SMemb reduction might due to cell degradation). Overall, these results suggested VIC activation occurred in the wounded model and SMemb positive cells are presumed to be one of the important sub-population of aVICs in valve injury repair. Interestingly, the other common aVIC marker α-SMA, no evident differential response was observed between floating Type 3 and the control construct at Day 2 and Day 6 after wounding. This further suggests distinction existing between α-SMA and SMemb positive cells.

The ultrastructure analysis on EM showed that there were viable cells surrounded by ECM at the 3D construct wound site at 6 days after damage. Moreover, a monolayer of cells were observed on the uneven fibrin matrix surface which might indicate cell migration from the deeper stroma. Although the cells were displaying an elongated endothelial-like morphology, the true identity of them requires further investigation. Since the above features were absent in the intact control construct (which was generally showing a cell-degraded endothelium), it can be proposed a wound repair process might be occurring in the damaged construct, possibly involves cell migration, and proliferation and ECM production. In previous studies using valve organ culture or standard cell culture techniques, mitral VICs have been found to have wound repair ability, in response to trauma (Durbin et al., 2005; Gotlieb et al., 2002; Lester et al., 1993; Lester et al., 1992; Tamura et al., 2000). By damaging

porcine mitral valve endothelium with linear wounds, VIC proliferation and migration was observed over a 6 day period in native valve explants (Lester and Gotlieb, 1988). VIC repairing processes were found to be associated with a number of cytokines, including FGF-2 (Gotlieb et al., 2002), NO (Durbin et al., 2005) and integrin (Fayet et al., 2007). The ECM component fibronectin has also been found at wounded sites (Fayet et al., 2007). This suggests, apart from cell proliferation and migration, VICs with a secretory phenotype are also involved in regulating wound healing. Durbin and Gotlieb (2002) suggest VIC response to valve injury, similarly to a vascular repair process (Clowes et al., 1983; Koo and Gotlieb, 1991), might be a cooperative process conducted by both motile and secretory VICs. In the early repairing stage, elongated VICs migrate towards wounds and proliferate; while in a second stage, cobblestone shape VICs secrete ECM and metabolic enzymes at the wounding edge while cell migration and proliferation are probably reduced by that point (Durbin and Gotlieb, 2002). This could explain the differences in α-SMA and SMemb positive aVICs observed in this study. It has been shown that the α-SMA phenotype is responsible for VIC migration, contractile function and force generation (Lester et al., 1993; Stephens et al., 2010a). However, the earliest possible response of VICs to endothelium damage (from Day 0-Day 2) was not examined in current study. And it is possible α-SMA protein up-regulation was missed in the damaged constructs. Apparent construct contraction ceased by Day 2 after injury, which might indicate cell mediated contractile activity may decrease after Day 2. Tracing changes in α-SMA expression at earlier time points in the future would be worthwhile.

The exact function of SMemb is not known. As mentioned before, this non-smooth muscle myosin has been identified in embryonic vascular tissue including foetal mitral valves (Aikawa et al., 1993; Kuro-o et al., 1991). It has also been described as a molecular marker of undifferentiated or synthetic type smooth muscle cells (Kuro-o et al., 1991). In normal adult heart valves, SMemb expression is minimal and it has been considered as a marker of mesenchymal cell activation (Disatian et al., 2008; Rabkin-Aikawa et al., 2004b). In Section 3, SMemb expression was demonstrated in 2D cultured VEC and VICs. In current endothelium injury model, SMemb positive cells were identified at sites close to the wounded area, moreover, their distribution

pattern matched that for collagen Type I and III and MMP-1, which suggests this phenotype might be more associated with ECM synthesis comparing to the α-SMA phenotype. This finding is consistent with previous studies by Disatian and colleagues, in which SMemb and α-SMA expression patterns were distinctly different and SMemb appeared to be more related to synthetic activity (Disatian et al., 2008; Disatian et al., 2010).

Valve cell-matrix mechanical interactions have attracted great attention recently (Balachandran et al., 2011; Blevins et al., 2008; Gupta et al., 2008b; Stephens et al., 2010b; Waxman et al., 2012). In the current study, detachment of the polystyrene substrate lead to decreased α-SMA and SMemb expression in the constructs. This effect appears to be dominant to that of endothelium wounding as it was apparent no matter whether endothelium damage was performed i.e. total SMemb and α-SMA deduction was observed in both Type 3-F and Control-F constructs. The similar decreasing trends between SMemb and α-SMA expression on Western blot suggest there might be a co-expression of these two cellular markers. A decrease in vimentin expression was also observed in floating constructs by Western blot and the EM analysis showed evident cell degradation in longer cultured floating constructs particularly in the proposed endothelium. These results indicate a decreased mesenchymal cell proliferation or presence of cell apoptosis. It might be argued that the reduced α-SMA and SMemb expression may be a pure result of total cell loss. However, it is unlikely to be the case. Immunofluorescence result showed the majority of cells on floating constructs were clearly positive for vimentin from Day 0 to Day 6 after manipulation. Therefore, cell death or decreased cell growth on constructs cannot fully explain the apparent loss of cell phenotypic activation. A more likely explanation is that with decreased external mechanical tension, VICs in the constructs transformed from an activated contractile phenotype to a more quiescent phenotype or a secretory phenotype (analogue to reversal of MMVD to a normal valve). Rabkin-Aikawa and colleagues have proposed a hypothesis regarding reversal of VIC plasticity (Rabkin-Aikawa et al., 2004b; Rabkin-Aikawa et al., 2005). They suggest during disease or physiological remodelling processes (‘a new, altered mechanical environment’), VICs tend to be activated and adapt to the new

environment in both biological and mechanical functions. When a new equilibrium is achieved, they will transform back to a quiescent phenotype (Rabkin-Aikawa et al., 2004b; Rabkin-Aikawa et al., 2005). They observed in tissue engineered heart valves, VICs transformed gradually from a myofibroblast phenotype into fibroblast phenotype, particularly after 16-20 weeks *in vivo* remodelling at ovine pulmonary valve site (Rabkin et al., 2002). It is known that VICs are responsive to substrate stiffness (Kural and Billiar, 2013; Stephens et al., 2011; Stephens et al., 2010b). With exogenous mechanical force or high culture substrate stiffness, α-SMA expression was found to increase in vascular smooth muscle cells and aortic VICs in 3D culture systems (Kural and Billiar, 2013; Pho et al., 2008). Presumably decreased mechanical tension in the current model modulated the contractile myofibroblasts to a more quiescent phenotype or secretory phenotype. This assumption is supported by TEM images on Day 6 Control-F construct, where some smooth muscle-like VICs were degrading while the others were viable and synthetically active.

The reversible phenotype plasticity of mitral VIC has been investigated in other 3D culture models. In a 3D collagen matrix culture system, 15% cyclic strain tended to regulate MMVD VICs from myofibroblast to fibroblast phenotype (Waxman et al., 2012). Reversible GAG production by porcine mitral VIC was observed in another collagen hydrogel model, in which GAG level is up-regulated with cyclic stretch and decreased with subsequent relaxation (Gupta et al., 2008a). All these data suggest mitral VICs are responsive to mechanical stimulation in both phenotype and synthesis activity.

There are several limitations to current study. Firstly, in the adherent Type 3 study, it was noticed that the construct fluorescence staining was affected by tissue fixation methodology. Four hour fixation in Methacarn fixative at room temperature (e.g. Day 2 samples) was found to be superior to 24 hour fixation at 4°C (e.g. Day 4 samples). Antigen epitope appeared to be masked in the tissue sample fixed for 24 hours. Control and wounded samples at each time point were collected and fixed using the same methodology therefore comparison results were still valid. Variation in construct morphology within the same group was another issue observed in T3-1 experiment. In the later floating construct study design, sample number was

increased at each time point (n=2 instead of n=1) to reduce the effect of individual sample variation. Reasonable consistency was achieved between individual batches of floating constructs. Moreover, the absence of α-SMA in all Type 3-A samples as well as in diseased mitral valve may be due to a technical issue possibly related to fixation methodology or primary antibody concentration. Further optimization would be necessary to resolve this issue. Secondly, the floating constructs were not planned in the original study design. However, in the second wounding experiment, when conducting endothelium damage, occasionally wounded constructs detached from the culture plate. This is considered to be a limitation of the manual damage techniques used. For future fabrication of Type 3-A construct, tissue stabilizing device (such as sterilized pins) would be necessary to use during the wounding procedure or an alternative damage method devised. Lastly, the ECM response to injury were not systemically evaluated, although collagen I and III and MMP-1 production appeared to be not affected by reduced α-SMA expression on immunofluorescence. Future investigation in assessing ECM related markers (such as MMP-1, MMP-3 and fibronectin) and known cytokines modulating VIC wound repair (such FGF-2, NO and integrin) would be necessary. Multiple immunofluorescence staining techniques possibly would help to get better understanding of the correlation between cell phenotypic and synthetic activation. Moreover, a direct assessment of cell migration (e.g. scanning electron microscopy), proliferation marker expression (e.g. Ki-67) (Disatian et al., 2008) and cell viability will also be useful to get a more complete image of VIC response in the current Type 3 model.

4.5 Conclusion

In summary, fibrin based 3D co-culture models were successfully generated using canine primary mitral valve cells and it is believed they are promising tools for valve cell biology and MMVD pathogenesis research.

Under static culture condition, fibrin/VECs-VICs 3D co-culture constructs assembled into a form more reminiscent of MMVD rather than a healthy valve, regardless if the VIC source was from healthy or diseased valves. This model, therefore, could be used to examine processes that might drive disease reversal. Mechanical stimulations

appeared to have apparent effects in modulating VIC phenotypes. In constructs with endothelium loss, cells appeared to have increased SMemb expression, which indicates cell activation occurred in response to the stimuli. Whereas in constructs challenged with endothelium injury combining decreased mechanical tension, overall SMemb and α-SMA expression were down-regulated. These suggest cells in constructs can undergo phenotypic transformation. The ultrastructure analysis suggests there was a degradation of some smooth muscle-like VICs when the mechanical tension decreased, but other cells were viable and participating in ECM synthesis. Moreover, it was noted that collagen Type I and III and MMP-1 expression was more associated with SMemb positive cells than α-SMA cells. This finding indicates heterogeneity existing in the aVICs population, and the SMemb positive cell population might be involved in ECM synthesis and catabolism.

Chapter 5: Tissue-Engineered Mitral Valve Tubular Construct Models under Dynamic Conditioning

Abstract

Tissue engineering has become an important technology recently in the field of heart valve regeneration. An application of this technology in establishing *in vitro* 3D research models has been considered as being of great value in contributing to the understanding of valve biology and pathology. In this study, the aim was to generate a tubular canine mitral valve construct using tissue engineering techniques. To date the feasibility of fabricating a prototype fibrin based mitral valve tubular construct, as well as construct endothelialisation has been determined. A customised bioreactor system has been designed to use for future dynamic conditioning. These preliminary data establish a foundation for future experiments and the model will be of benefit in researching of MMVD pathogenesis.

5.1 Introduction

Tissue engineering (TE) has recently become an important technology in the field of heart valve regeneration. Using a variety of cells, tissue scaffolds and bioreactor systems, attempts at developing tissue engineered valves have been made by research groups worldwide (Baraki et al., 2009; Flanagan et al., 2009; Jockenhoevel et al., 2001a; Kim et al., 2001; Shinoka et al., 1995; Steinhoff et al., 2000). Although substantial efforts have been made in artificial heart valve development, only a few have been applied to clinical usage in human medicine and the results have been controversial (Konertz et al., 2005; Simon et al., 1993). Inadequate understanding of valve cell biology as well as tissue *ex-vivo* development influences the progress of valve tissue engineering (Butcher and Nerem, 2006). Therefore, artificial three dimensional (3D) tissues have been proposed to be used as pre-clinical research models for answering fundamental questions of tissue physiology and pathophysiology *in vitro* (Gibbons et al., 2012; Griffith and Swartz, 2006).

Mitral valve tissue engineering has been investigated less compared to the aortic and pulmonic valve, mainly due to the complexity of the mitral valve apparatus (Black et al., 2009; Grande-Allen and Liao, 2011). Previous studies related to mitral valve tissue engineering mainly includes investigation of mitral valve cell biology and mechanobiology (Flanagan et al., 2006a; Grande-Allen and Liao, 2011), heart valve embryonic development biology and signalling pathways (Butcher and Markwald, 2007; Chiu et al., 2010; Stock and Vacanti, 2001), and bioreactor system development of mitral organ cultures *in vitro* (Barzilla et al., 2010; Gheewala and Grande-Allen, 2010; Lieber et al., 2010). To our knowledge, so far there have been no reported studies investigating the pathogenesis of myxomatous mitral valve disease (MMVD) utilising a tissue-engineered mitral valve model.

Canine MMVD is the most common cardiac disease in dog and the pathogenesis of this disease is not fully understood. A popular hypothesis of MMVD is long term shear stress of the valve leaflet causing valve endothelium denudation, which triggers sub-endothelial valve interstitial cell (VIC) activation and further extracellular matrix

(ECM) remodelling (Corcoran et al., 2004; Durbin and Gotlieb, 2002; Pedersen and Haggstrom, 2000; Prunotto et al., 2010; Stein et al., 1989). In this study, we aimed to develop a fibrin based canine mitral valve tubular construct using tissue engineering technology, that could be used to test the shear stress hypothesis in the aetiology of MMVD.

5.2 Materials and Methods

5.2.1 Fibrin Based Mitral Valve Tubular Construct Fabrication

Fibrin based canine mitral valve constructs were produced using a similar moulding methodology previously described for a vascular structure fabrication (Tschoeke et al., 2009). Details of protocols have been covered in Section 2.10.1 and 2.10.3. The cell source used for tubular construct generation was identical to the cultures used previously for 3D static cultures as described in Section 4. The schematic image in Figure 5.1 illustrates the fabrication process and the key devices involved in construct production are shown in Figure 5.2. The tubular construct mould and the medium reservoir for construct culture were kindly provided by the collaborators in RWTH Aachen University, Germany. Fabricated constructs were cultured in a 30 rpm continuous flow circulation system (Figure 5.3) for one week before measurement and analysis.

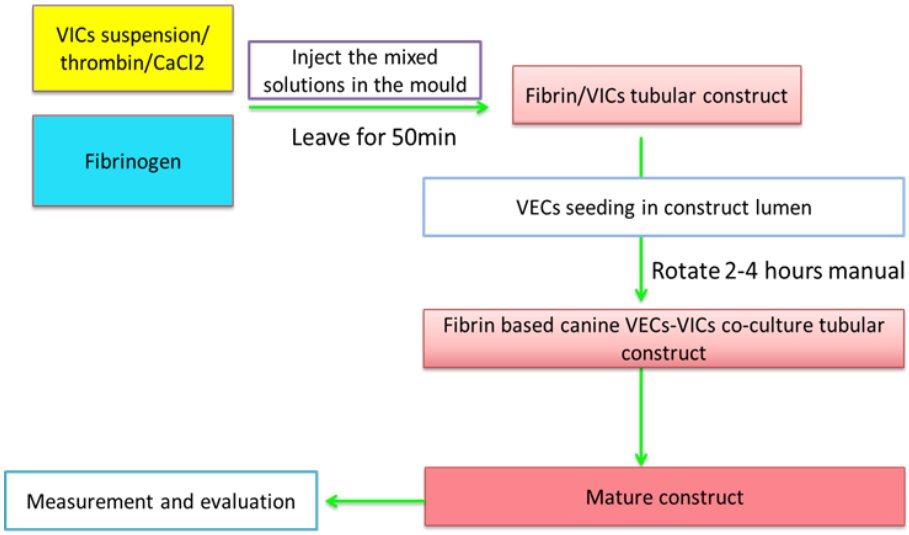

Figure 5.1. Schematic illustration of fibrin based canine mitral valve tubular construct fabrication process. Similar to static constructs, fibrin/VICs hydrogel was first generated in a dual cylinder mould (Figure 5.2 B). Endothelial cells were subsequently seeded on the luminal surface of the tubular constructs by manual rotation (Figure 5.2 D). Fabricated constructs were removed from the mould and transferred to a low rate flow circulation system (Figure 5.3) and cultured for one week before measurement and evaluation.

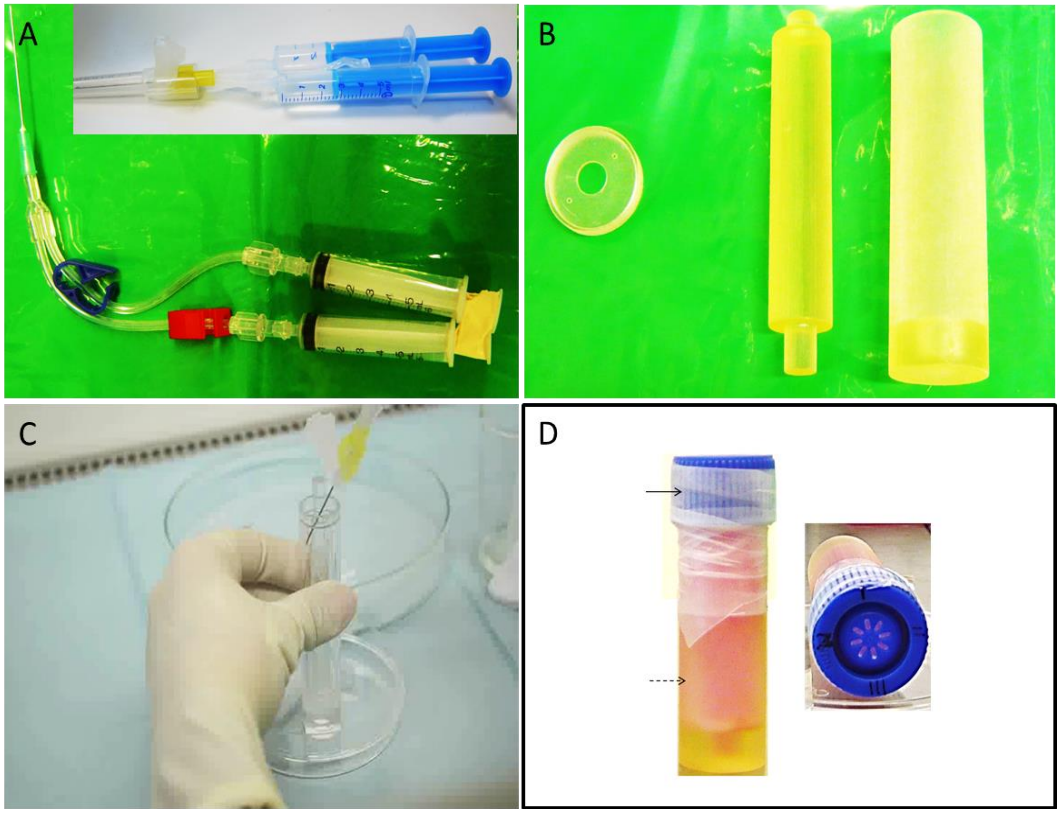

Figure 5.2. Key equipment for canine mitral valve tubular construct fabrication. A. Dual chamber syringe was used for simultaneously injection of VICs suspension/ thrombin/$CaCl_2$ and fibrinogen. A customised syringe was used in the current experiments (syringe on bottom) and a commercial product will be used in future fabrication (inset photo, kindly provided by Dr Tom Flanagan, University College Dublin, Ireland). B. Customised silicone moulding device composed of a sealing cap, a core cylinder and outer cylinder with lumen. C. Fibrin/VICs gel moulding process. Mixed solutions were injected in the mould lumen space at a constant speed (image was provided by RWTH Aachen University, Germany). D. Customised endothelial seeding device. Inner cylinder was removed subsequent to fibrin/VICs hydrogel polymerization, VEC suspension was added to the construct lumen (dash arrow in D) and filled up to the top of the mould. Seeding device was sealed with a T80 flask filter cap and secured with parafilm (solid arrow in D). The device was placed in standard tissue culture incubation and rotated by 90^{o} (in first experiment) or 45^{o} (in second experiment) every 15 min for 2 h or 4 h respectively following marked directions on the cap.

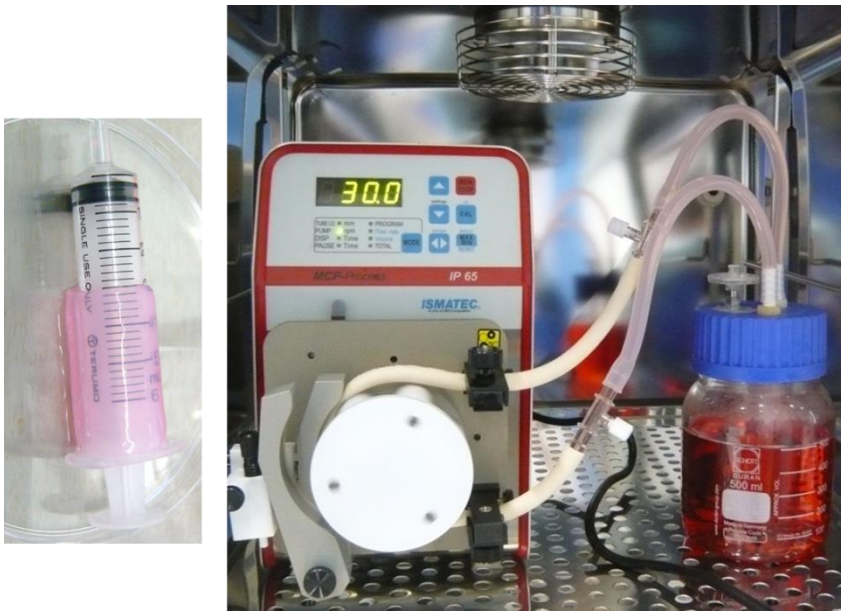

Figure 5.3. Equipment for canine mitral valve tubular construct culture at low rate flow circulation system. After endothelial cell seeding, constructs were removed from the mould and placed on a 5 ml supporting syringe to prevent collapsing. The tubular construct was then transferred to a sterile reservoir containing bioreactor culture medium and connected to a MCP process pump by rubber and silicone tubes. A sterile 0.2 µm venting filter was placed on the cap of the medium reservoir to allow gas exchange in the culture system. One direction continuous flow was set at a rate of 30 rpm. The assembled culture system was kept in a standard tissue culture incubator for 7 days.

5.2.2 Constructs Evaluation

5.2.2.1 Construct Contraction Assessment

After 7 days low rate flow circulation culture, constructs were harvested and measured for length, thickness and lumen diameter using an electronic vernier caliper. These parameters were compared to values obtained on Day 0 culture (right after fabrication). Details of the measurements are described in Table 5.1.

Table 5.1 Measurement of tubular construct length, thickness and lumen diameter

Construct	Length	Thickness	Inner diameter
Day 0	Direct measurement	Indirect measurement =½ (mould outer cylinder inner diameter – mould inner cylinder diameter)	Indirect measurement = mould inner cylinder diameter
Day 7	Direct measurement	Direct measurement	Indirect measurement = supporting syringe diameter

5.2.2.2 Endothelium Formation Assessment

Harvested tubular constructs were divided in to three parts and a 0.5 mm length tissue ring of the middle third of the construct was used for endothelium assessment. The ring was cut vertically and dissected into two strips. Luminal surface of construct strips was incubated with 0.5-1 ml diluted DiI-Ac-LDL for 4 h at 37°C and 5% CO_2, rinsed with 3 x 5 times sterile PBS and transferred construct strips to an invert glass slide for confocal microscopy (with endothelium side facing down). Constructs were maintained in small amount of sterile PBS during analysis. All treatments were carried out in a dark room to reduce light exposure. Stack images

were captured with Zen imaging software and the maximum intensity image is presented in Section 5.3.2.

5.3 Results

5.3.1 Tubular Construct Gross Morphology and Contraction Assessment

The current study demonstrated the feasibility of utilizing canine mitral VECs and VICs to fabricate a tubular construct. Constructs (n=2, 'n' indicates the number of construct fabrication experiment) cultured under low rate flow circulation were harvested on Day 7. They dramatically had shrunk in size and became less transparent compared to Day 0 (Figure 5.4). The length, thickness and inner diameter values of the two constructs are summarized in Table 5.2. After 7 days culture, the constructs showed a 29.1% and 33.7% decrease in length, 55% and 69% decrease in thickness and 0.7% decrease in inner diameter respectively.

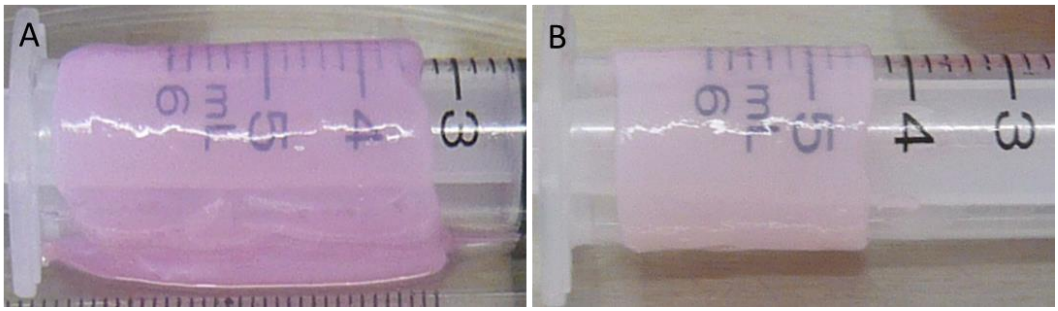

Figure 5.4. Mitral valve tubular construct morphology on gross inspection. Construct at 7 day culture (B) shrank in size compared to Day 0 culture (A), and demonstrated a more tissue-like less translucent appearance.

Table 5.2 Construct parameters before and post low rate flow circulation culture.

Construct 1 Measurement		Length (mm)	Thickness (mm)	Inner diameter (mm)
	Day 0	30.6	2.0	16.1
	Day 7	20.3	0.9	15.5
Ratio (Day 7:Day 0)		66.3%	45%	96.3%

Construct 2 Measurement		Length (mm)	Thickness (mm)	Inner diameter (mm)
	Day 0	36.5	2.0	16.1
	Day 7	29.5	0.62	15.5
Ratio (Day 7:Day 0)		80.9%	31%	96.3%

5.3.2 Construct Histology and Endothelium Formation Assessment

Cultured tubular construct showed tissue-like morphology on histology (Figure 5.5). Compared to static constructs (Figure 4.9), cells on tubular construct were more evenly distributed and a sub-endothelial dense cell-matrix layer was not observed. A number of lacunae were found interspersed between stromal cells, which may be caused by cell loss. Monolayer cells were found to line the construct luminal surface, however the coverage was not even between different areas within the same construct (Figure 5.5 B and C)

Tubular construct endothelium was assessed by up-take of DiI-Ac-LDL. Uneven positive cell coverage was observed on the luminal surface of both constructs examined (Figure 5.6).

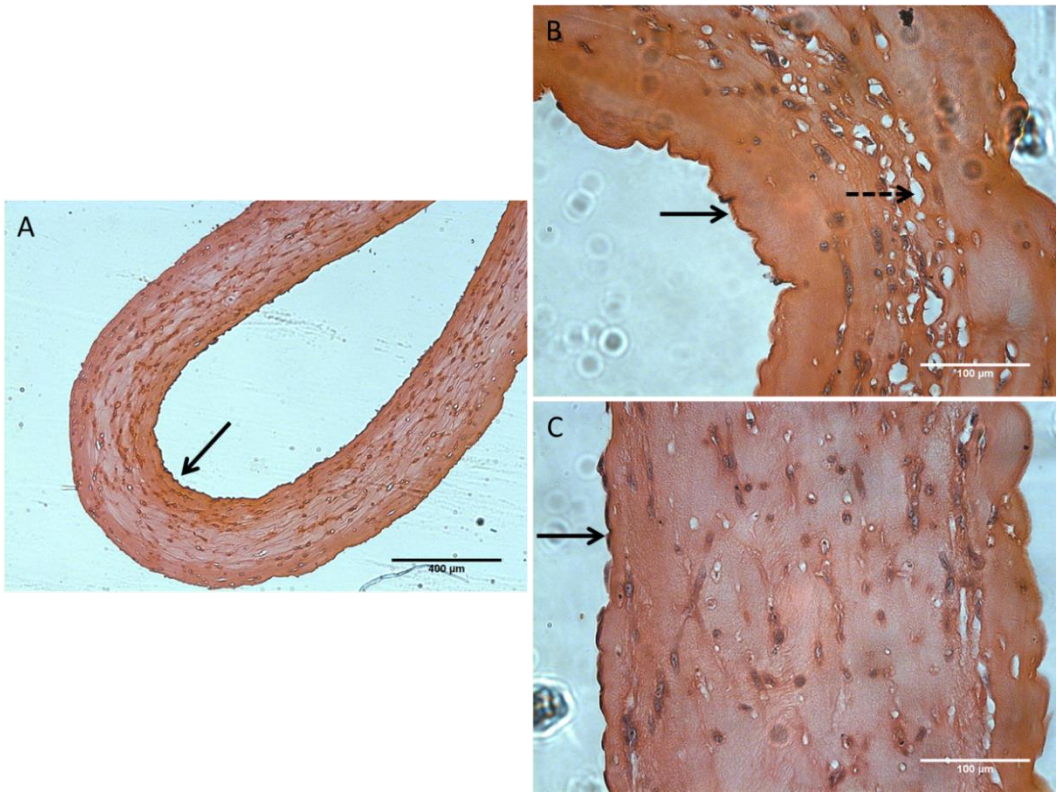

Figure 5.5. Histology of fibrin based mitral valve tubular construct cultured under a low rate continuous flow conditioning. Construct lumen surface is indicated by solid arrows. A. compared to static constructs in culture plate (Figure 4.9), the tubular construct demonstrated more even cell distribution and the sub-endothelial dense cell-matrix layer of the static construct was not observed in the tubular construct. B. cavernous areas were found in valve stroma (dash arrow). C. A monolayer of cells was observed on part of the construct luminal surface (presumed endothelium). Scale bar in A = 400 µm; scale bar in B and C =100 µm.

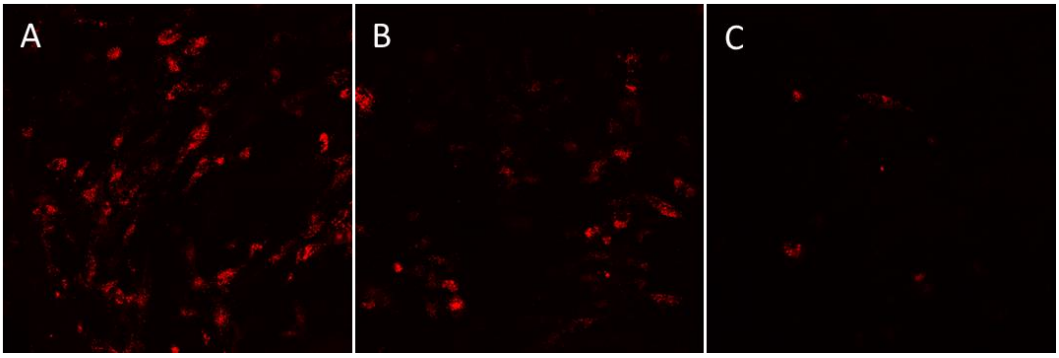

Figure 5.6. DiI-Ac-LDL labelled endothelial cells in one tubular construct luminal surface. Three separate area as shown in A, B and C. Uneven endothelial cell distribution was observed between different areas of the construct. Magnification x 200.

5.4 Discussion and Future Plan

The study design of the dynamic conditioned tubular construct comprises two stages and is shown in detail in Table 5.1. Results of the fabrication of the tubular construct in Stage 1 are presented in the current chapter, due to time constraints the results of Stage 2 have not been presented as part of this thesis and further work is planned and discussed in Section 5.4.2 and 5.4.3.

Table 5.3 Study design of dynamic conditioned tubular construct experiments

Stage	Experiments
Stage 1	Preparation for dynamic conditioning: testing the feasibility of generating a mitral tubular construct by using canine primary mitral valve cells and evaluating construct shrinkage and mechanical properties when cultured in a low rate flow circulation system for a 7 day period; and designing of a customised bioreactor system for Stage 2 pulsatile flow conditioning.
Stage 2	Applying dynamic conditionings to the tubular constructs. Three types of construct models will be generated: Dynamic Type 1 (pulsatile control)-constructs cultured in low rate flow loop for 14 days, which serve as 'static' controls for pulsatile flow conditioning; Dynamic Type 2 (physiological model)-constructs cultured in pulsatile flow condition in the bioreactor system for 14 days; Dynamic Type 3 (pathological model)-damage luminal endothelium of Dynamic Type 2 constructs and condition the constructs within the pulsatile flow bioreactor for another 7 days.

5.4.1 Development of A Fibrin Based Prototype Valve Tubular Construct

To date, a prototype valve tubular construct model using primary canine mitral valve cells has been generated. Preliminary data has shown the feasibility of tubular construct fabrication. Histologically morphology of the construct under low rate continuous flow conditioning demonstrated tissue-like morphology and relatively even cell distribution throughout the constructs. A number of lacunae existed in construct stroma possibly due to cell loss. This incidence of this phenomenon might be reduced or prevented by dynamic conditioning as it has been shown that this can enhance cell adherence to tissue engineering substrates (Flanagan et al., 2007; Schenke-Layland et al., 2003). By using a customised manual cell seeding device, endothelial lining of the construct lumen was partially achieved. The uneven endothelial cell distribution in the current method is not ideal. Dynamic seeding at low rotating speed would likely improve endothelial surface seeding (Flanagan et al., 2009; Lichtenberg et al., 2006; Tschoeke et al., 2009), which will be carried out in future experiments.

Cell contractility mediated construct shrinkage as well as tissue weakness are common concerns in hydrogel based tissue-engineered structures (Jockenhoevel et al., 2001b; Mol et al., 2005). In the current study design it was essential to obtain a tubular construct with relatively stable structure geometry and tissue strength prior to dynamic conditioning. Therefore, the shrinkage of the fibrin based tubular constructs was initially evaluated after a 7-day period low rate flow circulation culture. Pilot results from the two tubular constructs demonstrated that the construct contraction occurred in three dimensions: construct size decreased in length, thickness as well as luminal space. The ratios of construct parameters on Day 7 compared to Day 0 were fairly consistent between the two experimental runs: approximate 30% decrease in length (29.1% and 33.7% respectively) and 60% decrease in thickness (55% and 69% respectively). The shrinkage extent of constructs provides guidance for optimizing mould choice, as an appropriate construct configuration will be necessary for cyclic motion in the pulsatile flow bioreactor system. Moreover, in the future, it

will be necessary to test tissue strength of the tubular constructs prior to dynamic conditioning to get an idea of the maximum force the fibrin construct can withstand (Tschoeke et al., 2008).

5.4.2 Design of a Customized Bioreactor for Dynamic Conditioning

A bioreactor system for dynamic conditioning has been designed and produced by collaborators in RWTH Aachen University, Germany. The main body of the bioreactor is a silicone chamber (Figure 5.7A). It connects with a medium reservoir (Figure 5.7E) and a MCP processing pump (Figure 5.7D). Biochemical and flow mechanical parameters in the culture system can be programmed by a computer (Figure 5.7B) and monitored through a sensor (Figure 5.7C). By generating pulsatile flow with the pump, the flexible opening of the tubular construct (demonstrated by a plastic tube model in Figure 5.7A-1-3) is expected to open and close in response. This imitates native mitral valve motion in the systolic and diastolic phase of the cardiac cycle *in vivo*.

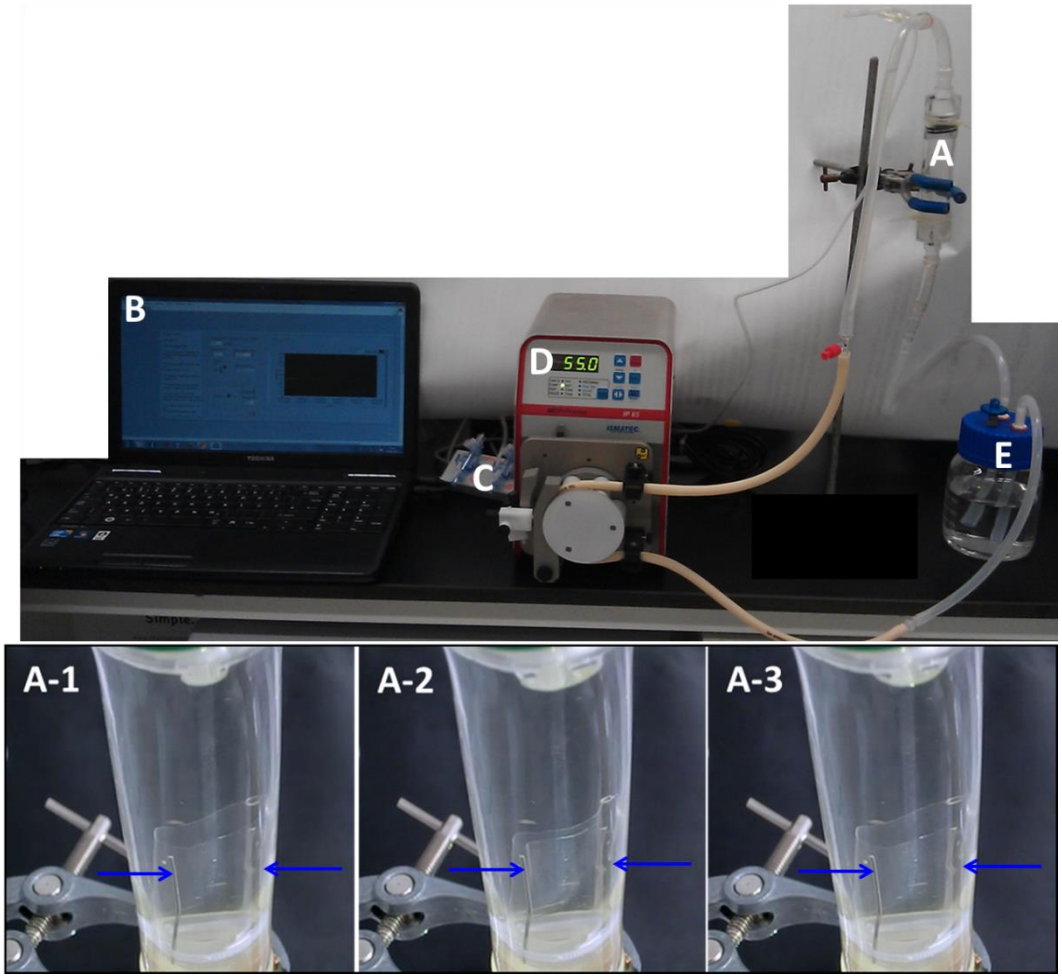

Figure 5.7. A bioreactor system (model) provides dynamic conditioning for a tubular construct. The customised dynamic conditioning system is composed of a MCP process pump (D) for generating cyclic flow, a bioreactor chamber (A) for construct culture, a medium reservoir (E) for nutrient supply and gas exchange, a sensor (C) and a computer (B) for culture condition monitoring and parameter control. The movement of the construct is expected to mimic native mitral valve movement during the cardiac cycle. An open-close-open cyclic motion (A-1-3) is demonstrated by a plastic tube model and the images are from a video file provided by collaborators in RWTH Aachen University, Germany. Arrows in A-1-3 indicated two mental stands which are supporting the plastic tube model to avoid collapsing.

Details of the planned design of the tubular constructs under dynamic culture conditions are summarized as follows: one opening of the tubular construct will be sutured to the silicone tube base of the bioreactor. The distal one third of the construct relative to the suture ring will represent mitral valve leaflets and the remainder will represent the left atrial wall (Figure 5.8). The distal one third flexible opening of the construct will mimic valve leaflet motion during the cardiac cycle. The luminal aspect of the construct represents the atrial part of the valve leaflet and the outer part of the construct the ventricular aspect of the valve leaflet. The atrial aspect of valve leaflet will experience physiological flow across the mitral orifice. When flow moves from the proximal opening of the construct to the distal end, 'tubular MV leaflets' in an open position will mimic the diastole phase of native cardiac cycles (Figure 5.8A); when flow moves from the distal part of tubular constructs to the proximal opening, 'leaflets' will close which imitates a systolic phase (Figure 5.8B), in which the flow direction within the tubular constructs is opposite to a native valve. As endothelium is absent on the construct outer surface it will not be investigated in the current study design.

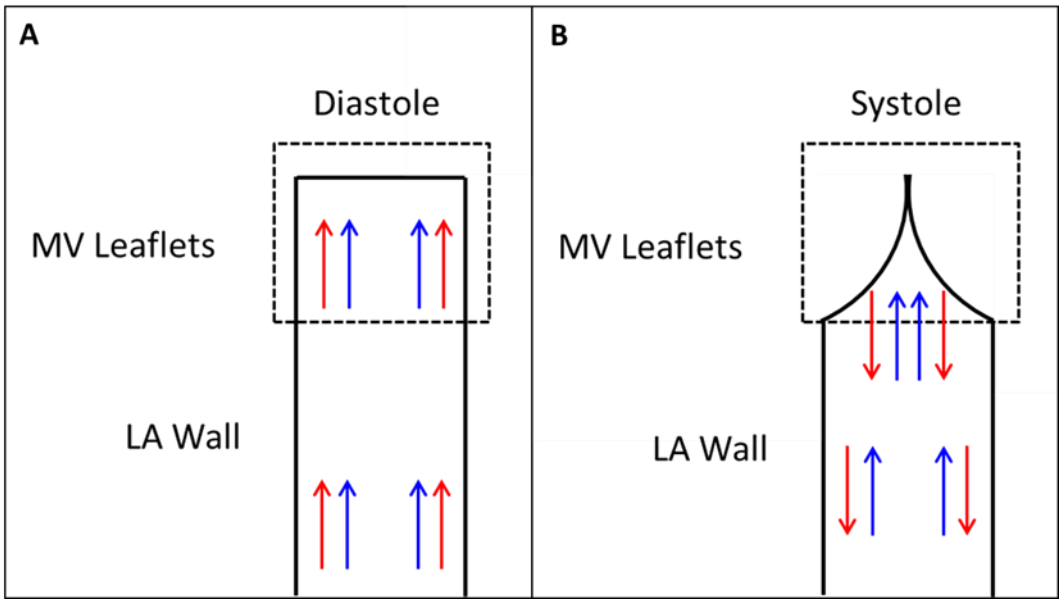

Figure 5.8. Schematic illustration of the design of pulsatile flow conditioned tubular constructs. The red arrows indicate flow directions in the bioreactor system; while the blue arrows indicate flow directions in native adult heart left atrium. During 'diastole', the flexible end of the tubular construct (represents MV leaflets) is in an open position with shear flow passing across (A); during 'systole', the flow reverses in direction and the 'MV leaflets' close (B).

To date, though basic design of the pulsatile flow bioreactor system has been developed, the detailed conditioning parameters have not been determined so far. In previous studies, dynamic conditioning systems have been developed for mitral valve organ culture (Barzilla et al., 2010; Gheewala and Grande-Allen, 2010; Lacerda et al., 2012a; Lacerda et al., 2012b; Lieber et al., 2010).

Typically adult heart physiological flow conditions were aimed to be reproduced in these systems as the cultivated organs were mature animal heart valves. For tissue-engineered valves, however, the application of physiological dynamic conditions for adult hearts would not necessarily be applicable for the early tissue development construct models. It has been suggested any type of TE cardiovascular structure should be conditioned following a foetal cardiac developmental protocol, which is less than 5% radial strain, low oxygen tension and a crescendo heart rate (Stock and Vacanti, 2001).

Gradually increased pulse rate dynamic conditioning as well as low shear stress conditioning has been found to enhance cell attachment and alignment as well as ECM remodeling in tissue engineered heart valves (Flanagan et al., 2007; Flanagan et al., 2009; Jockenhoevel et al., 2002; Weston and Yoganathan, 2001). Once a relatively mature neo structure is achieved, it would be reasonable to gradually adjust conditions towards a physiological level. In adult dog heart, maximum early diastolic transmitral pressure gradient (ETP_{max}) is 2.8 ± 0.8 mmHg (Courtois et al., 1988). Normal diastolic flow velocity peak across mitral valves is considered as a range of in 0.8-1.0 m/sec (Belanger, 2010). Adult dog heart rate is about 70-160 beats/min (Cote, 2010). All these physiological parameters should ideally be reproduced *in vitro* for mature canine tissue engineered mitral valve construct cultivation.

In summary, an integration of construct mechanical properties and general criteria of tissue engineered construct dynamic conditioning as well as native adult physiological cardiac flow parameters will determine the specific values of the dynamic conditioning in future experiments involving this model.

5.4.3 Potential Application of the Valve Tubular Construct for MMVD Pathogenesis Investigation

The initial application current valve tubular construct is planned to test the shear stress hypothesis in the aetiology of MMVD. As has been described in Table 5.1 (Stage 2), three types of tubular construct models will be generated in next step of this project. By utilizing pulsatile shear flow conditioning, it is predicted a superior physiological model will be achieved showing greater resemblance to native mitral valve compared to static 3D cultures. A pathological model (endothelial damage) will also be produced based on normal dynamic conditioned constructs. It is expected that myxomatous mitral valve disease related changes will occur in the wounded model, such as endothelial dysfunction, VIC phenotype transformation, proliferation and migration as well as ECM remodeling.

Potential further applications of this model could include application in drug discovery and therapeutic investigation, as well as MMVD putative marker examination. Potential examples include antagonists of endothelin receptors (Mow and Pedersen, 1999), serotonin receptor blockers (Orton et al., 2012; Oyama and Levy, 2010) and advanced glycation end products.

5.5 Conclusion

A tubular mitral valve construct has been developed and the principal and the feasibility of construct fabrication and endothelialisation has been confirmed. A customized bioreactor system has been designed and specific conditioning values will be decided at a later date. In future work, the dynamic conditioned valve tubular construct model will be used for research of MMVD.

Chapter 6: Expression of Advanced Glycation End Product Carboxymethyllysine in Canine Myxomatous Mitral Valve Disease

Abstract

In the current study, fibrin based mitral valve constructs have been developed. It is believed these *in vitro* models can be a research platform to investigate the role of a wide range of molecules with biochemical effects in valve function and disease. In this project the intention was firstly to investigate the role of advanced glycation end products (AGEs) in MMVD pathogenesis. Prior to the 3D construct based investigation, it was necessary to know if there is a link between AGEs and naturally developed MMVD.

The aim of this study was to determine the expression of the advanced glycation end product-carboxymethyllysine (CML) in native valve tissue and blood samples of dogs with myxomatous mitral valve disease, and to investigate the potential role of AGEs in canine MMVD, using a combination of protein immunoblotting (Western blot), immunohistochemistry and ELISA techniques.

CML expression was clearly identified in canine mitral valves. Comparing normal (n=3) and diseased valves (n=3), there was a clear difference with marked increased expression of CML in the diseased valves. When serum expression of CML in normal dogs (n=8) and dogs with confirmed MMVD (n=15) was compared, there was no difference in expression (1.15 ± 0.16 µg/ml vs 1.18 ± 0. 12µg/ml). There was a tendency for weak negative correlation between CML serum values and age.

These findings suggest CML might contribute to the pathogenesis of MMVD, and the role of CML in MMVD can be further investigated utilising current 3D static mitral valve construct model. This will be under-taken in future studies.

6.1 Introduction

In previous chapters, tissue engineered canine mitral valve 3D constructs have been developed. It is believed these are promising research tools for investigation of MMVD aetiology. They can be particularly useful in examining putative chemicals related to MMVD. For example, the advanced glycation end products.

Advanced glycation end products (AGEs), examples include pentosidine and carboxymethyllysine (CML), are complexes produced in the Maillard reaction that have important effects on extracellular matrix (ECM) biology. Once formed, AGEs are persistent compounds and natural age-associated accumulation has been found in many tissues including skin, bone and cartilage, and heart and blood vessels (Singh et al., 2001). AGEs can also be dietary in origin, with the main source being high heat processing or cooking of food which is also known to contribute to diabetic nephropathy in humans (Semba et al., 2010; Yamagishi, 2011). AGEs have high affinity for long-living proteins such as present in ECM and can impair tissue functions through a variety of pathways, including forming glucose-mediated intermolecular cross-links (Hartog et al., 2007). These cross-links are considered as having a primary effect on aging of collagen, increased biomechanical stiffness and enzyme-resistance, and reduced collagen turnover. AGEs also react with their receptor (RAGE) resulting in induction of oxidative stress, up-regulation of inflammatory signals and connective tissue growth factors which can then lead to expansion and remodelling of the ECM and endothelial dysfunction (Twigg et al., 2001).

The study of AGEs in cardiac disease has concentrated on diabetes mellitus and the consequent damaging effects on cardiac function, the increased risk of cardiovascular events, and atherosclerosis as part of the metabolic syndrome (Barlovic et al., 2011). In ageing and the diabetic heart, collagen acts as a target protein for AGEs accumulation. The reduced compliance of cardiovascular tissue in heart failure may be a result of AGEs cross-linking collagen and elastin, increased collagen production and reduced collagen degradation. Indeed, soluble RAGE and serum pentosidine are

recognised as independent risk factors for heart failure in human patients, and plasma CML level has been found to be associated with severity and prognosis of chronic heart failure in human patients (Koyama et al., 2007; Koyama et al., 2008). In the dog AGEs accumulation has been found in cerebellar neurons, aorta, cartilage, blood and atherosclerotic lesions of dogs, but not in myocardium (Chiers et al., 2010; Comazzi et al., 2008; DeGroot et al., 2004; Shapiro et al., 2008; Weber et al., 1998).

Myxomatous mitral valve disease (MMVD) involves changes in extra-cellular matrix components, including a disorganization of valve collagen and increased glycosaminoglycan (GAG) content. The extent and severity of connective tissue loss is closely associated with age-dependent disease status (Hadian et al., 2007; Han et al., 2010). An alteration in collagen fibril alignment and failure of maturation of newly produced collagen has been observed in canine MMVD previously (Hadian et al., 2010; Hadian et al., 2007). Since MMVD clearly involves changes in ECM production and organisation and alteration in collagen cross-links have previously documented with this disease, the aim of this pilot study was to investigate the possible role of CML in canine MMVD, by determining expression in valve tissue and measuring circulating CML levels. It has been hypothesized that the expression of CML is increased in myxomatous mitral valves.

6.2 Materials and Methods

6.2.1 Animals and Tissue Samples

Mitral valve samples (Table 6.1) from three adult dogs with gross pathological evidence of MMVD (Whitney grading 1/4-4/4), and three normal dogs were collected and prepared for examination as described in Section 2.1.

Table 6.1 Animals used for CML Western blot and immunohistochemistry

Animal	Age	Gender	Breed	MMVD Severity (Whitney Grade)
D-1	4Y	F	Mongrel	3/4
D-2	5Y	F	Mongrel	4/4
D-3	1Y	M	beagles	1/4
H-1	<1Y	M	beagles	0/4
H-2	1Y	F	beagles	0/4
H-3	1Y	F	beagles	0/4

Twenty three whole blood samples (15 MMVD cases and 8 dogs with no evidence of MMVD (control group)) were collected for ELISA analysis and the details are shown in Table 6.2. All blood samples were collected as part of an individual dog's clinical care and only unused remnant of a sample was retained for analysis in accordance with accepted institutional and national guidelines, and with informed owner consent. Detail of blood sample preparation is described in Section 2.1. All dogs were checked for evidence of diabetes mellitus and renal failure using standard biochemical tests, and found to be unaffected. Either serum or plasma sample of each dog was used for CML-ELISA analysis.

Table 6.2 Animal cases used for CML ELISA study

Group	Age (Year)	Gender		Breed	Blood Glucose Level (mmol/l)
	Range (Mean)	F	M	Breed (Number)	Range (Mean)
MMVD n=15	5.5-15 (10.1)	8	7	Labrador Retriever (1) Bichow prise (1) WHWT (1) Rottweiler (1) CKCS (6) Border Collie (3) Weimaraner (1) Mongrel (1)	4.2-6.7 (5.4)
Control n=8	5.0-12.5 (8.0)	3	5	CKCS (1) WHWT (2) Doberman (1) Springer Spaniel (1) Deerhound (1) Leonberger (1) Mongrel (1)	4.9-6.3 (5.8)

F, female; M, male

6.2.2 Western Blot

Related protocols of protein sample preparation and immunoblotting are described in Section 2.2. Protein samples derived from three MMVD valve and three normal mitral valves were probed with CML antibody (ab27684, Abcam, UK) at a concentration of 1 in 1,000 and the secondary antibody was same swine anti-rabbit antibody in Table 4.3 and the working concentration was 1 in 1,000. Ponceau S staining of the proteins on the membranes was carried out as loading control.

6.2.3 Immunohistochemistry

Detail of tissue section preparation and immunohistochemistry protocols are described in Section 2.11.5. Primary CML antibody was same as for immunoblotting at a concentration of 1 in 250. The rest of the reaction solutions including a secondary antibody were provided in the R.T.U. VECTASTAIN Elite ABC Kit. Detailed information has been described in Section 2.11.5. Canine skin tissue section

was used as a positive control for CML. Images were captured by using a Leica DMRB microscope. Representative images at magnification x 200 are presented in this chapter.

6.2.4 ELISA

A CycLex CML ELISA Kit (CY-8066, CycLex Co, Japan) was used to detect circulating CML levels. Prior to the assay, all reagents were brought to room temperature. First Antibody, 10 x Wash Buffer and CML-human serum albumin (HAS) Standard were provided in kit and the solutions were reconstituted according to manufacture instruction. CML-HAS Standard solution was prepared in a dilution series at concentration of 5.0 µg/ml, 2.5 µg/ml, 1.25 µg/ml, 0.63 µg/ml, 0.31 µg/ml, 0.16 µg/ml, 0.08 µg/ml and 0 µg/ml. Canine serum or plasma samples were 1 in 4 diluted with Sample Dilution Buffer (provided in the kit) in appropriate wells of a 96 well sample preparation microplate. 60 µl CML-HAS Standards and diluted samples were added in appropriate wells of the preparation microplate. 60 µl First Antibody working solution was added and mixed in each well. 100 µl prepared mixture was transferred to an Antigen Coated Microplate (provided in the kit) and incubated at room temperature for 1 h on an orbital microplate shaker. The microplate was washed by adding 350 µl Wash Buffer for 4 times. Subsequent to the washing step, 100 µl Substrate Reagent (provided in the kit) was added to each well and incubated for 20 min. The reaction ceased by adding 100 µl Stop Solution (provided in the kit). After all reactions, optical density (OD) value of each well was measured at 450nm using a VICTOR3™ V Multilable Counter (Perkin Elmer). A standard curve was obtained by plotting the optical density for the standard versus the concentration of the standard. The sample CML concentrations were then determined by a sigmoidal five parameter logistic equation calculated by using MasterPlex® EX 2010-Multiplex Expression Data Analysis Software (Hitachi Solutions America, Ltd. MiraiBio Group, USA). Dr.Uemoto Yoshinobu kindly provided help for statistical analysis with R program (The R Foundation, Austria). ANOVA test was performed to determine the data difference between normal and MMVD groups. Correlations

between CML level and age were obtained using the Pearson's product-moment correlation.

6.3 Results

6.3.1 Western Blot Analysis

When comparing CML modified protein expression in MMVD and normal dogs there were marked differences: CML modified proteins were clearly detected in three MMVD dogs, with band sizes between 20 and 105 kDa; While in the three normal mitral valves, very weak or no expression of CML was found (Figure 6.1).

Ponceau S staining demonstrates equal loading of the protein samples.

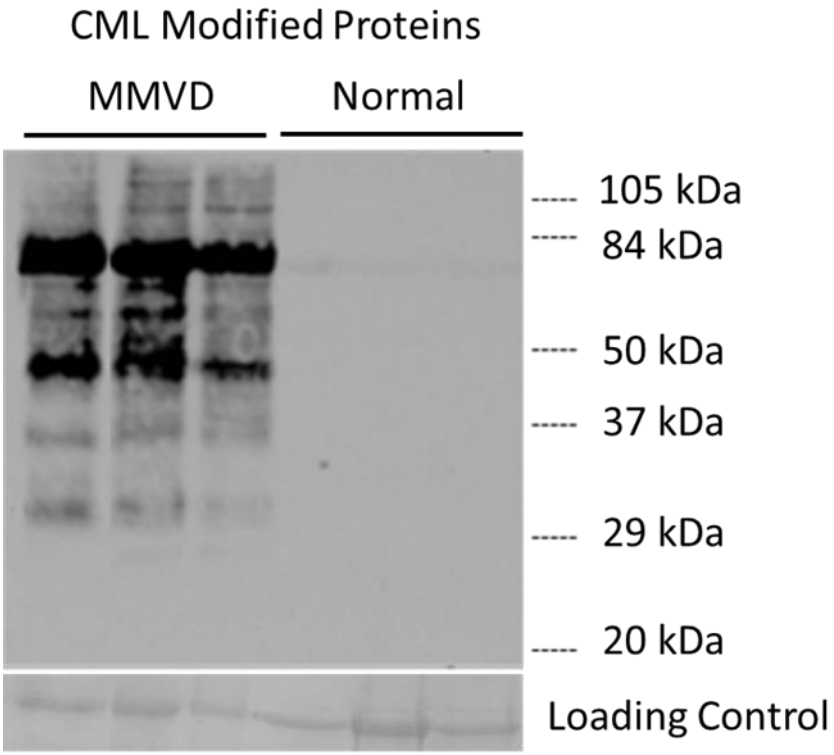

Figure 6.1. CML modified protein expression in canine MMVD and normal mitral valves on Western blot. Differential CML expression was observed between MMVD and normal group. CML modified protein bands between 20 and 105 kDa were detected in MMVD, while minimal CML expression was found in normal mitral valves. Ponceau S stained proteins were used as an equal loading control.

6.3.2 Immunohistochemistry

Consistent with findings of immunoblotting, there was marked difference of CML expression between MMVD and normal mitral valves on immunohistochemistry (Figure 6.2). In normal mitral valves from three young dogs, the CML expression was weak to absent. All three healthy valves showed no evidence of CML expression in valve distal edge (Figure 6.2A). In normal valve base, some cardiomyocytes were positive for CML and a faint stroma staining was observed in one valve (Figure 6.2 B). While in MMVD group, strong CML expression was detected in all three diseased valves. The CML staining in MMVD valve was present all through the valve leaflet length, from distal edge to valve base. The CML expression was evident in endothelium and interstitial cells in stroma of the valve distal edge (Figure 6.2D). In the proximal area, CML expression was prominent in cardiomyocytes as well as deep stroma, presumably the fibrosa lamina (Figure 6.2E).

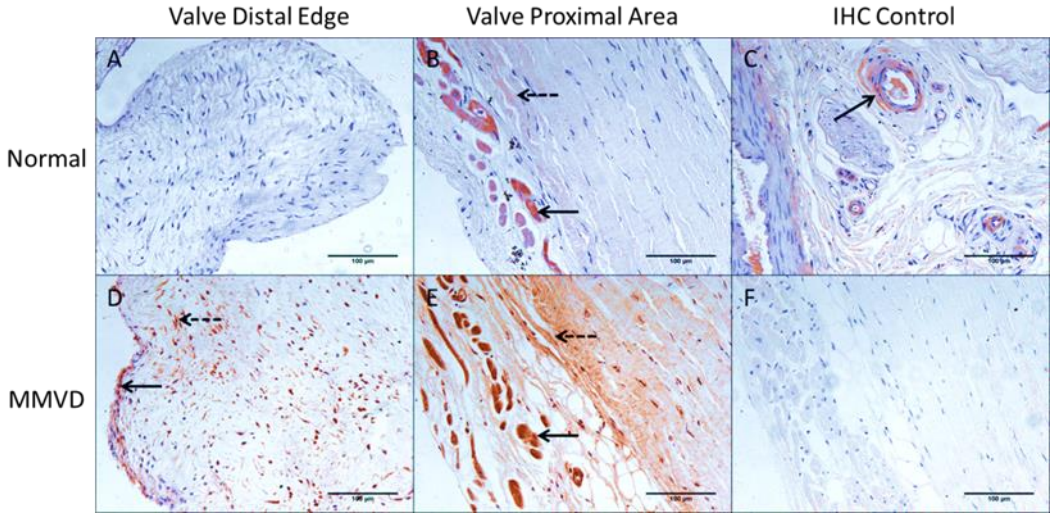

Figure 6.2. CML modified protein expression in canine MMVD and normal mitral valves on immunohistochemistry. In normal mitral valve, CML expression is absent in valve distal edge (A); weak to minimal staining was observed in myocytes (solid arrow in B) and weak stroma staining was observed in one valve (dash arrow in B); canine skin tissue was used as a positive staining control for normal valve CML immunohistochemistry (C), arrow in C indicates a stained blood vessel-like structure; while in MMVD valves, marked CML expression was observed in endothelium (solid arrow in D) and stroma interstitial cells (dash arrow in D) of valve distal area; towards to valve base, the CML staining was prominent in myocytes (solid arrow in E) and deep stroma (dash arrow in E); CML primary antibody omitted tissue section (F) was used as a negative control for MMVD valve CML immunohistochemistry. Scale bar =100 μm.

6.3.3 ELISA

The circulating CML ELISA results are shown in Figure 6.3. The mean CML level in blood sample was 1.18 ± 0.12 µg/ml in the MMVD group (n=15) and 1.15 ± 0.16 µg/ml in the control group (n=8). There was no statistically significantly difference between the two groups when comparing means or the variances. There was a tendency for weak negative correlation (r = -0.39) between circulating CML values and age for the combined groups (n=23), where MMVD cases were considered alone (r = -0.46), and for the control dogs only (r = -0.37), but these Pearson's product-moment correlations did not have associated p values less than 0.05 indicating a much large sample would be need to confirm if the correlations were real (Figure 6.4).

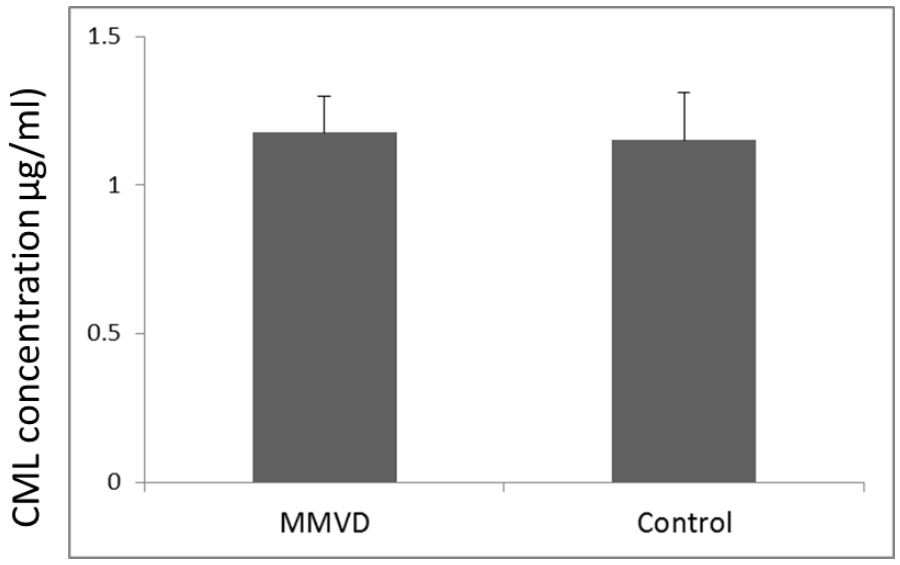

Figure 6.3. Circulating CML level in MMVD and normal control dogs. Statistically, the CML concentration in blood was not different between the two groups. The circulating CML level in MMVD group (n=15) was 1.18 ± 0.12 µg/ml, and was 1.15 ± 0.16 µg/ml in the control group (n=8).

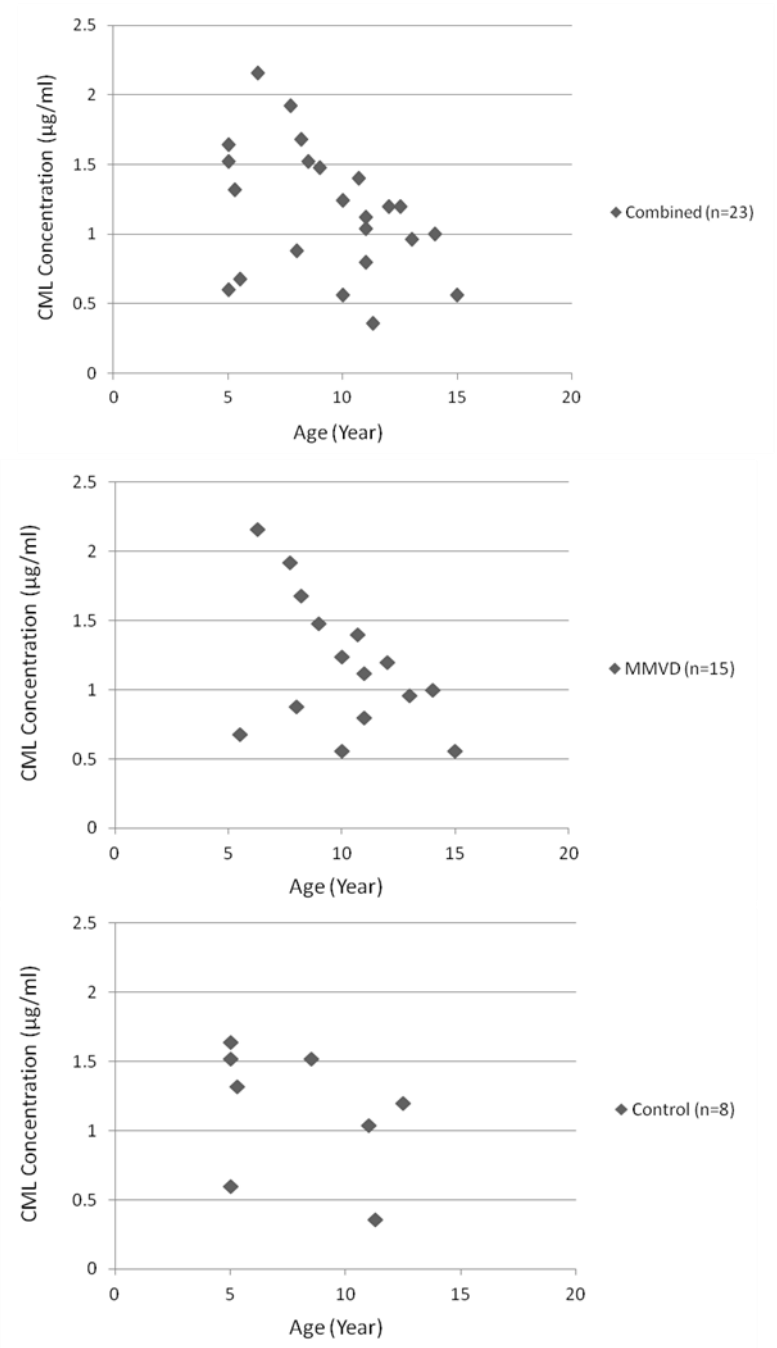

Figure 6.4. Correlation of circulating CML level and animal age. There was a tendency of weak negative correlation between CML level and age in the combined group, MMVD only and control only. However, statistically these correlations were not significant (P>0.05).

6.4 Discussion

This is the first study to demonstrate CML modified protein expression in the mitral valve of dogs. There were clear differences in expression between diseased and normal mitral valves. Apparently increased CML expression was found in MMVD valves, while the expression in normal valves was minimal. While the main interest in AGE products is their possible interaction with ECM, this study has shown clear evidence of intra-cellular expression of CML with staining of endothelial and stroma interstitial cells. CML positive endothelial and interstitial cells were observed in canine mitral valves which matches previously reported findings in human tissues (Baidoshvili et al., 2004). It should be noticed that the CML expression was prominent in predisposed myxomatous region (valve edge) in MMVD valves but not in normal valves, which indicates the AGEs may play a role in myxomatous lesion development.

AGEs interact with long-lived proteins through different pathways. CML is a non-crosslink AGE product and affects tissues by binding to the receptor of AGEs (RAGE) to cause oxidative modification. It is also known as a "dominant AGE product" and CML would appear to be one of the most important AGEs participating in disease processes (Yamagishi, 2011). Aberrant ECM remodeling is known to be a key feature of MMVD (Aupperle et al., 2009a; Hadian et al., 2010; Hadian et al., 2007), involves a complex series of events for which transforming growth factor beta (TGF-β) and serotonin signaling are thought to play major roles (Disatian et al., 2010; Disatian and Orton, 2009; Oyama and Levy, 2010; Zhong et al., 2006). AGEs have been shown to up-regulate TGF-β expression and are also associated with serotonin and, therefore, their presence in MMVD is not surprising.

The exact mechanism by which AGEs might interact with the valve ECM is unknown, but appears to involve stimulation of production of vascular endothelial growth factor (VEGF) which in turn allows stimulation of production of other growth factors, such as TGF-β and insulin like growth factor-1. These then contribute to increasing production of collagen, laminin and fibronectin (Yamagishi,

2011; Yamagishi et al., 2007). Furthermore AGEs interfere with matrix-to-matrix and matrix-to-cell interactions and reduce nitric oxide production by endothelial cells; functions that are important in life-long connective tissue remodelling and maintaining a healthy valve ECM (Yamagishi et al., 2007).

Since AGEs accumulate at sites of long-lived proteins it can be hypothesized that the endogenous production of AGEs or exogenous delivery through diet would increase in the valve where there is a large quantity of collagen. Furthermore, the documented changes in collagen cross-linkages in MMVD might suggest a role for AGEs (Hadian et al., 2010). However, ECM remodelling in MMVD differs from fibrosis as would occur in kidney, lung and myocardium. The matrix changes found with MMVD involve a loss rather than an increase in collagen content in overtly myxomatous areas of the valve (Hadian et al., 2010; Han et al., 2010). The data from this study shows there is increased expression of CML particularly in deep stroma (presumably collagen-rich fibrosa lamina) of MMVD valves, but whether this accumulation is a disease cause or consequence remain uncertain.

Raised circulating CML cannot be considered to be an independent risk factor for MMVD (Koyama et al., 2007; Koyama et al., 2008) as differences were not observed between dogs with MMVD and control dogs. This study has also shown that the circulating concentration for CML in dogs is approximately double that reported for normal human subjects and chronic renal failure human patients (Semba et al., 2010). There was a negative correlation between age and blood AGE levels, but this was too weak to be of any significance. Increased circulating AGEs concentrations have been shown to be associated with nephropathy in diabetes mellitus, renal failure and Alzheimer's disease in human patients (Mostafa et al., 2007; Sanaka et al. 2000; Bär et al., 2003). However, in the present study, there was no significant difference between mean circulating CML levels in MMVD and non-MMVD dogs, despite the clear differences in tissue expression. One explanation of this discrepancy is the elimination of circulating AGEs is dependent on renal function (Singh et al., 2001; Miyata et al., 1998). All dogs used for the CML ELISA study were unaffected by diabetes mellitus and renal failure, which indicate they must have adequate renal

function. Effective excretion of systemic AGEs therefore can be achieved. The discrepancy of systemic AGE level and local tissue AGE expression has been discussed previously in an Alzheimer's disease and vascular dementia study (Bär et al., 2003). CML level in cerebrospinal fluid of Alzheimer patients have been found be elevated and this change was not correlated with the serum values. It is believed the local tissue AGE expression can reveal the role of AGEs in specific tissue pathology, while the systemic AGE level is a less specific indicator that can be affected by many factors (for example, concurrent diseases). Therefore, the circulating AGE levels should be interpreted with cautions.

One limitation of this study is a small number of dog valves were examined. Moreover, the distinct age difference (two old dogs and one young dog) within the diseased animal group used for immunohistochemistry and Western blot induced a variation and may potentially affect the experimental results. Though in this study, there were no differences observed between the results from the young diseased dog and from the two old ones. Additional canine valve samples would be worthy to be investigated to confirm the current findings in the future.

6.5 Conclusion

This study has found CML modified protein expression increased in canine MMVD valves compared to normal dogs using a combination of protein immunoblotting and Immunohistochemistry. Circulating CML concentrations of MMVD dogs were not significantly different from normal dogs. On the basis of the current data it would appear that AGEs may play a role in canine MMVD pathogenesis. The intention in future studies is increase the native valve sample size and to challenge the 3D mitral valve constructs with AGEs.

Chapter 7: Discussion

The pathogenesis of MMVD is only partially understood. However, it is known that the major pathological changes of this disease include valve cell phenotype transformation as well as ECM remodelling (Barth et al., 2005; Black et al., 2005; Corcoran et al., 2004; Disatian et al., 2008; Disatian et al., 2010; Han et al., 2008) (Aupperle et al., 2009a; Cole et al., 1984; Hadian et al., 2010; Mow and Pedersen, 1999; Prunotto et al., 2010; Rabkin-Aikawa et al., 2004a; Stein et al., 1989; Tamura et al., 1995). In the current study, fibrin based canine mitral valve constructs were developed utilising primary cells and tissue engineering techniques. The intended aim will be to use these artificial models as *in vitro* platforms for studying MMVD pathogenesis, particularly focusing on the contribution of diseased VICs and/or damaged VECs. The findings of the study were as follows.

Characteristics of primary canine mitral valve endothelial and interstitial cells possess *in vitro* 2D culture

Prior to 3D mitral valve construct fabrication, primary canine mitral VECs and VICs were successfully isolated, cultivated and characterized in 2D culture. This provides an important platform for primary mitral valve cell biology studies as well as benefiting other aspects of valve research and tissue engineering.

Overall, relatively pure canine mitral VECs and VICs were obtained. With mesenchymal features having been found in both populations, endothelial marker expression enabled differentiation of VECs from VICs.

Canine mitral VECs were found to possess common endothelial properties, such as forming a predominantly cobblestone morphology in culture, expressing the marker CD31 and up-taking acetylated low density protein (DiI-Ac-LDL). These features differentiate them from mitral VICs. Cell pleomorphism was also observed within the VEC culture. In addition to the different cell morphologies, RT-PCR showed expression of myofibroblast markers in VEC cultures. These “myofibroblasts” in the VEC culture could either come from differentiated VECs or contaminating VICs. The activated mesenchymal marker SMemb was widely expressed in VEC cultures.

Previous *in vivo* studies have shown SMemb is highly expressed by embryonic VECs, but minimally expressed by adult VECs (Aikawa et al., 2006). To our knowledge, this is the first study showing apparent SMemb expression in adult VECs from any species. This suggests the VEC cultures are activated *in vitro* and possibly still possess developmental EndoMT potential, which is consistent with a VEC progenitor cell theory proposed previously (Bischoff and Aikawa, 2011). The EndoMT transformation of adult VECs have been investigated in a number of studies, and this mechanism is believed to be one of the key remodelling processes in valve diseases (Bischoff and Aikawa, 2011; Mahler et al., 2013; Paranya et al., 2001; Paruchuri et al., 2006). The hypothesis is that a subset of adult VECs possessing embryonic differentiation potential and could be a 'stock' cell source for replenishing VICs in disease or normal remodelling situations; similar to a foetal EndoMT development (Bischoff and Aikawa, 2011; Paruchuri et al., 2006).

The VIC contamination in VEC cultures has been discussed in previous reports, which has been considered as a common problem in primary isolated VECs using enzymatic digestion techniques (Butcher et al., 2004; Cheung et al., 2008). Additional VEC purification methods such as magnetic or fluorescence activated cell sorting or single clonal expansion appear to be effective solutions for the VIC contamination issue (Cheung et al., 2008; Gould and Butcher, 2010; Hoerstrup et al., 1998; Paranya et al., 2001). Moreover in purified VECs, using CD146 FACs as well as endothelial basal medium cultured VECs, the myofibroblast marker expression dramatically decreased. This suggests the proliferation of contaminating VICs and/ or differentiation of VECs were suppressed by both processes. To obtain a purer VEC population, a combination of cell sorting followed by endothelial specific medium culture should give optimal outcomes.

The VICs are the major cell type in all heart valves. It has been well known that sub-populations exist in this versatile population (Durbin and Gotlieb, 2002; Liu et al., 2007). However, there is no clear marker panel for differentiating VIC sub-populations. In this study, the entire VIC population has been defined as expressing vimentin but negative for endothelial markers (Heaney et al., 2009). Regarding sub-populations, cells in 2D VIC cultures have been found to express activated VIC

markers α-SMA, SM22 and SMemb (Blevins et al., 2006; Della Rocca et al., 2000; Disatian et al., 2008; Disatian et al., 2010; Han et al., 2008; Rabkin et al., 2001; Stephens et al., 2011; Wiester and Giachelli, 2003). This is distinct from healthy mitral VICs *in vivo*, which are predominantly a quiescent phenotype (vimentin positive only). The VIC phenotypic activation has been observed in a number of valve diseases such as the MMVD (Disatian et al., 2008; Han et al., 2008; Rabkin-Aikawa et al., 2004b; Rabkin et al., 2001). In pathological conditions, these activated myofibroblast-like cells (aVICs) have been implicated as a major player in ECM synthesis, remodelling (Aupperle et al., 2009a; Gupta et al., 2009a; Han et al., 2010) and degradation (Aupperle et al., 2009b; Disatian et al., 2008; Rabkin et al., 2001), and also responsible for cell proliferation and migration in the valve repair process (Black et al., 2005; Durbin et al., 2005; Lester et al., 1993; Lester and Gotlieb, 1988). Cell phenotypic markers in 2D VIC cultures were assessed in this study. Moreover SMemb protein was found in all cells in VIC culture, while α-SMA expression varied between different cultures. This is consistent with in vivo studies in which α-SMA and SMemb demonstrate differential distribution patterns in diseased valve (Disatian et al., 2008; Disatian et al., 2010; Rabkin et al., 2001). All this suggests heterogeneity exists even within the aVICs population. Future investigations of the aVICs phenotypic plasticity would be necessary to gain clearer understanding of valve disease or remodeling mechanisms.

Other future work directions using the 2D valve cell culture system may include identification of embryonic differentiation potential in the VECs, and comparison of ECM synthesis profile in healthy and diseased VICs. As has been mentioned before, cells in the adult VEC cultures have been found widely expressing SMemb protein. Counterstaining of SMemb and endothelial markers in the VECs would be necessary to carry out in order to confirm cell identity. If SMemb positive cells in the VEC culture were actually endothelial in nature, it can be proposed embryonic-like differentiation potential (EndoMT) may exist in the current VEC culture system. EndoMT pathways such as notch signalling would be worthwhile examining in the model in future studies (Orton et al., 2012).

Since ECM weakness is a cardinal feature in MMVD, it can be presumed that the diseased VICs may possess differential ECM remodelling capability to normal VICs. Although in the current study, when comparing mild diseased VICs to healthy VICs, there were no apparent differences in the cell activation and matrix catabolism markers. In future studies, it would be necessary to evaluate a panel of the native valve ECM markers (such as proteoglycan and GAGs, collagen and elastin) in these two cell populations. VICs from late stage MMVD valves should also be investigated.

The potential for using tissue-engineered mitral constructs as an *in vitro* platform for valve research, particularly for MMVD pathogenesis

Tissue engineering is fast becoming a commonly used technology in regenerative medicine. Though the majority of the attempts are focusing on generating artificial organs for clinical usage, the value of using TE constructs as preclinical research tools has also been recognized (Gibbons et al., 2012; Griffith and Swartz, 2006). Fibrin hydrogel systems are a relatively novel scaffold in the tissue engineering area. It has been described as 'excellent cell carrier' as they are favorable for cell distribution, cell communication and synthesis of ECM in a 3D culture system (Lee et al., 2008; Pikaart, 2008; Ye et al., 2000). Fibrin based canine mitral valve constructs in static culture were found to possess some native mitral valve properties including tissue-like gross and histological morphology, expression of native cell phenotypic markers and, demonstration of ECM synthesis and degradation capability. This suggests cultured mitral valve cells still have potential for organizing a native valve structure, which makes them an attractive cell source for heart valve tissue engineering. The good cell replication, without excessive cell number expansion, is another positive feature, such that cells derived from a medium size dog mitral valve can generate hundreds of static 3D constructs using current technologies. This could ameliorate the problems of native tissue shortage in valve research, in which the tissue engineered constructs could serve as partial substitutes for native valves.

Recently, the application of tissue engineered/3D culture models in valve research has attracted great attention. A numbers of fundamental questions were allowed to be examined through these models, examples including valve cell-cell interaction (Butcher and Nerem, 2006), cellular response to mechanical strain (Gupta et al., 2009b; Lacerda et al., 2012a; Lacerda et al., 2012b) and signaling pathways involved in valve embryonic development (Butcher and Markwald, 2007; Chiu et al., 2010; Stock and Vacanti, 2001).

In this project, the fibrin based tissue engineered VECs-VICs co-culture models have been particularly used for studying the pathogenesis of MMVD. The MMVD pathogenesis has been partially understood. Cellular transformation and interaction, mechanical stimuli and developmental-like signaling pathways are three major aspects in recent research of MMVD. The first two areas were examined in the current study.

Healthy and diseased VICs contribute similarly to MMVD marker expression in 3D static constructs

The most clearly identifiable cellular alteration in MMVD is VIC phenotype transformation and endothelium denudation over the lesion area (Barth et al., 2005; Black et al., 2005; Corcoran et al., 2004; Disatian et al., 2008; Disatian et al., 2010; Han et al., 2008; Mow and Pedersen, 1999; Prunotto et al., 2010; Rabkin-Aikawa et al., 2004b; Stein et al., 1989). However, it is uncertain if disease is initiated from abnormalities of VICs or from endothelial damage. It has been proposed the activated/diseased VICs might be a primary initiator for ECM alteration during disease development (Prunotto et al., 2010; Walker et al., 2004). In the current study, diseased VIC based mitral valve constructs were generated and compared with constructs containing VICs from healthy valves. Previous *in vivo* studies have shown the VICs in diseased valves are phenotypically activated and expressing excess ECM catabolic enzymes (Disatian et al., 2008; Disatian et al., 2010; Han et al., 2008; Rabkin et al., 2001). However, the diseased VICs and healthy VICs were found to show similar phenotypic and ECM remodeling behaviour in the fibrin based 3D culture system. In contrast to a native mitral valve (predominantly vimentin positive

cells), mesenchymal marker vimentin, activated VIC phenotypic marker α-SMA and SMemb were all evidently expressed in both diseased and healthy VIC based constructs. Collagenase MMP-1 and stromyslin MMP-3 expression have been found to be up-regulated in MMVD (Aupperle et al., 2009c; Disatian et al., 2008; Obayashi et al., 2011; Rabkin et al., 2001). The similar expression levels of MMP-1 and MMP-3 in diseased and healthy VICs based constructs suggest ECM synthesis and degradation activity is not different in both construct types. As most of the markers typically used to examine MMVD are minimally expressed in healthy mitral valves, but up-regulated in the diseased condition, their clear expression in both types of constructs suggests they are more closely modelling MMVD rather than the normal valve. The ultrastructure analysis results supporting the above assumption (variable cell morphology, cell degradation and activation as well as ECM synthesis) were observed which suggested a remodeling process.

The culture environment is likely to be the major contributor to cell activation in these tissue-engineered systems. Firstly, fibrin is not a native ECM component and there is a need for cells to 'clean up' this foreign protein and rebuild a more typical matrix environment which surrounds them *in vivo*. Activation of VICs is necessary to accomplish this remodeling process. It has been shown that MMP-3 is capable of cleaving fibrin cross links *in vitro* and MMP-3 is important in valve remodeling (Bini et al., 1996). Inadequate gas and nutrient perfusion into the deeper construct stroma is another possible cause which might lead to cell changes. Secondly, the mechanical properties of the culture system might trigger cell activation. Fibrin hydrogel has similar mechanical properties to a GAG environment, which is a characteristic of myxomatous lesions (Gupta et al., 2009a; Han et al., 2010; Tamura et al., 1995). Cells might be reacting as if they are in a "pathological" stroma and so begin to initiate ECM remodeling processes. Furthermore, it has been shown that a stiff culture substrate can also contribute to cell activation (Kural and Billiar, 2013; Pho et al., 2008). Further work is planned to examine the effects of movement on construct morphology using a custom built bioreactor system.

Though cell activation has been observed in the current model, the exact activation mechanism was not investigated. Previous reports have suggested the VIC activation

and repair in diseased heart valves as well as the tissue engineering heart valves share similar signaling pathways to embryonic heart valve development (Butcher and Markwald, 2007; Chiu et al., 2010; Goodwin et al., 2005; Orton et al., 2012). Serotonin/TGF-β signaling pathway has been proposed to be an initiator for the VIC activation (Merryman et al., 2007; Walker et al., 2004). Therefore, examination of this pathway would be necessary in future work examining this model.

An additional consideration is the potential effect of diseased VICs on overlying VEC function, but this has not been fully examined so far due to time constraints. Indeed, the ultrastructure study on the construct suggested morphological abnormality was present in the proposed endothelium. Future work will be necessary to functionally assess the endothelial layer in these constructs, which should help to examine the question of endothelium loss as a contributor to in MMVD.

This model could be used to examine the potential for disease reversal and to evaluate effects of mechanical and biochemical activation or therapeutic reagents on disease manifestation. As an example, since it is known that VIC activation involves the TGF-β signalling pathway, the effect of interference with that pathway can be examined, and in a controlled sequential manner.

Additionally, putative chemical triggers for MMVD could be applied to the constructs, and examined to see if characteristics of MMVD become more evident. For example, the advanced glycation end product (AGE) carboxymethyline (CML) is a biochemical compound known to affect long living protein such as collagen. Distinct CML expression in canine MMVD valves, examined in this project, suggests AGEs might be a putative regulator of MMVD pathogenesis. In future work, the role of AGEs in MMVD can be analyzed by introducing exogenous CML to the 3D construct system, followed by evaluation of changes on MMVD related markers.

Wound site changes in static 3D constructs after endothelium damaged

Endothelial damage is commonly observed in the MMVD lesion area (Corcoran et al., 2004; Stein et al., 1989). One possible hypothesis of MMVD pathogenesis is that

long term shear stress induced endothelial damage triggers sub-endothelial VIC activation and further ECM remodeling (Corcoran et al., 2004; Durbin and Gotlieb, 2002; Pedersen and Haggstrom, 2000; Prunotto et al., 2010; Stein et al., 1989). In this study, an endothelial damage model was developed (Type 3) based on the Fibrin/ VECs-VICs 3D co-culture mitral constructs in static culture condition. Depending on different manipulation techniques applied, the Type 3 constructs had been further divided in to adherent Type 3 (Type 3-A) and floating Type 3 (Type 3-F). After endothelial damage, the constructs were followed for a 6 day period. The hypothesis was that, in response to endothelial injury the VICs in the construct stroma would be activated and initiate a repair-like process. Indeed, increased expression of the activated mesenchymal marker SMemb was detected in Type 3A constructs when compared to intact control constructs, especially on Day 2 and Day 6. In the majority of Day 2 and Day 6 Type 3-F constructs, although total SMemb expression decreased (presumed due to mechanical alteration), some SMemb positive cells were found to be associated with the wounded surface. Transmission electron microscopy examination showed viable cells with ECM components surrounded at the wound site and also there was evidence of cells appearing to migrate from the deep stroma. These results suggest VICs have been activated in the wounding model and SMemb positive aVICs possibly play a role in valve injury repair. Interestingly, in contrast to SMemb, another aVIC marker α-SMA appears not to increase in response to the injury in Type 3-F constructs on Day 2 and Day 6. Moreover, any changes in α-SMA expression did not affect the expression of ECM related proteins (collagen Type I and III and MMP-1), whereas SMemb expression pattern appeared to be more associated with the ECM related proteins.

Mitral VIC repair has been investigated in previous organ culture or cell culture studies (Durbin et al., 2005; Gotlieb et al., 2002; Lester et al., 1993; Lester et al., 1992; Tamura et al., 2000). The repairing process involves cell proliferation and migration (Lester and Gotlieb, 1988), and expression of cytokines (e.g FGF-2, NO and integrin) (Durbin et al., 2005; Fayet et al., 2007; Gotlieb et al., 2002) and ECM products (e.g. fibronectin) (Fayet et al., 2007). It has been proposed both motile VICs and secretory VICs are required in the wound repair process; the former in an early

response mainly involving cell proliferation and migration towards the wound, while the latter being responsible for ECM synthesis and catabolism at the wound sites, which is believed to be subsequent to cell proliferation and migration (Durbin and Gotlieb, 2002). Based on the results of the current study it might be presumed that the α-SMA positive population is the motile phenotype, while the SMemb positive cells are more related to secretory activity. Similar findings have been reported in previous studies in which α-SMA and SMemb have shown distinct expression patterns in diseased canine mitral valves, and where the SMemb expression appears to be more related to synthesis (Disatian et al., 2008; Disatian et al., 2010). Previous reports also support the α-SMA association with motile activity and it has been shown the α-SMA positive VICs are responsible for cell migration, contractility and valve internal force generation (Lester et al., 1993; Stephens et al., 2010a). Given the fact that Type 3 constructs contraction mainly occurred within 48 hours, it is very likely the current study missed α-SMA up-regulation when assessed at the time points selected. It would be necessary to examine α-SMA protein alteration, cell proliferation and migration at earlier time points in future studies.

The SMemb protein has been identified to associate with undifferentiated or 'synthetic state' smooth muscle cells (Koo and Gotlieb, 1991; Sluiter et al., 2012), and it is likely SMemb positive VICs are the major synthetic cell population in heart valves. The signaling pathways involved in the repair process were not investigated in the current study due to time constraints, but several developmental pathways have been identified in the VIC wound healing process such as TGF-β/smad signaling (Han and Gotlieb, 2011) and Wnt/β-catenin signaling pathway (Xu and Gotlieb, 2013). This is of interest considering the similarity of the VICs in response to valve injury and the myxoid changes typical of MMVD and features of foetal valve development.

Apart from the VIC activation close to wound sites, it was also found that decreased mechanical tension resulted in down-regulation of total expression of the aVIC markers (SMemb and α-SMA) in Type 3F constructs. Ultrastructure analysis suggests there was smooth muscle-like phenotype cell degradation, which was likely to be a response to the decreased mechanical stretch. It is known that the VICs are

responsive to substrate stiffness (Kural and Billiar, 2013; Stephens et al., 2011; Stephens et al., 2010b), and α-SMA expression has been found to be up-regulated by exogenous mechanical forces or high culture substrate stiffness in vascular smooth muscle cells and aortic VICs (Kural and Billiar, 2013; Pho et al., 2008). In the current study, it is likely the decreased exogenous tension on the constructs modulated the activated VICs, especially their contractile phenotype, to a more quiescent and/or synthetic phenotype.

The reversal of phenotypic plasticity of mitral valve VICs has been discussed in previous studies. Rabkin and colleagues proposed VICs tend to be activated in response to novel altered mechanical environment (such as disease or physiological remodeling process) and once a steady-state equilibrium has been achieved the aVICs will then transform back to a quiescent phenotype (Rabkin-Aikawa et al., 2004b; Rabkin-Aikawa et al., 2005). VICs in tissue engineering heart valves transform gradually from activated myofibroblasts back to fibroblasts (quiescent VICs), particularly after implantation (Rabkin et al., 2002). Furthermore, applying 15% cyclic strain to a collagen hydrogel model has been shown to modify aVICs from myxomatous diseased mitral valves to a quiescent fibroblast phenotype (Waxman et al., 2012). Reversing GAG production by VICs has also been observed in a 3D collagen model in which the GAGs level was increased with cyclic stretch and decreased with subsequent relaxation (Gupta et al., 2008a). These data from various studies suggest mitral VICs have reverse plasticity capacity in both terms of cell phenotype and synthetic activity, potentially allowing strategies for disease reversal to be identified.

Advanced model-dynamic conditioned tissue engineered mitral valve construct

A major limitation of the static 3D constructs produced is that the effect of flow is excluded. Knowing that dynamic flow conditions are important to native valve functions and tissue-engineered heart valve development, a pulsatile flow conditioned tubular construct model has also been designed. Future work will use a bioreactor for accommodating the constructs and to allow tissue-flow interaction in the system, aimed to mimic as far as is possible physiological cardiac conditions. To

date, the study has preliminarily proved the feasibility of tubular construct fabrication and endothelisation. A customised bioreactor has also been developed and specific conditioning values will be determined based on tissue mechanical properties and tissue engineering conditioning criteria. In the next stage, both a physiological and a pathological (endothelium damage) tubular construct model will be generated and exposed to the dynamic conditioning. It is believed this would be a superior model to the static constructs in resembling naturally developed tissue. It has been shown that the dynamic conditioning of a tissue engineered construct can overcome the common gas/nutrient perfusion issue limitation in static culture, improve cell proliferation and viability and enhance extracellular matrix production and organization in tissue engineered heart valves (Flanagan et al., 2007; Schenke-Layland et al., 2003; Sodian et al., 2000; Wendt et al., 2009; Weston and Yoganathan, 2001). Moreover, a pulsatile flow system would allow examining the shear flow/stress effects on the mitral valve tubular construct endothelium, which may go some way to improving understanding of the role of shear stress induced VEC damage in the MMVD pathogenesis.

Conclusion

In summary, tissue-engineered mitral valve research models have been generated in the current project. MMVD-like features (i.e. VIC activation and excessive ECM catabolism) have been observed in the current model regardless of using VICs derived from healthy or MMVD valves. External mechanical stimuli have been found to modulate the VICs behaviour in the current 3D static model: the VICs are activated in response to endothelial damage, whereas the decreased mechanical tension appears to down-regulate the VIC activation. Moreover, in later stage of this project, a tissue engineered tubular construct model and a pulsatile shear flow conditioning bioreactor system have been generated for future work. By utilizing pulsatile shear flow conditioning, it is predicted a superior physiological and a shear stressing endothelial damage model will be achieved showing greater resemblance to naturally occurred biological processes compared to static 3D constructs.

It is believed the tissue engineered models developed in this project are promising research platforms for heart valve *in vitro* research. These will particularly benefit the investigation of MMVD pathogenesis.

Bibliography

Aikawa, M., Sivam, P.N., Kuro-o, M., Kimura, K., Nakahara, K., Takewaki, S., Ueda, M., Yamaguchi, H., Yazaki, Y., Periasamy, M., 1993. Human smooth muscle myosin heavy chain isoforms as molecular markers for vascular development and atherosclerosis. Circulation Research 73, 1000-1012.

Aikawa, E., Whittaker, P., Farber, M., Mendelson, K., Padera, R.F., Aikawa, M., Schoen, F.J., 2006. Human semilunar cardiac valve remodeling by activated cells from fetus to adult implications for postnatal adaptation, pathology, and tissue Engineering. Circulation 113, 1344-1352.

Aleksieva, G., Hollweck, T., Thierfelder, N., Haas, U., Koenig, F., Fano, C., Dauner, M., Wintermantel, E., Reichart, B., Schmitz, C., 2012. Use of a special bioreactor for the cultivation of a new flexible polyurethane scaffold for aortic valve tissue engineering. Biomedical Engineering Online 11, 1-11.

Anderson, R.H., Webb, S., Brown, N.A., Lamers, W., Moorman, A., 2003. Development of the heart:(2) Septation of the atriums and ventricles. Heart 89, 949-958.

Armstrong, E.J., Bischoff, J., 2004. Heart valve development: endothelial cell signaling and differentiation. Circulation Research 95, 459-470.

Atala, A., Bauer, S.B., Soker, S., Yoo, J.J., Retik, A.B., 2006. Tissue-engineered autologous bladders for patients needing cystoplasty. The Lancet 367, 1241-1246.

Aupperle, H., März, I., Thielebein, J., Schoon, H.-A., 2008. Expression of Transforming growth factor-β1,-β2 and-β3 in normal and diseased canine mitral valves. Journal of Comparative Pathology 139, 97-107.

Aupperle, H., Marz, I., Thielebein, J., Kiefer, B., Kappe, A., Schoon, H.A., 2009a. Immunohistochemical characterization of the extracellular matrix in normal mitral valves and in chronic valve disease (endocardiosis) in dogs. Research in Veterinary Science 87, 277-283.

Aupperle, H., Thielebein, J., Kiefer, B., Marz, I., Dinges, G., Schoon, H.A., 2009b. An immunohistochemical study of the role of matrix metalloproteinases and their tissue inhibitors in chronic mitral valvular disease (valvular endocardiosis) in dogs. Veterinary Journal 180, 88-94.

Aupperle, H., Thielebein, J., Kiefer, B., Marz, I., Dinges, G., Schoon, H.A., Schubert, A., 2009c. Expression of genes encoding matrix metalloproteinases (MMPs) and their tissue inhibitors (TIMPs) in normal and diseased canine mitral valves. Journal of Comparative Pathology 140, 271-277.

Aupperle, H., Disatian, S., 2012. Pathology, protein expression and signaling in myxomatous mitral valve degeneration: comparison of dogs and humans. Journal of Veterinary Cardiology 14, 59-71.

Baidoshvili, A., Niessen, H.W., Stooker, W., Huybregts, R.A., Hack, C.E., Rauwerda, J.A., Meijer, C.J., Eijsman, L., van Hinsbergh, V.W., Schalkwijk, C.G., 2004. N-epsilon-(carboxymethyl)lysine depositions in human aortic heart valves: similarities with atherosclerotic blood vessels. Atherosclerosis 174, 287-292.

Balachandran, K., Sucosky, P., Jo, H., Yoganathan, A.P., 2009. Elevated cyclic stretch alters matrix remodeling in aortic valve cusps: implications for degenerative aortic valve disease. American Journal of Physiology-Heart and Circulatory Physiology 296, H756-H764.

Balachandran, K., Alford, P.W., Wylie-Sears, J., Goss, J.A., Grosberg, A., Bischoff, J., Aikawa, E., Levine, R.A., Parker, K.K., 2011. Cyclic strain induces dual-mode endothelial-mesenchymal transformation of the cardiac valve. Proceedings of the National Academy of Sciences of the United States of America 108, 19943-19948.

Ballas, C.B., Zielske, S.P., Gerson, S.L., 2002. Adult bone marrow stem cells for cell and gene therapies: implications for greater use. Journal of Cellular Biochemistry 85, 20-28.

Bär, KJ., Franke, S., Wenda, B., Müller, S., Kientsch-Engel, R., Stein, G., Sauer, H., 2003. Pentosidine and N-(carboxymethyl)-lysine in Alzheimer's disease and vascular dementia. Neurobiology of Aging 24(2), 333-338.

Baraki, H., Tudorache, I., Braun, M., Hoffler, K., Gorler, A., Lichtenberg, A., Bara, C., Calistru, A., Brandes, G., Hewicker-Trautwein, M., Hilfiker, A., Haverich, A., Cebotari, S., 2009. Orthotopic replacement of the aortic valve with decellularized allograft in a sheep model. Biomaterials 30, 6240-6246.

Barlovic, D., Soro-Paavonen, A., Jandeleit-Dahm, K., 2011. RAGE biology, atherosclerosis and diabetes. Clinical Science 121, 43-55.

Barron, V., Lyons, E., Stenson-Cox, C., McHugh, P., Pandit, A., 2003. Bioreactors for cardiovascular cell and tissue growth: a review. Annals of Biomedical Engineering 31, 1017-1030.

Barth, P.J., Köster, H., Moosdorf, R., 2005. CD34+ fibrocytes in normal mitral valves and myxomatous mitral valve degeneration. Pathology-Research and Practice 201, 301-304.

Barzilla, J.E., McKenney, A.S., Cowan, A.E., Durst, C.A., Grande-Allen, K.J., 2010. Design and validation of a novel splashing bioreactor system for use in mitral valve organ culture. Annals of Biomedical Engineering 38, 3280-3294.

Bashey, R., Martinez-Hernandez, A., Jimenez, S., 1992. Isolation, characterization, and localization of cardiac collagen type VI. Associations with other extracellular matrix components. Circulation Research 70, 1006-1017.

Bassett, A.L., Fenoglio, J.J., Wit, A.L., Myerburg, R.J., Gelband, H., 1976. Electrophysiologic and ultrastructural characteristics of the canine tricuspid valve. American Journal of Physiology 230, 1366-1373.

Beardow, A.W., Buchanan, J., 1993. Chronic mitral valve disease in cavalier King Charles spaniels: 95 cases (1987-1991). Journal of the American Veterinary Medical Association 203, 1023-1029.

Behar, V.S., Whalen, R.E., McIntosh, H.D., 1967. The ballooning mitral valve in patients with the "precordial honk" or "whoop". The American Journal of Cardiology 20, 789-795.

Belanger, M.-C., 2010. Echocardiography. In: Ettinger, S.J., Feldman, E.C. (Eds.), Textbook of Veterinary Internal Medicine, Vol. 1.

Bernardo, A., Ball, C., Nolasco, L., Moake, J.F., Dong, J.-f., 2004. Effects of inflammatory cytokines on the release and cleavage of the endothelial cell–derived ultralarge von Willebrand factor multimers under flow. Blood 104, 100-106.

Berry, J.L., Steen, J.A., Williams, J.K., Jordan, J.E., Atala, A., Yoo, J.J., 2010. Bioreactors for development of tissue engineered heart valves. Annals of Biomedical Engineering 38, 3272-3279.

Bertipaglia, B., Ortolani, F., Petrelli, L., Gerosa, G., Spina, M., Pauletto, P., Casarotto, D., Marchini, M., Sartore, S., 2003. Cell characterization of porcine aortic valve and decellularized leaflets repopulated with aortic valve interstitial cells: the VESALIO project (vitalitate exornatum succedaneum aorticum labore ingenioso obtenibitur). The Annals of Thoracic Surgery 75, 1274-1282.

Bini, A., Itoh, Y., Kudryk, B.J., Nagase, H., 1996. Degradation of cross-linked fibrin by matrix metalloproteinase 3 (stromelysin 1): Hydrolysis of the γ Gly 404-Ala 405 peptide bond. Biochemistry 35, 13056-13063.

Bischoff, J., Aikawa, E., 2011. Progenitor cells confer plasticity to cardiac valve endothelium. Journal of Cardiovascular Translational Research 4, 710-719.

Bittar, N., Sosa, J.A., 1968. The Billowing Mitral Valve Leaflet Report on Fourteen Patients. Circulation 38, 763-770.

Black, A., French, A.T., Dukes-McEwan, J., Corcoran, B.M., 2005. Ultrastructural morphologic evaluation of the phenotype of valvular interstitial cells in dogs with myxomatous degeneration of the mitral valve. American Journal of Veterinary Research 66, 1408-1414.

Black, A., Corcoran, B.M., Heying, R., Jockenhoevel, S., Flanagan, T.C., 2009. The Mitral Valve: Development, Structure, Pathology & Tissue engineering, Vol. 1., 1-47.

Blevins, T.L., Carroll, J.L., Raza, A.M., Grande-Allen, K.J., 2006. Phenotypic characterization of isolated valvular interstitial cell subpopulations. The Journal of Heart Valve Disease 15, 815-822.

Blevins, T.L., Peterson, S.B., Lee, E.L., Bailey, A.M., Frederick, J.D., Huynh, T.N., Gupta, V., Grande-Allen, K.J., 2008. Mitral valvular interstitial cells demonstrate regional, adhesional, and synthetic heterogeneity. Cells Tissues Organs 187, 113-122.

Boontheekul, T., Mooney, D.J., 2003. Protein-based signaling systems in tissue engineering. Current Opinion in Biotechnology 14, 559-565.

Borgarelli, M., Tursi, M., La Rosa, G., Savarino, P., Galloni, M., 2011. Anatomic, histologic, and two-dimensional-echocardiographic evaluation of mitral valve anatomy in dogs. American Journal of Veterinary Research 72, 1186-1192.

Bouten, C.V., Dankers, P.Y., Driessen-Mol, A., Pedron, S., Brizard, A.M., Baaijens, F.P., 2011. Substrates for cardiovascular tissue engineering. Advanced Drug Delivery Reviews 63, 221-241.

Brendel, K., Duhamel, R.C., 1989. Body implants of extracellular matrix and means and methods of making and using such implants. In. Google Patents, City. http://www.google.com/patents/US4801299

Brody, S., Pandit, A., 2007. Approaches to heart valve tissue engineering scaffold design. Journal of Biomedical Materials Research Part B: Applied Biomaterials 83, 16-43.

Buchanan, J., 1977. Chronic valvular disease (endocardiosis) in dogs. Advances in Veterinary Science and Comparative Medicine 21, 75.

Butcher, J.T., Nerem, R.M., 2004. Porcine aortic valve interstitial cells in three-dimensional culture: Comparison of phenotype with aortic smooth muscle cells. The Journal of Heart Valve Disease 13, 478-485.

Butcher, J.T., Penrod, A.M., Garcia, A.J., Nerem, R.M., 2004. Unique morphology and focal adhesion development of valvular endothelial cells in static and fluid flow environments. Arteriosclerosis, Thrombosis, and Vascular Biology 24, 1429-1434.

Butcher, J.T., Nerem, R.M., 2006. Valvular endothelial cells regulate the phenotype of interstitial cells in co-culture: Effects of steady shear stress. Tissue Engineering 12, 905-915.

Butcher, J.T., Tressel, S., Johnson, T., Turner, D., Sorescu, G., Jo, H., Nerem, R.M., 2006. Transcriptional profiles of valvular and vascular endothelial cells reveal phenotypic differences: influence of shear stress. Arteriosclerosis, Thrombosis, and Vascular Biology 26, 69-77.

Butcher, J.T., Nerem, R.M., 2007. Valvular endothelial cells and the mechanoregulation of valvular pathology. Philosophical Transactions of the Royal Society B: Biological Sciences 362, 1445-1457.

Butcher, J.T., Markwald, R.R., 2007. Valvulogenesis: the moving target. Philosophical Transactions of the Royal Society B: Biological Sciences 362, 1489-1503.

Caira, F.C., Stock, S.R., Gleason, T.G., McGee, E.C., Huang, J., Bonow, R.O., Spelsberg, T.C., McCarthy, P.M., Rahimtoola, S.H., Rajamannan, N.M., 2006. Human degenerative valve disease is associated with up-regulation of low-density lipoprotein receptor-related protein 5 receptor-mediated bone formation. Journal of the American College of Cardiology 47, 1707-1712.

Carrier, R.L., Papadaki, M., Rupnick, M., Schoen, F.J., Bursac, N., Langer, R., Freed, L.E., Vunjak-Novakovic, G., 1999. Cardiac tissue engineering: cell seeding, cultivation parameters, and tissue construct characterization. Biotechnology and Bioengineering 64, 580-589.

Cebotari, S., Lichtenberg, A., Tudorache, I., Hilfiker, A., Mertsching, H., Leyh, R., Breymann, T., Kallenbach, K., Maniuc, L., Batrinac, A., Repin, O., Maliga, O., Ciubotaru, A., Haverich, A., 2006. Clinical application of tissue engineered human heart valves using autologous progenitor cells. Circulation 114, I132-137.

Chalajour, F., Treede, H., Ebrahimnejad, A., Lauke, H., Reichenspurner, H., Ergun, S., 2004. Angiogenic activation of valvular endothelial cells in aortic valve stenosis. Experimental Cell Research 298, 455-464.

Chen, Q., Bruyneel, A., Clarke, K., Carr, C., Czernuszka, J., 2012. Collagen-based scaffolds for potential application of heart valve tissue engineering. Journal of Tissue Science & Engineering 11:003.

Chen, Q., Bruyneel, A., Carr, C., Czernuszka, J., 2013. Bio-mechanical properties of novel bi-layer collagen-Elastin scaffolds for heart valve tissue engineering. Procedia Engineering 59, 247-254.

Cheng, T.-Y., Chen, M.-H., Chang, W.-H., Huang, M.-Y., Wang, T.-W., 2013. Neural stem cells encapsulated in a functionalized self-assembling peptide hydrogel for brain tissue engineering. Biomaterials 34(8), 2005-2016.

Chester, A.H., Taylor, P.M., 2007. Molecular and functional characteristics of heart-valve interstitial cells. Philosophical Transactions of the Royal Society B: Biological Sciences 362, 1437-1443.

Cheung, W.Y., Young, E.W.K., Simmons, C.A., 2008. Techniques for isolating and purifying porcine aortic valve endothelial cells. The Journal of Heart Valve Disease 17, 674-681.

Chiers, K., Vandenberge, V., Ducatelle, R., 2010. Accumulation of advanced glycation end products in canine atherosclerosis. Journal of Comparative Pathology 143, 65-69.

Chiu, Y.N., Norris, R.A., Mahler, G., Recknagel, A., Butcher, J.T., 2010. Transforming growth factor beta, bone morphogenetic protein, and vascular endothelial growth factor mediate phenotype maturation and tissue remodeling by embryonic valve progenitor cells: relevance for heart valve tissue engineering. Tissue Engineering Part A 16, 3375-3383.

Chun, I., Cooper, K., Fang, C.H., 2010. Tissue engineered blood vessels. In. Google Patents, City. http://www.google.ee/patents/US20110143429

Ci, H.B., Ou, Z.J., Chang, F.J., Liu, D.H., He, G.W., Xu, Z., Yuan, H.Y., Wang, Z.P., Zhang, X., Ou, J.S., 2013. Endothelial microparticles increase in mitral valve disease and impair mitral valve endothelial function. American Journal of Physiology-Endocrinology and Metabolism 304, E695-E702.

Clowes, A.W., Reidy, M.A., Clowes, M.M., 1983. Kinetics of cellular proliferation after arterial injury. I. Smooth muscle growth in the absence of endothelium. Laboratory Investigation 49, 327-333.

Colazzo, F., Sarathchandra, P., Smolenski, R.T., Chester, A.H., Tseng, Y.T., Czernuszka, J.T., Yacoub, M.H., Taylor, P.M., 2011. Extracellular matrix production by adipose-derived stem cells: implications for heart valve tissue engineering. Biomaterials 32, 119-127.

Cole, W., Chan, D., Hickey, A., Wilcken, D., 1984. Collagen composition of normal and myxomatous human mitral heart valves. Biochemical Journal 219, 451-460.

Comazzi, S., Bertazzolo, W., Bonfanti, U., Spagnolo, V., Sartorelli, P., 2008. Advanced glycation end products and sorbitol in blood from differently compensated diabetic dogs. Research in Veterinary Science 84, 341-346.

Combs, M.D., Yutzey, K.E., 2009. Heart valve development regulatory networks in development and disease. Circulation Research 105, 408-421.

Connell, P.S., Han, R.I., Grande-Allen, K.J., 2012. Differentiating the aging of the mitral valve from human and canine myxomatous degeneration. Journal of Veterinary Cardiology 14, 31-45.

Corcoran, B.M., Black, A., Anderson, H., McEwan, J.D., French, A., Smith, P., Devine, C., 2004. Identification of surface morphologic changes in the mitral valve leaflets and chordae tendineae of dogs with myxomatous degeneration. American Journal of Veteterinary Research 65, 198-206.

Cote, E., 2010. Electrocardiography and Cardiac Arrhythmias. In: Ettinger, S.J., Feldman, E.C. (Eds.), Textbook of Veterinary Internal Medicine Volume 2, Chapter 235, 1159-1187.

Courtois, M., Kovacs, S., Ludbrook, P., 1988. Transmitral pressure-flow velocity relation. Importance of regional pressure gradients in the left ventricle during diastole. Circulation 78, 661-671.

Culshaw, G.J., French, A.T., Han, R.I., Black, A., Pearson, G.T., Corcoran, B.M., 2010. Evaluation of innervation of the mitral valves and the effects of myxomatous degeneration in dogs. American Journal of Veterinary Research 71, 194-202.

Cuy, J.L., Beckstead, B.L., Brown, C.D., Hoffman, A.S., Giachelli, C.M., 2003. Adhesive protein interactions with chitosan: Consequences for valve endothelial cell growth on tissue ‐ engineering materials. Journal of Biomedical Materials Research Part A 67, 538-547.

Dal-Bianco, J.P., Aikawa, E., Bischoff, J., Guerrero, J.L., Handschumacher, M.D., Sullivan, S., Johnson, B., Titus, J.S., Iwamoto, Y., Wylie-Sears, J., 2009. Active adaptation of the tethered mitral valve insights into a compensatory mechanism for functional mitral regurgitation. Circulation 120, 334-342.

Davies, M., Moore, B., Braimbridge, M., 1978. The floppy mitral valve. Study of incidence, pathology, and complications in surgical, necropsy, and forensic material. British Heart Journal 40, 468.

Davies, P.F., Passerini, A.G., Simmons, C.A., 2004. Aortic valve: turning over a new leaf(let) in endothelial phenotypic heterogeneity. Arteriosclerosis, Thrombosis, and Vascular Biology 24, 1331-1333.

Davies, P.F., Spaan, J.A., Krams, R., 2005. Shear stress biology of the endothelium. Annals of Biomedical Engineering 33, 1714-1718.

de Lange, F.J., Moorman, A.F., Anderson, R.H., Männer, J., Soufan, A.T., de Gier-de Vries, C., Schneider, M.D., Webb, S., van den Hoff, M.J., Christoffels, V.M., 2004. Lineage and morphogenetic analysis of the cardiac valves. Circulation Research 95, 645-654.

Decker, R., Henney, A., Dingle, J., 1986. Porcine heart valves produce a protein that induces cell-mediated connective tissue degradation: II. Biochemical properties of the partially purified protein. Circulation Research 59, 329-341.

Decker, R.S., Dingle, J.T., 1982. Cardiac catabolic factors: the degradation of heart valve intercellular matrix. Science 215, 987-989.

DeGroot, J., Verzijl, N., Wijk, W.V., Marion, J., Jacobs, K.M., Van El, B., Van Roermund, P.M., Bank, R.A., Bijlsma, J.W., TeKoppele, J.M., 2004. Accumulation of advanced glycation end products as a molecular mechanism for aging as a risk factor in osteoarthritis. Arthritis & Rheumatism 50, 1207-1215.

Della Rocca, F., Sartore, S., Guidolin, D., Bertiplaglia, B., Gerosa, G., Casarotto, D., Pauletto, P., 2000. Cell composition of the human pulmonary valve: A comparative study with the aortic valve - The VESALIO* project. Annals of Thoracic Surgery 70, 1594-1600.

Dillon, A., Dell'Italia, L.J., Tillson, M., Killingsworth, C., Denney, T., Hathcock, J., Botzman, L., 2012. Left ventricular remodeling in preclinical experimental mitral regurgitation of dogs. Journal of Veterinary Cardiology 14, 73-92.

Disatian, S., Ehrhart, E.J., 3rd, Zimmerman, S., Orton, E.C., 2008. Interstitial cells from dogs with naturally occurring myxomatous mitral valve disease undergo phenotype transformation. The Journal of Heart Valve Disease 17, 402-411; discussion 412.

Disatian, S., Orton, E.C., 2009. Autocrine serotonin and transforming growth factor beta 1 signaling mediates spontaneous myxomatous mitral valve disease. The Journal of Heart Valve Disease 18, 44-51.

Disatian, S., Lacerda, C., Orton, E.C., 2010. Tryptophan hydroxylase 1 expression is increased in phenotype-altered canine and human degenerative myxomatous mitral valves. The Journal of Heart Valve Disease 19, 71-78.

Dreger, S., Taylor, P., Allen, S., Yacoub, M., 2002. Profile and localization of matrix metalloproteinases (MMPs) and their tissue inhibitors (TIMPs) in human heart valves. The Journal of Heart Valve Disease 11, 875-880.

Dreger, S.A., Thomas, P., Sachlos, E., Chester, A.H., Czernuszka, J.T., Taylor, P.M., Yacoub, M.H., 2006. Potential for synthesis and degradation of extracellular matrix proteins by valve interstitial cells seeded onto collagen scaffolds. Tissue Engineering 12, 2533-2540.

Duan, B., Hockaday, L.A., Kang, K.H., Butcher, J.T., 2013. 3D bioprinting of heterogeneous aortic valve conduits with alginate/gelatin hydrogels. Journal of Biomedical Materials Research Part A 101, 1255-1264.

Dumont, K., Yperman, J., Verbeken, E., Segers, P., Meuris, B., Vandenberghe, S., Flameng, W., Verdonck, P.R., 2002. Design of a new pulsatile bioreactor for tissue engineered aortic heart valve formation. Artificial Organs 26, 710-714.

Durbin, A.D., Gotlieb, A.I., 2002. Advances towards understanding heart valve response to in injury. Cardiovascular pathology 11, 69-77.

Durbin, A., Nadir, N.A., Rosenthal, A., Gotlieb, A.I., 2005. Nitric oxide promotes in vitro interstitial cell heart valve repair. Cardiovascular Pathology 14, 12-18.

Engelmayr, G.C., Hildebrand, D.K., Sutherland, F.W., Mayer, J.E., Sacks, M.S., 2003. A novel bioreactor for the dynamic flexural stimulation of tissue engineered heart valve biomaterials. Biomaterials 24, 2523-2532.

Engelmayr Jr, G.C., Rabkin, E., Sutherland, F.W., Schoen, F.J., Mayer Jr, J.E., Sacks, M.S., 2005. The independent role of cyclic flexure in the early in vitro development of an engineered heart valve tissue. Biomaterials 26, 175-187.

Engelmayr Jr, G.C., Sales, V.L., Mayer Jr, J.E., Sacks, M.S., 2006. Cyclic flexure and laminar flow synergistically accelerate mesenchymal stem cell-mediated engineered tissue formation: implications for engineered heart valve tissues. Biomaterials 27, 6083-6095.

Engelmayr Jr, G.C., Soletti, L., Vigmostad, S.C., Budilarto, S.G., Federspiel, W.J., Chandran, K.B., Vorp, D.A., Sacks, M.S., 2008. A novel flex-stretch-flow bioreactor for the study of engineered heart valve tissue mechanobiology. Annals of Biomedical Engineering 36, 700-712.

Engler, A.J., Sen, S., Sweeney, H.L., Discher, D.E., 2006. Matrix elasticity directs stem cell lineage specification. Cell 126, 677-689.

Olsen Lisebeth Hoier ; Häggstrom Jens ; Petersen Henrik Duelund, 2010. Aquired Vavular Heart Disease. Textbook of Veterinary Internal Medicine (7th Edition), Volume 2, Chapter 250, 1299-1319.

Evans, H.E., 1993. The Heart and Arteries. Miller's Anatomy of the Dog (3rd Edition), 11, 586-681.

Fayet, C., Bendeck, M.P., Gotlieb, A.I., 2007. Cardiac valve interstitial cells secrete fibronectin and form fibrillar adhesions in response to injury. Cardiovascular Pathology 16, 203-211.

Fenoglio, J.J., Jr., Tuan Duc, P., Wit, A.L., Bassett, A.L., Wagner, B.M., 1972. Canine mitral complex. Ultrastructure and electromechanical properties. Circulation Research 31, 417-430.

Ferrer, L., Fondevila, D., Rabanal, R., Vilafranca, M., 1995. Immunohistochemical detection of CD31 antigen in normal and neoplastic canine endothelial cells. Journal of Comparative Pathology 112, 319-326.

Fiegel, H.C., Kaufmann, P.M., Bruns, H., Kluth, D., Horch, R.E., Vacanti, J.P., Kneser, U., 2008. Hepatic tissue engineering: from transplantation to customized cell ‐ based liver directed therapies from the laboratory. Journal of Cellular and Molecular Medicine 12, 56-66.

Filip, D., Radu, A., Simionescu, M., 1986. Interstitial cells of the heart valves possess characteristics similar to smooth muscle cells. Circulation Research, Vol. 59(3), 310-320.

Flanagan, T.C., Black, A., O'Brien, M., Smith, T.J., Pandit, A.S., 2006a. Reference models for mitral valve tissue engineering based on valve cell phenotype and extracellular matrix analysis. Cells Tissues Organs 183, 12-23.

Flanagan, T.C., Wilkins, B., Black, A., Jockenhoevel, S., Smith, T.J., Pandit, A.S., 2006b. A collagen-glycosaminoglycan co-culture model for heart valve tissue engineering applications. Biomaterials 27, 2233-2246.

Flanagan, T.C., Cornelissen, C., Koch, S., Tschoeke, B., Sachweh, J.S., Schmitz-Rode, T., Jockenhoevel, S., 2007. The in vitro development of autologous fibrin-based tissue-engineered heart valves through optimised dynamic conditioning. Biomaterials 28, 3388-3397.

Flanagan, T.C., Sachweh, J.S., Frese, J., Schnoring, H., Gronloh, N., Koch, S., Tolba, R.H., Schmitz-Rode, T., Jockenhoevel, S., 2009. In vivo remodeling and structural characterization of fibrin-based tissue-engineered heart valves in the adult sheep model. Tissue Engineering Part A 15, 2965-2976.

Fosmire, S.P., Dickerson, E.B., Scott, A.M., Bianco, S.R., Pettengill, M.J., Meylemans, H., Padilla, M., Frazer-Abel, A.A., Akhtar, N., Getzy, D.M., 2006. Canine malignant hemangiosarcorma as a model of primitive angiogenic endothelium. Laboratory Investigation 84(5), 562-572.

Fox, P.R., Sisson, D., Moïse, N.S., 1999. Textbook of canine and feline cardiology: principles and clinical practice. Saunders Philadelphia.

Fox, P.R., 2012. Pathology of myxomatous mitral valve disease in the dog. Journal of Veterinary Cardiology 14, 103-126.

Frater, R.W., Ellis, F.H., 1961. The anatomy of the canine mitral valve: With notes on function and comparisons with other mammalian mitral valves. Journal of Surgical Research 1, 171-178.

Freed, L.E., Vunjak-Novakovic, G., 2000. Tissue engineering bioreactors. Principles of tissue engineering 2, 143-156.

French, A.T., Ogden, R., Eland, C., Hemani, G., Pong-Wong, R., Corcoran, B., Summers, K.M., 2012. Genome-wide analysis of mitral valve disease in Cavalier King Charles Spaniels. The Veterinary Journal 193, 283-286.

Fulton, D., Papapetropoulos, A., Zhang, X., Catravas, J.D., Hintze, T.H., Sessa, W.C., 2000. Quantification of eNOS mRNA in the canine cardiac vasculature by competitive PCR. American Journal of Physiology-Heart and Circulatory Physiology 278, H658-H665.

Gandaglia, A., Bagno, A., Naso, F., Spina, M., Gerosa, G., 2011. Cells, scaffolds and bioreactors for tissue-engineered heart valves: a journey from basic concepts to contemporary developmental innovations. European Journal Cardio-Thoracic Surgery 39, 523-531.

Gheewala, N., Grande-Allen, K.J., 2010. Design and mechanical evaluation of a physiological mitral valve organ culture system. Cardiovascular Engineering and Technology 1, 123-131.

Gibbons, M.C., Foley, M.A., Cardinal, K.O.H., 2012. Thinking inside the box: keeping tissue-engineered constructs in vitro for use as preclinical models. Tissue Engineering Part B: Reviews 19, 14-30.

Glasson, J.R., Komeda, M.K., Daughters, G.T., Niczyporuk, M.A., Bolger, A.F., Ingels, N.B., Miller, D.C., 1996. Three-dimensional regional dynamics of the normal mitral anulus during left ventricular ejection. The Journal of Thoracic and Cardiovascular Surgery 111, 574-585.

Goldstein, S., Black, K.S., 1999. Pulsatile flow system for developing heart valves. In. Google Patents, City. http://www.google.com/patents/US5899937

Goodwin, R.L., Nesbitt, T., Price, R.L., Wells, J.C., Yost, M.J., Potts, J.D., 2005. Three‐dimensional model system of valvulogenesis. Developmental Dynamics 233, 122-129.

Gotlieb, A.I., Boden, P., 1984. Porcine aortic organ culture: a model to study the cellular response to vascular injury. In Vitro 20, 535-542.

Gotlieb, A.I., Rosenthal, A., Kazemian, P., 2002. Fibroblast growth factor 2 regulation of mitral valve interstitial cell repair in vitro. The Journal of Thoracic and Cardiovascular Surgery 124, 591-597.

Gould, R.A., Butcher, J.T., 2010. Isolation of valvular endothelial cells. Journal of Visualized Experiments. http://www.ncbi.nlm.nih.gov/pmc/articles/PMC3159658/

Grande-Allen, K.J., Calabro, A., Gupta, V., Wight, T.N., Hascall, V.C., Vesely, I., 2004. Glycosaminoglycans and proteoglycans in normal mitral valve leaflets and chordae: association with regions of tensile and compressive loading. Glycobiology 14, 621-633.

Grande-Allen, K.J., Liao, J., 2011. The heterogeneous biomechanics and mechanobiology of the mitral valve: implications for tissue engineering. Current Cardiology Reports 13, 113-120.

Grau, J.B., Pirelli, L., Yu, P.J., Galloway, A.C., Ostrer, H., 2007. The genetics of mitral valve prolapse. Clinical Genetics 72, 288-295.

Grewal, J., Suri, R., Mankad, S., Tanaka, A., Mahoney, D.W., Schaff, H.V., Miller, F.A., Enriquez-Sarano, M., 2010. Mitral annular dynamics in myxomatous valve disease: new insights with real-time 3-dimensional echocardiography. Circulation 121, 1423-1431.

Grewal, J.S., Mukhin, Y.V., Garnovskaya, M.N., Raymond, J.R., Greene, E.L., 1999. Serotonin 5-HT2A receptor induces TGF-β1 expression in mesangial cells via ERK: proliferative and fibrotic signals. American Journal of Physiology-Renal Physiology 276, F922-F930.

Griffith, L.G., Swartz, M.A., 2006. Capturing complex 3D tissue physiology in vitro. Nature Reviews Molecular Cell Biology 7, 211-224.

Gross, L., Kugel, M., 1931. Topographic anatomy and histology of the valves in the human heart. The American Journal of Pathology 7, 445-474.

Gupta, V., Werdenberg, J.A., Lawrence, B.D., Mendez, J.S., Stephens, E.H., Grande-Allen, K.J., 2008a. Reversible secretion of glycosaminoglycans and proteoglycans by cyclically stretched valvular cells in 3D culture. Annals of Biomedical Engineering 36, 1092-1103.

Gupta, V., Werdenberg, J.A., Mendez, J.S., Jane Grande-Allen, K., 2008b. Influence of strain on proteoglycan synthesis by valvular interstitial cells in three-dimensional culture. Acta Biomaterialia 4, 88-96.

Gupta, V., Barzilla, J.E., Mendez, J.S., Stephens, E.H., Lee, E.L., Collard, C.D., Laucirica, R., Weigel, P.H., Grande-Allen, K.J., 2009a. Abundance and location of proteoglycans and hyaluronan within normal and myxomatous mitral valves. Cardiovascular pathology 18, 191-197.

Gupta, V., Tseng, H., Lawrence, B.D., Grande-Allen, K.J., 2009b. Effect of cyclic mechanical strain on glycosaminoglycan and proteoglycan synthesis by heart valve cells. Acta Biomaterialia 5, 531-540.

Hadian, M., Corcoran, B.M., Han, R.I., Grossmann, J.G., Bradshaw, J.P., 2007. Collagen organization in canine myxomatous mitral valve disease: an x-ray diffraction study. Biophysical Journal 93, 2472-2476.

Hadian, M., Corcoran, B.M., Bradshaw, J.P., 2010. Molecular changes in fibrillar collagen in myxomatous mitral valve disease. Cardiovascular pathology 19, e141-e148.

Hall, C.W., Liotta, D., De Bakey, M.E., 1966. Artificial skin. Transactions - American Society for Artificial Internal Organs 12, 340-345.

Han, L., Gotlieb, A.I., 2011. Fibroblast Growth Factor-2 Promotes in Vitro Mitral Valve Interstitial Cell Repair through Transforming Growth Factor-β/Smad Signaling. American Journal of Pathology 178, 119-127.

Han, R.I., Black, A., Culshaw, G.J., French, A.T., Else, R.W., Corcoran, B.M., 2008. Distribution of myofibroblasts, smooth muscle-like cells, macrophages, and mast cells in mitral valve leaflets of dogs with myxomatous mitral valve disease. American Journal of Veterinary Research 69, 763-769.

Han, R.I., Black, A., Culshaw, G., French, A.T., Corcoran, B.M., 2010. Structural and cellular changes in canine myxomatous mitral valve disease: an image analysis study. The Journal of Heart Valve Disease 19, 60-70.

Han, R., Clark, C., Black, A., French, A., Culshaw, G., Kempson, S., Corcoran, B., 2013. Morphological changes to endothelial and interstitial cells and to the extra-cellular matrix in canine myxomatous mitral valve disease (endocardiosis). The Veterinary Journal.

Hartog, J.W., Voors, A.A., Bakker, S.J., Smit, A.J., Veldhuisen, D.J., 2007. Advanced glycation end‐products (AGEs) and heart failure: Pathophysiology and clinical implications. European Journal of Heart Failure 9, 1146-1155.

Harvey, R.P., 2002. Patterning the vertebrate heart. Nature Reviews Genetics 3, 544-556.

Heaney, A.M., Bulmer, B.J., Ross, C.R., Schermerhorn, T., 2009. A technique for in vitro culture of canine valvular interstitial cells. Journal of Veterinary Cardiology 11, 1-7.

Hildebrand, D.K., Wu, Z.J., Mayer Jr, J.E., Sacks, M.S., 2004. Design and hydrodynamic evaluation of a novel pulsatile bioreactor for biologically active heart valves. Annals of Biomedical Engineering 32, 1039-1049.

Hoerstrup, S.P., Zünd, G., Schoeberlein, A., Ye, Q., Vogt, P.R., Turina, M.I., 1998. Fluorescence activated cell sorting: a reliable method in tissue engineering of a bioprosthetic heart valve. The Annals of Thoracic Surgery 66, 1653-1657.

Hoerstrup, S.P., Sodian, R., Daebritz, S., Wang, J., Bacha, E.A., Martin, D.P., Moran, A.M., Guleserian, K.J., Sperling, J.S., Kaushal, S., Vacanti, J.P., Schoen, F.J., Mayer, J.E., 2000a. Functional Living Trileaflet Heart Valves Grown In Vitro. Circulation 102, III-44-III-49.

Hoerstrup, S.P., Sodian, R., Sperling, J.S., Vacanti, J.P., Mayer Jr, J.E., 2000b. New pulsatile bioreactor for in vitro formation of tissue engineered heart valves. Tissue Engineering 6, 75-79.

Hopkins, R.A., 2005. Tissue engineering of heart valves: decellularized valve scaffolds. Circulation 111, 2712-2714.

Ilan, N., Madri, J.A., 2003. PECAM-1: old friend, new partners. Current Opinion in Cell Biology 15, 515-524.

Jaffe, A.S., Geltman, E., Rodey, G., Uitto, J., 1981. Mitral valve prolapse: a consistent manifestation of type IV Ehlers-Danlos syndrome. The pathogenetic role of the abnormal production of type III collagen. Circulation 64, 121-125.

Jian, B., Xu, J., Connolly, J., Savani, R.C., Narula, N., Liang, B., Levy, R.J., 2002. Serotonin mechanisms in heart valve disease I - Serotonin-induced up-regulation of transforming growth factor-beta 1 via G-protein signal transduction in aortic valve interstitial cells. American Journal of Pathology 161, 2111-2121.

Jockenhoevel, S., Chalabi, K., Sachweh, J.S., Groesdonk, H.V., Demircan, L., Grossmann, M., Zund, G., Messmer, B.J., 2001a. Tissue engineering: complete autologous valve conduit--a new moulding technique. The Journal of Thoracic and Cardiovascular Surgery 49, 287-290.

Jockenhoevel, S., Zund, G., Hoerstrup, S.P., Chalabi, K., Sachweh, J.S., Demircan, L., Messmer, B.J., Turina, M., 2001b. Fibrin gel -- advantages of a new scaffold in cardiovascular tissue engineering. European Journal Cardio-Thoracic Surgery 19, 424-430.

Jockenhoevel, S., Zund, G., Hoerstrup, S.P., Schnell, A., Turina, M., 2002. Cardiovascular tissue engineering: a new laminar flow chamber for in vitro improvement of mechanical tissue properties. American Society for Artificial Internal Organs Journal 48, 8-11.

Kanani, M., Deanfield, J., 2003. The anatomy of the mitral valve: a retrospective analysis of yesterday's future. The Journal of Heart Valve Disease 12, 543-547.

Kasimir, M., Rieder, E., Seebacher, G., Silberhumer, G., Wolner, E., Weigel, G., Simon, P., 2003. Comparison of different decellularization procedures of porcine heart valves. The International Journal of Artificial Organs 26, 421-427.

Kim, W., Cho, S., Kang, M., Lee, T., Park, J., 2001. Tissue-engineered heart valve leaflets: an animal study. The International Journal of Artificial Organs 24, 642.
Kittleson, M.D., Eyster, G.E., Knowlen, G.G., 1984. 'Myocardial function in small dogs with chronic mitral regurgitation and severe congestive heart failure. Group 4, 34.

Klement, P., Wilson, G.J., Yeger, H., 1988. Process for preparing biological mammalian implants. In. Google Patents, City. http://www.google.co.uk/patents/US4776853

Kofidis, T., Lenz, A., Boublik, J., Akhyari, P., Wachsmann, B., Mueller-Stahl, K., Hofmann, M., Haverich, A., 2003. Pulsatile perfusion and cardiomyocyte viability in a solid three-dimensional matrix. Biomaterials 24, 5009-5014.

Kogure, K., 1980. Pathology of chronic mitral valvular disease in the dog. Nihon Juigaku Zasshi 42, 323-335.

Konertz, W., Dohmen, P., Liu, J., Beholz, S., Dushe, S., Posner, S., Lembcke, A., Erdbrügger, W., 2005. Hemodynamic characteristics of the Matrix P decellularized xenograft for pulmonary valve replacement during the Ross operation. The Journal of Heart Valve Disease 14, 78.

Koo, E.W., Gotlieb, A.I., 1991. Neointimal formation in the porcine aortic organ culture. I. Cellular dynamics over 1 month. Laboratory Investigation64, 743-753.

Koyama, Y., Takeishi, Y., Arimoto, T., Niizeki, T., Shishido, T., Takahashi, H., Nozaki, N., Hirono, O., Tsunoda, Y., Nitobe, J., 2007. High serum level of pentosidine, an advanced glycation end product (AGE), is a risk factor of patients with heart failure. Journal of Cardiac Failure13, 199-206.

Koyama, Y., Takeishi, Y., Niizeki, T., Suzuki, S., Kitahara, T., Sasaki, T., Kubota, I., 2008. Soluble Receptor for advanced glycation end products (RAGE) is a prognostic factor for heart failure. Journal of Cardiac Failure 14, 133-139.

Ku, C.H., Johnson, P.H., Batten, P., Sarathchandra, P., Chambers, R.C., Taylor, P.M., Yacoub, M.H., Chester, A.H., 2006. Collagen synthesis by mesenchymal stem cells and aortic valve interstitial cells in response to mechanical stretch. Cardiovascular Research 71, 548-556.

Kunzelman, K.S., Cochran, R.P., 1990. Mechanical properties of basal and marginal mitral valve chordae tendineae. American Society for Artificial Internal Organs transactions 36, M405-408.

Kunzelman, K.S., Cochran, R., 1992. Stress/strain characteristics of porcine mitral valve tissue: parallel versus perpendicular collagen orientation. Journal of Cardiac Surgery 7, 71-78.

Kunzelman, K.S., Cochran, R.P., Murphree, S.S., Ring, W.S., Verrier, E.D., Eberhart, R.C., 1993. Differential collagen distribution in the mitral valve and its influence on biomechanical behaviour. The Journal of Heart Valve Disease 2, 236-244.

Kunzelman, K., Cochran, R., Verrier, E., Eberhart, R., 1994. Anatomic basis for mitral valve modelling. The Journal of Heart Valve Disease 3, 491.

Kural, M.H., Billiar, K.L., 2013. Mechanoregulation of valvular interstitial cell phenotype in the third dimension. Biomaterials 35(4), 1128-1137.

Kuro-o, M., Nagai, R., Nakahara, K.-I., Katoh, H., Tsai, R.-C., Tsuchimochi, H., Yazaki, Y., Ohkubo, A., Takaku, F., 1991. cDNA cloning of a myosin heavy chain isoform in embryonic smooth muscle and its expression during vascular development and in arteriosclerosis. Journal of Biological Chemistry 266, 3768-3773.

Lacerda, C.M., Kisiday, J., Johnson, B., Orton, E.C., 2012a. Local serotonin mediates cyclic strain-induced phenotype transformation, matrix degradation, and glycosaminoglycan synthesis in cultured sheep mitral valves. American Journal of Physiology-Heart and Circulatory Physiology 302, H1983-H1990.

Lacerda, C.M., MacLea, H.B., Kisiday, J.D., Orton, E.C., 2012b. Static and cyclic tensile strain induce myxomatous effector proteins and serotonin in canine mitral valves. Journal of Veterinary Cardiology 14, 223-230.

Langelaan, M.L., Boonen, K.J., Polak, R.B., Baaijens, F., Post, M.J., van der Schaft, D.W., 2010. Meet the new meat: tissue engineered skeletal muscle. Trends in Food Science & Technology 21, 59-66.

Langer, R., Vacanti, J.P., 1993. Tissue engineering. Science 260, 920-926.

Latif, N., Sarathchandra, P., Taylor, P., Antoniw, J., Yacoub, M., 2005. Localization and pattern of expression of extracellular matrix components in human heart valves. The Journal of Heart Valve Disease 14, 218-227.

Leask, R.L., Jain, N., Butany, J., 2003. Endothelium and valvular diseases of the heart. Microscopy Research and Technique 60, 129-137.

Lee, D.J., Steen, J., Jordan, J.E., Kincaid, E.H., Kon, N.D., Atala, A., Berry, J., Yoo, J.J., 2009. Endothelialization of heart valve matrix using a computer-assisted pulsatile bioreactor. Tissue Engineering Part A 15, 807-814.

Lee, J., Cuddihy, M.J., Kotov, N.A., 2008. Three-dimensional cell culture matrices: state of the art. Tissue Engineering Part B Reviews 14, 61-86.

Lester, W., Rosenthal, A., Granton, B., Gotlieb, A.I., 1988. Porcine mitral valve interstitial cells in culture. Laboratory Investigation 59, 710-719.

Lester, W.M., Gotlieb, A.I., 1988. In vitro repair of the wounded porcine mitral valve. Circulation Research 62, 833-845.

Lester, W.M., Damji, A.A., Tanaka, M., Gedeon, I., 1992. Bovine mitral valve organ culture: role of interstitial cells in repair of valvular injury. Journal of Molecular and Cellular Cardiology 24, 43-53.

Lester, W.M., Damji, A.A., Gedeon, I., Tanaka, M., 1993. Interstitial cells from the atrial and ventricular sides of the bovine mitral valve respond differently to denuding endocardial injury. In Vitro Cellular & Developmental Biology 29A, 41-50.

Li, N., Goodwin, R.L., Potts, J.D., 2013. Zyxin regulates cell migration and differentiation in EMT during chicken AV valve morphogenesis. Microscopy and Microanalysis 19(4):842-854.

Liao, J., Vesely, I., 2003. A structural basis for the size-related mechanical properties of mitral valve chordae tendineae. Journal of Biomechanics 36, 1125-1133.

Lichtenberg, A., Tudorache, I., Cebotari, S., Ringes-Lichtenberg, S., Sturz, G., Hoeffler, K., Hurscheler, C., Brandes, G., Hilfiker, A., Haverich, A., 2006. In vitro re-endothelialization of detergent decellularized heart valves under simulated physiological dynamic conditions. Biomaterials 27, 4221-4229.

Lieber, S.C., Kruithof, B.P., Aubry, N., Vatner, S.F., Gaussin, V., 2010. Design of a miniature tissue culture system to culture mouse heart valves. Annals of Biomedical Engineering 38, 674-682.

Liu, A.C., Joag, V.R., Gotlieb, A.I., 2007. The emerging role of valve interstitial cell phenotypes in regulating heart valve pathobiology. The American Journal of Pathology 171, 1407-1418.

Liu, A.C., Gotlieb, A.I., 2008. Transforming growth factor-β regulates in vitro heart valve repair by activated valve interstitial cells. The American Journal of Pathology 173, 1275-1285.

Lomholt, M., Nielsen, S.L., Hansen, S.B., Andersen, N.T., Hasenkam, J.M., 2002. Differential tension between secondary and primary mitral chordae in an acute in-vivo porcine model. The Journal of Heart Valve Disease 11, 337-345.

Lu., C.C., Liu., M.M., Culshaw., G., French., A., Corcoran., B., in press. Cellular changes in cavalier king charles spaniel myxomatous mitral valves are the same as for other dogs. Veterinary Journal in press.

Lyons, E., Prandit, A., 2005. Design of bioreactors for cardiovascular applications. In N. Ashammakhi and P.Ferreti, Topics in Tissue Engineering Volume 2, 1-32.

Madsen, M.B., Olsen, L.H., Haggstrom, J., Hoglund, K., Ljungvall, I., Falk, T., Wess, G., Stephenson, H., Dukes-McEwan, J., Chetboul, V., Gouni, V., Proschowsky, H.F., Cirera, S., Karlskov-Mortensen, P., Fredholm, M., 2011. Identification of 2 loci associated with development of myxomatous mitral valve disease in Cavalier King Charles Spaniels. Journal of Heredity 102 Issue Supplement 1, 62-67.

Mahler, G.J., Farrar, E.J., Butcher, J.T., 2013. Inflammatory cytokines promote mesenchymal transformation in embryonic and adult valve endothelial cells. Arteriosclerosis Thrombosis and Vascular Biology 33, 121-130.

Markwald, R.R., Fitzharris, T.P., Manasek, F.J., 1977. Structural development of endocardial cushions. American Journal of Anatomy 148, 85-119.

Marolt, D., Campos, I.M., Bhumiratana, S., Koren, A., Petridis, P., Zhang, G., Spitalnik, P.F., Grayson, W.L., Vunjak-Novakovic, G., 2012. Engineering bone tissue from human embryonic stem cells. Proceedings of the National Academy of Sciences 109, 8705-8709.

Mendelson, K., Schoen, F.J., 2006. Heart valve tissue engineering: concepts, approaches, progress, and challenges. Annals of Biomedical Engineering 34, 1799-1819.

Merrilees, M., Scott, L., 1982. Organ culture of rat carotid artery: maintenance of morphological characteristics and of pattern of matrix synthesis. In Vitro 18, 900-910.

Merryman, W.D., Lukoff, H.D., Long, R.A., Engelmayr, G.C., Hopkins, R.A., Sacks, M.S., 2007. Synergistic effects of cyclic tension and transforming growth factor-β1 on the aortic valve myofibroblast. Cardiovascular Pathology 16, 268-276.

Merryman, W.D., Youn, I., Lukoff, H.D., Krueger, P.M., Guilak, F., Hopkins, R.A., Sacks, M.S., 2006. Correlation between heart valve interstitial cell stiffness and transvalvular pressure: implications for collagen biosynthesis. American Journal of Physiology-Heart and Circulatory Physiology 290, H224-H231.

Metcalfe, A.D., Ferguson, M.W., 2007. Bioengineering skin using mechanisms of regeneration and repair. Biomaterials 28, 5100-5113.

Metzner, A., Stock, U.A., Iino, K., Fischer, G., Huemme, T., Boldt, J., Braesen, J.H., Bein, B., Renner, J., Cremer, J., Lutter, G., 2010. Percutaneous pulmonary valve replacement: autologous tissue-engineered valved stents. Cardiovascular Research 88, 453-461.

Mironov, V., Kasyanov, V., Markwald, R.R., 2011. Organ printing: from bioprinter to organ biofabrication line. Current Opinion in Biotechnology 22, 667-673.

Misfeld, M., Sievers, H.H., 2007. Heart valve macro- and microstructure. Philosophical Transactions of the Royal Society B: Biological Sciences 362, 1421-1436.

Miyata, Toshio, Ueda, Yasuhiko, Horie, Katsunori, Nangaku, Masaomi, Tanaka, Shuichi, de Strihou, Charles van Ypersele, Kurokawa, Kiyoshi, 1998. Renal catabolism of advanced glycation end products: the fate of pentosidine. Kidney International 53(2), 616-422.

Moesgaard, S.G., Olsen, L.H., Viuff, B.M., Baandrup, U., Pedersen, L.G., Thomsen, P.D., Pedersen, H.D., Harrison, A.P., 2007. Increased nitric oxide release and expression of endothelial and inducible nitric oxide synthases in mildly changed porcine mitral valve leaflets. The Journal of Heart Valve Disease 16, 67-75.

Moesgaard, S., Klostergaard, C., Zois, N., Teerlink, T., Molin, M., Falk, T., Rasmussen, C., Luis Fuentes, V., Jones, I., Olsen, L., 2012. Flow-mediated vasodilation measurements in cavalier king charles spaniels with increasing severity of myxomatous mitral valve disease. Journal of Veterinary Internal Medicine 26, 61-68.

Mol, A., Bouten, C., Zund, G., Gunter, C., Visjager, J., Turina, M., Baaijens, F., Hoerstrup, S., 2003. The relevance of large strains in functional tissue engineering of heart valves. Thoracic and Cardiovascular Surgeon 51, 78-83.

Mol, A., Driessen, N.J., Rutten, M.C., Hoerstrup, S.P., Bouten, C.V., Baaijens, F.P., 2005. Tissue engineering of human heart valve leaflets: a novel bioreactor for a strain-based conditioning approach. Annals of Biomedical Engineering 33, 1778-1788.

Mol, A., Rutten, M.C., Driessen, N.J., Bouten, C.V., Zund, G., Baaijens, F.P., Hoerstrup, S.P., 2006. Autologous human tissue-engineered heart valves: prospects for systemic application. Circulation 114, I152-158.

Mol, A., Smits, A.I., Bouten, C.V., Baaijens, F.P., 2009. Tissue engineering of heart valves: advances and current challenges. Expert Review of Medical Devices 6, 259-275.

Mostafa, A. A., Randell, E. W., Vasdev, S. C., Gill, V. D., Han, Y., Gadag, V., Raouf, A. A., El Said, H., 2007. Plasma protein advanced glycation end products, carboxymethyl cysteine, and carboxyethyl cysteine, are elevated and related to nephropathy in patients with diabetes. Molecular and Cellular Biochemistry 302(1-2), 35-42.

Mow, T., Pedersen, H.D., 1999. Increased endothelin-receptor density in myxomatous canine mitral valve leaflets. Journal of Cardiovascular Pharmacology 34, 254-260.

Mueller-Klieser, W., 1997. Three-dimensional cell cultures: from molecular mechanisms to clinical applications. American Journal of Physiology 273, C1109-1123.

Mulholland, D.L., Gotlieb, A.I., 1996. Cell biology of valvular interstitial cells. Canadian Journal of Cardiology 12, 231-236.

Mulholland, D.L., Gotlieb, A.I., 1997. Cardiac valve interstitial cells: Regulator of valve structure and function. Cardiovascular Pathology 6, 167-174.

Nehls, V., Drenckhahn, D., 1995. A novel, microcarrier-based in vitro assay for rapid and reliable quantification of three-dimensional cell migration and angiogenesis. Microvascular Research 50, 311-322.

Ng, C.M., Cheng, A., Myers, L.A., Martinez-Murillo, F., Jie, C., Bedja, D., Gabrielson, K.L., Hausladen, J.M., Mecham, R.P., Judge, D.P., 2004. TGF-β–dependent pathogenesis of mitral valve prolapse in a mouse model of Marfan syndrome. Journal of Clinical Investigation 114, 1586-1592.

Nielsen, S.L., Timek, T.A., Green, G.R., Dagum, P., Daughters, G.T., Hasenkam, J.M., Bolger, A.F., Ingels, N.B., Miller, D.C., 2003. Influence of anterior mitral leaflet second-order chordae tendineae on left ventricular systolic function. Circulation 108, 486-491.

Obadia, J.F., Casali, C., Chassignolle, J.F., Janier, M., 1997. Mitral subvalvular apparatus: different functions of primary and secondary chordae. Circulation 96, 3124-3128.

Obayashi, K., Miyagawa-Tomita, S., Matsumoto, H., Koyama, H., Nakanishi, T., Hirose, H., 2011. Effects of transforming growth factor-β3 and matrix metalloproteinase-3 on the pathogenesis of chronic mitral valvular disease in dogs. American Journal of Veterinary Research 72, 194-202.

Olive, P.L., Durand, R.E., 1994. Drug and radiation resistance in spheroids: cell contact and kinetics. Cancer and Metastasis Reviews 13, 121-138.

Olsen, L.H., Fredholm, M., Pedersen, H.D., 1999. Epidemiology and inheritance of mitral valve prolapse in Dachshunds. Journal of Veterinary Internal Medicine 13, 448-456.

Olsen, L.H., Martinussen, T., Pedersen, H.D., 2003a. Early echocardiographic predictors of myxomatous mitral valve disease in dachshunds. Veterinary Research 152, 293-297.

Olsen, L.H., Mortensen, K., Martinussen, T., Larsson, L.I., Baandrup, U., Pedersen, H.D., 2003b. Increased NADPH-Diaphorase activity in canine myxomatous mitral valve leaflets. Journal of Comparative Pathology 129, 120-130.

Oosthoek, P., Wenink, A.C., Vrolijk, B.C., Wisse, L.J., DeRuiter, M.C., Poelmann, R.E., Gittenberger-de Groot, A.C., 1998. Development of the atrioventricular valve tension apparatus in the human heart. Anatomy and Embryology (Berlin) 198, 317-329.

Opara, E.C., Mirmalek-Sani, S.-H., Khanna, O., Moya, M.L., Brey, E.M., 2010. Design of a bioartificial pancreas. Journal of investigative medicine: the official publication of the American Federation for Clinical Research 58, 831.

Orton, E.C., Lacerda, C.M., MacLea, H.B., 2012. Signaling pathways in mitral valve degeneration. Journal of Veterinary Cardiology 14, 7-17.

Ott, H.C., Matthiesen, T.S., Goh, S.-K., Black, L.D., Kren, S.M., Netoff, T.I., Taylor, D.A., 2008. Perfusion-decellularized matrix: using nature's platform to engineer a bioartificial heart. Nature Medicine 14, 213-221.

Oyama, M.A., Chittur, S.V., 2006. Genomic expression patterns of mitral valve tissues from dogs with degenerative mitral valve disease. American Journal of Veterinary Research 67, 1307-1318.

Oyama, M.A., Levy, R.J., 2010. Insights into serotonin signaling mechanisms associated with canine degenerative mitral valve disease. Journal of Veterinary Internal Medicine 24, 27-36.

Padala, M., Sacks, M.S., Liou, S.W., Balachandran, K., Zhaoming, H., Yoganathan, A.P., 2010. Mechanics of the mitral valve strut chordae insertion region. Journal of Biomechanical Engineering 132.

Paranya, G., Vineberg, S., Dvorin, E., Kaushal, S., Roth, S.J., Rabkin, E., Schoen, F.J., Bischoff, J., 2001. Aortic valve endothelial cells undergo transforming growth factor-β-mediated and non-transforming growth factor-β-mediated transdifferentiation in vitro. American Journal of Pathology 159, 1335-1343.

Paruchuri, S., Yang, J.H., Aikawa, E., Melero-Martin, J.M., Khan, Z.A., Loukogeorgakis, S., Schoen, F.J., Bischoff, J., 2006. Human pulmonary valve progenitor cells exhibit endothelial/mesenchymal plasticity in response to vascular endothelial growth factor-A and transforming growth factor-beta2. Circulation Research 99, 861-869.

Patten, B.M., Kramer, T.C., Barry, A., 1948. Valvular action in the embryonic chick heart by localized apposition of endocardial masses. The Anatomical Record 102, 299-311.

Pedersen, H.D., Haggstrom, J., 2000. Mitral valve prolapse in the dog: a model of mitral valve prolapse in man. Cardiovascular Research 47, 234-243.

Penna, V., Munder, B., Stark, G., Lang, E.M., 2011. An in vivo engineered nerve conduit—fabrication and experimental study in rats. Microsurgery 31, 395-400.

Perloff, J.K., Roberts, W.C., 1972. The mitral apparatus. Functional anatomy of mitral regurgitation. Circulation 46, 227-239.

Person, A.D., Klewer, S.E., Runyan, R.B., 2005. Cell biology of cardiac cushion development. International Review of Cytology 243, 287-335.

Petersen, T.H., Calle, E.A., Zhao, L., Lee, E.J., Gui, L., Raredon, M.B., Gavrilov, K., Yi, T., Zhuang, Z.W., Breuer, C., 2010. Tissue-engineered lungs for in vivo implantation. Science 329, 538-541.

Pho, M., Lee, W., Watt, D.R., Laschinger, C., Simmons, C.A., McCulloch, C., 2008. Cofilin is a marker of myofibroblast differentiation in cells from porcine aortic cardiac valves. American Journal of Physiology-Heart and Circulatory Physiology 294, H1767-H1778.

Pikaart, 2008. Human Fibrin As a Cell Carrier for Heart Valve Tissue Engineering Literature review.

Platt, J., Nagayasu, T., 1999. Current status of xenotransplantation*. Clinical and Experimental Pharmacology and Physiology 26, 1026-1032.

Pohost, G., Dinsmore, R., Rubenstein, J., O'Keefe, D., Grantham, R.N., Scully, H., Beierholm, E., Frederiksen, J., Weisfeldt, M., Daggett, W., 1975. The echocardiogram of the anterior leaflet of the mitral valve. Correlation with hemodynamic and cineroentgenographic studies in dogs. Circulation 51, 88-97.

Pomerance, A., Whitney, J.C., 1970. Heart valve changes common to man and dog: a comparative study. Cardiovascular Research 4, 61-66.

Prunotto, M., Caimmi, P.P., Bongiovanni, M., 2010. Cellular pathology of mitral valve prolapse. Cardiovascular Pathology 19, e113-117.

Pusztaszeri, M.P., Seelentag, W., Bosman, F.T., 2006. Immunohistochemical expression of endothelial markers CD31, CD34, von Willebrand factor, and Fli-1 in normal human tissues. Journal of Histochemistry & Cytochemistry 54, 385-395.

Rabkin-Aikawa, E., Aikawa, M., Farber, M., Kratz, J.R., Garcia-Cardena, G., Kouchoukos, N.T., Mitchell, M.B., Jonas, R.A., Schoen, F.J., 2004a. Clinical pulmonary autograft valves: pathologic evidence of adaptive remodeling in the aortic site. The Journal of Thoracic and Cardiovascular Surgery 128, 552-561.

Rabkin-Aikawa, E., Farber, M., Aikawa, M., Schoen, F.J., 2004b. Dynamic and reversible changes of interstitial cell phenotype during remodeling of cardiac valves. The Journal of Heart Valve Disease 13, 841-847.

Rabkin-Aikawa, E., Mayer, J.E., Schoen, F.J., 2005. Heart Valve Regeneration 94, 141-179.

Rabkin, E., Aikawa, M., Stone, J.R., Fukumoto, Y., Libby, P., Schoen, F.J., 2001. Activated interstitial myofibroblasts express catabolic enzymes and mediate matrix remodeling in myxomatous heart valves. Circulation 104, 2525-2532.

Rabkin, E., Hoerstrup, S., Aikawa, M., Mayer Jr, J., Schoen, F., 2002. Evolution of cell phenotype and extracellular matrix in tissue-engineered heart valves during in-vitro maturation and in-vivo remodeling. The Journal of Heart Valve Disease 11, 308.

Ramaswamy, S., Gottlieb, D., Engelmayr Jr, G.C., Aikawa, E., Schmidt, D.E., Gaitan-Leon, D.M., Sales, V.L., Mayer Jr, J.E., Sacks, M.S., 2010. The role of organ level conditioning on the promotion of engineered heart valve tissue development in-vitro using mesenchymal stem cells. Biomaterials 31, 1114-1125.

Reed, C.C., Iozzo, R.V., 2002. The role of decorin in collagen fibrillogenesis and skin homeostasis. Glycoconjugate Journal 19, 249-255.

Reinboth, B., Hanssen, E., Cleary, E.G., Gibson, M.A., 2002. Molecular interactions of biglycan and decorin with elastic fiber components biglycan forms a ternary complex with tropoelastin and microfibril-associated glycoprotein 1. Journal of Biological Chemistry 277, 3950-3957.

Ren, G., Michael, L.H., Entman, M.L., Frangogiannis, N.G., 2002. Morphological characteristics of the microvasculature in healing myocardial infarcts. Journal of Histochemistry & Cytochemistry 50, 71-79.

Richards, J., El-Hamamsy, I., Chen, S., Sarang, Z., Sarathchandra, P., Yacoub, M.H., Chester, A.H., Butcher, J.T., 2013. Side-specific endothelial-dependent regulation of aortic valve calcification: interplay of hemodynamics and nitric oxide signaling. The American Journal of Pathology 182(5), 1922-1931.

Richards, J.M., Farrar, E.J., Kornreich, B.G., Mosmall yi, U.N.S., Butcher, J.T., 2012. The mechanobiology of mitral valve function, degeneration, and repair. Journal of Veterinary Cardiology 14, 47-58.

Robinson, P.S., Johnson, S.L., Evans, M.C., Barocas, V.H., Tranquillo, R.T., 2008. Functional tissue-engineered valves from cell-remodeled fibrin with commissural alignment of cell-produced collagen. Tissue Engineering Part A 14, 83-95.

Ruel, J., Lachance, G., 2009. A new bioreactor for the development of tissue-engineered heart valves. Annals of Biomedical Engineering 37, 674-681.

Sacks, M.S., Enomoto, Y., Graybill, J.R., Merryman, W.D., Zeeshan, A., Yoganathan, A.P., Levy, R.J., Gorman, R.C., Gorman III, J.H., 2006. In-vivo

dynamic deformation of the mitral valve anterior leaflet. The Annals of Thoracic Surgery 82, 1369-1377.

Sacks, M.S., Schoen, F.J., Mayer, J.E., 2009. Bioengineering challenges for heart valve tissue engineering. Annual Review of Biomedical Engineering 11, 289-313.

Salgo, I.S., Gorman, J.H., 3rd, Gorman, R.C., Jackson, B.M., Bowen, F.W., Plappert, T., St John Sutton, M.G., Edmunds, L.H., Jr., 2002. Effect of annular shape on leaflet curvature in reducing mitral leaflet stress. Circulation 106, 711-717.

Salhiyyah, K., Yacoub, M.H., Chester, A.H., 2011. Cellular mechanisms in mitral valve disease. Journal of Cardiovascular Translational Research 4, 702-709.

Sanaka, T., Funaki, T., Tanaka, T., Hoshi, S., Niwayama, J., Taitoh, T., Nishimura, H., Higuchi, C., 2002. Plasma pentosidine levels measured by a newly developed method using ELISA in patients with chronic renal failure. Nephron 91, 64-73.

Sarphie, T., Allen, D.J., 1978. Scanning and transmission electron microscopy of normal and methotrexate-treated endocardial cell populations in dogs. Journal of Submicroscopic Cytology and Pathology 10, 15-25.

Sarphie, T., 1980. Pleomorphic surface features of mammalian endocardium: fine structure of canine bicuspid valves. Journal of Molecular and Cellular Cardiology 12, 241-255.

Schaefermeier, P., Szymanski, D., Weiss, F., Fu, P., Lueth, T., Schmitz, C., Meiser, B., Reichart, B., Sodian, R., 2008. Design and fabrication of three-dimensional scaffolds for tissue engineering of human heart valves. European Surgical Research 42, 49-53.

Schaefermeier, P.K., Cabeza, N., Besser, J.C., Lohse, P., Daebritz, S.H., Schmitz, C., Reichart, B., Sodian, R., 2009. Potential cell sources for tissue engineering of heart valves in comparison with human pulmonary valve cells. American Society for Artificial Internal Organs Journal 55, 86-92.

Schenke-Layland, K., Opitz, F., Gross, M., Döring, C., Halbhuber, K., Schirrmeister, F., Wahlers, T., Stock, U., 2003. Complete dynamic repopulation of decellularized heart valves by application of defined physical signals-an in vitro study. Cardiovascular Research 60, 497-509.

Schmidt, D., Hoerstrup, S.P., 2006. Tissue engineered heart valves based on human cells. Swiss Medical Weekly 136, 618.

Schoen, F.J., 2005. Cardiac valves and valvular pathology: update on function, disease, repair, and replacement. Cardiovascular Pathology 14, 189-194.

Schoen, F.J., 2008. Evolving concepts of cardiac valve dynamics: the continuum of development, functional structure, pathobiology, and tissue engineering. Circulation 118, 1864-1880.

Semba, R.D., Fink, J.C., Sun, K., Windham, B.G., Ferrucci, L., 2010. Serum carboxymethyl-lysine, a dominant advanced glycation end product, is associated with chronic kidney disease: the Baltimore longitudinal study of aging. Journal of Renal Nutrition 20, 74-81.

Shapiro, B.P., Owan, T.E., Mohammed, S.F., Meyer, D.M., Mills, L.D., Schalkwijk, C.G., Redfield, M.M., 2008. Advanced glycation end products accumulate in vascular smooth muscle and modify vascular but not ventricular properties in elderly hypertensive canines. Circulation 118, 1002-1010.

Shi, Y., Vesely, I., 2004. Characterization of statically loaded tissue-engineered mitral valve chordae tendineae. Journal of Biomedical Materials Research Part A 69, 26-39.

Shinoka, T., Breuer, C.K., Tanel, R.E., Zund, G., Miura, T., Ma, P.X., Langer, R., Vacanti, J.P., Mayer, J.E., Jr., 1995. Tissue engineering heart valves: valve leaflet replacement study in a lamb model. Annals of Thoracic Surgery 60, S513-516.

Shinoka, T., Ma, P.X., Shum-Tim, D., Breuer, C.K., Cusick, R.A., Zund, G., Langer, R., Vacanti, J.P., Mayer Jr, J.E., 1996. Tissue-engineered heart valves. Autologous valve leaflet replacement study in a lamb model. Circulation 94, II164-168.

Sierad, L.N., Simionescu, A., Albers, C., Chen, J., Maivelett, J., Tedder, M.E., Liao, J., Simionescu, D.T., 2010. Design and testing of a pulsatile conditioning system for dynamic endothelialization of polyphenol-stabilized tissue engineered heart valves. Cardiovascular Engineering and Technology 1, 138-153.

Silverman, M.E., Hurst, J.W., 1968. The mitral complex: interaction of the anatomy, physiology, and pathology of the mitral annulus, mitral valve leaflets, chordae tendineae, and papillary muscles. American Heart Journal 76, 399-418.

Simmons, C.A., Grant, G.R., Manduchi, E., Davies, P.F., 2005. Spatial heterogeneity of endothelial phenotypes correlates with side-specific vulnerability to calcification in normal porcine aortic valves. Circulation Research 96, 792-799.

Simon, A., Zavazava, N., Sievers, H.H., Müller‐Ruchholtz, W., 1993. In vitro cultivation and immunogenicity of human cardiac valve endothelium. Journal of Cardiac Surgery 8, 656-665.

Simon, P., Kasimir, M.T., Seebacher, G., Weigel, G., Ullrich, R., Salzer-Muhar, U., Rieder, E., Wolner, E., 2003. Early failure of the tissue engineered porcine heart valve SYNERGRAFT in pediatric patients. European Journal Cardio-Thoracic Surgery 23, 1002-1006; discussion 1006.

Singh, J.P., Evans, J.C., Levy, D., Larson, M.G., Freed, L.A., Fuller, D.L., Lehman, B., Benjamin, E.J., 1999. Prevalence and clinical determinants of mitral, tricuspid, and aortic regurgitation (the Framingham Heart Study). American Journal of Cardiology 83, 897-902.

Singh, R., Barden, A., Mori, T., Beilin, L., 2001. Advanced glycation end-products: a review. Diabetologia 44, 129-146.

Skowasch, D., Schrempf, S., Wernert, N., Steinmetz, M., Jabs, A., Tuleta, I., Welsch, U., Preusse, C.J., Likungu, J.A., Welz, A., Luderitz, B., Bauriedel, G., 2005. Cells of primarily extra-valvular origin in degenerative aortic valves and bioprostheses. European Heart Journal 26, 2576-2580.

Sluiter, I., van Heijst, A., Haasdijk, R., Kempen, M.B.-v., Boerema-de Munck, A., Reiss, I., Tibboel, D., Rottier, R.J., 2012. Reversal of pulmonary vascular remodeling in pulmonary hypertensive rats. Experimental and Molecular Pathology 93, 66-73.

Smith, P., French, A., Israïl, N., Smith, S., Swift, S., Lee, A., Corcoran, B., Dukes‐McEwan, J., 2005. Efficacy and safety of pimobendan in canine heart failure caused by myxomatous mitral valve disease. Journal of Small Animal Practice 46, 121-130.

Smith, S., Taylor, P.M., Chester, A.H., Allen, S.P., Dreger, S.A., Eastwood, M., Yacoub, M.H., 2007. Force generation of different human cardiac valve interstitial cells: relevance to individual valve function and tissue engineering. The Journal of Heart Valve Disease 16, 440.

Snopek, G., Pogorzelska, H., Korewicki, J., 2000. Influence of valve replacement on plasma endothelin-1 level in mitral stenosis. The Journal of Heart Valve Disease 9, 82.

Sodian, R., Hoerstrup, S.P., Sperling, J.S., Martin, D.P., Daebritz, S., Mayer Jr, J.E., Vacanti, J.P., 2000. Evaluation of biodegradable, three-dimensional matrices for tissue engineering of heart valves. American Society for Artificial Internal Organs Journal 46, 107-110.

Sodian, R., Schaefermeier, P., Abegg-Zips, S., Kuebler, W.M., Shakibaei, M., Daebritz, S., Ziegelmueller, J., Schmitz, C., Reichart, B., 2010. Use of human umbilical cord blood-derived progenitor cells for tissue-engineered heart valves. The Annals of Thoracic Surgery 89, 819-828.

Sonnenblick, E.H., Napolitano, L.M., Daggett, W.M., Cooper, T., 1967. An intrinsic neuromuscular basis for mitral valve motion in the dog. Circulation Research 21, 9-15.

Stein, P.D., Wang, C.-H., Riddle, J.M., Sabbah, H.N., Magilligan Jr, D.J., Hawkins, E.T., 1989. Scanning electron microscopy of operatively excised severely regurgitant floppy mitral valves. American Journal of Cardiology 64, 392-394.

Steinhoff, G., Stock, U., Karim, N., Mertsching, H., Timke, A., Meliss, R.R., Pethig, K., Haverich, A., Bader, A., 2000. Tissue engineering of pulmonary heart valves on allogenic acellular matrix conduits - In vivo restoration of valve tissue. Circulation 102, 50-55.

Stephens, E.H., de Jonge, N., McNeill, M.P., Durst, C.A., Grande-Allen, K.J., 2009. Age-related changes in material behavior of porcine mitral and aortic valves and correlation to matrix composition. Tissue Engineering Part A 16, 867-878.

Stephens, E.H., Durst, C.A., Swanson, J.C., Grande-Allen, K.J., Ingels Jr, N.B., Miller, D.C., 2010a. Functional coupling of valvular interstitial cells and collagen via α2β1 integrins in the mitral leaflet. Cellular and Molecular Bioengineering 3, 428-437.

Stephens, E.H., Huynh, T.N., Cieluch, J.D., Grande-Allen, K.J., 2010b. Fibronectin-based isolation of valve interstitial cell subpopulations: relevance to valve disease. Journal of Biomedical Materials Research Part A 92, 340-349.

Stephens, E.H., Durst, C.A., West, J.L., Grande-Allen, K.J., 2011. Mitral valvular interstitial cell responses to substrate stiffness depend on age and anatomic region. Acta Biomaterialia 7, 75-82.

Stock, U.A., Vacanti, J.P., 2001. Cardiovascular physiology during fetal development and implications for tissue engineering. Tissue Engineering 7, 1-7.

Sun, L., Rajamannan, N.M., Sucosky, P., 2011. Design and validation of a novel bioreactor to subject aortic valve leaflets to side-specific shear stress. Annals of Biomedical Engineering 39, 2174-2185.

Sun, W., Zhao, R., Yang, Y., Wang, H., Shao, Y., Kong, X., 2013. Comparative study of human aortic and mitral valve interstitial cell gene expression and cellular function. Genomics 101(6), 326-335.

Sutherland, Robert M, McCredie, John A, Inch, W Rodger, 1971. Growth of multiple spheroids inm tissue culture as a model of nodular carcinomas. Journal of the National Cancer Institute 46(1), 113-120.

Sutherland, F.W., Perry, T.E., Yu, Y., Sherwood, M.C., Rabkin, E., Masuda, Y., Garcia, G.A., McLellan, D.L., Engelmayr, G.C., Jr., Sacks, M.S., Schoen, F.J., Mayer, J.E., Jr., 2005. From stem cells to viable autologous semilunar heart valve. Circulation 111, 2783-2791.

Swenson, L., Haggstrom, J., Kvart, C., Juneja, R.K., 1996. Relationship between parental cardiac status in Cavalier King Charles spaniels and prevalence and severity of chronic valvular disease in offspring. Journal of American Veterinary Medical Association 208, 2009-2012.

Syedain, Z.H., Tranquillo, R.T., 2009. Controlled cyclic stretch bioreactor for tissue-engineered heart valves. Biomaterials 30, 4078-4084.

Tamura, K., Fukuda, Y., Ishizaki, M., Masuda, Y., Yamanaka, N., Ferrans, V.J., 1995. Abnormalities in elastic fibers and other connective-tissue components of floppy mitral valve. American Heart Journal 129, 1149-1158.

Tamura, K., Jones, M., Yamada, I., Ferrans, V.J., 2000. Wound healing in the mitral valve. The Journal of Heart Valve Disease 9, 53-63.

Tao, G., Kotick, J.D., Lincoln, J., 2012. Heart Valve Development, Maintenance, and Disease: The Role of Endothelial Cells. Heart Development 100, 203-232.

Taylor, P.M., Allen, S.P., Yacoub, M.H., 2000. Phenotypic and functional characterization of interstitial cells from human heart valves, pericardium and skin. The Journal of Heart Valve Disease 9, 150-158.

Taylor, P.A., Batten, P., Brand, N.J., Thomas, P.S., Yacoub, M.H., 2003. The cardiac valve interstitial cell. International Journal of Biochemistry & Cell Biology 35, 113-118.

Thamm, D.H, Dickerson, E.B, Akhtar, N., Lewis, R., Auerbach, R., Helfand, S.C., MacEwen, E.G., 2006. Biological and molecular characterization of a canine hemangiosarcoma-derived cell line. Research in Veterinary Science 81(1), 76-86.

Timek, T.A., Lai, D.T., Dagum, P., Tibayan, F., Daughters, G.T., Liang, D., Berry, G.J., Miller, D.C., Ingels, N.B., Jr., 2003. Ablation of mitral annular and leaflet muscle: effects on annular and leaflet dynamics. American Journal of Physiology-Heart and Circulation Physiology 285, H1668-1674.

Tschoeke, B., Flanagan, T.C., Cornelissen, A., Koch, S., Roehl, A., Sriharwoko, M., Sachweh, J.S., Gries, T., Schmitz‐Rode, T., Jockenhoevel, S., 2008. Development of a composite degradable/nondegradable tissue-engineered vascular graft. Artificial Organs 32, 800-809.

Tschoeke, B., Flanagan, T.C., Koch, S., Harwoko, M.S., Deichmann, T., Ellå, V., Sachweh, J.S., Kellomåki, M., Gries, T., Schmitz-Rode, T., 2009. Tissue-engineered small-caliber vascular graft based on a novel biodegradable composite fibrin-polylactide scaffold. Tissue Engineering Part A 15, 1909-1918.

Tudorache, I., Cebotari, S., Sturz, G., Kirsch, L., Hurschler, C., Hilfiker, A., Haverich, A., Lichtenberg, A., 2007. Tissue engineering of heart valves: biomechanical and morphological properties of decellularized heart valves. The Journal of Heart Valve Disease 16, 567.

Twigg, S.M., Chen, M.M., Joly, A.H., Chakrapani, S.D., Tsubaki, J., Kim, H.-S., Oh, Y., Rosenfeld, R.G., 2001. Advanced glycosylation end products up-regulate

connective tissue growth factor (insulin-like growth factor-binding protein-related protein 2) in human fibroblasts: a potential mechanism for expansion of extracellular matrix in diabetes mellitus 1. Endocrinology 142, 1760-1769.

Ulijn, R.V., 2006. Enzyme-responsive materials: a new class of smart biomaterials. Journal of Materials Chemistry 16, 2217-2225.

Vesely, I., 2005. Heart valve tissue engineering. Circulation Research 97, 743-755.
Vismara, R., Soncini, M., Talò, G., Dainese, L., Guarino, A., Redaelli, A., Fiore, G.B., 2010. A bioreactor with compliance monitoring for heart valve grafts. Annals of Biomedical Engineering 38, 100-108.

Visse, R., Nagase, H., 2003. Matrix metalloproteinases and tissue inhibitors of metalloproteinases structure, function, and biochemistry. Circulation Research 92, 827-839.

Voyta, J.C., Via, D.P., Butterfield, C.E., Zetter, B.R., 1984. Identification and isolation of endothelial cells based on their increased uptake of acetylated-low density lipoprotein. The Journal of Cell Biology 99, 2034-2040.

Walker, G.A., Masters, K.S., Shah, D.N., Anseth, K.S., Leinwand, L.A., 2004. Valvular myofibroblast activation by transforming growth factor-beta: implications for pathological extracellular matrix remodeling in heart valve disease. Circulation Research 95, 253-260.

Walmsley, T., 1929. The heart. Quain's elements of anatomy 4, 354-367.

Walter, E.M., Sales, V.L., Sill, B., Martin, D., Rusk, E., Emani, S., Hetzer, R., Mayer, J.E., 2010. In vivo implantation of a functional tissue engineered stentless pulmonary valve using bone-marrow-derived mesenchymal stem cells and circulating endothelial progenitor cells. Circulation 122.

Warnock, J.N., Burgess, S.C., Shack, A., Yoganathan, A.P., 2006. Differential immediate-early gene responses to elevated pressure in porcine aortic valve interstitial cells. The Journal of Heart Valve Disease 15, 34-41.

Waxman, A.S., Kornreich, B.G., Gould, R.A., Sydney Moïse, N., Butcher, J.T., 2012. Interactions between TGFβ1 and cyclic strain in modulation of myofibroblastic differentiation of canine mitral valve interstitial cells in 3D culture. Journal of Veterinary Cardiology 14, 211-221.

Weber, B., Emmert, M.Y., Hoerstrup, S.P., 2012. Stem cells for heart valve regeneration. Swiss Medical Weekly 142, w13622.

Weber, K., Schmahl, W., Münch, G., 1998. Distribution of advanced glycation end products in the cerebellar neurons of dogs. Brain Research 791, 11-17.

Weber, M., Heta, E., Moreira, R., Gesché, V., Schermer, T., Frese, J., Jockenhoevel, S., Mela, P., 2014. Tissue-engineered fibrin-based heart valve with a tubular leaflet design. Tissue Engineering Part C 20(4), 265-275.

Wendt, D., Riboldi, S.A., Cioffi, M., Martin, I., 2009. Potential and bottlenecks of bioreactors in 3D cell culture and tissue manufacturing. Advanced Materials 21, 3352-3367.

Weston, M.W., LaBorde, D.V., Yoganathan, A.P., 1999. Estimation of the shear stress on the surface of an aortic valve leaflet. Annals of Biomedical Engineering 27, 572-579.

Weston, M.W., Yoganathan, A.P., 2001. Biosynthetic activity in heart valve leaflets in response to in vitro flow environments. Annals of Biomedical Engineering 29, 752-763.

Whitney, J., 1967. Cardiovascular Pathology. Journal of Small Animal Practice 8, 459-465.

Whitney, J., 1974. Observations on the effect of age on the severity of heart valve lesions in the dog. Journal of Small Animal Practice 15, 511-522.

Wiester, L., Giachelli, C., 2003. Expression and function of the integrin alpha9beta1 in bovine aortic valve interstitial cells. The Journal of Heart Valve Disease 12, 605.

Wills, T.B., Heaney, A.M., Wardrop, K.J., Haldorson, G.J., 2009. Immunomagnetic isolation of canine circulating endothelial and endothelial progenitor cells. Veterinary Clinical Pathology 38(4), 437-442.

Williams, C., Johnson, S.L., Robinson, P.S., Tranquillo, R.T., 2006. Cell sourcing and culture conditions for fibrin-based valve constructs. Tissue Engineering 12, 1489-1502.

Wong, M.L., Leach, J.K., Athanasiou, K.A., Griffiths, L.G., 2011. The role of protein solubilization in antigen removal from xenogeneic tissue for heart valve tissue engineering. Biomaterials 32, 8129-8138.

Woodfin, A., Voisin, M.-B., Nourshargh, S., 2007. PECAM-1: a multi-functional molecule in inflammation and vascular biology. Arteriosclerosis, Thrombosis, and Vascular Biology 27, 2514-2523.

Woollard, H., 1926. The innervation of the heart. Journal of Anatomy 60, 345.

Wylie-Sears, J., Aikawa, E., Levine, R.A., Yang, J.H., Bischoff, J., 2011. Mitral valve endothelial cells with osteogenic differentiation potential. Arteriosclerosis, Thrombosis, and Vascular Biology 31, 598-607.

Xu, S., Liu, A.C., Kim, H., Gotlieb, A.I., 2012. Cell density regulates in vitro activation of heart valve interstitial cells. Cardiovascular Pathology 21, 65-73.

Xu, S., Gotlieb, A.I., 2013. Wnt3a/beta-catenin increases proliferation in heart valve interstitial cells. Cardiovascular Pathology 22, 156-166.

Yacoub, M.H., Cohn, L.H., 2004. Novel approaches to cardiac valve repair: from structure to function: Part I. Circulation 109, 942-950.

Yamagishi, S.-i., Fukami, K., Ueda, S., Okuda, S., 2007. Molecular mechanisms of diabetic nephropathy and its therapeutic intervention. Current Drug Targets 8, 952-959.

Yamagishi, S.-i., 2011. Role of advanced glycation end products (AGEs) and receptor for AGEs (RAGE) in vascular damage in diabetes. Experimental Gerontology 46, 217-224.

Yang, C.-H., Culshaw, G., Liu, M.-M., Lu, C.-C., French, A., Clements, D., Corcoran, B., 2012. Canine tissue-specific expression of multiple small leucine rich proteoglycans. The Veterinary Journal 193, 374-380.

Ye, Q., Zünd, G., Benedikt, P., Jockenhoevel, S., Hoerstrup, S.P., Sakyama, S., Hubbell, J.A., Turina, M., 2000. Fibrin gel as a three dimensional matrix in cardiovascular tissue engineering. European Journal of Cardio-Thoracic Surgery 17, 587-591.

Zacks, S., Rosenthal, A., Granton, B., Havenith, M., Opas, M., Gotlieb, A.I., 1991. Characterization of cobblestone mitral valve interstitial cells. Archives of Pathology & Laboratory Medicine 115, 774-779.

Zhong, Y., Li, S.-H., Liu, S.-M., Szmitko, P.E., He, X.-Q., Fedak, P.W., Verma, S., 2006. C-reactive protein upregulates receptor for advanced glycation end products expression in human endothelial cells. Hypertension 48, 504-511.

Ziegelmueller, J.A., Zaenkert, E.K., Schams, R., Lackermair, S., Schmitz, C., Reichart, B., Sodian, R., 2010. Optical monitoring during bioreactor conditioning of tissue-engineered heart valves. American Society for Artificial Internal Organs Journal 56, 228-231.

Appendix

Publications

Conference Proceedings

1. MM Liu, LY Pang, BM Corcoran, GJ Gulshaw, AT French. Expression of carboxymethyllysine, an advanced glycation end product, in myxomatous mitral valve disease and the mitral valve of healthy dogs. Volume 3-Issue 01, Proceedings of the British Society of Animal Science and the Association of Veterinary Teaching and Research Work, April 2012. Oral Presentation.

2. Mengmeng M. Liu, Tom C. Flanagan, Stefan Jockenhoevel, Alexander Black, David J. Argyle, Anne T. French, Brendan M. Corcoran. Tissue-Engineered Canine Mitral Valve Constructs as In vitro Research Models for Myxomatous Mitral Valve Disease. Proceeding of SHVD 7th Biennial Meeting, June 2013. Poster Presentation.

Journal Articles

1. Yang CH, Culshaw GJ, Liu MM, Lu CC, French AT, Clements DN, Corcoran BM. Canine tissue-specific expression of multiple small leucine rich proteoglycans. Veterinary Journal. 2012 Aug;193 (2):374-80.

2. Lu CC, Liu MM, Culshaw GJ, French AT, Corcoran BM. Cellular changes in Cavalier King Charles Spaniel myxomatous mitral valves are the same as for other dogs. Veterinary Journal. 2013. In press.